



QUANTITATIVE ANALYSIS OF BULK WATER IN WATER/LITHIUM BROMIDE MIXTURES WITH IONIC LIQUIDS AS A WORKING FLUID IN ABSORPTION HEAT PUMPS AND INFLUENCE ON THE THERMOPHYSICAL PROPERTIES

David Latorre Arca

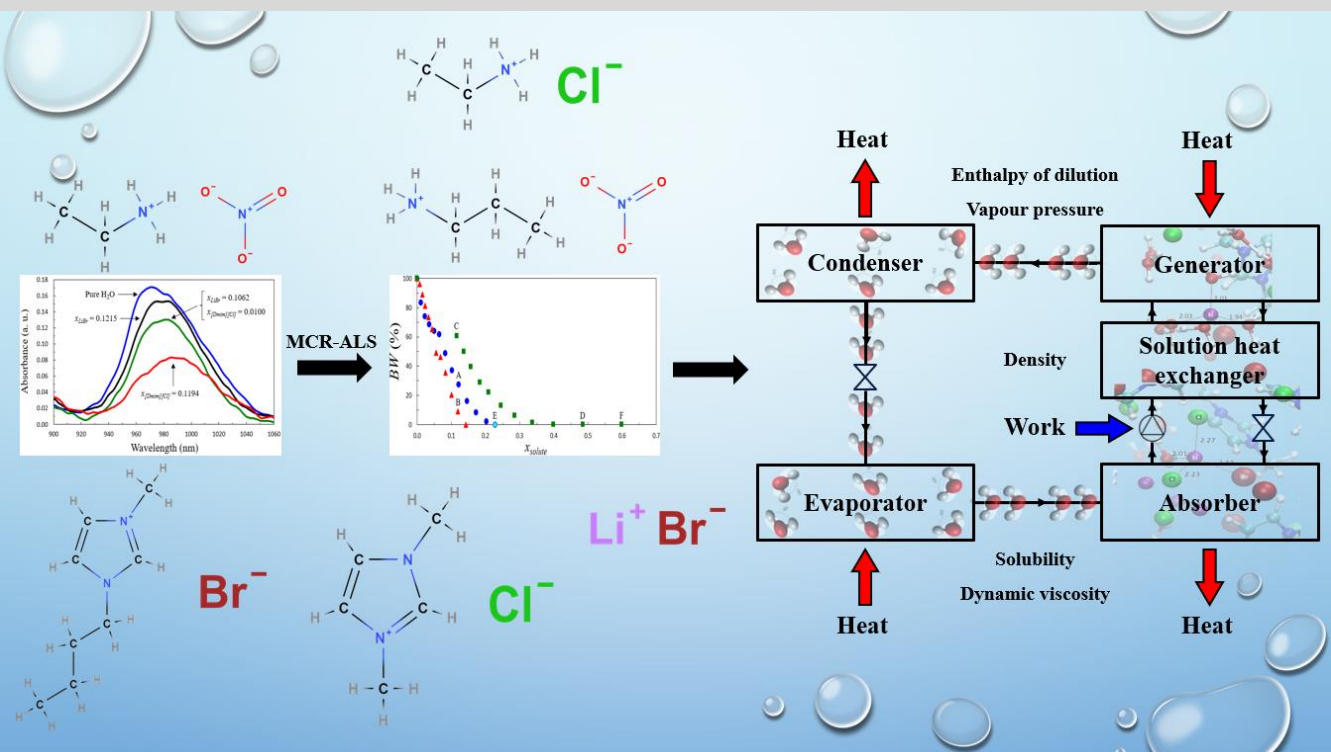
ADVERTIMENT. L'accés als continguts d'aquesta tesi doctoral i la seva utilització ha de respectar els drets de la persona autora. Pot ser utilitzada per a consulta o estudi personal, així com en activitats o materials d'investigació i docència en els termes establerts a l'art. 32 del Text Refós de la Llei de Propietat Intel·lectual (RDL 1/1996). Per altres utilitzacions es requereix l'autorització prèvia i expressa de la persona autora. En qualsevol cas, en la utilització dels seus continguts caldrà indicar de forma clara el nom i cognoms de la persona autora i el títol de la tesi doctoral. No s'autoritza la seva reproducció o altres formes d'explotació efectuades amb finalitats de lucre ni la seva comunicació pública des d'un lloc aliè al servei TDX. Tampoc s'autoritza la presentació del seu contingut en una finestra o marc aliè a TDX (framing). Aquesta reserva de drets afecta tant als continguts de la tesi com als seus resums i índexs.

ADVERTENCIA. El acceso a los contenidos de esta tesis doctoral y su utilización debe respetar los derechos de la persona autora. Puede ser utilizada para consulta o estudio personal, así como en actividades o materiales de investigación y docencia en los términos establecidos en el art. 32 del Texto Refundido de la Ley de Propiedad Intelectual (RDL 1/1996). Para otros usos se requiere la autorización previa y expresa de la persona autora. En cualquier caso, en la utilización de sus contenidos se deberá indicar de forma clara el nombre y apellidos de la persona autora y el título de la tesis doctoral. No se autoriza su reproducción u otras formas de explotación efectuadas con fines lucrativos ni su comunicación pública desde un sitio ajeno al servicio TDR. Tampoco se autoriza la presentación de su contenido en una ventana o marco ajeno a TDR (framing). Esta reserva de derechos afecta tanto al contenido de la tesis como a sus resúmenes e índices.

WARNING. Access to the contents of this doctoral thesis and its use must respect the rights of the author. It can be used for reference or private study, as well as research and learning activities or materials in the terms established by the 32nd article of the Spanish Consolidated Copyright Act (RDL 1/1996). Express and previous authorization of the author is required for any other uses. In any case, when using its content, full name of the author and title of the thesis must be clearly indicated. Reproduction or other forms of for profit use or public communication from outside TDX service is not allowed. Presentation of its content in a window or frame external to TDX (framing) is not authorized either. These rights affect both the content of the thesis and its abstracts and indexes.

Quantitative analysis of bulk water in water/lithium bromide mixtures with ionic liquids as a working fluid in absorption heat pumps and influence on the thermophysical properties

DAVID LATORRE ARCA



UNIVERSITAT ROVIRA I VIRGILI
QUANTITATIVE ANALYSIS OF BULK WATER IN WATER/LITHIUM BROMIDE MIXTURES WITH IONIC LIQUIDS
AS A WORKING FLUID IN ABSORPTION HEAT PUMPS AND INFLUENCE ON THE THERMOPHYSICAL PROPERTIES
David Latorre Arca

UNIVERSITAT ROVIRA I VIRGILI
QUANTITATIVE ANALYSIS OF BULK WATER IN WATER/LITHIUM BROMIDE MIXTURES WITH IONIC LIQUIDS
AS A WORKING FLUID IN ABSORPTION HEAT PUMPS AND INFLUENCE ON THE THERMOPHYSICAL PROPERTIES
David Latorre Arca

UNIVERSITAT ROVIRA I VIRGILI
QUANTITATIVE ANALYSIS OF BULK WATER IN WATER/LITHIUM BROMIDE MIXTURES WITH IONIC LIQUIDS
AS A WORKING FLUID IN ABSORPTION HEAT PUMPS AND INFLUENCE ON THE THERMOPHYSICAL PROPERTIES
David Latorre Arca

David Latorre Arca

**Quantitative analysis of bulk water in water/lithium
bromide mixtures with ionic liquids as a working fluid
in absorption heat pumps and influence on the
thermophysical properties**

DOCTORAL THESIS

Supervised by

Dr. Daniel Salavera

Departament d'Enginyeria Mecànica

Dra. M. Soledad Larrechi

Departament de Química Analítica i Química Orgànica



UNIVERSITAT ROVIRA I VIRGILI

Tarragona

2024

UNIVERSITAT ROVIRA I VIRGILI
QUANTITATIVE ANALYSIS OF BULK WATER IN WATER/LITHIUM BROMIDE MIXTURES WITH IONIC LIQUIDS
AS A WORKING FLUID IN ABSORPTION HEAT PUMPS AND INFLUENCE ON THE THERMOPHYSICAL PROPERTIES
David Latorre Arca



UNIVERSITAT ROVIRA i VIRGILI
Departament d'Enginyeria Mecànica

WE STATE that the present study, entitled “Quantitative analysis of free water in water/lithium bromide mixtures with ionic liquids as a working fluid in absorption heat pumps and influence on the thermophysical properties”, presented by David Latorre Arca for the award of the degree of Doctor, has been carried out under our supervision at the Department of Mechanical Engineering of the Universitat Rovira i Virgili (URV), and it fulfils all the requirements to be eligible for the International Doctorate Award.

Tarragona, 21st August 2024

Doctoral Thesis Supervisors

Dr. Daniel Salavera Muñoz

Dra. María Soledad Larrechi García



UNIVERSITAT ROVIRA i VIRGILI

UNIVERSITAT ROVIRA I VIRGILI
QUANTITATIVE ANALYSIS OF BULK WATER IN WATER/LITHIUM BROMIDE MIXTURES WITH IONIC LIQUIDS
AS A WORKING FLUID IN ABSORPTION HEAT PUMPS AND INFLUENCE ON THE THERMOPHYSICAL PROPERTIES
David Latorre Arca

The work performed in this Doctoral Thesis has been possible thanks to the Project Reversible Water/LiBr Absorption Heat Pumps: Additives, Thermodynamic Properties, Design and Applications (PID2020-119004RB-C21), financed by MCIN/AEI/10.13039/501100011033, and the financial support of the Diputació de Tarragona and Universitat Rovira i Virgili.

UNIVERSITAT ROVIRA I VIRGILI
QUANTITATIVE ANALYSIS OF BULK WATER IN WATER/LITHIUM BROMIDE MIXTURES WITH IONIC LIQUIDS
AS A WORKING FLUID IN ABSORPTION HEAT PUMPS AND INFLUENCE ON THE THERMOPHYSICAL PROPERTIES
David Latorre Arca

Acknowledgements

First, I would like to thank my supervisors, Dr. Daniel Salavera Muñoz and Dr. María Soledad Larrechi García, for their dedication and the help and advice you have given me from the beginning of the thesis, and for the countless things I have learned throughout this stage.

I would also like to thank Dr. Alberto Coronas Salcedo for the support he has given me, as well as for his words of encouragement and the enriching discussions we have had.

My thanks also go to Dr. Yohann Coulier for letting me stay at the Équipe TIM of the Université Clermont Ferrand, and for his involvement and help both in carrying out the experiments and in analysing the results.

A special thank you to my family for their support and care during all this time, especially my mother, Maricarmen, and my sister, Laura.

Thanks to all my friends, who have witnessed this long process and have lent me a hand when I needed it. Carlota, Javi, Patri, Isma, Xián, Jesús, Sara, María, Xavier, Emilio, María, Gabriel, and Iván, thank you from the bottom of my heart.

I would also like to thank the friends I made in Tarragona because you made my stay there better and much more fun. Thank you, Sara, for the quality time and for making me remember my homeland and the Atlantic Ocean. Thank you, María, for the walks we took and for sharing with me your passion for trying new food. Thank you, Xavier, for being a fantastic friend and for making living together an enjoyable experience.

Thanks to Hussain, Tegen, Cristina, Aman, and Francesco, with whom I have shared time and space in labs 113 and 115. Talking to you about anything and making plans has always been pleasant and has helped me to get through the difficult days better.

I would also like to thank Julián and Alaa for the time and effort they put into hosting me in Clermont-Ferrand and making me feel at home. My stay in France would not have been the same without you and I am glad to have met you.

UNIVERSITAT ROVIRA I VIRGILI
QUANTITATIVE ANALYSIS OF BULK WATER IN WATER/LITHIUM BROMIDE MIXTURES WITH IONIC LIQUIDS
AS A WORKING FLUID IN ABSORPTION HEAT PUMPS AND INFLUENCE ON THE THERMOPHYSICAL PROPERTIES
David Latorre Arca

Abbreviations

[Bmim][Br]: 1-butyl-3-methylimidazolium bromide

[Dmim][Cl]: 1,3-dimethylimidazolium chloride

[EA][Cl]: ethylammonium chloride

[EA][NO₃]: ethylammonium nitrate

[PA][NO₃]: propylammonium nitrate

abs: absorbent

ALS: alternating least squares

C: concentration profile matrix

c: speed of sound

CFC: chlorofluorocarbon

COP: coefficient of performance

D: spectral data matrix

E: matrix of residuals

EFA: evolving factor analysis

H₂O: water

HCFC: hydrochlorofluorocarbon

HFC: hydrofluorocarbon

HFO: hydrofluoroolefin

HVAC: heating, ventilation, and air conditioning

i: dissociation factor

IL: ionic liquid

k: coverage factor

LiBr: lithium bromide

LOF: lack of fit

M: molar mass

MCR: multivariate curve resolution

MD: molecular dynamics

N: number of factors

n : number of moles

NH₃: ammonia

NIR: near infrared

p : pressure

PCA: principal component analysis

r : correlation coefficient

RMSE: root mean square error

r_n : solute/solvent mole ratio

S: spectral profile matrix

SLE: solid-liquid equilibria

SVD: singular value decomposition

T : temperature

U : uncertainty

VLE: vapour-liquid equilibria

V_ϕ : apparent molar volume

V_ϕ^0 : apparent molar volume at infinite dilution

w : mass fraction

w_{IL}/w_{abs} : mass fraction ratio between ionic liquid and lithium bromide + ionic liquid

x : mole fraction

x_{IL}/x_{LiBr} : mole fraction ratio between IL and LiBr

x_{LiBr}/x_{H_2O} : mole fraction ratio between lithium bromide and water

$\Delta(\Delta h_{dil})/\Delta h_{dil}$: relative enthalpy of dilution difference

Δh_{dil} : enthalpy of dilution

$\Delta p/p$: relative vapour pressure difference

$\Delta x/x$: relative lithium bromide/water mole fraction ratio difference

$\Delta\eta/\eta$: relative dynamic viscosity difference

$\Delta\lambda/\lambda$: relative thermal conductivity difference

$\Delta\rho/\rho$: relative density difference

η : dynamic viscosity

κ_S : isentropic compressibility

κ_φ : apparent molar isentropic compressibility

κ_φ^0 : limiting apparent molar isentropic compressibility

λ : thermal conductivity

ρ : density

σ : electrical conductivity

UNIVERSITAT ROVIRA I VIRGILI
QUANTITATIVE ANALYSIS OF BULK WATER IN WATER/LITHIUM BROMIDE MIXTURES WITH IONIC LIQUIDS
AS A WORKING FLUID IN ABSORPTION HEAT PUMPS AND INFLUENCE ON THE THERMOPHYSICAL PROPERTIES
David Latorre Arca

Abstract

Global energy consumption for space heating and cooling systems is substantial, with buildings accounting for 30 % of global energy use. Current heating, ventilation, and air conditioning (HVAC) systems predominantly rely on vapor compression technology, which has high energy consumption and environmental impact due to the refrigerants used. Absorption refrigeration systems and heat pump systems, which utilize thermal energy instead of electrical power, present a promising alternative to the traditional vapor compression technology. These systems offer benefits such as longer service life, less maintenance, and the use of natural refrigerants. However, conventional working pairs, such as $\text{NH}_3/\text{H}_2\text{O}$ and $\text{H}_2\text{O}/\text{LiBr}$, face limitations including toxicity and crystallisation risks.

This doctoral thesis explores the enhancement of the $\text{H}_2\text{O}/\text{LiBr}$ working pair by incorporating ionic liquids (ILs) as additives to improve the thermophysical properties of the working fluid. The primary objective is to determine quantitatively the free water content in an $\text{H}_2\text{O}/\text{LiBr}$ working pair with ionic liquids as additives and estimate its effect on the thermophysical properties using near-infrared spectroscopy coupled with the multivariate curve resolution method based on alternating least squares. Five ILs were investigated: three protic (ethylammonium nitrate, propylammonium nitrate, and ethylammonium chloride) and two aprotic (1-butyl-3-methylimidazolium bromide and 1,3-dimethylimidazolium chloride).

The research of ion hydration and association in $\text{H}_2\text{O}/(\text{LiBr}+\text{IL})$ solutions with high IL composition in the solute ($\text{LiBr}+\text{IL}$) revealed that, in the presence of ILs, there is a greater amount of water (bulk water) that preserves its structural properties compared to $\text{H}_2\text{O}/\text{LiBr}$. This result, that evidences stronger solute-solute interactions in $\text{H}_2\text{O}/(\text{LiBr}+\text{IL})$ mixtures, suggests that there are interactions between lithium bromide and ionic liquids. The amount of bulk water in $\text{H}_2\text{O}/(\text{LiBr}+1,3\text{-dimethylimidazolium chloride})$ solutions does not vary significantly at mole fraction ratios between IL and LiBr lower than 0.0942 shows that the composition of IL. The amount of bulk water in $\text{H}_2\text{O}/(\text{LiBr}+\text{IL})$ solutions remains essentially constant between 20 °C and 60 °C.

Analysis of solid-liquid equilibria showed that the addition of ILs effectively delays crystallisation, which is attributed to cation-cation interactions between lithium bromide and ionic liquid. The magnitude of these interactions depends on both the

ionic liquid and its composition in the mixture. The operation range of absorption refrigeration and heat pump systems could be extended in the presence of ILs.

The influence of ILs on vapor-liquid equilibria highlighted that these ionic liquids can both increase and decrease the vapor pressure of the working fluid, depending on composition and temperature. The analysis allowed finding the most interesting mixtures for the absorption applications considered.

The experimental values of density, speed of sound, enthalpy of dilution, electrical conductivity, thermal conductivity, and dynamic viscosity of liquid $\text{H}_2\text{O}/(\text{LiBr}+\text{IL})$ were analysed and compared to that of $\text{H}_2\text{O}/\text{LiBr}$. The results indicate the presence of ILs lowers the heat of dilution, density, and thermal conductivity, and increases dynamic viscosity. The higher amount of bulk water can be directly related to changes in thermodynamic properties, but not to changes in transport properties.

Derived volumetric properties, namely apparent molar volume at infinite dilution, isentropic compressibility, and limiting apparent molar isentropic compressibility, were used to qualitatively compare interactions between $\text{H}_2\text{O}/(\text{LiBr}+\text{IL})$ and $\text{H}_2\text{O}/\text{LiBr}$ mixtures. The results show that solute-solvent interactions are weaker in the presence of ionic liquids, which can be related to the greater amount of bulk water in the mixtures with additive.

Contents

Chapter I. Introduction	1
I.1. Current energy consumption of space heating and cooling systems	2
I.2. Absorption refrigeration and heat pump systems	4
I.3. Working fluids	6
I.3.1 Conventional working fluids	6
I.3.2 Other working fluids	7
I.3.3 Ionic liquids as additives of H ₂ O/LiBr	8
I.4. Motivation	16
I.5. Hypothesis	18
I.6. Objectives	19
I.7. Thesis structure	19
Chapter II. Theoretical background	23
II.1. Near-infrared spectroscopy	24
II.2. Multivariate curve resolution. Optimisation by alternating least squares	25
II.2.1 Determination of the number of factors	26
II.2.2 Initial estimation. Evolving factor analysis	28
II.2.3 Solution optimisation by alternating least squares	28
II.2.4 Quality parameters	29
II.3. Thermophysical properties	30
II.3.1 Solid-liquid equilibria: solubility	30
II.3.2 Vapour-liquid equilibria: vapour pressure	31
II.3.3 Density and speed of sound	31
II.3.4 Enthalpy of dilution	35
II.3.5 Electrical conductivity	36
II.3.6 Thermal conductivity	37

II.3.7 Dynamic viscosity.....	38
II.4. Derived volumetric properties.....	39
II.4.1 Apparent molar volume	39
II.4.2 Isentropic compressibility	41
Chapter III. Ion hydration and association in H₂O/(LiBr+IL) mixtures.....	43
III.1. Introduction.....	44
III.2. Determination of the amount of bulk water in the H ₂ O/LiBr mixture.....	47
III.2.1 Experimental part.....	47
III.2.2 Results and Discussion.....	49
III.2.3 Influence of the hydration on the solid-liquid equilibria and vapour-liquid equilibria of H ₂ O/LiBr.....	55
III.3. Determination of the amount of bulk water in H ₂ O/(LiBr+[Dmim][Cl]) mixtures with high IL composition	60
III.3.1 Introduction	60
III.3.2 Experimental part.....	61
III.3.3 Results and Discussion.....	62
III.4. Selection of ionic liquid composition in H ₂ O/(LiBr+[Dmim][Cl]) mixtures using IL as an additive	69
III.4.1 Introduction	69
III.4.2 Experimental part.....	69
III.4.3 Results and Discussion.....	71
III.5. Influence of the ionic liquid structure on the bulk water content in H ₂ O/(LiBr+IL) mixtures using IL as an additive	75
III.5.1 Introduction	75
III.5.2 Experimental part.....	76
III.5.3 Results and Discussion.....	78
III.6. Influence of temperature on the bulk water in H ₂ O/(LiBr+IL) mixtures at the same mole ratio between LiBr and IL.....	85

III.6.1 Introduction	85
III.6.2 Results and Discussion	85
III.7. Conclusions	93
Chapter IV. Solid-liquid and vapour-liquid equilibria of H₂O/(LiBr+IL) mixtures	95
IV.1. Introduction.....	96
IV.2. Solid-liquid equilibria	96
IV.2.1 Introduction	96
IV.2.2 Experimental device.....	97
IV.2.3 Experimental procedure.....	98
IV.2.4 Reference mixture: H ₂ O/LiBr.....	99
IV.2.5 Experimental results and discussion.....	100
IV.2.6 Comparison of results with the literature.....	112
IV.3. Vapour-liquid equilibria	115
IV.3.1 Introduction	115
IV.3.2 Experimental device.....	116
IV.3.3 Experimental procedure.....	117
IV.3.4 Reference mixture: H ₂ O/LiBr.....	118
IV.3.5 Experimental results and discussion.....	119
IV.3.6 Comparison of results with the literature.....	129
IV.4. Conclusions	131
Chapter V. Thermophysical properties of liquid H₂O/(LiBr+IL) mixtures.....	133
V.1. Introduction.....	134
V.2. Density and speed of sound.....	135
V.2.1 Experimental device.....	135
V.2.2 Experimental procedure.....	135
V.2.3 Reference mixture: H ₂ O/LiBr.....	136

V.2.4 Experimental results and discussion.....	137
V.3. Enthalpy of dilution	151
V.3.1 Experimental device.....	151
V.3.2 Experimental procedure	152
V.3.3 Reference mixture: H ₂ O/LiBr.....	153
V.3.4 Experimental results and discussion.....	154
V.4. Electrical conductivity	156
V.4.1 Experimental device.....	156
V.4.2 Experimental procedure	157
V.4.3 Reference mixture: H ₂ O/LiBr.....	157
V.4.4 Experimental results and discussion.....	158
V.5. Thermal conductivity.....	164
V.5.1 Experimental device.....	164
V.5.2 Experimental procedure	164
V.5.3 Reference mixture: H ₂ O/LiBr.....	164
V.5.4 Experimental results and discussion.....	165
V.6. Dynamic viscosity	168
V.6.1 Experimental device.....	168
V.6.2 Experimental procedure	168
V.6.3 Reference mixture: H ₂ O/LiBr.....	169
V.6.4 Experimental results and discussion.....	170
V.7. Summary of the influence of ILs on the thermophysical properties of H ₂ O/LiBr	173
V.8. Conclusions	175
Chapter VI. Analysis of the influence of ionic liquid on the solute-solvent interaction in H₂O/(LiBr+IL) mixtures using derived volumetric properties...	177
VI.1. Introduction	178
VI.2. Apparent molar volume at infinite dilution	179

VI.3. Isentropic compressibility	188
VI.4. Conclusions.....	199
Chapter VII. Conclusions and future work.....	201
VII.1. Conclusions.....	202
VII.2. Future work	206
References	207

List of Tables

Table I.1. Generations of refrigerants used in vapour compression cycles.....	3
Table I.2. Advantages and disadvantages of NH ₃ /H ₂ O and H ₂ O/LiBr for absorption refrigeration and heat pump systems.	7
Table I.3. Summary of experimentally determined thermophysical properties of H ₂ O/(LiBr+IL) mixtures using ILs as additives available in the literature.	9
Table I.4. Selected ionic liquids used as additives of H ₂ O/LiBr.	17
Table III.1. Conditions at which the mixtures were analysed by NIR+MCR-ALS.	46
Table III.2. Mass (<i>m</i>) and mole fraction (<i>x</i>) of H ₂ O/LiBr solutions.	47
Table III.3. Singular value decomposition of H ₂ O/LiBr spectra at 293.15 K.	50
Table III.4. MCR-ALS results for the H ₂ O/LiBr mixture at 293.15 K.	53
Table III.5. Used <i>a</i> , <i>b</i> and <i>c</i> values in the mass balance.	57
Table III.6. Vapour pressure estimation of H ₂ O/LiBr solutions at 293.15 K.	58
Table III.7. Mass (g) of H ₂ O/[Dmim][Cl] and H ₂ O/(LiBr+[Dmim][Cl]) solutions.	61
Table III.8. MCR-ALS results for H ₂ O/[Dmim][Cl] at 293.15 K.....	63
Table III.9. MCR-ALS results for H ₂ O/(LiBr+[Dmim][Cl]) at 293.15 K and high IL compositions.....	64
Table III.10. Mass (g) of H ₂ O/(LiBr+[Dmim][Cl]) solutions at the selected x_{IL}/x_{LiBr} ratios.	70
Table III.11. MCR-ALS results for H ₂ O/(LiBr+[Dmim][Cl]) at 293.15 K and $x_{IL}/x_{LiBr} = 0.0202$	72
Table III.12. MCR-ALS results for H ₂ O/(LiBr+[Dmim][Cl]) at 293.15 K and $x_{IL}/x_{LiBr} = 0.0418$	73
Table III.13. MCR-ALS results for H ₂ O/(LiBr+[Dmim][Cl]) at 293.15 K and $x_{IL}/x_{LiBr} = 0.0648$	74
Table III.14. Mass (g) of H ₂ O/(LiBr+IL) solutions at a similar x_{IL}/x_{LiBr} ratio for [EA][NO ₃], [PA][NO ₃], [EA][Cl] and [Bmim][Br].	77
Table III.15. MCR-ALS results for H ₂ O/(LiBr+[EA][NO ₃]) at 293.15 K and $x_{IL}/x_{LiBr} = 0.0205$	79

Table III.16. MCR-ALS results for H ₂ O/(LiBr+[PA][NO ₃]) at 293.15 K and $x_{IL}/x_{LiBr} = 0.0205$	80
Table III.17. MCR-ALS results for H ₂ O/(LiBr+[EA][Cl]) at 293.15 K and $x_{IL}/x_{LiBr} = 0.0205$	81
Table III.18. MCR-ALS results for H ₂ O/(LiBr+[Bmim][Br]) at 293.15 K and $x_{IL}/x_{LiBr} = 0.0208$	82
Table III.19. MCR-ALS results for H ₂ O/LiBr at 313.15 K and 333.15 K.....	86
Table III.20. MCR-ALS results for H ₂ O/(LiBr+[EA][NO ₃]) at 313.15 K and 333.15 K, and $x_{IL}/x_{LiBr} = 0.0205$	87
Table III.21. MCR-ALS results for H ₂ O/(LiBr+[PA][NO ₃]) at 313.15 K and 333.15 K, and $x_{IL}/x_{LiBr} = 0.0205$	88
Table III.22. MCR-ALS results for H ₂ O/(LiBr+[EA][Cl]) at 313.15 K and 333.15 K, and $x_{IL}/x_{LiBr} = 0.0205$	89
Table III.23. MCR-ALS results for the H ₂ O/(LiBr+[Bmim][Br]) at 313.15 K and $x_{IL}/x_{LiBr} = 0.0208$	90
Table III.24. MCR-ALS results for the H ₂ O/(LiBr+[Bmim][Br]) at 333.15 K and $x_{IL}/x_{LiBr} = 0.0208$	91
Table III.25. Average bulk water difference between H ₂ O/(LiBr+IL) and H ₂ O/LiBr mixtures additive at different temperatures.	93
Table IV.1. Summary of the conditions at which the solid-liquid equilibria of H ₂ O/(LiBr+IL) mixtures was determined at atmospheric pressure.	96
Table IV.2. Solid phase composition of H ₂ O/LiBr mixtures.....	100
Table IV.3. Mass fraction of absorbent and temperature at the solid-liquid equilibria of H ₂ O/(LiBr+IL) mixtures using [EA][NO ₃], [PA][NO ₃] and [EA][Cl].	101
Table IV.4. Mass fraction of absorbent and temperature at the solid-liquid equilibria of H ₂ O/(LiBr+[Bmim][Br]) mixtures at different IL/absorbent mass ratios.....	102
Table IV.5. Mass fraction of absorbent and temperature at the solid-liquid equilibria of H ₂ O/(LiBr+[Dmim][Cl]) mixtures at different IL/absorbent mass ratios.....	103
Table IV.6. Composition range, coefficients and <i>RMSE</i> of the SLE correlation for H ₂ O/(LiBr+IL) mixtures.	105

Table IV.7. Summary of the average relative increase in x_{LiBr}/x_{H_2O} as a function of x_{IL}/x_{LiBr} and temperature. w_{IL}/w_{abs} : mass fraction ratio between ionic liquid and absorbent.....	110
Table IV.8. Summary of the average relative differences in x_{LiBr}/x_{H_2O} as a function of x_{IL}/x_{LiBr} and T for the SLE of $H_2O/(LiBr+IL)$ found in the literature.....	112
Table IV.9. Summary of the conditions at which the vapor-liquid equilibria was determined for $H_2O/(LiBr+IL)$ mixtures.....	116
Table IV.10. Vapour pressure of the $H_2O/(LiBr+[EA][NO_3])$ mixture with $x_{IL}/x_{LiBr} = 0.0205$	120
Table IV.11. Vapour pressure of the $H_2O/(LiBr+[Bmim][Br])$ mixture with $x_{IL}/x_{LiBr} = 0.0205$	120
Table IV.12. Vapour pressure of the $H_2O/(LiBr+[Dmim][Cl])$ mixture with $x_{IL}/x_{LiBr} = 0.0204$	121
Table IV.13. Vapour pressure of the $H_2O/(LiBr+[Dmim][Cl])$ mixture with $x_{IL}/x_{LiBr} = 0.0427$	121
Table IV.14. Coefficients and $RMSE$ of the VLE correlation for $H_2O/(LiBr+IL)$ mixtures as a function of mass fraction of absorbent.....	123
Table IV.15. Coefficients and $RMSE$ of the VLE correlation for $H_2O/(LiBr+IL)$ mixtures as a function of mole fraction of absorbent.....	123
Table IV.16. Average relative vapour pressure difference between $H_2O/(LiBr+IL)$ mixtures and $H_2O/LiBr$	129
Table V.1. Summary of the conditions at which density and speed of sound were determined for $H_2O/(LiBr+IL)$ mixtures.....	136
Table V.2. Density and speed of sound of the $H_2O/(LiBr+[EA][NO_3])$ mixture at $x_{IL}/x_{LiBr} = 0.0205$ and atmospheric pressure.....	138
Table V.3. Density and speed of sound of the $H_2O/(LiBr+[PA][NO_3])$ mixture at $x_{IL}/x_{LiBr} = 0.0205$ and atmospheric pressure.....	139
Table V.4. Density and speed of sound of the $H_2O/(LiBr+[EA][Cl])$ mixture at $x_{IL}/x_{LiBr} = 0.0205$ and atmospheric pressure.....	140
Table V.5. Density and speed of sound of the $H_2O/(LiBr+[Bmim][Br])$ mixture at $x_{IL}/x_{LiBr} = 0.0208$ and atmospheric pressure.....	141

Table V.6. Density and speed of sound of the H ₂ O/(LiBr+[Dmim][Cl]) mixture at $x_{IL}/x_{LiBr} = 0.0203$ and atmospheric pressure.	142
Table V.7. Density of the H ₂ O/(LiBr+[Dmim][Cl]) mixture at $x_{IL}/x_{LiBr} = 0.0423$ and atmospheric pressure.	143
Table V.8. Coefficients and <i>RMSE</i> of the density correlation for H ₂ O/(LiBr+IL) mixtures as a function of the mass fraction of absorbent.	145
Table V.9. Coefficients and <i>RMSE</i> of the density correlation for H ₂ O/(LiBr+IL) mixtures as a function of the mole fraction of absorbent.	145
Table V.10. Coefficients and <i>RMSE</i> of the speed of sound correlation for H ₂ O/LiBr and H ₂ O/(LiBr+IL) mixtures.	147
Table V.11. Average relative density difference between H ₂ O/(LiBr+IL) and H ₂ O/LiBr mixtures from (293.15 to 343.15) K as as function of x_{LiBr}/x_{H_2O}	150
Table V.12. Summary of the conditions at which the enthalpy of dilution was determined at 298.15 K.	153
Table V.13. Summary of the conditions at which the electrical conductivity was determined for H ₂ O/(LiBr+IL) mixtures.	157
Table V.14. Summary of available electrical conductivity values of H ₂ O/LiBr in the literature.	158
Table V.15. Electrical conductivity of H ₂ O/(LiBr+[EA][NO ₃]) solutions with $x_{IL}/x_{LiBr} = 0.0204$	160
Table V.16. Electrical conductivity of H ₂ O/(LiBr+[EA][Cl]) solutions with $x_{IL}/x_{LiBr} = 0.0209$	160
Table V.17. Electrical conductivity of H ₂ O/(LiBr+[Dmim][Cl]) solutions with $x_{IL}/x_{LiBr} = 0.0203$	161
Table V.18. Electrical conductivity of H ₂ O/(LiBr+[Dmim][Cl]) solutions with $x_{IL}/x_{LiBr} = 0.0421$	161
Table V.19. Coefficients and <i>RMSE</i> of the electrical conductivity correlation for H ₂ O/LiBr and H ₂ O/(LiBr+IL) mixtures.	163
Table V.20. Thermal conductivity of H ₂ O/(LiBr+[Dmim][Cl]) with $x_{IL}/x_{LiBr} = 0.0449$	165

Table V.21. Coefficients and <i>RMSE</i> of the correlation for the thermal conductivity of H ₂ O/(LiBr+[Dmim][Cl]) with $x_{IL}/x_{LiBr} = 0.0449$	167
Table V.22. Dynamic viscosity of H ₂ O/(LiBr+[Dmim][Cl]) with $x_{IL}/x_{LiBr} = 0.0423$..	171
Table V.23. Coefficients and <i>RMSE</i> of the correlation for the dynamic viscosity of H ₂ O/(LiBr+[Dmim][Cl]) with $x_{IL}/x_{LiBr} = 0.0423$	172
Table VI.1. Summary of conditions at which the analysis was carried out for each mixture.....	178
Table VI.2. Apparent molar volume of H ₂ O/LiBr solutions. <i>b</i> : molality; x_{LiBr}/x_{H2O} : mole fraction ratio between LiBr and H ₂ O; <i>T</i> : temperature.	180
Table VI.3. Apparent molar volume of H ₂ O/(LiBr+[EA][NO ₃]) solutions with $x_{IL}/x_{LiBr} = 0.0205$	181
Table VI.4. Apparent molar volume of H ₂ O/(LiBr+[PA][NO ₃]) solutions with $x_{IL}/x_{LiBr} = 0.0205$	182
Table VI.5. Apparent molar volume of H ₂ O/(LiBr+[EA][Cl]) solutions with $x_{IL}/x_{LiBr} = 0.0205$	182
Table VI.6. Apparent molar volume of H ₂ O/(LiBr+[Bmim][Br]) solutions with $x_{IL}/x_{LiBr} = 0.0208$	183
Table VI.7. Apparent molar volume of H ₂ O/(LiBr+[Dmim][Cl]) solutions with $x_{IL}/x_{LiBr} = 0.0203$	183
Table VI.8. Redlich-Rosenfeld-Meyer fitting of the apparent molar volume of H ₂ O/LiBr solutions.	184
Table VI.9. Redlich-Rosenfeld-Meyer fitting of the apparent molar volume of H ₂ O/(LiBr+IL) solutions.....	185
Table VI.10. <i>A</i> , <i>B</i> and <i>C</i> coefficients of the apparent molar volume at infinite dilution of H ₂ O/LiBr and H ₂ O/(LiBr+IL) solutions from (293.15 to 343.15) K.	187
Table VI.11. Hepler's constant for H ₂ O/LiBr and H ₂ O/(LiBr) solutions at $x_{IL}/x_{LiBr} \approx 0.0205$ from (293.15 to 343.15) K.....	188
Table VI.12. Isentropic compressibility of H ₂ O/LiBr solutions.....	189
Table VI.13. Isentropic compressibility of H ₂ O/(LiBr+[EA][NO ₃]) solutions with $x_{IL}/x_{LiBr} = 0.0205$	189

Table VI.14. Isentropic compressibility of H ₂ O/(LiBr+[PA][NO ₃]) solutions with $x_{IL}/x_{LiBr} = 0.0205$.	190
Table VI.15. Isentropic compressibility of H ₂ O/(LiBr+[EA][Cl]) solutions with $x_{IL}/x_{LiBr} = 0.0205$.	190
Table VI.16. Isentropic compressibility of H ₂ O/(LiBr+[Bmim][Br]) solutions with $x_{IL}/x_{LiBr} = 0.0208$.	191
Table VI.17. Isentropic compressibility of H ₂ O/(LiBr+[Dmim][Cl]) solutions with $x_{IL}/x_{LiBr} = 0.0203$.	191
Table VI.18. Convergence points of isentropic compressibility of H ₂ O/LiBr and H ₂ O/(LiBr+IL) solutions at $x_{IL}/x_{LiBr} \approx 0.0205$.	192
Table VI.19. Apparent molar isentropic compressibility of H ₂ O/LiBr solutions.	193
Table VI.20. Apparent molar isentropic compressibility of H ₂ O/(LiBr+[EA][NO ₃]) solutions with $x_{IL}/x_{LiBr} = 0.0205$.	194
Table VI.21. Apparent molar isentropic compressibility of H ₂ O/LiBr+[PA][NO ₃]) solutions with $x_{IL}/x_{LiBr} = 0.0205$.	194
Table VI.22. Apparent molar isentropic compressibility of H ₂ O/(LiBr+[EA][Cl]) solutions with $x_{IL}/x_{LiBr} = 0.0205$.	195
Table VI.23. Apparent molar isentropic compressibility of H ₂ O/(LiBr+[Bmim][Br]) solutions with $x_{IL}/x_{LiBr} = 0.0208$.	195
Table VI.24. Apparent molar isentropic compressibility of H ₂ O/(LiBr+[Dmim][Cl]) solutions with $x_{IL}/x_{LiBr} = 0.0203$.	196
Table VI.25. Fitting of the apparent molar isentropic compressibility of H ₂ O/(LiBr+IL) solutions.	197

List of Figures

Figure I.1. General scheme of single-effect absorption refrigeration and heat pump systems.....	5
Figure II.1. Reflection, absorption, and transmission of light.	24
Figure II.2. Outline of the MCR-ALS resolution.	26
Figure II.3. Singular value decomposition of a data matrix.	27
Figure II.4. EFA results of a data matrix.	28
Figure II.5. Scheme of a U-shape vibrating tube to determine the density of fluids.	32
Figure II.6. Scheme of a pulse measure to determine the speed of sound of fluids.	34
Figure II.7. Scheme of the electrode method for the electrical conductivity determination.	36
Figure II.8. Scheme of a hot wire method to determine the thermal conductivity of a fluid from the slope of the linear function of temperature vs logarithm of time.....	38
Figure II.9. Cutaway view of the viscometer measuring chamber.	39
Figure III.1. Spectra of H ₂ O/LiBr solutions at 293.15 K.	50
Figure III.2. EFA results of H ₂ O/LiBr solutions at 293.15 K.	51
Figure III.3. Concentration and spectral profiles recovered by MCR-ALS for H ₂ O/LiBr at 293.15 K.	52
Figure III.4. <i>BW</i> (%) of H ₂ O/LiBr solutions against LiBr mole fraction at 293.15 K.	54
Figure III.5. Chemical species.	54
Figure III.6. Vapour pressure of H ₂ O/LiBr solutions against mole fraction of LiBr at 293.15 K.	59
Figure III.7. Arbitrary ionic aggregate in the second coordination shell of H ₂ O/LiBr.	59
Figure III.8. Experimental spectra of water and mixtures with similar solute composition.	65
Figure III.9. Bulk water of the analysed solutions against mole fraction of solute (LiBr, [Dmim][Cl] or LiBr+[Dmim][Cl]) at 293.15 K.	66
Figure III.10. Mole ratio against mole fraction of solute at 293.15 K.	67

Figure III.11. Structure of the first solvation shell of Li ion in a snapshot of the CPMD trajectory for (a) relatively concentrated solution and (b) very concentrated solution.	68
Figure III.12. Bulk water of the H ₂ O/(LiBr+[Dmim][Cl]) solutions against mole fraction ratio between LiBr and H ₂ O at 293.15 K.	75
Figure III.13. Bulk water of H ₂ O/LiBr and H ₂ O/(LiBr+IL) solutions against LiBr/H ₂ O mole fraction ratio at 293.15 K.	83
Figure III.14. Average bulk water difference between solutions with and without additive at 293.15 K as a function of the molar mass of the ionic liquid.	84
Figure III.15. Bulk water in H ₂ O/LiBr solutions against mole fraction ratio between LiBr and H ₂ O.....	92
Figure III.16. Bulk water against mole fraction ratio between LiBr and H ₂ O at 313.15 K and 333.15 K.....	93
Figure IV.1. Experimental device used to determine the solid-liquid equilibria by means of the visual polythermal method.	97
Figure IV.2. Solid-liquid equilibria of the H ₂ O/LiBr mixture at 1 bar.	99
Figure IV.3. Solid-liquid equilibria of H ₂ O/LiBr and H ₂ O/(LiBr+IL) mixtures.	107
Figure IV.4. Solid-liquid equilibria of H ₂ O/LiBr and H ₂ O/(LiBr+IL) mixtures at a similar x_{IL}/x_{LiBr} ratio.....	108
Figure IV.5. Solid-liquid equilibria of H ₂ O/LiBr and H ₂ O/(LiBr+IL) mixtures at different x_{IL}/x_{LiBr} ratios.	109
Figure IV.6. Relative LiBr/H ₂ O mole ratio difference between H ₂ O/(LiBr+IL) and H ₂ O/LiBr.....	110
Figure IV.7. Influence of the amount of [Bmim][Br] on the solubility of LiBr in H ₂ O.	115
Figure IV.8. Experimental device used to determine the vapour-liquid equilibria by means of the static, isothermal, isochoric, synthetic and variable pressure methods.	117
Figure IV.9. Pressure-temperature-composition phase diagram for the H ₂ O/LiBr mixture.....	119

Figure IV.10. Pressure-temperature-composition phase diagram for the H ₂ O/(LiBr+[EA][NO ₃]) mixture with $x_{IL}/x_{LiBr} = 0.0205$.	124
Figure IV.11. Pressure-temperature-composition phase diagram for the H ₂ O/(LiBr+[Bmim][Br]) mixture with $x_{IL}/x_{LiBr} = 0.0205$.	124
Figure IV.12. Pressure-temperature-composition phase diagram for the H ₂ O/(LiBr+[Dmim][Cl]) mixture with $x_{IL}/x_{LiBr} = 0.0204$.	125
Figure IV.13. Pressure-temperature-composition phase diagram for the H ₂ O/(LiBr+[Dmim][Cl]) mixture with $x_{IL}/x_{LiBr} = 0.0427$.	125
Figure IV.14. Relative vapour pressure difference between H ₂ O/(LiBr+[EA][NO ₃]) and H ₂ O/LiBr at $x_{IL}/x_{LiBr} = 0.0205$ against temperature.	126
Figure IV.15. Relative vapour pressure difference between H ₂ O/(LiBr+[Bmim][Br]) and H ₂ O/LiBr at $x_{IL}/x_{LiBr} = 0.0205$ against temperature.	126
Figure IV.16. Relative vapour pressure difference between H ₂ O/(LiBr+[Dmim][Cl]) and H ₂ O/LiBr at $x_{IL}/x_{LiBr} = 0.0204$ against temperature.	127
Figure IV.17. Relative vapour pressure difference between H ₂ O/(LiBr+[Dmim][Cl]) and H ₂ O/LiBr at $x_{IL}/x_{LiBr} = 0.0427$ against temperature.	127
Figure IV.18. Summary of relative vapour pressure difference between H ₂ O/(LiBr+IL) mixtures and H ₂ O/LiBr against temperature.	128
Figure V.1. Density of H ₂ O/LiBr solutions at 1 bar.	136
Figure V.2. Speed of sound of H ₂ O/LiBr solutions at 1 bar.	137
Figure V.3. Summary of density differences between H ₂ O/(LiBr+IL) mixtures and H ₂ O/LiBr over the entire temperature and composition range.	148
Figure V.4. Experimental device used to determine the enthalpy of dilution.	151
Figure V.5. Calculated enthalpy of dilution of H ₂ O/LiBr solutions at 298.15 K starting from an initial solution with mole fraction of lithium bromide equal to 0.23.	154
Figure V.6. Experimental enthalpy of dilution of H ₂ O/LiBr and H ₂ O/(LiBr+IL) mixtures at 298.15 K.	155
Figure V.7. Summary of enthalpy of dilution relative difference between H ₂ O/(LiBr+IL) and H ₂ O/LiBr mixtures at 298.15 K and $x_{IL}/x_{LiBr} \approx 0.0205$.	156

Figure V.8. Literature data of electrical conductivity of H ₂ O/LiBr against mass fraction of lithium bromide.	158
Figure V.9. Electrical conductivity of H ₂ O/(LiBr+IL) solutions at 293.15 K against mass fraction of absorbent.	159
Figure V.10. Electrical conductivity of H ₂ O/(LiBr+IL) solutions at 298.15 K against mass fraction of absorbent.	159
Figure V.11. Thermal conductivity of H ₂ O/LiBr as a function of mass fraction of lithium bromide and temperature.....	165
Figure V.12. Thermal conductivity of H ₂ O/(LiBr+[Dmim][Cl]) with $x_{IL}/x_{LiBr} = 0.0449$	166
Figure V.13. Relative thermal conductivity difference between H ₂ O/(LiBr+[Dmim][Cl]) with $x_{IL}/x_{LiBr} = 0.0449$ and H ₂ O/LiBr.	168
Figure V.14. Estimated dynamic viscosity of H ₂ O/LiBr against temperature and mass fraction of lithium bromide.....	169
Figure V.15. Dynamic viscosity of the H ₂ O/(LiBr+[Dmim][Cl]) mixture with $x_{IL}/x_{LiBr} = 0.0423$ against temperature and mass fraction of absorbent.	172
Figure V.16. Summary of average relative difference of the experimentally determined thermophysical properties of H ₂ O/(LiBr+IL) mixtures with respect to H ₂ O/LiBr.....	174
Figure VI.1. Apparent molar volume of (LiBr+IL) in H ₂ O/(LiBr+IL) mixtures as a function of molality and temperature.	181
Figure VI.2. Apparent molar volume at infinite dilution of LiBr and LiBr+IL in aqueous solutions at $x_{IL}/x_{LiBr} \approx 0.0205$	186
Figure VI.3. Hepler's constant solutes in H ₂ O/LiBr and H ₂ O/(LiBr+IL) solutions in water from (293.15 to 343.15) K.....	188
Figure VI.4. Limiting apparent molar isentropic compressibility of LiBr and LiBr+IL in aqueous solutions at $x_{IL}/x_{LiBr} \approx 0.0205$	198

Chapter I. Introduction

I.1. Current energy consumption of space heating and cooling systems

Global energy consumption has increased exponentially over the last 30 years, and about 80% of the primary energy consumed comes from fossil fuels.^[1,2] Since the Paris Agreement was enacted in 2016, international efforts have focused on limiting the global temperature increase to 1.5 °C above pre-industrial levels. Achieving this goal requires a gradual process of decarbonisation, which can be achieved by using renewable energy sources and improving the efficiency of existing energy systems, where up to 30% of primary energy is lost during conversion and transportation. Renewable energies provided 30% of the electricity consumed in the world in 2022, and investments to develop and install renewable technologies are increasing year by year.^[3]

In the case of energy consumption in buildings, it was 133 EJ in 2022,^[3] representing 30 % of the total energy consumed worldwide. Regarding the energy demand of buildings, the main primary sources are fossil fuels (30 %) and electricity (33 %). Specifically, consumption of the latter has increased steadily in recent years due to the increased use of household appliances and air conditioners. On average, 50 % of the energy consumed in buildings was used for space heating or cooling through heating, ventilation, and air conditioning (HVAC) systems.^[4]

Space conditioning in buildings is typically carried out using vapour compression refrigeration and heat pump systems, as well as heating, ventilation, and air conditioning (HVAC) systems. These systems have high coefficients of performance (COP), which is advantageous considering the large amount of energy dedicated to space conditioning. However, besides the high electrical energy consumption of these systems, they have the significant drawback of the high environmental impact of the refrigerants used, which have been changing throughout history to meet the needs of each moment (Table I.1).^[5]

The first generation of refrigerants, based on natural substances, was based on their availability and performance in existing machines.

Chapter I

Table I.1. Generations of refrigerants used in vapour compression cycles.^[5]

Generation	Period	Suitable refrigerants	Primary requirements of the refrigerant*
1 st	S.XIX – 1930s	Natural refrigerants ethyl chloride, diethyl ether, ammonia, propane, sulfur dioxide, carbon dioxide...	Availability and that they could be used in the systems of that time
2 nd	1930s – 1990s	CFCs and HCFCs	Stable, nontoxic, nonflammable, and boiling point ranging from (-40 to 0) °C
3 rd	1990s – 2010	HFCs and natural refrigerants: water, ammonia, carbon dioxide...	Null ozone depletion potential
4 th	2010 – onwards	Mainly HFOs, some HFCs and natural refrigerants	Low global warming potential

*The requirements were maintained in each subsequent generation and expanded from the second generation onwards.^[5]

In the second generation, the focus was on the safety and durability of refrigerants. Chlorofluorocarbons (CFCs) and hydrochlorofluorocarbons (HCFCs) were explicitly synthesised for use in vapour compression refrigeration and heat pump systems. From a thermodynamic cycle performance standpoint, these refrigerants were very competitive. However, after it was discovered that the presence of chlorine in these substances destroys the atmospheric ozone layer, their use was banned following the Vienna Convention for the Protection of the Ozone Layer in 1985 and the Montreal Protocol on Substances that Deplete the Ozone Layer in 1987.

The third generation of refrigerants was based on HFCs (hydrofluorocarbons) and natural refrigerants, which did not affect the ozone layer. However, it was soon discovered that these gases contributed to the greenhouse effect. In the Kyoto Protocol of 1997, it was agreed to phase down their use.

Currently, we are using the fourth generation of refrigerants to mitigate global warming caused by the greenhouse effect. Most refrigerants today are

hydrofluoroolefins (HFOs), HFCs, and natural refrigerants.^[5] Nevertheless, in 2016, it was agreed to reduce the use of HFCs by 85% through the Kigali Amendment to the Montreal Protocol, further limiting the number of available refrigerants.

Given the high electrical energy consumption of vapour compression systems and the increasingly limited use of refrigerants, other types of systems, such as those based on absorption, are attracting increasing interest.

I.2. Absorption refrigeration and heat pump systems

The technology of absorption refrigeration and heat pump systems constitutes an alternative to traditional vapour compression systems to mitigate global warming and ozone depletion.^[6-9] The energy required by these systems is not supplied as electrical power but as thermal power, which can come from natural gas combustion, waste heat from industrial processes, geothermal energy or solar energy. Other advantages of absorption systems, compared to those based on vapour compression, include more extended service life, less maintenance, more flexible operation, lower noise and absence of vibration.^[6,10] In addition, they allow the use of natural refrigerants, such as water or ammonia, instead of the synthetic refrigerants mentioned above.

The general scheme of a single-effect absorption refrigeration and heat pump system is shown in Figure I.1. The refrigerant evaporates from the working fluid in the generator as it receives heat, circulating through the condenser-expansion valve-evaporator circuit. Upon leaving the evaporator, the refrigerant enters the absorber and mixes with an absorber-rich stream, generating heat. The stream exiting the absorber, rich in refrigerant, is pumped through the solution heat exchanger before entering the generator. The stream leaving the generator, rich in absorbent, circulates through the solution heat exchanger and an expansion device before returning to the absorber. The purpose of the solution heat exchanger is to preheat the refrigerant-rich stream at the expense of the stream leaving the generator, which increases the efficiency of the system.

The power consumption of absorption refrigeration and heat pump systems is significantly lower than that of vapour compression-based systems because they compress a liquid instead of a vapour.

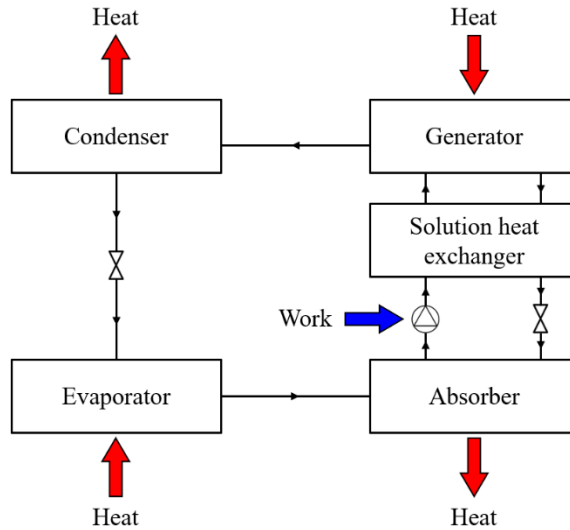


Figure I.1. General scheme of single-effect absorption refrigeration and heat pump systems.

Although absorption systems are expected to cover a large part of the cooling and heating demand in the present and near future, their operating coefficients are considerably lower than those of vapour compression systems. Three alternatives are available to improve their performance:^[6–8,11]

- 1) Using modifications or expansions of the single-effect cycle, such as the single-effect double-lift cycle, the half-effect cycle, multi-effect cycles, the generator/absorber heat exchange (GAX) cycle, and the resorption cycle.
- 2) Improving the design of components to increase mass and heat transfer, with particular emphasis on the absorber, which is the most critical component of absorption systems. The actual mass of refrigerant that is absorbed in the absorbent-rich stream is considerably less than the theoretical mass it can absorb due to the non-equilibrium conditions in which the absorber operates.
- 3) Improving the properties of the working fluid, which can be achieved by using different pairs of refrigerant and absorbent or by adding substances to existing working fluids.

On the one hand, modifications of the single-effect cycle are conditioned by the amount of heat available and its temperature, so its use depends on the specific application. On the other hand, improving the design of the components and the properties of the working fluid would be helpful in all applications, as they play a crucial role in this type of system.

I.3. Working fluids

I.3.1 Conventional working fluids

The requirements that refrigerants and working pairs must meet regarding their properties to be used in refrigeration and absorption heat pump systems are as follows:^[6,7,9–12]

- 1) High latent heat and low melting temperature of the refrigerant.
- 2) High affinity between absorbent and refrigerant.
- 3) Absorbent with low vapour pressure and working fluid with moderate pressure.
- 4) Low viscosity to enhance mass and heat transfer and compactness of the system components.
- 5) High diffusion coefficients and thermal conductivity to favour mass and heat transfer and compactness of the system components.
- 6) Non-crystallisation of the absorbent.
- 7) Non-toxic, non-corrosive, and chemically stable working pair.
- 8) Cost-effective.

Although no working fluids exist that meet all these requirements, $\text{NH}_3/\text{H}_2\text{O}$ and $\text{H}_2\text{O}/\text{LiBr}$ are the most used working pairs in absorption refrigeration and heat pump systems.^[6,7,9–11] Table I.2 summarises the main advantages and disadvantages of the two traditional working fluids. Furthermore, neither of these refrigerants nor absorbents contributes to ozone depletion or global warming, which is an advantage compared to vapour compression systems that do not use natural refrigerants.

Table I.2. Advantages and disadvantages of NH₃/H₂O and H₂O/LiBr for absorption refrigeration and heat pump systems.

Working fluid	Advantages	Disadvantages
NH ₃ /H ₂ O	High latent heat of ammonia Low fusion temperature of ammonia (-78.2 °C) Low viscosities of ammonia and working fluid Complete miscibility of refrigerant and absorbent	Toxicity of ammonia High vapour pressure of the refrigerant (NH ₃) Non-negligible vapour pressure of the absorbent (H ₂ O) Need of a rectifier to separate refrigerant and absorbent
H ₂ O/LiBr	High latent heat of water Non-volatility of the absorbent Low viscosity of water	Crystallisation of lithium bromide Corrosivity of the working fluid High fusion temperature of water (0.01 °C) Need of vacuum due to the low vapour pressure of water, which increases the component size High viscosity of the working fluid

The H₂O/LiBr mixture has been used in refrigeration systems and absorption heat pumps since the second half of the 20th century because it is one of the best existing options, thanks to the favourable characteristics of both the refrigerant and the absorbent, coupled with the high affinity between them. However, as shown in Table I.2, some drawbacks limit the applications of this working fluid, highlighting the risk of crystallisation in the absorbent-rich stream at low temperatures. Therefore, to overcome this limitation, some alternatives exist to use H₂O/LiBr as working fluid.

I.3.2 Other working fluids

Although other working fluids for refrigeration and absorption heat pump systems based on alcohols or halogenated hydrocarbons, such as HCFCs and HFCs, were proposed in the literature, the properties of these mixtures do not globally improve those of H₂O/LiBr.^[6,7,11,13]

More recently, new working fluids have been proposed in which ionic liquids play the role of absorbent in H₂O/IL, NH₃/IL, alcohol/IL, or H₂O/(inorganic salt+IL).^[11–14]

Chapter I

Ionic liquids (ILs) are salts composed of ions that have a low melting point.^[12,15,16] Their structure is based on organic cations and organic or inorganic anions, which gives them unique physicochemical properties, such as negligible vapour pressure and flammability, liquid phase over a wide temperature range, thermal stability, and the ability to solvate compounds with different polarities. Their thermophysical properties can be tuned depending on the chosen cation and anion, making them versatile substances of interest for various applications.

To date, the results show that the use of ILs as absorbents presents a lower coefficient of performance than with H₂O/LiBr or NH₃/H₂O,^[11,12,14] since they exhibit other problems, especially related to transport properties. Nevertheless, an option of great interest is using these ionic liquids as additives of lithium bromide to improve the properties of the mixture, with particular interest in solubility.

I.3.3 Ionic liquids as additives of H₂O/LiBr

Many substances have been proposed over the years as additives of lithium bromide to increase its solubility, such as inorganic salts,^[10,17–22] organic salts,^[23] zwitterionic compounds,^[24,25] or glycols.^[21,26–31] More recently, ionic liquids have also started to be used as additives of this working fluid.^[25,32–44]

Table I.3 summarises the pressure, temperature and composition ranges in which thermophysical properties of H₂O/(LiBr+IL) mixtures were experimentally determined in the literature using ILs as additives.

Table I.3. Summary of experimentally determined thermophysical properties of H₂O/(LiBr+IL) mixtures using ILs as additives available in the literature. w_{abs} : mass fraction of absorbent (LiBr+IL).

Property	Reference	Ionic liquid	T range (K)	p range (kPa)	w_{abs} range	IL/LiBr mole ratio
Solid-liquid equilibria	Yang <i>et al.</i> ^[33]	1-ethyl-3-methylimidazolium chloride	253 – 307	100	0.69 – 0.75	0.24
	Kim <i>et al.</i> ^[34]	1-butyl-3-methylimidazolium bromide	286 – 362	Atmospheric pressure	0.62 – 0.75	0.06 – 0.10
	Królikowska and Hofman ^[32]	N-ethyl-N-methylmorpholinium bromide	243 – 352	100	0.58 – 0.71	0.05
			235 – 343	100	0.61 – 0.73	0.11
			228 – 351	100	0.64 – 0.77	0.17
		N-butyl-N-methylmorpholinium bromide	228 – 363	100	0.57 – 0.71	0.04
			241 – 349	100	0.61 – 0.74	0.09
			238 – 366	100	0.64 – 0.78	0.16
		N-hexyl-N-methylmorpholinium bromide	239 – 352	100	0.58 – 0.70	0.04
			235 – 350	100	0.61 – 0.74	0.08
			243 – 340	100	0.64 – 0.75	0.14
		1-butyl-3-methylimidazolium bromide	246 – 352	100	0.58 – 0.72	0.05
			250 – 354	100	0.61 – 0.74	0.10
			245 – 363	100	0.64 – 0.77	0.17
		N-ethyl-N-methylpiperidinium bromide	239 – 353	100	0.57 – 0.70	0.05

Table I.3 (continued)

Property	Reference	Ionic liquid	T range (K)	p range (kPa)	w_{abs} range	IL/LiBr mole ratio
Solid-liquid equilibria	Królikowska and Hofman ^[32]	N-ethyl-N-methylpiperidinium bromide	250 – 340	100	0.61 – 0.71	0.10
			241 – 334	100	0.64 – 0.75	0.18
		N-butyl-N-methylpiperidinium bromide	249 – 358	100	0.59 – 0.72	0.04
			264 – 336	100	0.62 – 0.72	0.09
			250 – 363	100	0.64 – 0.76	0.16
		N-butyl-N-methylpyrrolidinium bromide	249 – 353	100	0.59 – 0.70	0.04
			239 – 345	100	0.61 – 0.73	0.10
			243 – 355	100	0.64 – 0.76	0.17
		N-butylpyridinium bromide	250 – 352	100	0.59 – 0.70	0.05
			249 – 352	100	0.61 – 0.73	0.10
			246 – 341	100	0.64 – 0.75	0.17
		Tri(ethyl)butylammonium bromide	254 – 353	100	0.59 – 0.71	0.04
	245 – 362		100	0.61 – 0.74	0.09	
	246 – 359		100	0.64 – 0.76	0.16	
	Królikowska <i>et al.</i> ^[25]	N-(2-hydroxyethyl)-N,N,N-triethylammonium bromide	255 – 353	100	0.59 – 0.71	0.04
254 – 355			100	0.62 – 0.74	0.10	
250 – 349			100	0.65 – 0.77	0.16	

Table I.3 (continued)

Property	Reference	Ionic liquid	T range (K)	p range (kPa)	w_{abs} range	IL/LiBr mole ratio
Solid-liquid equilibria	Królikowska <i>et al.</i> ^[25]	N-(cyanomethyl)-N,N,N-triethylammonium bromide	261 – 338	100	0.58 – 0.68	0.04
			263 – 363	100	0.55 – 0.75	0.10
			266 – 348	100	0.56 – 0.76	0.17
		N-(2-hydroxyethyl)-N,N-dimethyl-N-butylammonium bromide	253 – 360	100	0.59 – 0.71	0.04
			250 – 355	100	0.62 – 0.74	0.10
			250 – 352	100	0.65 – 0.77	0.16
		N,N-di(2-hydroxyethyl)-N,N-dimethylammonium bromide	265 – 369	100	0.57 – 0.68	0.05
			242 – 353	100	0.62 – 0.75	0.10
			248 – 351	100	0.66 – 0.78	0.17
		N-methyl-N-(2-hydroxyethyl)morpholinium bromide	244 – 341	100	0.65 – 0.77	0.17
		N-(2-acetyloxy)ethyl-N-methylmorpholinium bromide	251 – 358	100	0.65 – 0.79	0.14
		N-methyl-N-(2-ethoxy-2-oxoethyl)morpholinium bromide	247 – 332	100	0.65 – 0.76	0.14
1-methyl-3-(2-hydroxyethyl)imidazolium bromide	249 – 345	100	0.65 – 0.77	0.18		
N-methyl-N-(2-hydroxyethyl)pyrrolidinium bromide	257 – 352	100	0.65 – 0.77	0.18		

Table I.3 (continued)

Property	Reference	Ionic liquid	T range (K)	p range (kPa)	w_{abs} range	IL/LiBr mole ratio
Solid-liquid equilibria	Królikowska <i>et al.</i> ^[25]	N-methyl-N-(2-hydroxyethyl)pyrrolidinium bromide	248 – 350	100	0.65 – 0.78	0.18
Vapour-liquid equilibria	Jing <i>et al.</i> ^[35]	1,3-dimethylimidazolium chloride	309 – 439	3 – 103	0.30 – 0.69	0.218
		1,3-dimethylimidazolium tetrafluoroborate	311 – 424	4 – 102	0.30 – 0.70	0.236
	Zhang <i>et al.</i> ^[36]	1-ethyl-3-methylimidazolium acetate	304 – 405	5 – 101	0.20 – 0.60	0.170
	Yang <i>et al.</i> ^[33]	1-ethyl-3-methylimidazolium chloride	305 – 434	1 – 102	0.55 – 0.70	0.237
	Xuan <i>et al.</i> ^[37]	1-ethyl-3-methylimidazolium chloride	320 – 410	4 – 103	0.30 – 0.60	0.296
	Rafiee and Frouzesh ^[38]	1-ethyl-3-methylimidazolium hydrogen sulfate	298	2 – 3	0.10 – 0.42	0.24 – 1.68
	Xuan <i>et al.</i> ^[39]	1,3-dimethylimidazolium iodide	351 – 410	32 – 106	0.30 – 0.60	0.194
		1-ethyl-3-methylimidazolium iodide	351 – 414	32 – 106	0.30 – 0.57	0.091
	Dong <i>et al.</i> ^[41]	1,3-dimethylimidazolium dimethylphosphate	299 – 410	2 – 103	0.20 – 0.60	0.130
Królikowska <i>et al.</i> ^[40]	3-(1-methyl-morpholinium)propane-1-sulfonate	338 – 368	6 – 84	0.02 – 0.30	0.167	

Table I.3 (continued)

Property	Reference	Ionic liquid	T range (K)	p range (kPa)	w_{abs} range	IL/LiBr mole ratio
Vapour-liquid equilibria	Królikowska <i>et al.</i> ^[40]	N,N-di(2-hydroxyethyl)-N,N-dimethylammonium bromide	338 – 368	5 – 84	0.03 – 0.36	0.173
		N,N,N-tri(2-hydroxyethyl)-N-methylammonium bromide	338 – 368	6 – 84	0.02 – 0.31	0.167
Density	Rafiee and Frouzesh ^[38]	1-ethyl-3-methylimidazolium hydrogen sulfate	293 – 313	87	0.06 – 0.19	0.08 – 0.25
	Rafiee and Frouzesh ^[44]	1-ethyl-3-methylimidazolium chloride	298 - 318	87	0.06 – 0.28	0.17 – 0.68
	Shekaari <i>et al.</i> ^[42]	1-butyl-3-methylimidazolium thiocyanate	298	86	0.02 – 0.04	0.04 – 0.17
		1-methyl-3-octyl-1H-imidazolium thiocyanate	298	86	0.02 – 0.04	0.03 – 0.12
		1-hexyl-3-methylimidazolium thiocyanate	298	86	0.02 – 0.04	0.03 – 0.15
	Yang <i>et al.</i> ^[33]	1-ethyl-3-methylimidazolium chloride	303 – 373	100	0.30 – 0.45	0.237
	Królikowska <i>et al.</i> ^[40]	3-(1-methyl-morpholinium)propane-1-sulfonate	298 – 348	100	0.06 – 0.70	0.167
		N,N-di(2-hydroxyethyl)-N,N-dimethylammonium bromide	298 – 348	100	0.11 – 0.71	0.173

Table I.3 (continued)

Property	Reference	Ionic liquid	T range (K)	p range (kPa)	w_{abs} range	IL/LiBr mole ratio
Density	Królikowska <i>et al.</i> ^[40]	N,N,N-tri(2-hydroxyethyl)-N-methylammonium bromide	298 – 348	100	0.16 – 0.73	0.167
	Bagheri <i>et al.</i> ^[43]	2-hydroxyethylammonium acetate	288 – 318	87.1	0.01 – 0.04	0.54 – 1.25
		bis-2-hydroxyethylammonium acetate	288 – 318	87.1	0.01 – 0.05	0.53 – 1.25
		tris-2-hydroxyethylammonium acetate	288 – 318	87.1	0.01 – 0.05	0.54 – 1.25
Speed of sound	Shekaari <i>et al.</i> ^[42]	1-butyl-3-methylimidazolium thiocyanate	298	86	0.02 – 0.04	0.04 – 0.17
		1-methyl-3-octyl-1H-imidazolium thiocyanate	298	86	0.02 – 0.04	0.03 – 0.12
		1-hexyl-3-methylimidazolium thiocyanate	298	86	0.02 – 0.04	0.03 – 0.15
	Bagheri <i>et al.</i> ^[43]	2-hydroxyethylammonium acetate	288 – 318	87.1	0.01 – 0.04	0.54 – 1.25
		bis-2-hydroxyethylammonium acetate	288 – 318	87.1	0.01 – 0.05	0.53 – 1.25
		tris-2-hydroxyethylammonium acetate	288 – 318	87.1	0.01 – 0.05	0.54 – 1.25
Heat capacity at constant pressure	Yang <i>et al.</i> ^[33]	1-ethyl-3-methylimidazolium chloride	303 – 373	100	0.30 – 0.45	0.237

Table I.3 (continued)

Property	Reference	Ionic liquid	T range (K)	p range (kPa)	w_{abs} range	IL/LiBr mole ratio
Viscosity	Yang <i>et al.</i> ^[33]	1-ethyl-3-methylimidazolium chloride	303 – 373	100	0.30 – 0.45	0.237
	Shekaari <i>et al.</i> ^[42]	1-butyl-3-methylimidazolium thiocyanate	298	86	0.02 – 0.04	0.04 – 0.17
		1-methyl-3-octyl-1H-imidazolium thiocyanate	298	86	0.02 – 0.04	0.03 – 0.12
		1-hexyl-3-methylimidazolium thiocyanate	298	86	0.02 – 0.04	0.03 – 0.15
	Królikowska <i>et al.</i> ^[40]	3-(1-methyl-morpholinium)propane-1-sulfonate	298 – 348	100	0.06 – 0.70	0.167
		N,N-di(2-hydroxyethyl)-N,N-dimethylammonium bromide	298 – 348	100	0.11 – 0.71	0.173
		N,N,N-tri(2-hydroxyethyl)-N-methylammonium bromide	298 – 348	100	0.16 – 0.73	0.167
	Bagheri <i>et al.</i> ^[43]	2-hydroxyethylammonium acetate	288 – 318	87.1	0.01 – 0.04	0.53 – 1.25
		bis-2-hydroxyethylammonium acetate	288 – 318	87.1	0.01 – 0.05	0.53 – 1.25
		tris-2-hydroxyethylammonium acetate	288 – 318	87.1	0.01 – 0.05	0.53 – 1.25

As Table I.3 shows,^[25,32–41] most ionic liquids proposed as additives of lithium bromide are based on the imidazolium cation. Królikowska and Hofman^[32] and Królikowska *et al.*^[25,40] also used ionic liquids based on other cations, such as ammonium and morpholinium. However, the pressure, temperature, and composition ranges are limited, especially regarding the operation ranges of absorption refrigeration and heat pump systems: many properties were measured only at 25 °C, low absorbent compositions, and large amounts of ionic liquid.

I.4. Motivation

The thermophysical properties of a working pair in absorption refrigeration and heat pumps systems can improve by using additives, such as ionic liquids, due to their special characteristics. This can help to increase the cycle performance and extend the applications of these technologies. On the one hand, the analysis of the solid-liquid equilibria results of LiBr in water in the presence of ionic liquids as additives, as mentioned in the literature,^[25,32–34] evidences the potential of these substances to delay the crystallisation of lithium bromide in H₂O/LiBr mixtures. On the other hand, vapour pressure results reported in the literature suggest that, for the same mass fraction of absorbent in the working fluid, the vapour pressure is higher in the presence of ionic liquids,^[33,35–41] which may have a negative effect on the conditions required for the working fluids in the application. Both aspects vary depending on the nature of the ionic liquid considered and the composition of the mixture.

However, the large number of existing ionic liquids and the number of essential properties required, especially the solid-liquid and liquid-vapour phase equilibria, to properly design absorption refrigeration and heat pump systems,^[32] makes it difficult to select the adequate ionic liquid and its composition only by measuring thermophysical properties. This requires a great experimental effort, both in time and money, which is reflected in the scarce and limited studies reporting experimental data on thermophysical properties of H₂O/LiBr mixtures with ionic liquids as additives (Table I.3).

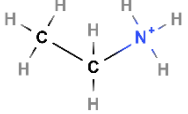
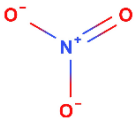
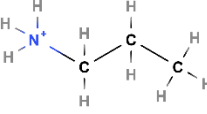
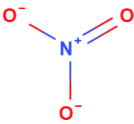
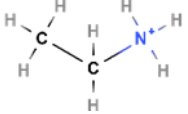

For this reason, the motivation of this doctoral thesis is to establish an analysis strategy to estimate the influence of ionic liquids on the thermophysical properties of

Chapter I

the H₂O/LiBr working pair. The approach is based on near-infrared spectroscopy coupled with the curve resolution method based on alternating least squares, and the results are contrasted and complemented with the properties of solid-liquid and vapour-liquid equilibria and thermophysical properties measured and calculated for H₂O/(LiBr+IL) mixtures. The acquired knowledge will help to choose better the adequate ionic liquid and composition in the mixture.

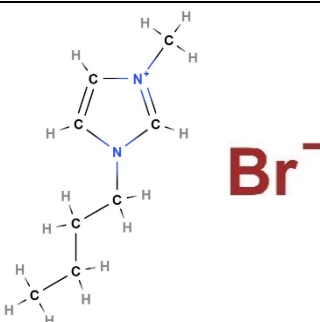
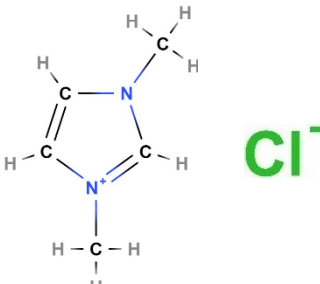
The case study (Table I.4) involves a set of five ionic liquids: three of them (ethylammonium nitrate [EA][NO₃], propylammonium nitrate [PA][NO₃], and ethylammonium chloride [EA][Cl]) are protic and have not been used yet in any published work in the literature, and two others (1-butyl-3-methylimidazolium bromide [Bmim][Br] and 1,3-dimethylimidazolium chloride [Dmim][Cl]) are aprotic and have already been referenced in the literature,^[32,34,35] extending the range of conditions in which thermophysical properties are determined according to the application of interest.

Table I.4. Selected ionic liquids used as additives of H₂O/LiBr.

Ionic liquid Abbreviation CAS number Supplier and mass purity (%)	Cation	Anion	<i>M</i> (g·mol ⁻¹)
Ethylammonium nitrate [EA][NO ₃] 22113-86-6 IOLITEC (> 97)			108.11
Propylammonium nitrate [PA][NO ₃] 22113-88-8 IOLITEC (> 97)			122.12
Ethylammonium chloride [EA][Cl] 557-66-4 Sigma-Aldrich (> 99.3)			81.545

Chapter I

Table I.4 (continued)

1-butyl-3-methylimidazolium bromide [Bmim][Br] 85100-77-2 IOLITEC (> 99)		219.12
1,3-dimethylimidazolium chloride [Dmim][Cl] 79917-88-7 Angene (> 97)		132.59

I.5. Hypothesis

The considered hypotheses in this doctoral thesis are the following:

- Understanding how the presence of ionic liquids affects the solvation of LiBr will help us understand their influence on the thermophysical properties of mixtures.
- Quantifying the extent of LiBr hydration in the presence of the ionic liquid relative to that of the H₂O/LiBr mixture will help estimate the most appropriate composition of the ionic liquid in the working fluid.
- Analyzing the changes produced in the thermophysical properties of the H₂O/LiBr mixture in the presence of ionic liquids will allow to evaluate their potential to improve the performance of the mixture as a working fluid in absorption refrigeration and heat pump systems, and to corroborate and complement the above hypotheses.
- Determining volumetric derived properties of (H₂O/LiBr+IL) solutions, which allows interpreting the solute-solvent interactions from a thermodynamic point of view, will also help support the above hypotheses.

I.6. Objectives

The general objective of this doctoral thesis is to establish an analysis strategy to estimate the influence of an additive on the properties of the H₂O/LiBr working pair. The approach is based on near-infrared spectroscopy coupled with the curve resolution method based on alternating least squares. The conclusions derived from these results will be contrasted and complemented with the results found from the measurement of phase equilibria, some thermophysical properties and calculation of derived volumetric properties.

The specific objectives required to fulfil this general objective are:

- 1) To determine the hydration and association in solutions with and without additive over a wide composition range at different temperatures using a multivariate curve resolution method applied to near-infrared spectra.
- 2) To determine the solid-liquid equilibria of H₂O/(LiBr+IL) mixtures over wide composition and temperature ranges.
- 3) To determine the vapour-liquid equilibria of H₂O/(LiBr+IL) mixtures over wide composition and temperature ranges.
- 4) To determine density, speed of sound, enthalpy of dilution, electrical conductivity, thermal conductivity, and dynamic viscosity of liquid H₂O/(LiBr+IL) mixtures over comprehensive composition and temperature ranges.
- 5) To analyse the influence of selected ionic liquids on the solid-liquid equilibria, vapour-liquid equilibria and thermophysical properties of the working fluid.
- 6) To compare interactions in solutions with and without additive from a thermodynamic point of view based on derived volumetric properties.

I.7. Thesis structure

This doctoral thesis is divided into seven different chapters. The first chapter is the introduction, discussing the need to mitigate climate change. Then, the single-effect absorption refrigeration and heat pump systems are briefly described, along with the advantages and disadvantages of the most used working fluids. Subsequently, a literature review on using ionic liquids as additives of H₂O/LiBr is

Chapter I

presented. Finally, the motivation, hypotheses and objectives of this thesis are defined.

In the second chapter, the theoretical background of the experimental part is described. In the first section, the theoretical foundations of near-infrared spectroscopy are detailed. The second section describes the theoretical background of the used multivariate curve resolution method. The theoretical foundations regarding solid-liquid equilibria, vapour-liquid equilibria, density, speed of sound, enthalpy of dilution, electrical conductivity, thermal conductivity, and dynamic viscosity are described in the third section. The final section briefly summarises the theoretical background regarding derived properties obtained from density and speed of sound.

The third chapter presents the ion hydration and association in $\text{H}_2\text{O}/(\text{LiBr}+\text{IL})$ mixtures and discusses using a multivariate curve resolution method to near-infrared spectra. Calculating bulk water content is detailed for the $\text{H}_2\text{O}/\text{LiBr}$ mixture at 20 °C. Then, the quantitative analysis of water association in $\text{H}_2\text{O}/(\text{LiBr}+\text{IL})$ mixtures is analysed with 1,3-dimethylimidazolium chloride to determine the maximum quantity of IL that should be used in solution. Subsequently, the influence of the IL composition on the bulk water of $\text{H}_2\text{O}/(\text{LiBr}+\text{IL})$ with 1,3-dimethylimidazolium chloride used as an additive is discussed. Then, the influence of the structure of the selected ionic liquids on the bulk water is presented and discussed at 20 °C. Finally, the impact of temperature on the bulk water of $\text{H}_2\text{O}/(\text{LiBr}+\text{IL})$ mixtures is discussed at 40 °C and 60 °C.

The fourth chapter presents and discusses the experimental solid-liquid and vapour-liquid equilibria of $\text{H}_2\text{O}/(\text{LiBr}+\text{IL})$ mixtures. Generally, the experimental work carried out is guided by the conclusions drawn in the previous chapter. Firstly, the solid-liquid equilibria results are discussed depending on the absorbent composition, on the $\text{LiBr}/\text{H}_2\text{O}$ mole ratio, and on the influence of the chemical structure of the IL. Then, the results are compared with the referenced values in the literature. Subsequently, the vapour-liquid equilibria results are discussed as a function of the $\text{LiBr}/\text{H}_2\text{O}$ mole ratio and are compared with those found in the literature.

The fifth chapter is devoted to the thermophysical properties of $\text{H}_2\text{O}/(\text{LiBr}+\text{IL})$ mixtures in the liquid phase. According to the previous chapters, the results of density,

Chapter I

speed of sound, enthalpy of dilution, electrical conductivity, thermal conductivity, and dynamic viscosity are presented and discussed concerning the referenced values of H₂O/LiBr at the selected IL/LiBr ratios.

In the sixth chapter, the influence of ionic liquids on the solute-solvent interactions in H₂O/(LiBr+IL) mixtures is analysed by comparison of derived volumetric properties. The apparent molar volume at infinite dilution, the isentropic compressibility, and the limiting apparent molar isentropic compressibility of H₂O/(LiBr+IL) solutions are compared to that of H₂O/LiBr as a function of temperature over a wide composition range.

Finally, the main findings are summarised in the concluding chapter along with future work recommendations.

As a clarification, although *solute* and *absorbent* refer to LiBr or (LiBr+IL), and *solvent* and *refrigerant* refer to water, their use depends on the specific context. For this reason, the terms *solute* and *solvent* are generally more appropriate for the discussion in Chapters III and VI. At the same time, *absorbent* and *refrigerant* are preferred in Chapters IV and V. Similarly, the terms *solution*, *mixture*, *working fluid*, and *working pair* refer to the combination of two or more substances. In general, *solution* is preferred in Chapters III and VI, while *mixture*, *working fluid* and *working pair* are used indistinctly in Chapters IV and V.

Chapter II. Theoretical background

II.1. Near-infrared spectroscopy

The near-infrared (NIR) covers the region of the electromagnetic spectrum of wavelength from (700 to 2500) nm. The absorption bands in this region are characteristic of the overtones and combination bands of the fundamental vibrations of the functional group bonds in the mid-infrared. The highest intensity bands correspond to the vibrations of the C-H, O-H and N-H groups. These groups are characterised by broad bands and low intensity, which facilitates the quantitative determination of compounds with high composition without the need to pretreat samples.

Infrared radiation can change when it travels through a sample due to reflection, absorption and transmission phenomena (Figure II.1). As a consequence, a part of the intensity of the incident radiation (P_o) will be reflected (P_r), another part will be absorbed (P_a), and another part will be transmitted (P_t).

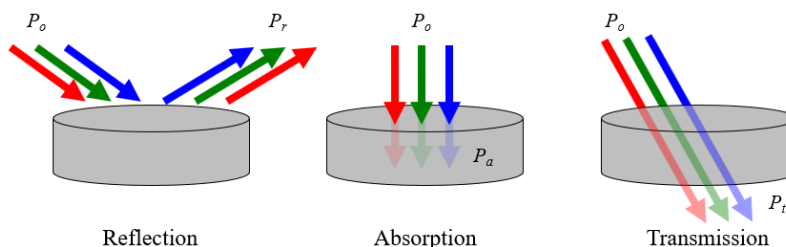


Figure II.1. Reflection, absorption, and transmission of light.

Measurements in the near-infrared region can be carried out based on any of the three phenomena mentioned above, according to Eqs. II.1-II.3, where S_λ , B_λ y R_λ are the sample intensity, background intensity and reference intensity at wavelength λ , respectively, expressed in $W \cdot m^{-2}$.

$$R_\lambda(\%) = 100 \cdot \frac{S_\lambda - B_\lambda}{R_\lambda - B_\lambda} \quad \text{Eq. II.1}$$

$$A_\lambda = -\log_{10} \left(\frac{S_\lambda - B_\lambda}{R_\lambda - B_\lambda} \right) \quad \text{Eq. II.2}$$

$$T_{\lambda} (\%) = 100 \cdot \frac{S_{\lambda} - B_{\lambda}}{R_{\lambda} - B_{\lambda}} \quad \text{Eq. II.3}$$

The experiments carried out in this thesis were performed using transmitted/absorbed radiation (absorption measurements), which is the most common mode used when working with liquid samples.

II.2. Multivariate curve resolution. Optimisation by alternating least squares

Curve resolution methods applied to multivariate data (MCR), introduced by Lawton and Sylvestre,^[45] are a technique based on factor analysis used to estimate the pure factors in a two-component system. The use of MCR was later extended to solve more complex systems.^[46,47]

The objective of multivariate curve resolution – alternating least squares (MCR-ALS)^[48] is the decomposition of the initial data matrix **D** into the product of two matrices that contain the pure concentration and response profiles of all the active species present in the system (Eq. II.4). This can only be done assuming that the experimental data follow a bilinear model of analogous structure to the generalised law of Beer-Lambert ($A = \varepsilon \cdot b \cdot c$), where A is the absorbance, ε is the molar absorptivity of the species ($\text{m}^2 \cdot \text{mol}^{-1}$), b is the path length (m), and c is the concentration of the species ($\text{mol} \cdot \text{m}^{-3}$).

In this work, **D** is the matrix containing the infrared spectra of the $\text{H}_2\text{O}/\text{LiBr}$, $\text{H}_2\text{O}/[\text{Dmim}][\text{Cl}]$ or $\text{H}_2\text{O}/(\text{LiBr}+\text{IL})$ mixtures, **C** and **S** are the concentration and spectral profiles of the different chemical species in the analysed solutions, respectively, and **E** is the matrix of residuals that are not explained by the model.

$$\mathbf{D} = \mathbf{C} \cdot \mathbf{S}^T + \mathbf{E} \quad \text{Eq. II.4}$$

The dimensions of these matrices are: **D** ($I \times J$), **C** ($I \times N$), **S**^T ($N \times J$) and **E** ($I \times J$), where I is the number of samples analysed, J is the number of wavelengths at which they spectra are acquired, and N is the number of chemical species or compounds present.

An outline of the steps involved in the resolution of Eq. II.4 is shown in Figure II.2. It starts from an original space, where the data are represented with as many dimensions as variables considered in the response (J in this case), and ends in a reduced space of new factors (N), which are representative of the pure spectra of the chemical species in the analysed samples.

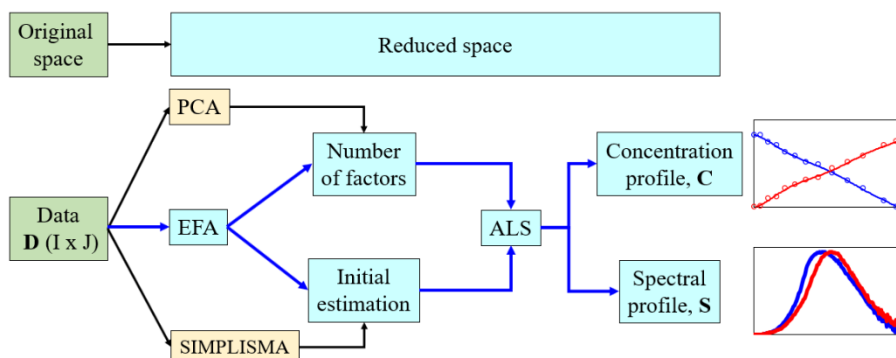


Figure II.2. Outline of the MCR-ALS resolution.

This process requires determining the number of factors (N), creating an initial estimation of the concentration matrix (\mathbf{C}^*) or the spectra matrix (\mathbf{S}^{T*}) and optimising the response.

II.2.1 Determination of the number of factors

There are many procedures for determining the number of factors that make up the system.^[49] Two of the most widely used are Principal Component Analysis (PCA) and Evolving Factor Analysis (EFA).

The factorial decomposition into principal components^[50] of a bilinear data matrix \mathbf{D} allows for the variability of the data in the matrix to be represented in a reduced number of factors. Each factor is a linear combination of the original variables. If a sample in the original space is represented by a vector x_j of j variables, then the expression of a principal component is as given in Eq. II.5.

Chapter II

$$PC_a = p_{1a} \cdot x_1 + p_{2a} \cdot x_2 + \dots + p_{ja} \cdot x_j \quad \text{Eq. II.5}$$

With this method, the matrix **D** is then decomposed, as shown in Eq. II.6, where **T** is the matrix of the sample values in the new principal component space, **P** is the matrix of the coefficients of the variables, and **E** is the residual matrix.

$$\mathbf{D} = \mathbf{T} \cdot \mathbf{P}^T + \mathbf{E} \quad \text{Eq. II.6}$$

The singular value decomposition (SVD)^[51] is one of the algorithms used to perform the factorial decomposition of the matrix **D** into the product of three matrices according to Eq. II.7. The values on the diagonal of the matrix **W** are called singular values, which are ordered from largest to smallest and correspond to the square root of the eigenvalues (λ). The product of the matrices **U** and **W** is equivalent to the score matrix **T** mentioned in the previous paragraph, while the matrix **V^T** is equivalent to the matrix **P^T**.

$$\mathbf{D} = \mathbf{U} \cdot \mathbf{W} \cdot \mathbf{V}^T + \mathbf{E} \quad \text{Eq. II.7}$$

The analysis of the singular values allows for determining the number of factors needed to represent the variability of the data. As illustrated in Figure II.3, factors with low singular values only represent information associated with experimental noise.

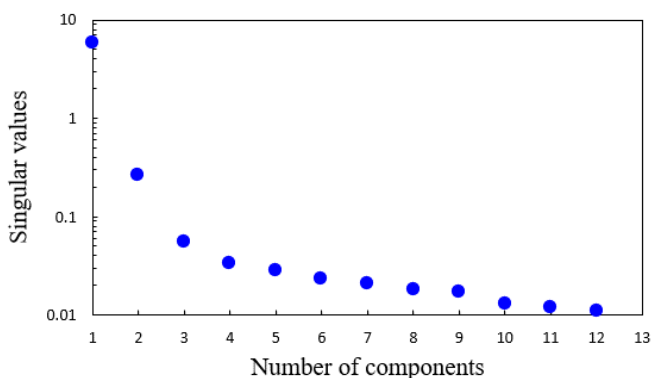


Figure II.3. Singular value decomposition of a data matrix.

II.2.2 Initial estimation. Evolving factor analysis

Creating the initial estimation is necessary as a starting point for determining \mathbf{C} or \mathbf{S}^T . The estimation can be obtained from techniques based on pure variable detection (SIMPLISMA)^[52] or evolving factor analysis (EFA),^[53] among others. EFA has been used in this doctoral thesis because it provides more descriptive information SIMPLISMA. Its fundamentals are briefly described below.

The objective of EFA is to determine the number of factors at each time a factor decomposition is performed in the data matrix \mathbf{D} . The process is started by applying the singular value decomposition (SVD) to a submatrix containing only the first two rows of the initial data matrix and continues as the number of rows in the matrix is consecutively increased. The computational process is performed in both matrix directions (Figure II.4 a). It is possible to detect the emergence or decay of the different factors by observing the evolution of the singular values versus the number of rows of the data matrix. Figure II.4 b shows the initial estimation of the concentration matrix, \mathbf{C}^* , if two factors are retained.

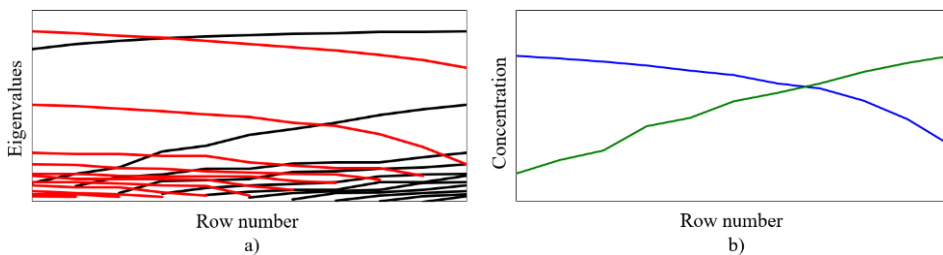


Figure II.4. EFA results of a data matrix. a) Eigenvalues. Black lines: forward; red lines: backwards. b) Initial estimation.

II.2.3 Solution optimisation by alternating least squares

The initial estimations \mathbf{C}^* or \mathbf{S}^{T*} are optimized solving Eq. II.4 iteratively using the Alternating Least Squares (ALS) method.^[54] On the one hand, if an initial estimation of the concentration profile is available, the least-squares solution is obtained according to Eq. II.8, where \mathbf{C}^+ is the pseudoinverse of the matrix \mathbf{C} , and \mathbf{D}^* is the

Chapter II

experimental data matrix reproduced by PCA for the considered number of factors. On the other hand, if an initial estimation of the spectral profile is available, then the least-squares solution for the concentration is obtained as shown in Eq. II.9 from the pseudoinverse matrix of \mathbf{S}^T and \mathbf{D}^* . These two steps are repeated until the difference in the residual of two consecutive iterations between the obtained solution and the experimental spectra is lower than set tolerance.

$$\mathbf{S}^T = \mathbf{C}^+ \cdot \mathbf{D}^* \quad \text{Eq. II.8}$$

$$\mathbf{C} = \mathbf{D}^* \cdot (\mathbf{S}^T)^+ \quad \text{Eq. II.9}$$

The results obtained by Alternative Least Squares (ALS) can be improved by using constraints on the \mathbf{C} and/or \mathbf{S}^T matrices that provide additional information based on physical and chemical knowledge of the studied system.^[55,56] Constraints are any chemical or mathematical property systematically satisfied in the whole system or in the parts of pure contributions.^[57,58]

The most frequently used restrictions are:

- 1) Non-negativity: the concentrations of the recovered chemical species and/or spectra must be equal to or greater than 0.
- 2) Unimodality: a maximum value is imposed on the profiles obtained. It is usually applied in concentration profiles but not in spectral profiles.
- 3) Closure: the sum of concentrations of all species in the system is constant.
- 4) Selectivity: it can be used when it is known that only one species exists in the system.

II.2.4 Quality parameters

Several parameters can be used to evaluate the goodness of the solutions obtained by MCR-ALS. One of them is the lack of fit (*LOF*) and is defined by Eq. II.10, where d_{ij} is the element of the experimental matrix \mathbf{D} and e_{ij} is the residual obtained as the difference between the experimental value of the matrix \mathbf{D} and the MCR-ALS solution. The *LOF* is calculated from the solution obtained by PCA (*LOF* PCA) and for the solution obtained with constraints (*LOF* exp).

The quality of the solution was also evaluated by the correlation coefficient r (Eq. II.11), where γ is the angle between the vectors of the spectrum recovered by the MCR-ALS (\hat{S}_i) and the spectrum of pure water ($|S_i|$).

$$LOF (\%) = 100 \cdot \frac{\sqrt{\sum_{ij} e_{ij}^2}}{\sqrt{\sum_{ij} d_{ij}^2}} \quad \text{Eq. II.10}$$

$$r = \cos \gamma = \frac{S_i^T \cdot \hat{S}_i}{\|S_i\| \cdot \|\hat{S}_i\|} \quad \text{Eq. II.11}$$

II.3. Thermophysical properties

II.3.1 Solid-liquid equilibria: solubility

The IUPAC Gold Book defines the solubility of a solute in a solvent^[59] as the analytical composition of a saturated solution (solution with the exact composition of a solute as one that is in equilibrium with undissolved solute at specific values or pressure and temperature), expressed in terms of the proportion of a designated solute in a designated solvent. It may be expressed as a concentration, molality, mole or mass fraction, etc.

The solid-liquid equilibrium is vital in absorption refrigeration and heat pumps when salts are used as absorbents because it indicates a limit in the use of soluble solutions. The salts precipitate at lower temperatures or higher compositions, and the machine cannot operate.

Different methods to determine the solubility of a solute in a solvent have been reported in the literature.^[60] In this work, a visual-polythermal-synthetic method has been used. This method consists of observing the phase change of a solution whose masses are known. The starting point is a supersaturated mixture to which the temperature is increased steadily over time while stirring until the solid phase is no longer observed. The phase change from solid to liquid is chosen due to the reproducibility of the experiments since there is a difference between the crystallisation temperature and the dissolution temperature that ranges from (0.8 to 3) K. This temperature difference arises from the complexity of the salt

crystallisation, which depends on more factors than salt dissolution, resulting in lower reproducibility.^[10]

From the point of view of the selected application, the working fluid should have a greater solubility than H₂O/LiBr to increase its operating range.

II.3.2 Vapour-liquid equilibria: vapour pressure

The vapour pressure is the equilibrium pressure of a vapour above its liquid (or solid). That is, the pressure of the vapour resulting from the evaporation of a liquid (or solid) above a sample of that liquid (or solid) in a closed container. The unit of this property in the international system is the Pascal (Pa).

Vapour-liquid equilibria of refrigerant-absorbent pairs are fundamental properties in absorption refrigeration and heat pumps because they are directly related to the absorption and desorption processes and define the operation range of the thermodynamic cycle.

A usual method to measure the vapour pressure of a fluid is the static method, where a specific quantity of a fluid (pure or mixture) is introduced in a closed equilibrium cell, whose temperature can be chosen by external means. The pressure registered directly by a pressure transducer is the vapour pressure of the fluid at that temperature. Repeating the measurement at different temperatures and compositions, the pressure-temperature-composition relation is obtained in the case of mixtures, and the vapour-liquid equilibrium can be represented.

On the one hand, it is thought that absorption refrigeration systems will benefit from operating with a working fluid with a lower vapour pressure than H₂O/LiBr since the pure water will come out colder from the generator. On the other hand, using a working pair with a higher vapour pressure than H₂O/LiBr would benefit absorption heat pumps because the pure water would leave the generator at a higher temperature.

II.3.3 Density and speed of sound

Density expresses the ratio of mass to volume of a substance. In the international system, its unit is the kilogram per cubic meter (kg·m⁻³).

Chapter II

Density is related to other thermophysical properties, such as pressure, temperature, and dynamic viscosity. On the one hand, as the pressure exerted on a material increases, it undergoes compression, increasing its density. On the other hand, density is inversely related to temperature since an increase in temperature implies a greater kinetic energy in the molecules, which translates into a greater volume occupied by a given amount of matter. The relationship with viscosity is generally directly proportional for substances in the liquid phase: an increase in density is usually associated with an increase in dynamic viscosity due to the smaller distance between molecules.

The device used to determine density and speed of sound is an Anton Paar DMS 5000, based on the vibrating tube and ultrasonic pulse method.^[61]

The operating principle of a vibrating tube densimeter is based on the variation of the natural oscillation period (τ) of an oscillator, of known mass (m) and internal volume (V_0), when filled with a liquid whose density ρ is to be measured, compared to the oscillation period when it is empty (Eq. II.12). In this equation, K is the oscillation constant.

$$\tau = 2 \cdot \pi \sqrt{\frac{m + \rho \cdot V_0}{K}} \quad \text{Eq. II.12}$$

Figure II.5 shows a schematic of the interior of a measuring cell. The mechanical oscillator is a tuning fork-shaped tube (U-shaped tube) into which the liquid whose density is to be determined is introduced. Once filled, the system is electronically excited to determine the resonance period under these conditions.

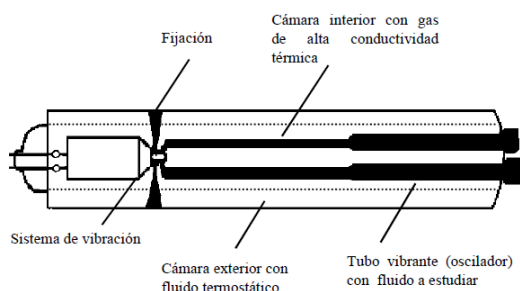


Figure II.5. Scheme of a U-shape vibrating tube to determine the density of fluids.

Chapter II

By rearranging Eq. II.12, the density can be determined as shown in Eq. II.13.

$$\rho = \frac{K \cdot \tau^2}{4 \cdot \pi^2 \cdot V_0} - \frac{m}{V_0} \quad \text{Eq. II.13}$$

The constant parameters of this equation can be grouped into only two constants:

$$\rho = A(\tau^2 - B) \quad \text{Eq. II.14}$$

It should be considered that both K and V_0 , which are specific equipment values, can vary with temperature and pressure, so they must be calculated for different operating conditions by using a previous calibration. This calibration, which allows the values of A and B to be calculated directly, is carried out with two fluids of known density, or with a fluid and vacuum ($\rho = 0$). In this way, the values of the constants A and B are obtained directly for the working conditions determined according to Eqs. II.15-II-16.

$$A = \frac{\rho_1 - \rho_2}{\tau_1^2 - \tau_2^2} \quad \text{Eq. II.15}$$

$$B = \frac{\tau_2^2 \cdot \rho_1 - \tau_1^2 \cdot \rho_2}{\tau_1^2 - \tau_2^2} \quad \text{Eq. II.16}$$

The measuring cell was calibrated from 10 °C to 80 °C with deionised water and vacuum and from 90 °C to 100 °C with toluene and vacuum.

Regarding the application, it is of interest that the density of the working fluid is as high as possible since the pump circulates a certain volume flow rate. If the density increases, the mass flow rate increases, increasing heat transfer.

Speed of sound is defined as the phase velocity of sound waves in a medium, i.e., the speed at which a sound wave propagates in that medium. Its SI unit is the meter per second ($\text{m} \cdot \text{s}^{-1}$). Mathematically, this property is defined as the square root of the partial derivative of pressure concerning density at constant entropy (Eq. II.17).

$$c = \sqrt{\left(\frac{\partial p}{\partial \rho}\right)_s} \quad \text{Eq. II.17}$$

The speed of sound is related to other thermophysical properties, such as density, viscosity, and temperature. On the one hand, for a given fluid, in general, the

Chapter II

relationship with density is inverse: the lower the density, the higher the speed of sound since the number of molecules through which the wave propagates decreases, making it easier to transmit. On the other hand, the more viscous the medium, the easier the transmission of sound. The higher the composition of the absorbent, the higher the viscosity, and therefore, the higher the speed of sound. Regarding temperature, the higher it is, the higher the kinetic energy of the molecules and, thus, the higher the speed of sound transmission.

A standard method for determining the speed of sound is the pulse method through a piezoelectric transducer flight,^[62] where the time it takes for the wave to travel a known distance is measured. The sample is introduced into the measuring cell, bordered by an ultrasonic transmitter on one side and a receiver on the other (Figure II.6).

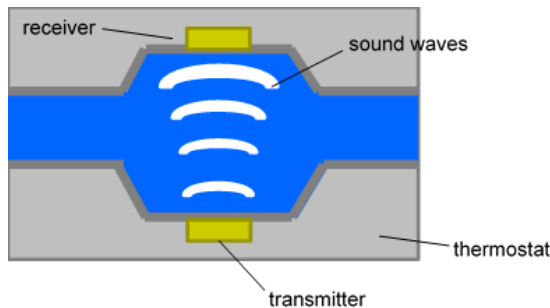


Figure II.6. Scheme of a pulse measure to determine the speed of sound of fluids.

The transmitter sends sound waves of a well-known period through the sample at a known distance. The speed of sound can be calculated by determining the period of received sound waves and the distance between the transmitter and the receiver (Eq. II.18). In this expression, p_l is the path length of the sound waves (5000 μm), ΔT the temperature deviation with respect to 20 $^\circ\text{C}$, P_s the oscillation period of the received sound waves, K' a constant of the device previously determined by calibration, and f_3 a correction term for temperature.

$$c = \frac{p_l \cdot (1 + 1.6 \cdot 10^{-5} \cdot \Delta T)}{\frac{P_s}{512} - K' \cdot f_3} \quad \text{Eq. II.18}$$

Although the speed of sound does not influence the application in a relevant way, it is helpful in qualitatively analysing the solute-solvent interactions in solutions using isentropic compressibility and calculations derived from it.

II.3.4 Enthalpy of dilution

The enthalpy of dilution is the amount of heat rejected or absorbed when a solution of known composition is diluted. Depending on the solute-solvent interactions, its value can be either negative (exothermic) or positive (endothermic). Its SI units are $\text{J} \cdot \text{kg}^{-1}$ or $\text{J} \cdot \text{mol}^{-1}$.

The enthalpy of dilution can be experimentally determined with a calorimeter using Eq. II.19, where ΔSignal is the signal difference between the signal obtained when diluting the solution and the baseline, \dot{n}_{abs} is the absorbent (solute) mole flow rate, and K is a calibration constant.

$$\Delta h_{dil} = \frac{\Delta \text{Signal}}{K \cdot \dot{n}_{abs}} \quad \text{Eq. II.19}$$

The enthalpy of dilution can also be calculated as the difference of relative apparent molar enthalpy between the final and initial composition of the solution (Eq. II.20).^[63]

$$\Delta h_{dil} = \Phi_L(x_{abs_{final}}) - \Phi_L(x_{abs_{initial}}) \quad \text{Eq. II.20}$$

In absorption refrigeration and heat pump systems, it is important that the working fluid has a low enthalpy of dilution since the lower the enthalpy of dilution, the lower the amount of heat required in the generator to run the cycle. In addition, if the amount of heat that the working fluid rejects in the absorber and gains in the generator decreases, the size of these components could be decreased, leading to greater compactness of the system.

II.3.5 Electrical conductivity

Electrical conductivity is the capacity of a solution to conduct electrical current. It is a measurement of the total concentration of ions. In the international system, the unit of measurement of this transport property is siemens per meter ($S \cdot m^{-1}$).

The electrical conductivity depends strongly on temperature because it has a dual effect on electrolytes: it affects how far they dissolve and ion mobility. The electrical conductivity increases with temperature.

In this work, an electrode method (CRISON), shown in Figure II.7, has been used to measure the electrical conductivity. An electrical field is applied to two electrodes, and the resistance of the solution is measured.

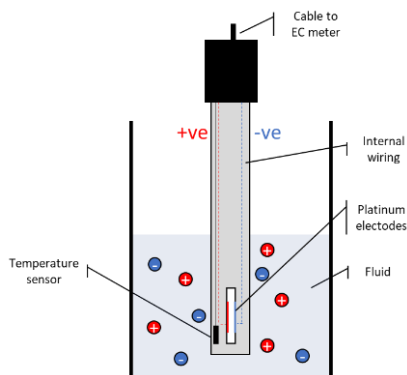


Figure II.7. Scheme of the electrode method for the electrical conductivity determination.

The temperature at which the electrical conductivity is determined is often compensated to give the value at a reference temperature (usually 20 °C or 25 °C).

The conductivity probe must be calibrated with one, two or three points using standard solutions.

Although electrical conductivity is not directly used in the thermodynamic cycle calculations in the selected application, it adds information regarding relevant transport properties that influence the performance of real absorption systems, such as diffusion coefficients and dynamic viscosity.^[64,65]

II.3.6 Thermal conductivity

Thermal conductivity is the rate at which heat passes through a material or fluid, expressed as the amount of heat that flows per unit time through a unit area with a temperature gradient of one degree per unit distance. Thermal conductivity depends on the free electrons in metallic substances and on the vibration of molecular bonds in non-metallic substances.^[66] Its SI unit is the watt per meter and Kelvin ($\text{W}\cdot\text{m}^{-1}\cdot\text{K}^{-1}$).

The instrument used in this work to measure thermal conductivity (Thermal Analyzer Decagon KD2-Pro) is based on the transient hot wire method. The probe consists of a needle with a heater and temperature sensor inside. A current is passed through the heater and the temperature of the probe is monitored over time. An analysis of the probe temperature is used to determine thermal conductivity. The probe is relatively large and robust, making it easy to use. Heating times are kept as short as possible to minimise thermally induced water movement and time required for a measurement. Heat input is also minimised to minimise water movement and free convection. The use of relatively short heating times and low heating rates requires high-resolution temperature measurements and special algorithms to measure thermal properties. Special algorithms are used to analyse measurements made during heating and cooling intervals and to separate the effects of the heat pulse from ambient temperature changes. The temperature during heating and cooling is computed from Eq. II.21, where m_1 is the ambient temperature during heating, m_2 is the rate of background temperature drift, m_3 is the slope of a line relating temperature rise to logarithm of temperature, and t_h is the heating time.

$$T = m_1 + m_2 \cdot t_h + m_3 \cdot \ln t_h \quad \text{Eq. II.21}$$

During cooling (after heating), the temperature model is:

$$T = m_1 + m_2 \cdot t + m_3 \cdot \ln \left[\frac{t}{(t - t_h)} \right] \quad \text{Eq. II.22}$$

In this equation, t is the time. Eqs. II.21-II.22 are solved for m_1 , m_2 and m_3 by linear least squares from experimental temperature and time data. The value of m_3 is then related to the thermal conductivity of the sample according to Eq. II.23.

$$\lambda = \frac{q}{4 \cdot \pi \cdot m_3} \quad \text{Eq. II.23}$$

Figure II.8 shows a scheme of the hot wire method and the calculation of thermal conductivity from the slope of the temperature vs logarithm of time in the linear region during the heating interval.

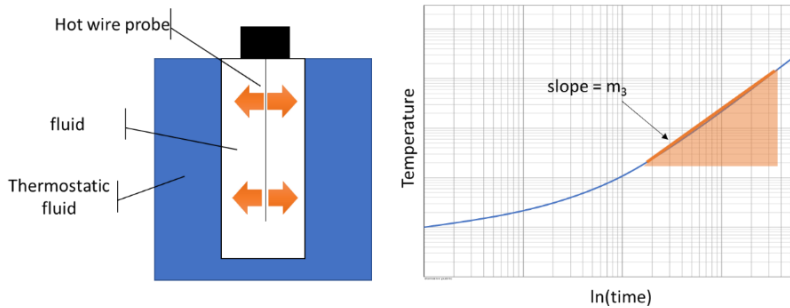


Figure II.8. Scheme of a hot wire method to determine the thermal conductivity of a fluid from the slope of the linear function of temperature vs logarithm of time.

From the point of view of absorption refrigeration and heat pump systems, it is desirable to use working fluids with high thermal conductivity to maximise the heat transfer, which could lead to more compact heat exchangers.

II.3.7 Dynamic viscosity

Viscosity is a transport property that measures the resistance of a fluid to flow and depends on intermolecular forces in the medium.^[67] Its SI unit is the Pascal per second (Pa·s). It is related to electrical conductivity, as it influences the mobility of ions, and is inversely proportional to the diffusion coefficient.^[65]

The Cambridge Applied Systems piston-style viscometer has two magnetic coils within a stainless-steel sensor and a magnetic piston surrounded by the fluid sample deflected into the measurement chamber, as shown in Figure II.9. Two coils inside the sensor body are used to magnetically force the piston back and forth a predetermined distance (about 5 mm). By alternatively powering the coils with a constant force, the piston round trip travel time is measured. An increase in viscosity is perceived as a slowdown in piston travel time. The time required for the piston to

Chapter II

complete a two-way cycle is an accurate measure of viscosity. The deflecting fence continuously deflects fresh samples into the measurement chamber.

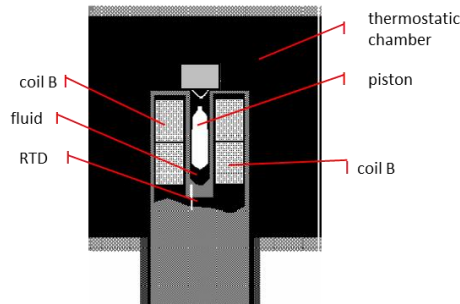


Figure II.9. Cutaway view of the viscometer measuring chamber.

Since measurement of the piston motion is in two directions, variations due to gravity or flow forces are annulled. In addition, since the piston has very little mass, magnetic forces greatly exceed any disturbance due to vibration.

There are different sensors for different viscosity ranges. In this work, a (1-20) cP sensor range was used.

As mentioned in Section I.3.1, the working fluids considered for this application are required to have low viscosity to avoid impairing the mass and heat transfer processes. Furthermore, if the working fluid is highly viscous, both the electrical power required to pump it and the pressure drop through pipes and components will be high, which is not desirable from operational and design points of view.

II.4. Derived volumetric properties

II.4.1 Apparent molar volume

The analysis of the volumetric properties of a solution can be performed through its partial molar properties, keeping temperature and pressure constant.^[68] This analysis provides information about the change in volume resulting from the addition of the solute, as well as on solute-solvent, solvent-solvent, and solute-solute interactions.

Chapter II

Thus, the partial molar volume of a component i in solution is defined as:

$$\bar{V}_i = \left(\frac{\partial V}{\partial n_i} \right)_{T,p,n_{j \neq i}} \quad \text{Eq. II.24}$$

In the case of an aqueous solution consisting of a solvent (1) and a solute (2), the volume of this solution will be the sum of the molar volumes of the components:

$$V = n_1 \cdot \bar{V}_1 + n_2 \cdot \bar{V}_2 \quad \text{Eq. II.25}$$

A different way of expressing the volume of the solution is from the molar volume of the solvent (V_1^0) and the apparent molar volume of the solute (V_ϕ). In this case, the contribution to the molar volume of the solution by the solvent is considered to correspond to the molar volume of the pure solvent itself at the same pressure and temperature, while all the contributions to the non-ideality are associated with the solute through its apparent molar volume:

$$V = n_1 \cdot V_1^0 + n_2 \cdot V_\phi \quad \text{Eq. II.26}$$

Rearranging this equation:

$$V_\phi = \frac{V - n_1 \cdot V_1^0}{n_2} \quad \text{Eq. II.27}$$

Moreover, this equation can be expressed in terms of the densities of the solution (ρ) and the pure solvent (ρ_0), in $\text{kg} \cdot \text{m}^{-3}$, the molar mass of the solute (M_2), in $\text{kg} \cdot \text{mol}^{-1}$, and the molality (b), in $\text{mol} \cdot \text{kg}^{-1}$:

$$V_\phi = \frac{M_2}{\rho} - \frac{\rho - \rho_0}{b \cdot \rho \cdot \rho_0} \quad \text{Eq. II.28}$$

The dependence of the apparent molar volume on the solute composition can be expressed by the Redlich-Rosenfeld-Meyer equation:^[69]

$$V_\phi = V_\phi^0 + S_V \cdot \sqrt{b} + B_V \cdot b \quad \text{Eq. II.29}$$

In this equation, S_V is the slope, and B_V is the empirical deviation constant for each solute.^[70] On the one hand, the limiting value of S_V for each solute can be determined both theoretically^[69] and empirically.^[43,44] On the other hand, although Eq. II.29 is

Chapter II

applicable to very dilute solutions,^[70] it has also been used in solutions with high solute composition.^[71]

V_{φ}^0 , which is the apparent molar volume at infinite dilution, when the solute composition tends to zero, is also known as the partial molar volume at infinite dilution (V_{φ}^{∞}), and coincides with the partial molar volume of the solute (\bar{V}_2^0):

$$\lim_{b \rightarrow 0} V_{\varphi} = V_{\varphi}^{\infty} = \bar{V}_2^0 \quad \text{Eq. II.30}$$

In this limiting condition, the solute molecules are sufficiently separated from each other to assume that there are no solute-solute interactions, so this parameter makes it possible to analyze solute-solvent interactions. The value of V_{φ}^0 depends on three different contributions (Eq. II.31)^[72] related to the volume change in the solute molecules (V_{int}^0), the decrease in the volume of the solution due to electrostatic interactions between solute and solvent (V_{elec}^0), and the volume change in the solvent surrounding the solute (V_{str}^0).

$$V_{\varphi}^0 = V_{int}^0 + V_{elec}^0 + V_{str}^0 \quad \text{Eq. II.31}$$

Hepler^[73] proposed a criterion for analysing the influence of the solute on the solvent structure based on the dependence of the apparent molar volume on temperature:

$$\left(\frac{\partial \bar{C}_p}{\partial p} \right)_T = -T \cdot \left(\frac{\partial^2 \bar{V}_2^0}{\partial T^2} \right)_p \quad \text{Eq. II.32}$$

Positive values of $\left(\frac{\partial^2 \bar{V}_2^0}{\partial T^2} \right)_p$ are associated with structure making solutes, while negative values are associated with structure breaking solutes.

II.4.2 Isentropic compressibility

Isoentropic compressibility indicates the facility to compress or expand a substance as a function of pressure at constant entropy. Its unit in the international system is the inverse of the Pascal (Pa^{-1}).

This property is mathematically defined according to Eq. II.33, where v is the specific volume of the solution, p the pressure, and s the entropy. The smaller its

Chapter II

value, the greater the stiffness of the fluid, and the more difficult it is to compress it. This property provides information about the compression responses of molecules and ions in solution, which are related to intermolecular interactions.

$$\kappa_S = -\frac{1}{v} \cdot \left(\frac{\partial v}{\partial p} \right)_s \quad \text{Eq. II.33}$$

The isentropic compressibility is determined with experimental values of density (ρ) and speed of sound (c) using the Newton-Laplace equation:^[74]

$$\kappa_S = \frac{1}{\rho \cdot c^2} \quad \text{Eq. II.34}$$

The isentropic compressibility values of aqueous electrolyte solutions converge to a certain solute composition,^[75] which can be related to the interactions in the solution.

The apparent molar isentropic compressibility (κ_φ) is defined similarly to the apparent molar volume (Eq. II.35), where κ_S and κ_{S_0} are the isentropic compressibility of the solution and the pure solvent, respectively.

$$\kappa_\varphi = \frac{\kappa_S \cdot M_2}{\rho} - \frac{\kappa_{S_0} \cdot \rho - \kappa_S \cdot \rho_0}{b \cdot \rho \cdot \rho_0} \quad \text{Eq. II.35}$$

The limiting apparent molar isentropic compressibility (κ_φ^0), i.e., the apparent molar isentropic compressibility in an environment in which there are no solute-solute interactions (infinite dilution), can be obtained by fitting the values of the apparent molar isentropic compressibility to a Redlich-Rosenfeld-Meyer type equation:

$$\kappa_\varphi = \kappa_\varphi^0 + S_\kappa \cdot \sqrt{b} \quad \text{Eq. II.36}$$

In this expression, S_κ is a fitting coefficient analogous to the apparent molar volume at infinite dilution. The analysis of κ_φ^0 allows qualitative interpretation of the interactions in solution.^[76]

Chapter III. Ion hydration and association in H₂O/(LiBr+IL) mixtures

III.1. Introduction

Analysing the relationship between the thermophysical properties of aqueous electrolyte solutions and their composition is relevant in those applications where the processes of interest take place in that chemical environment. In the context of absorption refrigeration and heat pump systems, understanding the relationship between the composition of H₂O/(LiBr+IL) mixtures and properties such as solubility and vapour pressure is important for three reasons: to explain the influence of ionic liquids on the properties of the working fluid, to select the most suitable ionic liquid, and to estimate the most appropriate composition of ionic liquid in the working fluid.

Many different approaches have been proposed from the beginning of the theory of electrolytes to understand the relationship between the anhydrous composition of electrolytes in solutions and their properties. The phenomena that are always mentioned in the literature to explain the processes in which solutes are involved are the solvation/hydration of ions in solution^[77] and ion pairing.^[78]

Modelling the hydration of ions in solution has been a topic of interest since the early days of electrolyte theory.^[79,80] Although the first electrostatic approaches^[81–84] admit that ions in solution are solvated, they ignore the impact of hydration on the solvent composition, which makes it difficult to explain the behaviour of those solution properties that depend on the composition, e.g., vapour pressure.

On the one hand, researchers have recently focused more attention on hydration models, where a distinction is made between bulk water and solvated (solute-bound) water so that the total solvent composition in the solution varies.^[85–90]

On the other hand, evaluating the extent to which the ion pairing phenomenon occurs in solutions is an unresolved challenge due to the complexity of the ion pairing phenomenon.^[78,91–93] However, experimental measurements indicate that some degree of pairing exists in all electrolytes in the solution. The formation of ion pairs in electrolyte mixtures has been studied, among other methods, on the basis of dissociation constants.^[78,91,94,95]

The Molecular Dynamics (MD) simulation methods have been of great value in analyzing and interpreting the solvation and formation of ion pairs in the solutions.

Chapter III

From this brief literature review it is evident that the hydration of ions and the formation of ion pairs condition the effective composition of the solute in solution. Therefore, the evaluation of both phenomena is necessary if one wants to relate the anhydrous composition of the solutes to the thermophysical properties of the working fluids.

Ion solvation can be studied either experimentally with diffusion coefficients,^[96] electrical conductivity and Raman spectroscopy,^[97] neutron diffraction,^[98,99] and ¹H NMR,^[100] or computationally with MD simulations.^[101,102] Although these methods provide valuable information regarding the behaviour of ions in solution, many of them are not available in all laboratories due to their inherent complexity.

It is worth mentioning that the interest of this PhD thesis in the study of solvation is not focused on modelling the relation between the anhydrous composition of the solutes and the thermophysical properties of H₂O/(LiBr+IL) mixtures, but on quantitatively analysing the extent to which solute hydration occurs, since it may constitute a measure of the absorption capacity of the working fluid, as was indicated above. This does not require knowledge of the molecular structure of the solvates formed or the extent of solute aggregation, but it does require knowledge of the amount of water that does not participate in solute solvation.

With the aim of studying the behaviour of aqueous electrolyte solutions, the CREVER research group started using a methodology based on the intense absorption band of water in the near-infrared region between 850 nm and 1100 nm^[103] and the potential of the curve resolution method based on alternating least squares (MCR-ALS) for the analysis of mixtures.^[104,105]

The studies carried out using this methodology^[106–109] have shown its utility for the quantitative determination of the amount of bulk water in binary aqueous mixtures with strong electrolytes and ionic liquids.

This methodology is used in this doctoral thesis to compare the solvation in H₂O/LiBr and H₂O/(LiBr+IL) mixtures.

As a summary, Table III.1 shows the temperature and composition ranges of the mixtures in which solvation has been studied using this methodology. The mole fraction ratio between ionic liquid and lithium bromide (x_{IL}/x_{LiBr}) was set to 0.0205 in

Chapter III

all H₂O/(LiBr+IL) mixtures, which is approximately equal to 1 mole of IL per 49 moles of LiBr. In the case of solutions with [Dmim][Cl], two additional x_{IL}/x_{LiBr} compositions were selected: 0.0418 and 0.0648, which correspond to approximate mole ratios of 1 [Dmim][Cl]:24 LiBr and 1 [Dmim][Cl]:15 LiBr, respectively.

Table III.1. Conditions at which the mixtures were analysed by NIR+MCR-ALS. T : temperature. w_{solute} : mass fraction of solute; x_{solute} : mole fraction of solute. x_{IL}/x_{LiBr} : mole fraction ratio between IL and LiBr

Mixture	T (K)	w_{solute}	x_{solute}	x_{IL}/x_{LiBr}
H ₂ O/LiBr	293.15	0 – 0.55	0 – 0.20	–
H ₂ O/[Dmim][Cl]	293.15	0 – 0.55	0 – 0.14	–
	293.15	0.40 – 0.90	0.12 – 0.60	0.0941 – 1.03
H ₂ O/(LiBr+[Dmim][Cl])	293.15	0 – 0.58	0 – 0.22	0.0202 0.0418 0.0648
	293.15			
H ₂ O/(LiBr+[Bmim][Br])	313.15 333.15	0 – 0.58	0 – 0.22	0.0208
	293.15			
H ₂ O/(LiBr+[EA][NO ₃])	313.15 333.15	0 – 0.58	0 – 0.22	0.0205
	293.15			
H ₂ O/(LiBr+[PA][NO ₃])	313.15 333.15	0 – 0.58	0 – 0.22	0.0205
	293.15			
H ₂ O/(LiBr+[EA][Cl])	313.15 333.15	0 – 0.58	0 – 0.22	0.0205

The fundamentals of the used methodology and the calculation procedure are summarized in this chapter along with the discussion of the results obtained for H₂O/LiBr at 20 °C. The discussion of the results obtained for H₂O/(LiBr+IL) mixtures focuses on the novel aspects with respect to what is discussed for the mixture without additive.

III.2. Determination of the amount of bulk water in the H₂O/LiBr mixture

The main objective of this section is to analyse the amount of water remaining as bulk water in aqueous solutions of lithium bromide. This analysis has been carried out at 20 °C, covering a wide LiBr composition range.

The amount of water involved in the solvation of the ions is calculated as the difference between the total amount of water and the amount of bulk water.

The obtained results were used to relate the amount of bulk water to the solid-liquid equilibrium composition of H₂O/LiBr and to estimate the vapour pressure of the analysed solutions using values of the coordination number of Li⁺ and Br⁻ ions in aqueous solution reported in the literature. These values were compared with those determined by experimental methods to support the validity of the methodology used to analyse the behaviour of the solutions under study.

III.2.1 Experimental part

Analysed samples

A set of solutions prepared by dilution of a H₂O/LiBr mother solution was analysed. Lithium bromide (CAS No: 7550-35-8) was purchased from Sigma-Aldrich with a mass purity greater than 99 %. Information regarding ionic liquids is presented in Table I.4. The mother solution was prepared by weighing with a solute mass fraction of 0.58. The masses and mole fractions of the prepared H₂O/LiBr solutions are shown in Table III.2.

Table III.2. Mass (m) and mole fraction (x) of H₂O/LiBr solutions.

m_{H_2O} (g)	m_{LiBr} (g)	x_{LiBr}
5.3194	0	0
5.1682	0.2722	0.0108
3.9101	0.4322	0.0224
4.3068	0.7585	0.0352
4.2382	1.0578	0.0492
$U(m) = \pm 0.0001$ g		

Table III.2 (continued)

m_{H_2O} (g)	m_{LiBr} (g)	x_{LiBr}
3.9855	1.3278	0.0646
3.9353	1.6876	0.0817
5.2366	2.8387	0.1011
6.8127	4.5407	0.1215
5.9973	4.9212	0.1455
6.4967	6.4979	0.1718
5.9397	7.2762	0.2026
$U(m) = \pm 0.0001$ g		

Spectra acquisition

The short-wave near-infrared (SW-NIR) spectra of the solutions shown in Table III.2 were acquired with a UV-Visible 8453 Agilent spectrophotometer using the absorbance mode. In this spectral region, where the molar absorptivity of the functional groups is very weak, it is possible to measure the spectrum of pure water accurately. The 100 % of the transmittance was established with a 1 cm path length quartz cell filled with air before the sample analysis. The cell was flushed with pure water and acetone three times after acquiring the spectrum of each sample. The spectra were acquired at 20 °C from (900 to 1060) nm. The characteristic absorption band of water -OH groups can be observed in this spectral region at around 970 nm.

Data treatment

The data were processed with the Matlab programming language (The MathWorks Inc. (2022). Matlab version 9.10 (R2021a), Natick, Massachusetts). The spectra of the solutions were exported from the software of the instrument (UV-Visible Chemstation, version B.05.02) and sequentially arranged in a single matrix ($\mathbf{D}_{H_2O/LiBr}$) of dimensions (12 x 380) containing the 380 absorbance values measured between (900 and 1060) nm for each of the 12 samples.

The spectra were pretreated before performing the analysis by means of the weighted least-squares baseline function of PLs-Toolbox v7 (the Eigenvector

Chapter III

Research, Manson, Washington) to correct the baseline shift, which is characteristic of the selected measurement mode.

Then, the MCR-ALS algorithm was run using the toolbox developed by Jaumot *et al.*^[110] to decompose the matrix $\mathbf{D}_{\text{H}_2\text{O}/\text{LiBr}}$ (12 x 380) according to Eq. II.4. Following what was explained in Section II.2, the matrix \mathbf{C}_i , of dimensions (12 x f), contains the concentration profiles, and the matrix \mathbf{S}_i , of dimensions (f x 380), contains the spectral profiles. The matrix \mathbf{E}_i , of dimensions (12 x 380), contains information that the model cannot explain.

The number of factors (f) required to retain the spectral variability, which is representative of the different chemical species in the aqueous solutions, was determined by analysing the explained variance of the singular values^[51] obtained in the factorial decomposition of the spectral data matrix $\mathbf{D}_{\text{H}_2\text{O}/\text{LiBr}}$.

An initial estimation of the concentration matrix \mathbf{C} (12 x f) was obtained from evolving factor analysis (EFA).^[53] Then, the mathematical solutions were optimised by using MCR-ALS^[110] with the following constraints: non-negativity in spectrum and concentration profiles, unimodality in the concentration profile and vertical normalisation of the spectra. The convergence criteria of the unimodality constraint and the ALS were set to 0.01.

The goodness of the solution obtained by MCR-ALS was evaluated using the quality parameters described in Section II.2.4.

III.2.2 Results and Discussion

Figure III.1 a shows the experimental spectra acquired from the prepared $\text{H}_2\text{O}/\text{LiBr}$ solutions. The baseline shift, characteristic of single beam spectrophotometers, can be visualized. The pretreated spectra, without baseline shift, are shown in Figure III.1 b and are stored in the $\mathbf{D}_{\text{H}_2\text{O}/\text{LiBr}}$ matrix for the subsequent calculations.

As one would expect, the analysis of the spectra obtained shows that the maximum of the absorption band characteristic of the -OH functional group, observed at 971 nm, decreases as the water composition of the samples decreases.^[106] Nevertheless, the existence of a solvatochromic shift of the band maximum can also

Chapter III

be observed. This shift can be attributed to the formation of different structures as a consequence of the interactions between salt ions and water molecules depending on the composition of the solution.^[106,111]

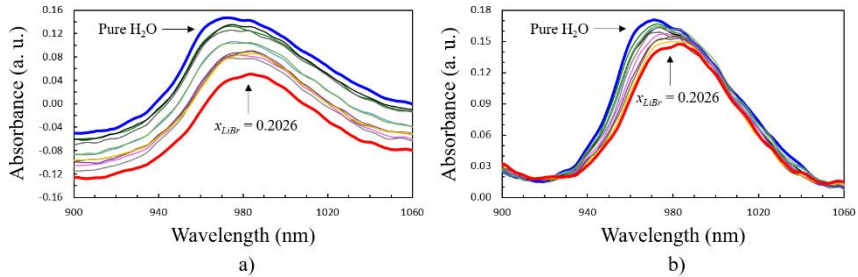


Figure III.1. Spectra of H₂O/LiBr solutions at 293.15 K. a) Experimental. b) Pretreated. Blue line: pure water; red line: most concentrated solution in LiBr.

Table III.3 shows the eigenvalues obtained in the decomposition of the data matrix $D_{H_2O/LiBr}$ by SVD with their corresponding percentages of explained variance. The first two factors account for almost all the variability of the data (99.98 %).

Table III.3. Singular value decomposition of H₂O/LiBr spectra at 293.15 K.

Factor	Singular value	Variance (%)	Cumulative variance (%)
1	5.891	99.783	99.783
2	0.262	0.197	99.980
3	0.055	0.009	99.989
4	0.033	0.003	99.992
5	0.028	0.002	99.994
6	0.023	0.002	99.996
7	0.021	0.001	99.997
8	0.018	0.001	99.998
9	0.017	0.001	99.999
10	0.013	< 0.001	99.999
11	0.012	< 0.001	100
12	0.010	< 0.001	100

Chapter III

The results obtained from the application of evolving factor analysis (EFA),^[53] shown in Figure III.2 a), confirm that there are only two significant factors over the entire composition range. For this reason, two factors were selected to perform the decomposition of the $D_{H_2O/LiBr}$ matrix by MCR-ALS. Figure III.2 b) shows the resulting initial estimation of the concentration profiles considering two factors.

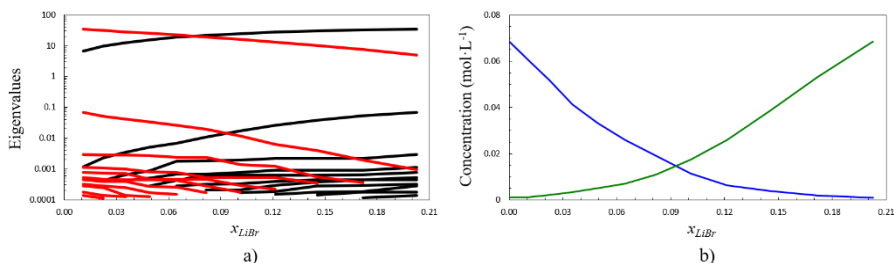


Figure III.2. EFA results of H₂O/LiBr solutions at 293.15 K. a) Factor evolution obtained from EFA. Black lines: forward; red lines: backward. b) Initial estimate of the concentration profiles.

The concentration (C) and spectral (S^T) profiles obtained for the analysed H₂O/LiBr solutions at 20 °C are plotted in Figure III.3. It is observed that one of the spectral profiles recovered has the maximum absorbance value at 971 nm, as was observed in Figure III.1 b) for pure water. Furthermore, the correlation coefficient between pure water spectrum, obtained experimentally, and the spectrum recovered by MCR-ALS is 0.9999. Therefore, this recovered spectrum can be considered representative of pure water. The other recovered spectrum shows the absorbance peak at a higher wavelength, which can be attributed to the water associated with the ions in the solvate.

Regarding the concentration profile, it is observed that as the LiBr composition in the samples increases, less amount of water remains as pure water because it is associated with ions in a new species.

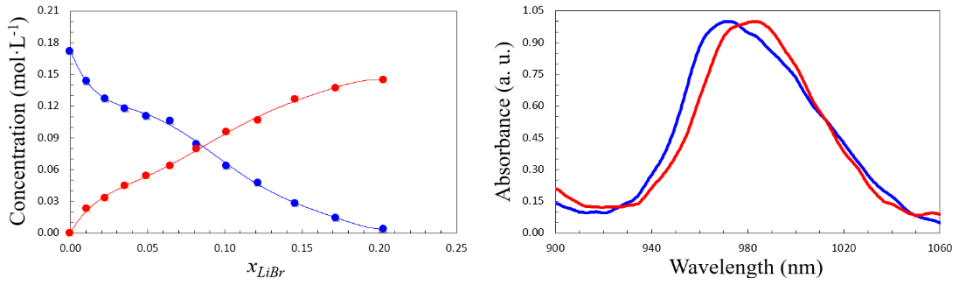


Figure III.3. Concentration and spectral profiles recovered by MCR-ALS for H₂O/LiBr at 293.15 K. Blue data series: bulk water; red data series: water in the solvate.

The *LOF* PCA and *LOF* exp are 0.00 % and 1.40 %, respectively, for the solution shown in Figure III.3. Thus, the obtained solution is satisfactory.

The values of the concentration profile of pure water have been used to calculate the amount of water that participates in the hydration of the solute and the amount of water that preserves its structural properties, referred to as bulk water (*BW*)^[95,112,113] from now on. Assuming that the acquired data satisfy the Beer-Lambert law, each species has a spectral profile representative of its molar absorptivity spectrum and a concentration profile proportional to its molar concentration. Therefore, the water percentage that keeps the same molecular structure as pure water can be calculated for each solution as given in Eq. III.1, where x_{H_2O} represents the mole fraction of total water and $x_{H_2O,r}$ represents the recovered mole fraction of water.

$$BW (\%) = 100 \cdot \frac{x_{H_2O,r}}{x_{H_2O}} \quad \text{Eq. III.1}$$

The mole fraction of bulk water ($x_{H_2O,BW}$) is calculated as follows: first, the concentration of bulk water in each solution, obtained from the concentration profile, is divided by the concentration in the first solution, which is pure water. Second, the obtained coefficient is multiplied by the prepared mole fraction of water. The difference between the prepared mole fraction of water and the mole fraction of bulk water indicates the mole fraction of water in the solvate ($x_{H_2O,S}$).^[109] The calculated mole fractions of bulk water and water in the solvate for the H₂O/LiBr at 20 °C given in Table III.4.

Chapter III

Table III.4. MCR-ALS results for the H₂O/LiBr mixture at 293.15 K. *x*: mole fraction. *BW*: bulk water. *r_n*: mole ratio.

Prepared		Recovered from MCR-ALS			Calculated
<i>x</i> _{H₂O}	<i>x</i> _{LiBr}	<i>BW</i> (%)	<i>x</i> _{H₂O,<i>BW</i>}	<i>x</i> _{H₂O,<i>S</i>}	<i>r_n</i> (mole ratio)
1	0	100	1	0	-
0.9892	0.0108	83.6	0.8265	0.1627	15.1
0.9776	0.0224	74.0	0.7237	0.2539	11.3
0.9648	0.0352	68.6	0.6615	0.3033	8.60
0.9508	0.0492	64.2	0.6106	0.3402	6.91
0.9354	0.0646	61.8	0.5781	0.3573	5.53
0.9183	0.0817	49.0	0.4504	0.4679	5.73
0.8989	0.1011	37.2	0.3340	0.5649	5.59
0.8785	0.1215	27.6	0.2425	0.6360	5.24
0.8545	0.1455	16.3	0.1394	0.7151	4.92
0.8282	0.1718	8.4	0.0697	0.7585	4.41
0.7974	0.2026	2.1	0.0171	0.7803	3.85

The bulk water of the analysed solutions is plotted in Figure III.4, where it is observed that the percentage of bulk water decreases as the mole fraction of LiBr increases. The mole ratio (*r_n*) shown in Table III.4, calculated as the ratio between the moles of water in the solvate and the moles of LiBr (Eq. III.2), decreases with increasing lithium bromide composition. As discussed below, this fact suggests a change in the hydration structure of the ions in solution. The mole ratio will prove useful later in interpreting the vapour pressure behaviour.

$$r_n = \frac{n_{H_2O,S}}{n_{LiBr}} \quad \text{Eq. III.2}$$

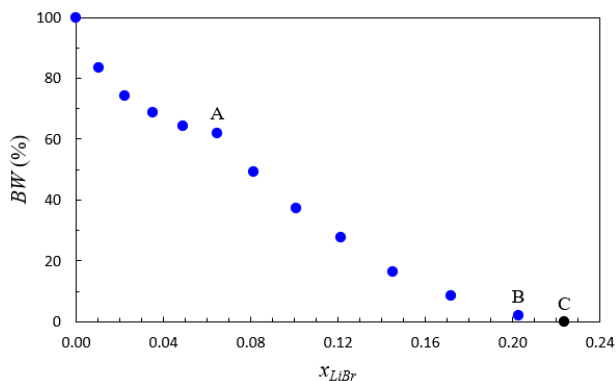


Figure III.4. BW (%) of H₂O/LiBr solutions against LiBr mole fraction at 293.15 K.

According to the cited literature,^[114–116] it is necessary to consider the phenomena of hydration of ions and ion pairing, illustrated in Figure III.5, to relate the properties of the solution to the anhydrous composition of the solute. The interpretation of the results obtained in this thesis is based on these two phenomena.

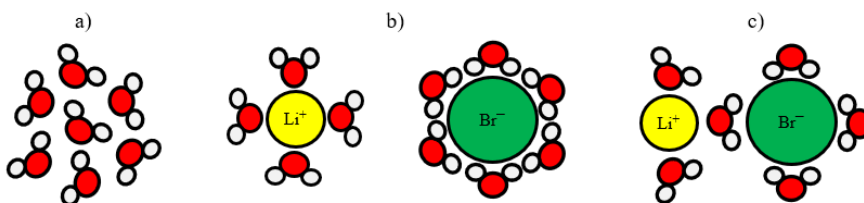
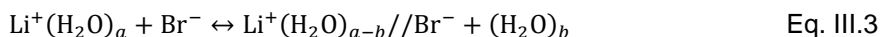


Figure III.5. Chemical species. a) Bulk water. b) Hydrated ions. c) Ion pair.

On the one hand, it is observed that when the anhydrous mole fraction of LiBr is lower than 0.0646 (point A in Figure III.4), the mole ratio of the analysed solutions is much higher than the coordination number usually referenced in the literature for both Li⁺(3.29-6)^[112,116–121] and Br⁻ (4.83-8).^[116–121] This result suggests that hydration predominates over ion pairing at low LiBr mole fractions. On the other hand, at LiBr mole fractions higher than 0.0646, the values of r_n keep decreasing, but more gradually. One possible explanation for this behaviour is that ion pairing predominates over ion hydration from this composition.

Understanding the behaviour of a solute in a solvent is crucial to correctly estimating the properties of mixtures and justifying their variations when the composition is varied. Recently, Zavitsas,^[88,89] Wilson,^[91,95] and Reynolds,^[90] and earlier Heyrovská^[85,86] argued that the properties of electrolyte mixtures are not directly correlated with their anhydrous composition in mixtures, regardless of the unit used for their expression. According to these authors, a good representation of the ion-pair formation equilibria of LiBr in solution would be given by Eq. III.3,^[89] where hydrated ions are in equilibrium with ion pairs, and bulk water appears as a separate product of ion pairing and hydrated ions.



With this approach, water molecules are bound around the ions in different ways, and there is an equilibrium between water-water and solute-water groups, regardless of the structure of the chemical species. This point of view, which influences the calculation of the composition of all chemical species in the solution, will be used in the next section to relate the results obtained by MCR-ALS to experimental data of the SLE and VLE of H₂O/LiBr at 20 °C.

III.2.3 Influence of the hydration on the solid-liquid equilibria and vapour-liquid equilibria of H₂O/LiBr

The eutectic point of aqueous LiBr solutions where crystals are observed should correspond to a solution in which the amount of bulk water is zero. Therefore, the mole fraction of LiBr could be estimated by extrapolation of the values in Figure III.4 from point B ($x_{\text{LiBr}} = 0.2026$), where the bulk water represents 2.7 % of the total amount water in the solution. A quadratic fit in this region of the curve provides an estimation of $x_{\text{LiBr}} = 0.2240$ for $BW = 0$ (point C), which is very similar to the reported mole fraction of LiBr at the solid-liquid equilibrium at 18.99 °C ($x_{\text{LiBr}} = 0.2274$).^[122]

Vapour pressure is another property directly related to the bulk water in the solution. According to Raoult's law (Eq. III.4), the vapour pressure of a mixture is proportional to the mole fraction of solvent in the solution at a given temperature.

Chapter III

$$p_{\text{H}_2\text{O}/\text{LiBr}} = p_{\text{H}_2\text{O}} \cdot x_a \quad \text{Eq. III.4}$$

This law is satisfied by ideal solutions, while for real solutions it is necessary to replace the solvent mole fraction with the *effective* mole fraction, which, as mentioned above, will depend on ionic species in the medium as well as on their respective compositions.

The experimental approach used in this thesis relies on estimating the effective mole fraction of water ($x_{a,eff}$) that participates in the vapour-liquid equilibria by applying a mass balance. The effective mole fraction of water is calculated from the results obtained by MCR-ALS along with the prepared amount of solute. It is worth noting that this approach constitutes a novelty with respect to what is usually referenced in the literature.

In aqueous LiBr solutions there are hydrated species, represented as $\text{Li}^+(\text{H}_2\text{O})_a$ and $\text{Br}^-(\text{H}_2\text{O})_b$ (Eqs. III.5-III.6), and ion pairs, represented as $\text{Li}^+(\text{H}_2\text{O})_c//\text{Br}^-$ (Eq. III.7). In these equations, a and b are the coordination numbers of Li^+ and Br^- , respectively, and c is the number of moles of water per mole of ion pairs. The total number of moles of hydrated chemical species in solution (n_{hs}) can be calculated as the sum of the moles of the considered chemical species (Eq. III.8).

$$S_1 = \text{Li}^+(\text{H}_2\text{O})_a \quad \text{Eq. III.5}$$

$$S_2 = \text{Br}^-(\text{H}_2\text{O})_b \quad \text{Eq. III.6}$$

$$S_3 = \text{Li}^+(\text{H}_2\text{O})_c//\text{Br}^- \quad \text{Eq. III.7}$$

$$n_{hs} = S_1 + S_2 + S_3 \quad \text{Eq. III.8}$$

The number of water moles participating in the different species ($n_{\text{H}_2\text{O},S}$) can be estimated from the mole fraction of water in the solvate ($x_{\text{H}_2\text{O},S}$ in Table III.4), and it can be related to the moles of ions of each species by means of their respective coordination numbers (Eq. III.9). Consequently, a mass balance can be written for the initial moles of Li^+ and Br^- in the prepared solutions, as shown in Eqs. III.10-III.11. This set of equations constitutes a linear system of three equations and six unknowns (a, b, c, S_1, S_2, S_3).

Chapter III

$$n_{H_2O,S} = a \cdot S_1 + b \cdot S_2 + c \cdot S_3 \quad \text{Eq. III.9}$$

$$n_{(Li^+)} = S_1 + S_3 \quad \text{Eq. III.10}$$

$$n_{(Br^-)} = S_2 + S_3 \quad \text{Eq. III.11}$$

Considering that the amounts of initial moles of Li^+ and Br^- are the same as the amount of anhydrous moles of $LiBr$ in the solution (Eq. III.12), the above equations have been combined to clear S_1 , as shown in Eq. III.13.

$$n_{(Li^+)} = n_{(Br^-)} = n_{LiBr} \quad \text{Eq. III.12}$$

$$S_1 = \frac{n_{H_2O,S} - c \cdot n_{LiBr}}{a + b - c} \quad \text{Eq. III.13}$$

The most referenced coordination numbers of Li^+ and Br^- ions in aqueous solutions are 4^[112,116–121] and 6,^[116–121] respectively. However, to the best of my knowledge, there are no available values for the number of water moles per mole of ion pair (c). For this reason, the considered values for this parameter in the mass balance, shown in Table III.5, range from 0 to 4 based on the mole ratio (r_n), previously shown in Table III.4.

Table III.5. Used a , b and c values in the mass balance. x_{LiBr} : mole fraction of $LiBr$. a : coordination number of Li^+ . b : coordination number of Br^- . c : number of water moles per mole of ion pair.

Composition range	a	b	c
$0 < x_{LiBr} \leq 0.0224$	6	8	0
$0.0224 < x_{LiBr} < 0.0646$	6	8	1
$0.0646 \leq x_{LiBr} \leq 0.1011$	4	6	2
$0.1011 < x_{LiBr} < 0.1455$	4	6	3
$0.1455 \leq x_{LiBr} \leq 0.2026$	4	6	4

The effective mole fraction of water can be estimated with Eq. III.14 from the total moles of hydrated species (Eq. III.8) and the bulk water moles. This effective mole fraction is used to estimate the vapour pressure according to Raoult's law. Table III.6 shows the results for the analysed $H_2O/LiBr$ solutions.

Chapter III

$$x_{a,eff} = \frac{n_{H_2O,BW}}{n_{H_2O,BW} + n_{hs}} \quad \text{Eq. III.14}$$

Table III.6. Vapour pressure estimation of H₂O/LiBr solutions at 293.15 K. *x*: mole fraction. *n*: number of moles. *p*: vapour pressure. Δp : relative vapour pressure difference. *i*: dissociation factor.

Prepared	Calculated						
x_{LiBr}	n_{hs} (mol)	$n_{H_2O,BW}$ (mol)	$x_{a,eff}$	p_{est} (kPa)	p_{lit} (kPa)	$\Delta p/p$ (%)	<i>i</i>
0	0	0.295	1	2.339	2.339	0	0
0.0108	0.0065	0.240	0.974	2.277	2.277	0	2.00
0.0224	0.0090	0.161	0.947	2.215	2.232	-0.8	1.81
0.0352	0.0132	0.164	0.926	2.165	2.183	-0.8	1.51
0.0492	0.0170	0.151	0.899	2.103	2.105	-0.1	1.39
0.0646	0.0199	0.137	0.873	2.042	1.972	3.5	1.30
0.0817	0.0255	0.107	0.808	1.889	1.773	6.6	1.31
0.1011	0.0425	0.108	0.718	1.680	1.501	12	1.30
0.1215	0.0613	0.104	0.630	1.474	1.200	23	1.17
0.1455	0.0604	0.054	0.473	1.107	0.872	27	1.07
0.1718	0.0770	0.030	0.282	0.660	0.582	14	1.03
0.2026	0.0829	0.007	0.077	0.180	0.346	-48	0.99

It is observed in Figure III.6 that the obtained results from the mass balance (p_{est}) follow the same trend as the values taken from the literature (p_{lit})^[123] over the entire composition range. Furthermore, there is an excellent agreement between both vapour pressure values in dilute solutions, where the hydration of ions predominates over ion pairing. However, as the LiBr composition increases, the difference between the estimated vapour pressure and that obtained from the literature also increases. These differences are more significant when the LiBr composition approaches the composition at the solid-liquid equilibrium.

Chapter III

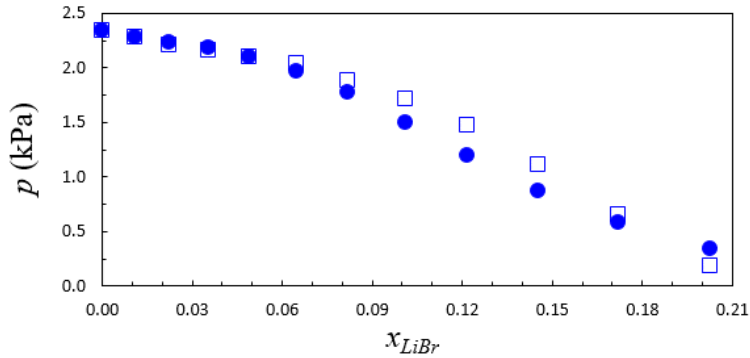


Figure III.6. Vapour pressure of $H_2O/LiBr$ solutions against mole fraction of $LiBr$ at 293.15 K. ●: literature values;^[123] □: estimated values.

These differences can be attributed to the predominance of the ion pairing at high $LiBr$ compositions. The mass balance proposed in this thesis is only valid if the ion pairs can be represented by $Li^+(H_2O)_d/Br^-$ (Eq. III.7), where there is one Li^+ for each Br^- . One could think of the formation of ionic aggregates in which a Li^+ cation coordinates with more than one Br^- anion, as was arbitrarily represented in Figure III.7. In that case, a second coordination sphere would exist where these large ionic aggregates would be bound together by water molecules^[124] in a similar way to that postulated in mixtures containing protic ILs and $LiNO_3$.^[125] This possibility in the mass balances of Li^+ and Br^- ions is possible only if the stoichiometry of the solvated species in the medium is known, and this will be the subject of study in future work.

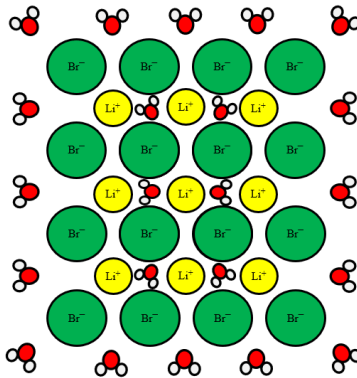


Figure III.7. Arbitrary ionic aggregate in the second coordination shell of $H_2O/LiBr$.

Until now, it can be deduced that the vapour pressure depends not only on the amount of water interacting with the solvate, but also on the molecular structure of the solvated species. Depending on the stoichiometry of these species, the dissociation factor (i), calculated as the number of ions in solution per initial mole of solute, will vary significantly, affecting the actual composition of the solute in the solution.

Table III.6 shows the calculated dissociation factor on the basis of the results discussed in this section. It can be observed that its value decreases as the LiBr composition increases. Values of $i = 2$ in aqueous solutions of 1:1 electrolytes, such as LiBr, can only be assumed at very low solute composition, such as $x_{LiBr} < 0.0224$. The dissociation factor decreases significantly at higher salt compositions, which could be observed in the most concentrated solution ($x_{LiBr} = 0.2026$). At that composition, the dissociation factor required to find a good agreement between both pressure values would have to be 0.5, which is far from the value found using the proposed mass balance. This finding highlights the importance of the formation of ion pairs and ionic aggregates when working with high solute composition.

III.3. Determination of the amount of bulk water in H₂O/(LiBr+[Dmim][Cl]) mixtures with high IL composition

III.3.1 Introduction

The methodology explained in the previous section, based on NIR and MCR-ALS, has also been used in this section to analyse the effect of an ionic liquid ([Dmim][Cl]) on the solvation of ions in aqueous LiBr solutions. For this purpose, the amount of bulk water in mixtures of H₂O/[Dmim][Cl] and H₂O/(LiBr+[Dmim][Cl]) at high IL compositions has been determined.

The choice of using [Dmim][Cl] was made because this substance was already used by the CREVER research group and because it is mentioned in the literature as a promising additive of lithium bromide.^[35]

The solvation in the H₂O/[Dmim][Cl] mixture has also been studied in order to facilitate the interpretation of the results of ternary H₂O/(LiBr+[Dmim][Cl]) solutions.

III.3.2 Experimental part

The analysed samples, spectra acquisition and data processing of H₂O/[Dmim][Cl] and H₂O/(LiBr+[Dmim][Cl]) solutions over a wide range of solute composition ($0.094 \leq x_{IL}/x_{LiBr} \leq 1.03$) are described in this section.

Analysed samples

Two different sets of 12 aqueous solutions of IL and (LiBr+IL) were prepared: one of them with [Dmim][Cl] mole fractions varying between 0 and 0.1426, and one with lithium bromide and ionic liquid mole fractions ranging from (0-0.2944) and (0-0.3043), respectively. The masses of the analysed samples are given in Table III.7.

Table III.7. Mass (g) of H₂O/[Dmim][Cl] and H₂O/(LiBr+[Dmim][Cl]) solutions.

H ₂ O/[Dmim][Cl]		H ₂ O/(LiBr+[Dmim][Cl])		
m_{H_2O}	$m_{[Dmim][Cl]}$	m_{H_2O}	m_{LiBr}	$m_{[Dmim][Cl]}$
4.9582	0	5.1376	0	0
4.7834	0.2517	4.9049	2.8398	0.4078
3.8527	0.4285	4.6260	2.9876	0.8361
4.6542	0.8188	4.8247	3.3902	1.4258
3.8824	0.9717	4.5501	3.5773	2.0490
4.2415	1.4165	3.7824	3.2865	2.3565
4.1601	1.7825	2.9127	2.9257	2.5203
3.4481	1.8559	2.9161	3.3934	3.3799
3.3485	2.2303	2.0188	2.8402	3.2263
3.0089	2.4602	1.8078	3.1364	4.0516
2.8244	2.8189	1.3597	3.2038	4.5424
2.6705	3.2691	0.8810	3.1166	4.9185

$U(m) = \pm 0.0001$ g

Data treatment

The data were treated as was explained in the previous section. The acquired spectra of the samples were stored in matrices named $D_{H_2O/[Dmim][Cl]}$ and $D_{H_2O/(LiBr+[Dmim][Cl])}$, both with (12 x 380) dimensions. These spectra were then pretreated to correct the baseline shift.

The MCR-ALS was used to estimate the spectral and concentration profiles that are representative of the different chemical environments in which water molecules can be found. The process was carried out following the same steps as those described in the previous section.

III.3.3 Results and Discussion

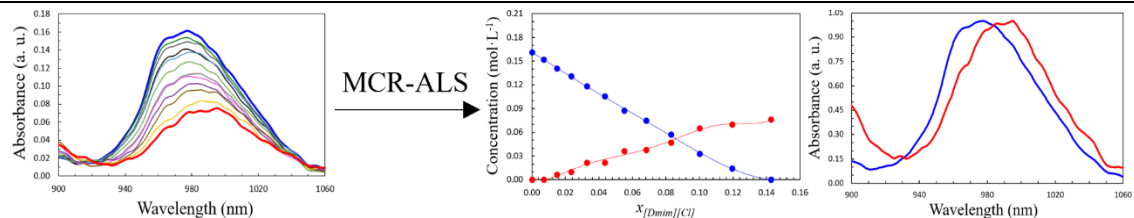
Pretreated spectra, MCR-ALS solutions, quality parameters, bulk water percentage, mole fractions of bulk water and water in the solvate and mole ratio (r_n) are presented in tables arranged in horizontal pages to facilitate the exposition and discussion of the results obtained for $H_2O/[Dmim][Cl]$ and $H_2O/(LiBr+[Dmim][Cl])$ mixtures.

It can be observed in Tables III.8-III.9 that the MCR-ALS solutions represent more than 99.9 % of the variance of the original data and that the correlation coefficients between the spectrum of pure water and that recovered by ALS are close to 1 in both mixtures. This allows assuming that the bulk water percentage and the mole fractions of bulk water and water in the solvate will provide a good estimation for comparatively analysing the influence of IL composition on the amount of bulk water in the solution.

To avoid repetition, this section emphasises the main findings derived from comparing the results obtained for $H_2O/[Dmim][Cl]$ and $H_2O/(LiBr+[Dmim][Cl])$ solutions with those obtained for $H_2O/LiBr$.

The strong decrease of the water absorption band with increasing IL composition observed in the spectra of $H_2O/[Dmim][Cl]$ solutions, shown in Table III.8, confirms the general strong tendency of ionic liquids,^[126,127] and $[Dmim][Cl]$ ^[107] in particular, to interact with water.

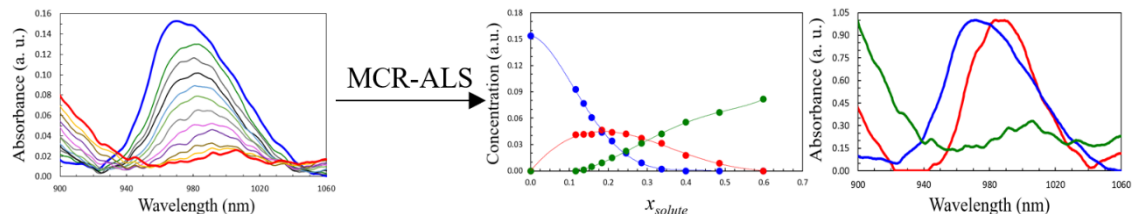
Table III.8. MCR-ALS results for H₂O/[Dmim][Cl] at 293.15 K.



Variance (%)	99.97
LOF PCA (%)	0.21
LOF exp (%)	1.83
r	0.9999

x_{H_2O}	$x_{[Dmim][Cl]}$	BW (%)	$x_{H_2O,BW}$	$x_{H_2O,S}$	r_n (mole ratio)
1	0	100	1	0	-
0.9929	0.0071	96.1	0.9538	0.0391	5.50
0.9851	0.0149	89.2	0.8785	0.1066	7.16
0.9767	0.0233	81.2	0.7931	0.1836	7.86
0.9671	0.0329	73.4	0.7103	0.2568	7.81
0.9566	0.0434	65.5	0.6269	0.3297	7.60
0.9450	0.0550	49.1	0.4643	0.4807	8.74
0.9319	0.0681	46.4	0.4322	0.4997	7.33
0.9170	0.0830	35.5	0.3258	0.5912	7.12
0.9000	0.1000	20.4	0.1835	0.7165	7.17
0.8806	0.1194	8.9	0.0785	0.8021	6.72
0.8574	0.1426	0	0	0.8574	6.01

Table III.9. MCR-ALS results for $\text{H}_2\text{O}/(\text{LiBr}+[\text{Dmim}][\text{Cl}])$ at 293.15 K and high IL compositions.



Variance (%)	99.94
LOF PCA (%)	0.48
LOF exp (%)	2.53
r	0.9998

$x_{\text{H}_2\text{O}}$	x_{LiBr}	$x_{[\text{Dmim}][\text{Cl}]}$	x_{solute}	BW (%)	$x_{\text{H}_2\text{O},\text{BW}}$	$x_{\text{H}_2\text{O},\text{S}}$	r_n (mole ratio)
1	0	0	0	100	1	0	-
0.8839	0.1062	0.0100	0.1162	60.4	0.5339	0.3500	3.02
0.8632	0.1156	0.0212	0.1368	49.9	0.4306	0.4326	3.16
0.8432	0.1229	0.0339	0.1568	39.5	0.3332	0.5100	3.25
0.8168	0.1332	0.0500	0.1832	28.7	0.2341	0.5827	3.18
0.7906	0.1425	0.0669	0.2094	22.1	0.1748	0.6158	2.94
0.7542	0.1571	0.0887	0.2458	13.0	0.0984	0.6558	2.67
0.7148	0.1726	0.1126	0.2852	6.0	0.0430	0.6718	2.36
0.6627	0.1934	0.1439	0.3373	1.4	0.0092	0.6535	1.94
0.6008	0.2162	0.1830	0.3992	0	0	0.6008	1.51
0.5148	0.2516	0.2336	0.4852	0	0	0.5148	1.06
0.4013	0.2944	0.3043	0.5987	0	0	0.4013	0.67

The spectral analysis of the evolution of the water absorption band in the data for the H₂O/(LiBr+[Dmim][Cl]) mixture (Table III.9) reveals that ternary solutions with lower solute (LiBr+[Dmim][Cl]) composition have lower absorbance than H₂O/LiBr solutions with higher solute (LiBr) composition. As an example, this is visualized in Figure III.8, where the absorbance of solutions with similar solute mole fraction are ordered as follows: H₂O/LiBr ($x_{LiBr} = 0.1215$) > H₂O/(LiBr+[Dmim][Cl]) ($x_{LiBr} = 0.1062$ and $x_{[Dmim][Cl]} = 0.0100$) > H₂O/[Dmim][Cl] ($x_{[Dmim][Cl]} = 0.1194$). Although the water affinity of this ionic liquid is higher than that of lithium bromide, its composition in the ternary solution is very low, and the LiBr mole fraction in the H₂O/(LiBr+IL) solution is 0.0153 lower than in the H₂O/LiBr solution. This significant difference in the absorbance between the H₂O/(LiBr+IL) and H₂O/LiBr solutions, which cannot be explained exclusively by the lower solute mole fraction, could be related to interactions between LiBr and [Dmim][Cl].^[109]

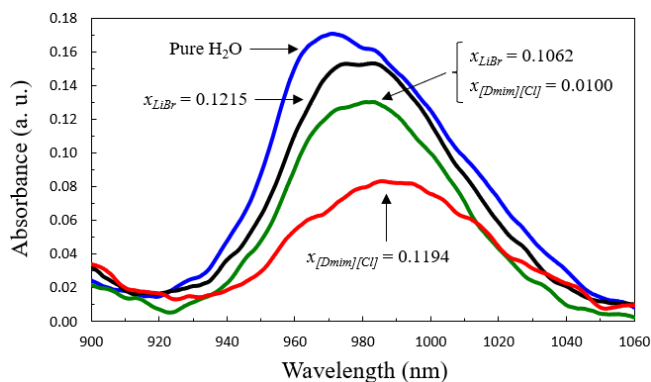


Figure III.8. Experimental spectra of water and mixtures with similar solute composition. Blue data series: pure water. Black data: H₂O/LiBr with $x_{LiBr} = 0.1215$. Red data: H₂O/[Dmim][Cl] with $x_{[Dmim][Cl]} = 0.1194$. Green data: H₂O/(LiBr+[Dmim][Cl]) with $x_{LiBr} = 0.1062$ and $x_{[Dmim][Cl]} = 0.0100$.

Quantitatively, the influence of IL composition on the amount of bulk water is visualised in Figure III.9, where the bulk water percentage in H₂O/[Dmim][Cl] and H₂O/(LiBr+[Dmim][Cl]) solutions (Tables III.8-III.9) is represented along with the *BW* of H₂O/LiBr solutions (Table III.4). Points A, B, and C are representative of the spectra shown in Figure III.8, corresponding to solutions with similar solute molar fraction.

Chapter III

The bulk water percentage in these particular solutions follows the order $\text{H}_2\text{O}/[\text{Dmim}][\text{Cl}] < \text{H}_2\text{O}/\text{LiBr} < \text{H}_2\text{O}/(\text{LiBr}+[\text{Dmim}][\text{Cl}])$, with values of 8.9 %, 27.6 %, and 60.4 % at points B, A, and C, respectively. These values reflect the two aforementioned findings: the strong interaction of this IL with water (8.9 % vs 27.6 %), and the interaction between lithium bromide and $[\text{Dmim}][\text{Cl}]$ (27.6 % vs 60.4 %).

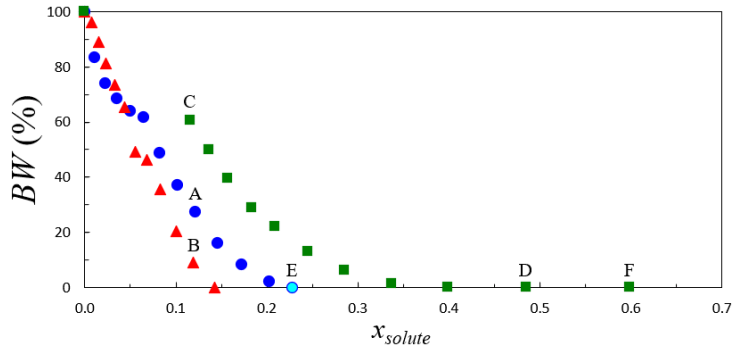


Figure III.9. Bulk water of the analysed solutions against mole fraction of solute (LiBr, $[\text{Dmim}][\text{Cl}]$ or $\text{LiBr}+[\text{Dmim}][\text{Cl}]$) at 293.15 K. Blue dots: $\text{H}_2\text{O}/\text{LiBr}$; red triangles: $\text{H}_2\text{O}/[\text{Dmim}][\text{Cl}]$; green squares: $\text{H}_2\text{O}/(\text{LiBr}+[\text{Dmim}][\text{Cl}])$.

One of the fundamental requirements for working fluids used in absorption refrigeration and heat pump systems is that the vapour pressure of the mixture must be considerably lower than that of the pure refrigerant.^[9] Taking this into account, these results suggest that the $x_{\text{IL}}/x_{\text{LiBr}}$ ratio should be lower than that calculated at point C ($x_{\text{IL}} = 0.0100$, $x_{\text{LiBr}} = 0.1062$, $x_{\text{IL}}/x_{\text{LiBr}} = 0.0942$) to avoid impairing the absorption capacity of the mixture.

It is noteworthy to observe that, although the $\text{H}_2\text{O}/(\text{LiBr}+[\text{Dmim}][\text{Cl}])$ solutions prepared with high solute compositions ($0.3992 \leq x_{\text{solute}} \leq 0.5987$) have zero bulk water percentage, no solid phase was observed in the samples (points D and F, Figure III.9). This fact is interpreted as a consequence of the influence of IL on the solubility of LiBr. For example: the ternary solution with the highest solute composition (point F, Figure III.9), was prepared with $x_{\text{LiBr}} = 0.2944$ and $x_{[\text{Dmim}][\text{Cl}]} = 0.3043$. This LiBr composition is significantly higher than the solubility limit of lithium bromide in water at 18.99 °C ($x_{\text{LiBr}} = 0.2274$).^[122] From the point of view of ion hydration and

ion pairing, it is reasonable to think that the formation of ionic aggregates similar to the one represented in Figure III.7 predominates in these compositions, as mentioned in Section III.2.3.

As expected, the values of r_n (moles of water in the solvate per mole of solute) in $\text{H}_2\text{O}/(\text{LiBr}+[\text{Dmim}][\text{Cl}])$ solutions (Table III.9) are lower than in $\text{H}_2\text{O}/\text{LiBr}$ solutions (Table III.4). Figure III.10 shows that, regardless of the solute composition, the r_n values in ternary solutions is lower than the minimum value found for $\text{H}_2\text{O}/\text{LiBr}$ (3.85). This finding is significant since the composition of that $\text{H}_2\text{O}/\text{LiBr}$ solution is close to one in the solid-liquid equilibrium, where the formation of ion pairs between Li^+ and Br^- ions would be enhanced with respect to ion hydration. This suggests that solute-solute interactions compete with solute-solvent interactions, favouring the formation of large ionic aggregates^[115,124] over the entire composition range considered. The low mole ratio value (0.67) for the solution with the highest solute composition ($x_{\text{solute}} = 0.5987$) is noteworthy.

Considering the values of the mole ratio (r_n) and the dissociation factor (i) of LiBr in aqueous solutions, it is likely that the presence of ionic liquid causes a decrease in the dissociation of LiBr, decreasing its effective composition in solution.

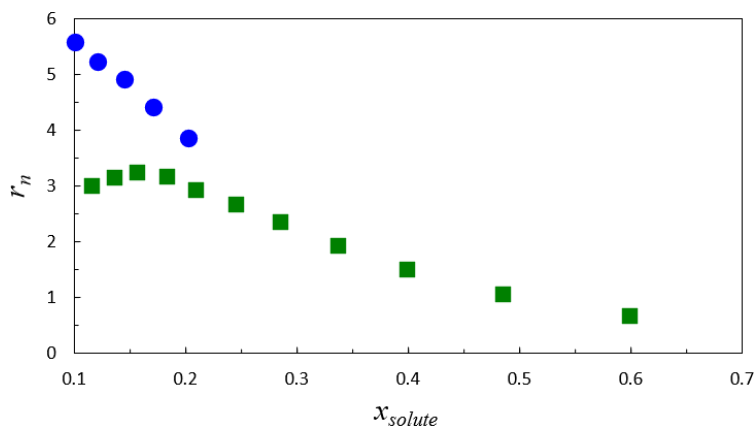


Figure III.10. Mole ratio against mole fraction of solute at 293.15 K. ●: $\text{H}_2\text{O}/\text{LiBr}$; ■: $\text{H}_2\text{O}/(\text{LiBr}+[\text{Dmim}][\text{Cl}])$.

Chapter III

Results obtained by NIR+MCR-ALS show good agreement with computational results regarding the structure and distribution of water molecules in $\text{H}_2\text{O}/(\text{LiBr}+[\text{Dmim}][\text{Cl}])$ ternary solutions.^[109] Studies based on atomistic (classical) Molecular Dynamics simulations (MD) were carried out by the research group of L. Miguel Varela, from Universidade de Santiago de Compostela, and Car-Parrinello Molecular Dynamics simulations (CPMD) were carried out by Professor Antonio Fortea, from Universitat Rovira i Virgili. Figure III.11 shows one representative snapshot of the CPMD trajectory of two solutions: one with $x_{[\text{Dmim}][\text{Cl}]} = 0.0357$ and $x_{\text{solute}} = 0.1429$ (Figure III.11 a), and another one with $x_{[\text{Dmim}][\text{Cl}]} = 0.3000$ and $x_{\text{solute}} = 0.6000$ (Figure III.11 b). This figure has been included to provide a good representation of the arrangement of water molecules in the solutions. It can be observed that, in the solution with a lower solute composition, a Li^+ cation coordinates with four water molecules, while in the solution with a higher solute composition, a predominance of ion-ion interactions (Li^+-Cl^- and Li^+-Br^-) is observed.

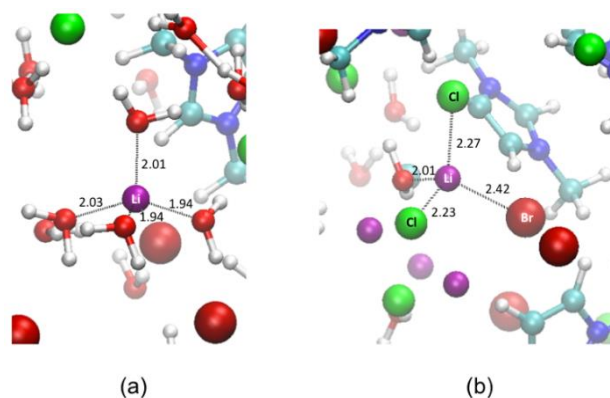


Figure III.11. Structure of the first solvation shell of Li ion in a snapshot of the CPMD trajectory for (a) relatively concentrated solution and (b) very concentrated solution. Colour code for the atoms: Li (magenta), Br (dark red), Cl (green), O (red), C (light blue), N (dark blue), H (white). Distances are in Angstrom.^[109]

On one hand, the discussed results demonstrate that the effective solute composition depends both on the amount of bulk water and on the structure of the solvates. On the other hand, the considered $x_{\text{IL}}/x_{\text{LiBr}}$ ratio should be lower than

Chapter III

0.0942 ($x_{LiBr} = 0.1062$, $x_{IL} = 0.0100$) to avoid a strong competition for water molecules between ionic liquid and lithium bromide in $H_2O/(LiBr+IL)$ solutions that would be detrimental to the application performance.

III.4. Selection of ionic liquid composition in $H_2O/(LiBr+[Dmim][Cl])$ mixtures using IL as an additive

III.4.1 Introduction

The procedure described in Section II.2 is used to determine the bulk water content in $H_2O/(LiBr+[Dmim][Cl])$ solutions over a wide range of solute composition to select the most suitable x_{IL}/x_{LiBr} ratio.

III.4.2 Experimental part

Twenty different samples were prepared from three $H_2O/(LiBr+[Dmim][Cl])$ solutions, with molar ratios between IL and LiBr of 0.0202, 0.0418, and 0.0648, and solute mole fractions varying from pure water to $x_{solute} = 0.22$ (Table III.10).

Table III.10. Mass (g) of H₂O/(LiBr+[Dmim][Cl]) solutions at the selected x_{IL}/x_{LiBr} ratios.

$x_{IL}/x_{LiBr} = 0.0202$			$x_{IL}/x_{LiBr} = 0.0418$			$x_{IL}/x_{LiBr} = 0.0648$		
m_{H_2O}	m_{LiBr}	m_{IL}	m_{H_2O}	m_{LiBr}	m_{IL}	m_{H_2O}	m_{LiBr}	m_{IL}
1.7655	0	0	1.5286	0	0	1.4852	0	0
2.9203	0.0823	0.0025	2.9590	0.0751	0.0048	3.2648	0.0799	0.0079
1.3953	0.0823	0.0025	1.3655	0.0751	0.0048	1.5038	0.0799	0.0079
2.5479	0.2330	0.0072	3.1701	0.2741	0.0175	3.4501	0.2883	0.0285
1.8459	0.2334	0.0072	2.2691	0.2741	0.0175	2.4737	0.2883	0.0285
1.4236	0.2334	0.0072	1.7444	0.2741	0.0175	1.9061	0.2883	0.0285
2.5224	0.5134	0.0158	1.4057	0.2741	0.0175	1.5227	0.2883	0.0285
2.0801	0.5134	0.0158	2.2726	0.5369	0.0343	1.2606	0.2883	0.0285
1.7535	0.5134	0.0158	1.9221	0.5369	0.0343	2.1836	0.5909	0.0585
1.5007	0.5134	0.0158	1.6383	0.5369	0.0343	1.8689	0.5909	0.0585
1.3016	0.5134	0.0158	1.4114	0.5369	0.0343	1.6178	0.5909	0.0585
1.1307	0.5134	0.0158	1.2292	0.5369	0.0343	1.4089	0.5909	0.0585
1.9463	1.1418	0.0352	1.0835	0.5369	0.0343	1.2324	0.5909	0.0585
1.7150	1.1418	0.0352	2.1126	1.1977	0.0765	1.0772	0.5909	0.0585
1.5258	1.1418	0.0352	1.8732	1.1977	0.0765	1.6389	1.0153	0.1004
1.3525	1.1418	0.0352	1.6631	1.1977	0.0765	1.4571	1.0153	0.1004
1.2059	1.1418	0.0352	1.4795	1.1977	0.0765	1.2924	1.0153	0.1004
1.0696	1.1418	0.0352	1.3246	1.1977	0.0765	1.1527	1.0153	0.1004
0.9529	1.1418	0.0352	1.1763	1.1977	0.0765	1.0326	1.0153	0.1004
0.8492	1.1418	0.0352	1.0414	1.1977	0.0765	0.9114	1.0153	0.1004
			0.9225	1.1977	0.0765	0.8084	1.0153	0.1004

$U(m) = \pm 0.0001 \text{ g}$

Chapter III

The infrared spectra between 900 nm and 1060 nm for each set of samples with the same IL/LiBr mole ratio were acquired at 20 °C using the same instrument and conditions described in Section III.3.

III.4.3 Results and Discussion

Tables III.11-III.13 show the pretreated spectra of $\text{H}_2\text{O}/(\text{LiBr}+[\text{Dmim}][\text{Cl}])$ solutions as well as the obtained solutions from NIR+MCR-ALS and the performed calculations. In all cases, two factors were considered after performing the singular value decomposition of the spectral matrices $\mathbf{D}_{\text{H}_2\text{O}/(\text{LiBr}+[\text{Dmim}][\text{Cl}]}$.

Table III.11. MCR-ALS results for $\text{H}_2\text{O}/(\text{LiBr}+[\text{Dmim}][\text{Cl}])$ at 293.15 K and $x_{\text{IL}}/x_{\text{LiBr}} = 0.0202$.

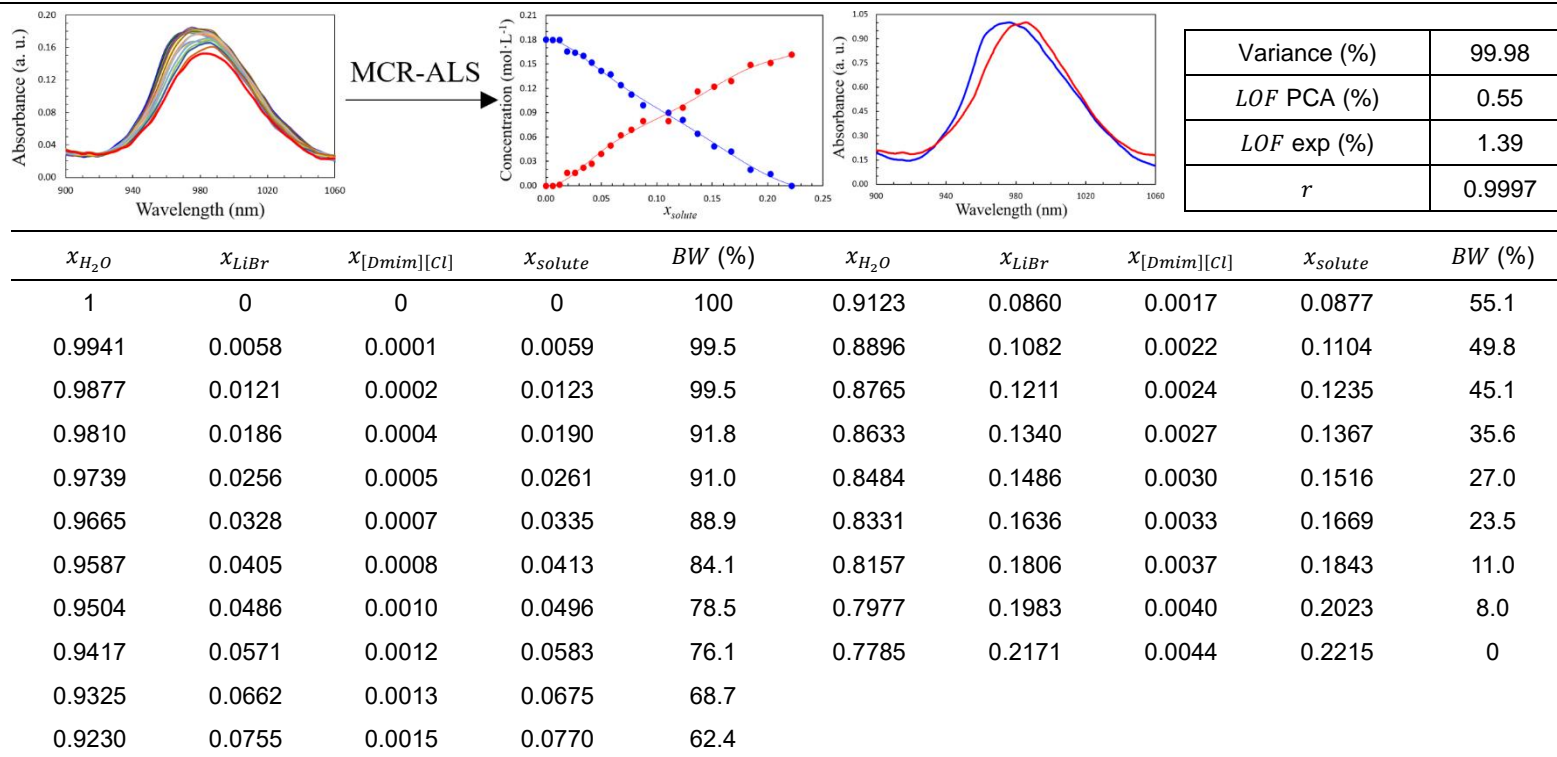
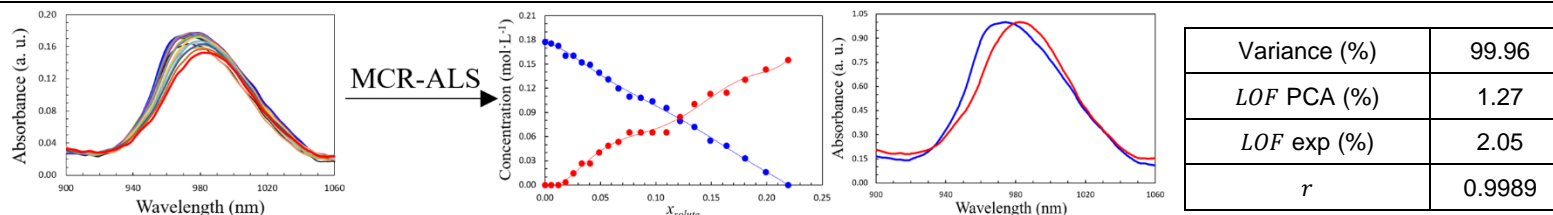
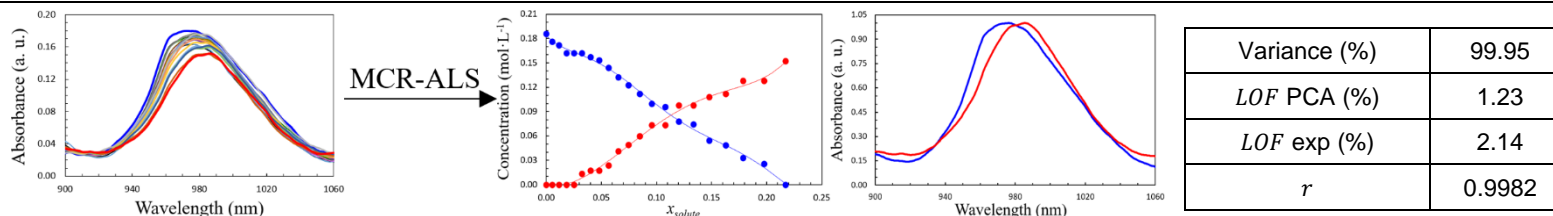


Table III.12. MCR-ALS results for $\text{H}_2\text{O}/(\text{LiBr}+[\text{Dmim}][\text{Cl}])$ at 293.15 K and $x_{\text{IL}}/x_{\text{LiBr}} = 0.0418$.



$x_{\text{H}_2\text{O}}$	x_{LiBr}	$x_{[\text{Dmim}][\text{Cl}]}$	x_{solute}	BW (%)	$x_{\text{H}_2\text{O}}$	x_{LiBr}	$x_{[\text{Dmim}][\text{Cl}]}$	x_{solute}	BW (%)
1	0	0	0	100	0.9137	0.0828	0.0035	0.0863	60.8
0.9945	0.0053	0.0002	0.0055	98.7	0.9033	0.0928	0.0039	0.0967	58.5
0.9882	0.0113	0.0005	0.0118	97.2	0.8909	0.1047	0.0044	0.1091	53.8
0.9817	0.0176	0.0007	0.0183	90.2	0.8786	0.1165	0.0049	0.1214	44.7
0.9746	0.0244	0.0010	0.0254	90.2	0.8653	0.1293	0.0054	0.1347	40.5
0.9672	0.0315	0.0013	0.0328	85.6	0.8511	0.1429	0.0060	0.1489	31.0
0.9596	0.0388	0.0016	0.0404	83.9	0.8365	0.1569	0.0066	0.1635	27.3
0.9514	0.0466	0.0020	0.0486	78.6	0.8196	0.1732	0.0072	0.1804	18.6
0.9431	0.0546	0.0023	0.0569	73.9	0.8009	0.1911	0.0080	0.1991	9.0
0.9339	0.0634	0.0027	0.0661	67.4	0.7809	0.2103	0.0088	0.2191	0
0.9240	0.0729	0.0031	0.0760	61.7					

Table III.13. MCR-ALS results for $\text{H}_2\text{O}/(\text{LiBr}+[\text{Dmim}][\text{Cl}])$ at 293.15 K and $x_{\text{IL}}/x_{\text{LiBr}} = 0.0648$.



$x_{\text{H}_2\text{O}}$	x_{LiBr}	$x_{[\text{Dmim}][\text{Cl}]}$	x_{solute}	BW (%)	$x_{\text{H}_2\text{O}}$	x_{LiBr}	$x_{[\text{Dmim}][\text{Cl}]}$	x_{solute}	BW (%)
1	0	0	0	100	0.9152	0.0796	0.0052	0.0848	60.2
0.9946	0.0051	0.0003	0.0054	94.8	0.9042	0.0900	0.0058	0.0958	53.6
0.9884	0.0109	0.0007	0.0116	92.4	0.8919	0.1015	0.0066	0.1081	51.6
0.9819	0.0170	0.0011	0.0181	87.3	0.8796	0.1131	0.0073	0.1204	41.9
0.9749	0.0236	0.0015	0.0251	87.3	0.8666	0.1253	0.0081	0.1334	40.0
0.9677	0.0303	0.0020	0.0323	87.2	0.8521	0.1389	0.0090	0.1479	29.4
0.9599	0.0377	0.0024	0.0401	84.7	0.8371	0.1530	0.0099	0.1629	26.1
0.9519	0.0452	0.0029	0.0481	82.5	0.8216	0.1675	0.0109	0.1784	17.6
0.9436	0.0530	0.0034	0.0564	77.6	0.8025	0.1855	0.0120	0.1975	13.8
0.9347	0.0613	0.0040	0.0653	71.2	0.7828	0.2040	0.0132	0.2172	0
0.9253	0.0702	0.0045	0.0747	66.1					

Chapter III

Figure III.12 shows the percentage of bulk water against the ratio between mole fractions of LiBr and H₂O. where no significant differences in the percentage of bulk water are observed as a function of the ratio between IL and LiBr mole fractions when working with small compositions of ionic liquid in the solute. This finding suggests a similar behaviour regarding ion solvation in these solutions and, therefore, similar values of the effective solute composition in all cases.

In view of this behaviour, subsequent analyses were carried out using the lowest composition of ionic liquid in the solute ($x_{IL}/x_{LiBr} \approx 0.0205$).

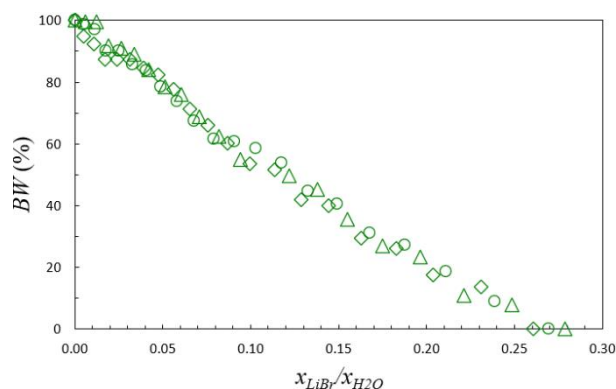


Figure III.12. Bulk water of the H₂O/(LiBr+[Dmim][Cl]) solutions against mole fraction ratio between LiBr and H₂O at 293.15 K. \triangle : H₂O/(LiBr+[Dmim][Cl]) with $x_{IL}/x_{LiBr} = 0.0202$; \circ : H₂O/(LiBr+[Dmim][Cl]) with $x_{IL}/x_{LiBr} = 0.0418$; \diamond : H₂O/(LiBr+[Dmim][Cl]) with $x_{IL}/x_{LiBr} = 0.0648$.

III.5. Influence of the ionic liquid structure on the bulk water content in H₂O/(LiBr+IL) mixtures using IL as an additive

III.5.1 Introduction

The procedure detailed in Section II.2 has been used again to analyse the behaviour of aqueous H₂O/LiBr solutions with four ionic liquids of different chemical characteristics as additives. Three of them are protic ionic liquids with acid-base

Chapter III

characteristics: ethylammonium nitrate ([EA][NO₃]), propylammonium nitrate (PA)[NO₃], and ethylammonium chloride ([EA][Cl]) The other ionic liquid used is 1-butyl-3-methylimidazolium bromide ([Bmim][Br]), with bromide anion, as well as LiBr.

The main objective of this section is to provide useful evidence to select the most suitable ionic liquid among them as an additive for H₂O/LiBr in absorption refrigeration and heat pump systems. The composition of the mixtures analysed is detailed below, and the results are briefly presented and discussed to avoid repetition.

III.5.2 Experimental part

Thirteen H₂O/(LiBr+IL) solutions with [EA][NO₃], [PA][NO₃] and [EA][Cl], and 20 solutions with [Bmim][Br] were prepared. The mole fraction of solute in these solutions range from pure water to 0.22, and the ratio of mole fractions between IL and LiBr (x_{IL}/x_{LiBr}) is approximately 0.0205. The spectra of the solutions shown in Table III.14 were acquired at 20 °C.

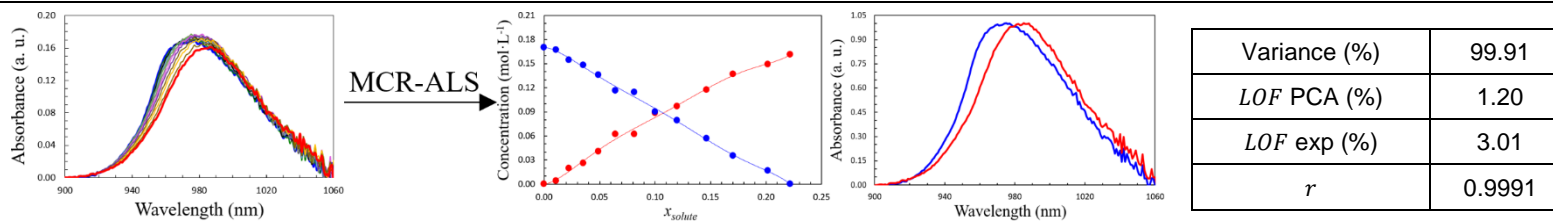
Table III.14. Mass (g) of H₂O/(LiBr+IL) solutions at a similar x_{IL}/x_{LiBr} ratio for [EA][NO₃], [PA][NO₃], [EA][Cl] and [Bmim][Br].

H ₂ O/(LiBr+[EA][NO ₃]) $x_{IL}/x_{LiBr} = 0.0205$			H ₂ O/(LiBr+[PA][NO ₃]) $x_{IL}/x_{LiBr} = 0.0205$			H ₂ O/(LiBr+[EA][Cl]) $x_{IL}/x_{LiBr} = 0.0205$			H ₂ O/(LiBr+[Bmim][Br]) $x_{IL}/x_{LiBr} = 0.0208$					
m_{H_2O}	m_{LiBr}	m_{IL}	m_{H_2O}	m_{LiBr}	m_{IL}	m_{H_2O}	m_{LiBr}	m_{IL}	m_{H_2O}	m_{LiBr}	m_{IL}	m_{H_2O}	m_{LiBr}	m_{IL}
8.6629	0	0	8.6221	0	0	8.5675	0	0	9.0920	0	0	6.0471	3.7723	0.1976
7.9301	0.4072	0.0104	8.7612	0.4499	0.0130	8.0889	0.4181	0.0080	8.3444	0.2422	0.0127	6.0050	4.2322	0.2217
8.6481	0.9333	0.0238	8.1222	0.8691	0.0250	8.2752	0.9012	0.0173	8.5759	0.5275	0.0276	5.8417	4.7026	0.2463
7.8668	1.3583	0.0346	8.0289	1.3488	0.0388	7.9026	1.3677	0.0263	8.3233	0.8018	0.0420	5.4527	5.1905	0.2719
7.9104	1.9223	0.0490	8.1265	1.9597	0.0564	8.2215	2.0182	0.0388	6.9788	0.8899	0.0466	5.7468	5.9251	0.3103
7.2437	2.3537	0.0600	7.6805	2.4775	0.0713	7.5545	2.4655	0.0474	7.2911	1.2458	0.0653	4.8222	5.5589	0.2912
7.2055	3.0173	0.0770	7.5533	3.1506	0.0907	7.3991	3.1085	0.0598	7.7439	1.6407	0.0859	5.2787	6.8492	0.3587
6.8060	3.5793	0.0913	7.3392	3.8124	0.1098	7.1648	3.7950	0.0730	8.3311	2.0830	0.1091	7.3403	3.0509	0.1598
6.6282	4.2662	0.1088	6.9668	4.4941	0.1294	7.0780	4.6439	0.0894	7.5950	2.3312	0.1221	6.6280	3.1891	0.1670
6.0740	4.9240	0.1256	6.7864	5.3627	0.1544	6.9887	5.6143	0.1080	7.8642	2.8194	0.1477	6.1499	3.3821	0.1771
5.9774	5.8009	0.1480	6.5190	6.3194	0.1819	6.8910	6.7487	0.1299	7.3403	3.0509	0.1598	6.0471	3.7723	0.1976
5.7907	6.9082	0.1762	6.1344	7.2865	0.2098	6.0485	7.2803	0.1401	6.6280	3.1891	0.1670	6.0050	4.2322	0.2217
5.9476	8.0124	0.2044	6.2552	8.3972	0.2417	5.9973	8.1353	0.1565	6.1499	3.3821	0.1771	5.8417	4.7026	0.2463
$U(m) = \pm 0.0001 \text{ g}$														

III.5.3 Results and Discussion

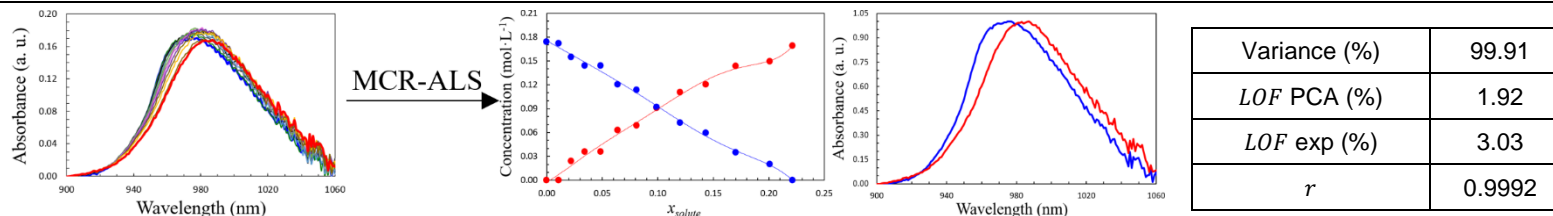
The pretreated infrared spectra of the analysed $\text{H}_2\text{O}/(\text{LiBr}+\text{IL})$ solutions are shown in Tables III.15-III.18 together with the solutions obtained and the calculations performed. The number of factors necessary to retain as much information as possible was estimated by singular value decomposition of the spectral matrices $\mathbf{D}_{\text{H}_2\text{O}/(\text{LiBr}+\text{IL})}$. The quality parameters of the solution, with explained variance percentages higher than 99.9 % and correlation coefficients (r) close to 1 between the recovered spectrum, representative of pure water, and the experimental spectrum of water, show the goodness of the solutions obtained by decomposing the spectra matrices.

Table III.15. MCR-ALS results for $\text{H}_2\text{O}/(\text{LiBr}+[\text{EA}][\text{NO}_3])$ at 293.15 K and $x_{\text{IL}}/x_{\text{LiBr}} = 0.0205$.



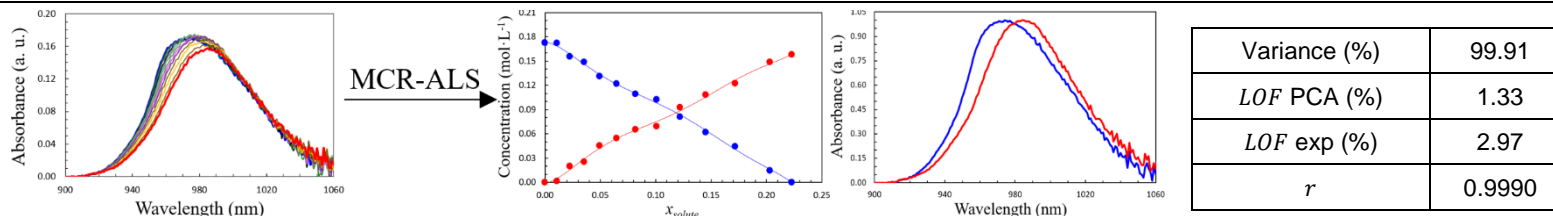
$x_{\text{H}_2\text{O}}$	x_{LiBr}	$x_{[\text{EA}][\text{NO}_3]}$	x_{solute}	BW (%)
1	0	0	0	100
0.9892	0.0106	0.0002	0.0108	98.1
0.9777	0.0219	0.0004	0.0223	90.5
0.9647	0.0346	0.0007	0.0353	87.0
0.9511	0.0479	0.0010	0.0489	79.7
0.9356	0.0631	0.0013	0.0644	68.5
0.9186	0.0798	0.0016	0.0814	67.2
0.8998	0.0982	0.0020	0.1002	52.8
0.8801	0.1175	0.0024	0.1199	46.5
0.8535	0.1436	0.0029	0.1465	33.3
0.8296	0.1670	0.0034	0.1704	20.6
0.7984	0.1976	0.0040	0.2016	9.7
0.7781	0.2174	0.0045	0.2219	0

Table III.16. MCR-ALS results for $\text{H}_2\text{O}/(\text{LiBr}+[\text{PA}][\text{NO}_3])$ at 293.15 K and $x_{\text{IL}}/x_{\text{LiBr}} = 0.0205$.



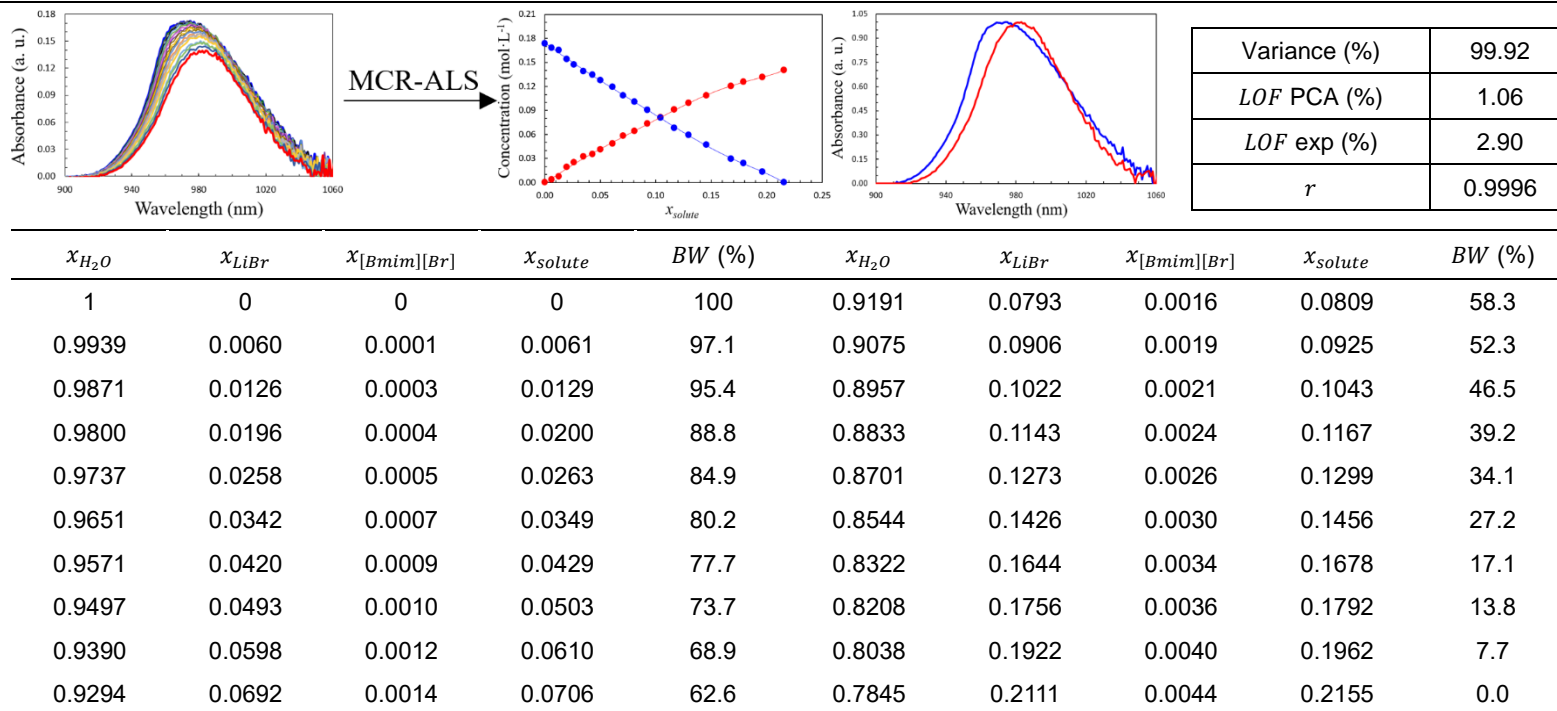
$x_{\text{H}_2\text{O}}$	x_{LiBr}	$x_{[\text{PA}][\text{NO}_3]}$	x_{solute}	BW (%)
1	0	0	0	100
0.9892	0.0106	0.0002	0.0108	98.9
0.9778	0.0218	0.0004	0.0222	89.1
0.9657	0.0336	0.0007	0.0343	82.8
0.9514	0.0476	0.0010	0.0486	82.8
0.9361	0.0626	0.0013	0.0639	69.1
0.9189	0.0795	0.0016	0.0811	65.1
0.9009	0.0971	0.0020	0.0991	52.7
0.8799	0.1177	0.0024	0.1201	41.6
0.8567	0.1404	0.0029	0.1433	34.3
0.8297	0.1669	0.0034	0.1703	20.1
0.7991	0.1969	0.0040	0.2009	11.4
0.7787	0.2169	0.0044	0.2213	0

Table III.17. MCR-ALS results for $\text{H}_2\text{O}/(\text{LiBr}+[\text{EA}][\text{Cl}])$ at 293.15 K and $x_{\text{IL}}/x_{\text{LiBr}} = 0.0205$.



$x_{\text{H}_2\text{O}}$	x_{LiBr}	$x_{[\text{EA}][\text{Cl}]}$	x_{solute}	BW (%)
1	0	0	0	100
0.9892	0.0106	0.0002	0.0108	99.8
0.9775	0.0220	0.0005	0.0225	90.1
0.9647	0.0346	0.0007	0.0353	86.3
0.9506	0.0484	0.0010	0.0494	76.1
0.9354	0.0633	0.0013	0.0646	70.8
0.9183	0.0801	0.0016	0.0817	63.4
0.8992	0.0988	0.0020	0.1008	59.4
0.8780	0.1196	0.0024	0.1220	46.9
0.8547	0.1424	0.0029	0.1453	35.9
0.8283	0.1683	0.0034	0.1717	25.6
0.7969	0.1990	0.0041	0.2031	8.5
0.7769	0.2186	0.0045	0.2231	0

Table III.18. MCR-ALS results for $\text{H}_2\text{O}/(\text{LiBr}+[\text{Bmim}][\text{Br}])$ at 293.15 K and $x_{\text{IL}}/x_{\text{LiBr}} = 0.0208$.



Chapter III

To compare the results, Figure III.13 shows the percentage of bulk water of the new solutions against x_{LiBr}/x_{H_2O} along with that of H₂O/LiBr (Table III.4) and H₂O/(LiBr+[Dmim][Cl]) solutions (Table III.11). It is observed that, regardless of the IL considered, the amount of bulk water is higher than that of H₂O/LiBr. The average bulk water differences between mixtures with and without additive follow the order: [EA][Cl] (14.6 %) > [EA][NO₃] (13.0 %) ≈ [PA][NO₃] (12.2 %) ≈ [Dmim][Cl] (11.7 %) > [Bmim][Br] (7.9 %).

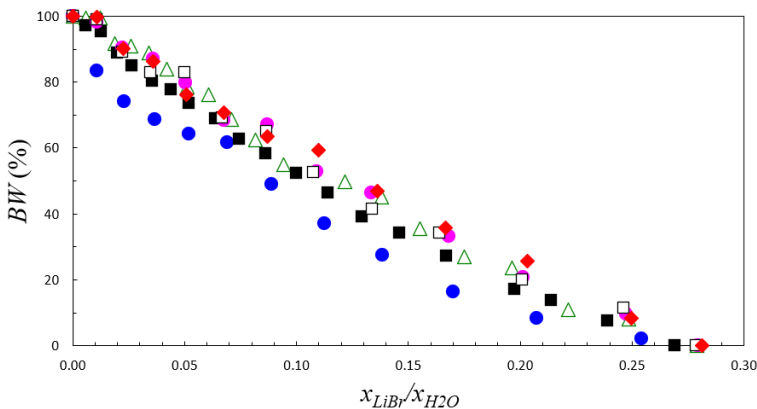


Figure III.13. Bulk water of H₂O/LiBr and H₂O/(LiBr+IL) solutions against LiBr/H₂O mole fraction ratio at 293.15 K. ●: H₂O/LiBr; ●: H₂O/(LiBr+[EA][NO₃]) with $x_{IL}/x_{LiBr} = 0.0205$; □: H₂O/(LiBr+[PA][NO₃]) with $x_{IL}/x_{LiBr} = 0.0205$; ◆: H₂O/(LiBr+[EA][Cl]) with $x_{IL}/x_{LiBr} = 0.0205$; ■: H₂O/(LiBr+[Bmim][Br]) with $x_{IL}/x_{LiBr} = 0.0208$; △: H₂O/(LiBr+[Dmim][Cl]) with $x_{IL}/x_{LiBr} = 0.0202$.

These results suggest that the protic character of the ionic liquids based on the ammonium cation ([EA][NO₃], [PA][NO₃], and [EA][Cl]) favours interaction with the lithium cation,^[108,125] and that this interaction is greater when the cation size is smaller. The difference observed between the mixtures with [Dmim][Cl] and [Bmim][Br] can be attributed to the larger radius of the bromide anion compared to the chloride anion.^[128] The influence of ion size is reflected in the coordination numbers usually referenced in the literature for aqueous solutions with these anions: 8 for Br⁻ and 7 for Cl⁻.^[120]

Chapter III

Figure III.14 shows the average bulk water difference $\text{H}_2\text{O}/(\text{LiBr}+\text{IL})$ and $\text{H}_2\text{O}/\text{LiBr}$ mixtures at 20 °C over the entire composition range at $x_{\text{IL}}/x_{\text{LiBr}} \approx 0.0205$. It is observed that the difference in bulk water decreases linearly as the molar mass of the IL increases, which evidences that the solvation mechanism is similar in all the mixtures.

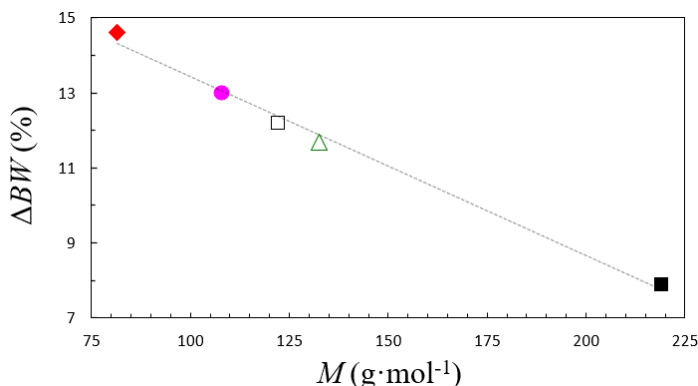


Figure III.14. Average bulk water difference between solutions with and without additive at 293.15 K against molar mass of IL. ●: $\text{H}_2\text{O}/(\text{LiBr}+[\text{EA}][\text{NO}_3])$ with $x_{\text{IL}}/x_{\text{LiBr}} = 0.0205$; □: $\text{H}_2\text{O}/(\text{LiBr}+[\text{PA}][\text{NO}_3])$ with $x_{\text{IL}}/x_{\text{LiBr}} = 0.0205$; ◆: $\text{H}_2\text{O}/(\text{LiBr}+[\text{EA}][\text{Cl}])$ with $x_{\text{IL}}/x_{\text{LiBr}} = 0.0205$; ■: $\text{H}_2\text{O}/(\text{LiBr}+[\text{Bmim}][\text{Br}])$ with $x_{\text{IL}}/x_{\text{LiBr}} = 0.0208$; △: $\text{H}_2\text{O}/(\text{LiBr}+[\text{Dmim}][\text{Cl}])$ with $x_{\text{IL}}/x_{\text{LiBr}} = 0.0202$. The dotted line is only a guide to the eye.

From the point of view of absorption refrigeration and heat pump systems, these results indicate that the water absorption capacity of the absorbent is higher with aprotic ILs, such as $[\text{Dmim}][\text{Cl}]$ or $[\text{Bmim}][\text{Br}]$, since the amount of bulk water is lower in the presence of these, implying that there is more water in the solvate.

III.6. Influence of temperature on the bulk water in H₂O/(LiBr+IL) mixtures at the same mole ratio between LiBr and IL

III.6.1 Introduction

The objective of this section is to evaluate whether the findings stated in the previous sections vary with increasing temperature.

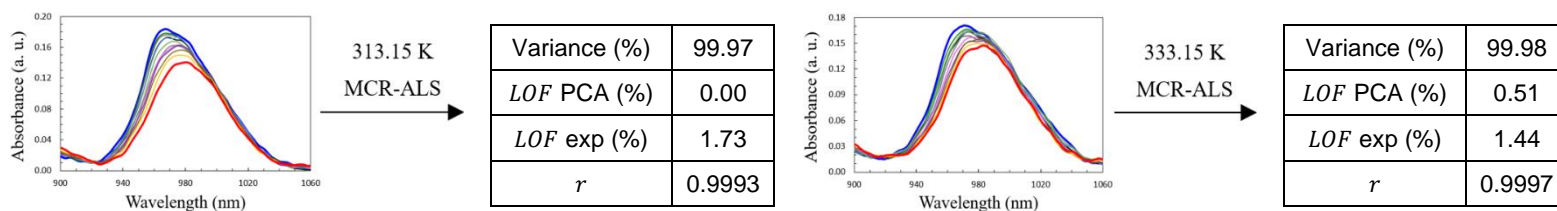
The study has been carried out by comparatively analysing the percentage of bulk water in H₂O/LiBr and H₂O/(LiBr+IL) solutions with spectra acquired at 20 °C, 40 °C and 60 °C.

III.6.2 Results and Discussion

Tables III.19-III.24 summarise the pretreated spectra and the calculations derived from the MCR-ALS solutions.

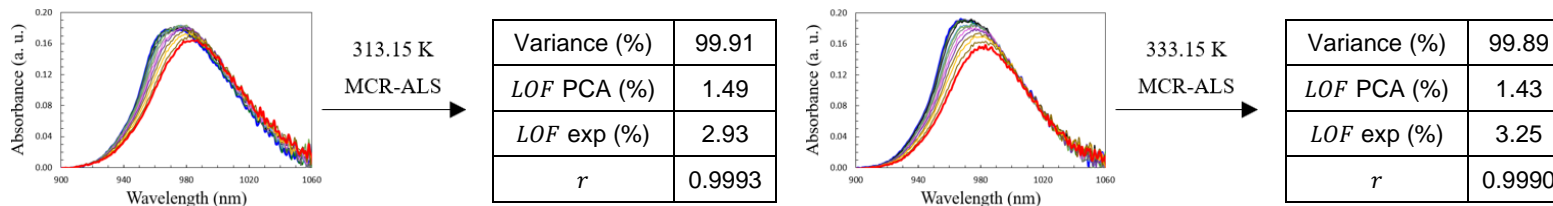
To facilitate the analysis, Figure III.15 shows the percentage of bulk water in H₂O/LiBr solutions at the three temperatures considered. In agreement with what would be expected considering that solute-solute, solute-solvent and solvent-solvent interactions will decrease with increasing temperature,^[120] it is observed that the amount of bulk water increases with increasing temperature over the whole composition range. This effect is more significant in solutions with low LiBr composition ($x_{LiBr}/x_{H_2O} < 0.05$), where ion pairing does not predominate.

Table III.19. MCR-ALS results for H₂O/LiBr at 313.15 K and 333.15 K.



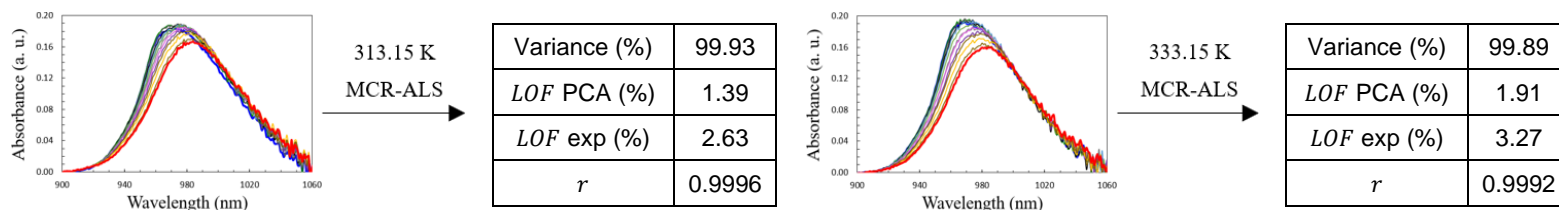
x_{H_2O}	x_{LiBr}	BW (%) at 313.15 K	BW (%) at 333.15 K
1	0	100	100.0
0.9929	0.0071	97.6	95.9
0.9851	0.0149	88.4	95.1
0.9767	0.0233	76.2	80.3
0.9671	0.0329	70.2	73.8
0.9566	0.0434	61.1	58.5
0.9450	0.0550	53.7	44.8
0.9319	0.0681	43.5	42.3
0.9170	0.0830	34.0	34.7
0.9000	0.1000	21.5	19.5
0.8806	0.1194	11.9	9.4
0.8574	0.1426	0	0

Table III.20. MCR-ALS results for $\text{H}_2\text{O}/(\text{LiBr}+[\text{EA}][\text{NO}_3])$ at 313.15 K and 333.15 K, and $x_{\text{IL}}/x_{\text{LiBr}} = 0.0205$.



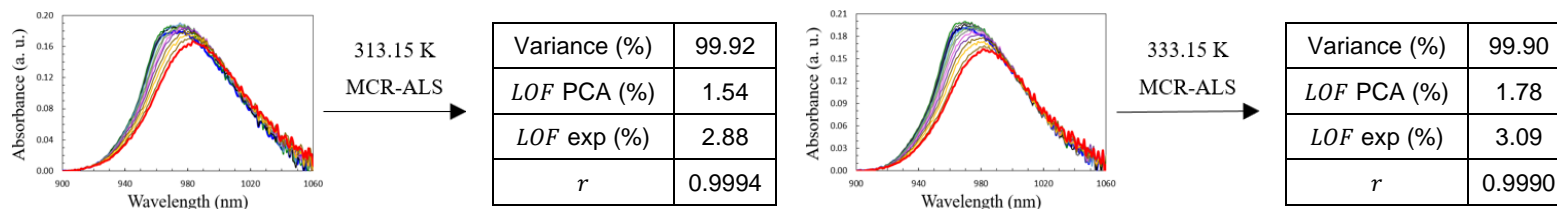
$x_{\text{H}_2\text{O}}$	x_{LiBr}	$x_{[\text{EA}][\text{NO}_3]}$	x_{solute}	BW (%) at 313.15 K	BW (%) at 333.15 K
1	0	0	0	100	100
0.9892	0.0106	0.0002	0.0108	95.1	99.3
0.9777	0.0219	0.0004	0.0223	91.1	99.3
0.9647	0.0346	0.0007	0.0353	77.1	85.4
0.9511	0.0479	0.0010	0.0489	77.1	79.4
0.9356	0.0631	0.0013	0.0644	66.3	76.1
0.9186	0.0798	0.0016	0.0814	61.0	67.6
0.8998	0.0982	0.0020	0.1002	54.9	55.4
0.8801	0.1175	0.0024	0.1199	43.1	47.6
0.8535	0.1436	0.0029	0.1465	32.4	35.7
0.8296	0.1670	0.0034	0.1704	25.5	21.5
0.7984	0.1976	0.0040	0.2016	8.0	3.8
0.7781	0.2174	0.0045	0.2219	0.4	0

Table III.21. MCR-ALS results for $\text{H}_2\text{O}/(\text{LiBr}+[\text{PA}][\text{NO}_3])$ at 313.15 K and 333.15 K, and $x_{\text{IL}}/x_{\text{LiBr}} = 0.0205$.



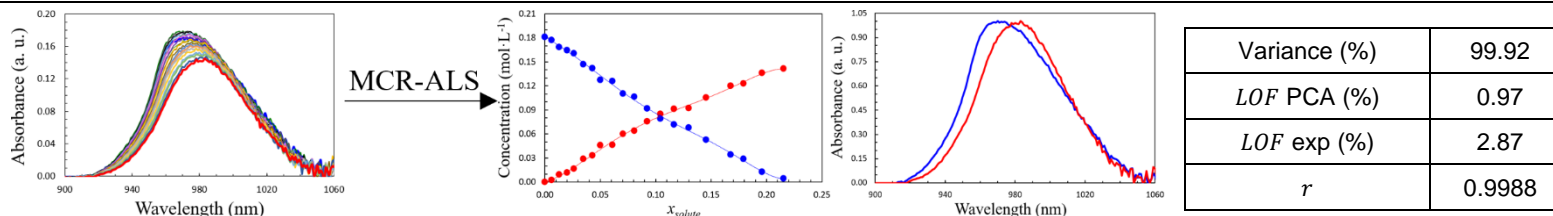
$x_{\text{H}_2\text{O}}$	x_{LiBr}	$x_{[\text{PA}][\text{NO}_3]}$	x_{solute}	BW (%) at 313.15 K	BW (%) at 333.15 K
1	0	0	0	100	100
0.9892	0.0106	0.0002	0.0108	97.2	98.4
0.9778	0.0218	0.0004	0.0222	93.5	93.4
0.9657	0.0336	0.0007	0.0343	82.8	93.0
0.9514	0.0476	0.0010	0.0486	74.7	82.3
0.9361	0.0626	0.0013	0.0639	69.7	76.1
0.9189	0.0795	0.0016	0.0811	62.2	60.9
0.9009	0.0971	0.0020	0.0991	51.7	56.9
0.8799	0.1177	0.0024	0.1201	44.0	45.1
0.8567	0.1404	0.0029	0.1433	37.0	38.0
0.8297	0.1669	0.0034	0.1703	20.3	25.9
0.7991	0.1969	0.0040	0.2009	9.5	12.1
0.7787	0.2169	0.0044	0.2213	0.6	0

Table III.22. MCR-ALS results for $\text{H}_2\text{O}/(\text{LiBr}+[\text{EA}][\text{Cl}])$ at 313.15 K and 333.15 K, and $x_{\text{IL}}/x_{\text{LiBr}} = 0.0205$.



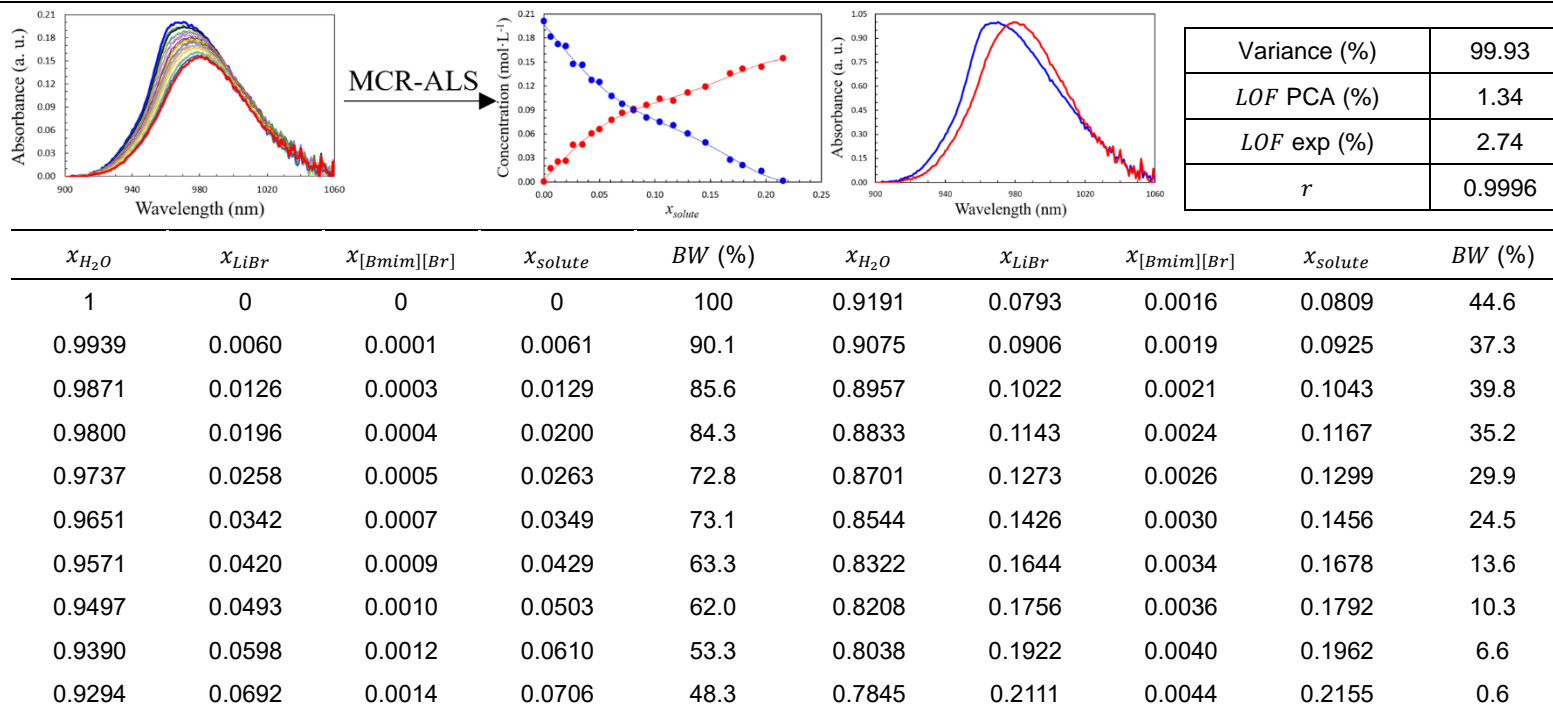
$x_{\text{H}_2\text{O}}$	x_{LiBr}	$x_{[\text{EA}][\text{Cl}]}$	x_{solute}	BW (%) at 313.15 K	BW (%) at 333.15 K
1	0	0	0	100	100
0.9892	0.0106	0.0002	0.0108	94.0	97.1
0.9775	0.0220	0.0005	0.0225	89.4	92.4
0.9647	0.0346	0.0007	0.0353	89.3	87.2
0.9506	0.0484	0.0010	0.0494	81.2	79.6
0.9354	0.0633	0.0013	0.0646	71.2	70.5
0.9183	0.0801	0.0016	0.0817	67.1	65.6
0.8992	0.0988	0.0020	0.1008	55.0	55.1
0.8780	0.1196	0.0024	0.1220	48.1	44.2
0.8547	0.1424	0.0029	0.1453	36.7	34.2
0.8283	0.1683	0.0034	0.1717	26.5	27.9
0.7969	0.1990	0.0041	0.2031	8.9	10.0
0.7769	0.2186	0.0045	0.2231	0	0

Table III.23. MCR-ALS results for the $\text{H}_2\text{O}/(\text{LiBr}+[\text{Bmim}][\text{Br}])$ at 313.15 K and $x_{\text{IL}}/x_{\text{LiBr}} = 0.0208$.



$x_{\text{H}_2\text{O}}$	x_{LiBr}	$x_{[\text{Bmim}][\text{Br}]}$	x_{solute}	BW (%)	$x_{\text{H}_2\text{O}}$	x_{LiBr}	$x_{[\text{Bmim}][\text{Br}]}$	x_{solute}	BW (%)
1	0	0	0	100	0.9191	0.0793	0.0016	0.0809	58.8
0.9939	0.0060	0.0001	0.0061	98.0	0.9075	0.0906	0.0019	0.0925	50.6
0.9871	0.0126	0.0003	0.0129	93.1	0.8957	0.1022	0.0021	0.1043	43.8
0.9800	0.0196	0.0004	0.0200	90.9	0.8833	0.1143	0.0024	0.1167	39.6
0.9737	0.0258	0.0005	0.0263	88.7	0.8701	0.1273	0.0026	0.1299	37.6
0.9651	0.0342	0.0007	0.0349	69.6	0.8544	0.1426	0.0030	0.1456	29.0
0.9571	0.0420	0.0009	0.0429	81.2	0.8322	0.1644	0.0034	0.1678	18.9
0.9497	0.0493	0.0010	0.0503	78.5	0.8208	0.1756	0.0036	0.1792	15.9
0.9390	0.0598	0.0012	0.0610	70.3	0.8038	0.1922	0.0040	0.1962	6.9
0.9294	0.0692	0.0014	0.0706	61.0	0.7845	0.2111	0.0044	0.2155	2.2

Table III.24. MCR-ALS results for the $\text{H}_2\text{O}/(\text{LiBr}+[\text{Bmim}][\text{Br}])$ at 333.15 K and $x_{\text{IL}}/x_{\text{LiBr}} = 0.0208$.



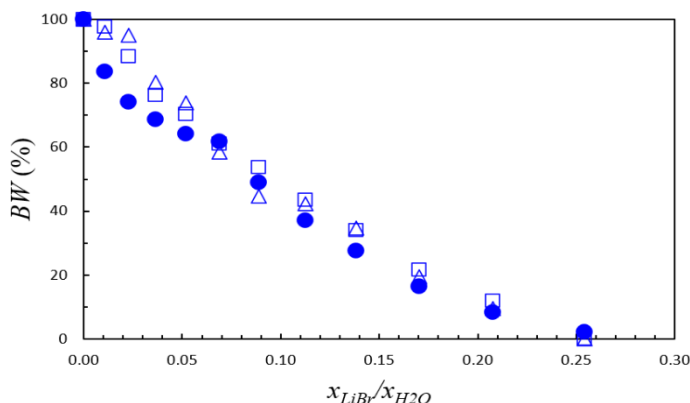


Figure III.15. Bulk water in H₂O/LiBr solutions against mole fraction ratio between LiBr and H₂O. ●: 293.15 K; □: 313.15 K; △: 333.15 K.

The bulk water values in solutions with and without additives determined at 40 °C and 60 °C are shown in Figure III.16 a) and b), respectively. The values at 20 °C were previously shown in Figure III.13. The comparative analysis of these figures reveals that, regardless of temperature, the percentage of bulk water in the H₂O/(LiBr+[Bmim][Br]) mixture is lower than that in mixtures with ionic liquids based on the ammonium cation. At 60 °C, generally, it is observed that the mixture with [Bmim][Br] has slightly lower values of bulk water than H₂O/LiBr, which could indicate a greater water absorption capacity of lithium bromide in the presence of this additive.

To provide information on the influence of temperature, Table III.25 shows the average bulk water difference (ΔBW) of H₂O/(LiBr+L) mixtures with respect to H₂O/LiBr over the entire composition range. In general, although the differences are smaller with increasing temperature, the increase in bulk water depends on the ionic liquid. However, this phenomenon cannot be interpreted solely on the basis of NIR+MCR-ALS, but it could be analysed using computational methods that allow further study of the interactions between ions in these solutions.

Chapter III

Table III.25. Average bulk water difference between H₂O/(LiBr+IL) and H₂O/LiBr mixtures additive at different temperatures.

Mixture	x_{IL}/x_{LiBr}	ΔBW (%)		
		293.15 K	313.15 K	333.15 K
H ₂ O/(LiBr+[EA][NO ₃])	0.0205	13.0	6.9	10.0
H ₂ O/(LiBr+[PA][NO ₃])	0.0205	12.2	7.0	11.4
H ₂ O/(LiBr+[EA][Cl])	0.0205	14.6	10.2	10.7
H ₂ O/(LiBr+[Bmim][Br])	0.0208	7.9	3.6	-2.6

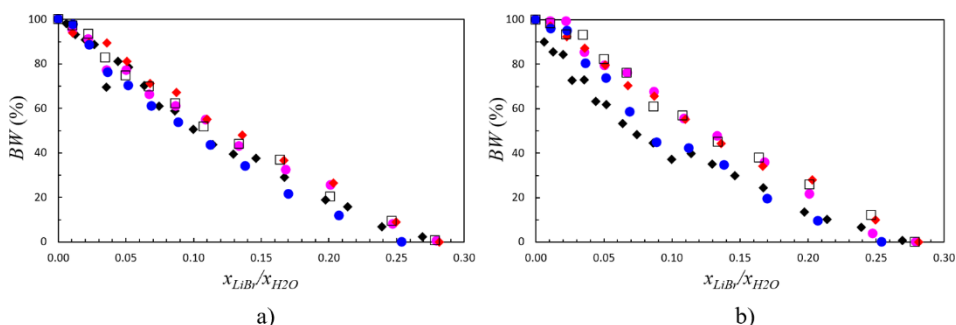


Figure III.16. Bulk water against mole fraction ratio between LiBr and H₂O at a) 313.15 K and b) 333.15 K. ●: H₂O/LiBr; ●: H₂O/(LiBr+[EA][NO₃]) with $x_{IL}/x_{LiBr} = 0.0205$; □: H₂O/(LiBr+[PA][NO₃]) with $x_{IL}/x_{LiBr} = 0.0205$; ◆: H₂O/(LiBr+[EA][Cl]) with $x_{IL}/x_{LiBr} = 0.0205$; ◆: H₂O/(LiBr+[Bmim][Br]) with $x_{IL}/x_{LiBr} = 0.0208$.

III.7. Conclusions

The conclusions drawn in this chapter correspond to the specific objective 1 (Section I.6).

The analytical methodology based on infrared spectroscopy together with the multivariate curve resolution is a useful tool to interpret and quantify the solvation of lithium bromide in aqueous solutions.

Chapter III

In aqueous lithium bromide solutions, water preserves the tridimensional network structure of pure water (bulk water), and water interacts with salt ions.

The values of bulk water in $\text{H}_2\text{O}/\text{LiBr}$ can be used to estimate the vapour pressure of its solutions by means of Raoult's law and a mass balance.

The ratio between the mole fractions of IL and LiBr should be less than 0.0942 to avoid impairing the water absorption capacity of the working fluid in absorption refrigeration and heat pump systems.

The amount of bulk water in $\text{H}_2\text{O}/\text{LiBr}$ solutions with 1,3-dimethylimidazolium chloride is greater than in $\text{H}_2\text{O}/\text{LiBr}$ solutions at 20 °C.

There are no significant differences in the bulk water of $\text{H}_2\text{O}/\text{LiBr}$ mixtures with 1,3-dimethylimidazolium chloride when working with IL to LiBr mole fraction ratios of 0.0202, 0.0418, and 0.0648.

The amount of bulk water in mixtures with protic ionic liquids based on the ammonium cation is higher than in mixtures with aprotic ionic liquids based on the imidazolium cation.

In the analysed mixtures, there are no significant differences between the percentage of bulk obtained at 20 °C, 40 °C, and 60 °C.

The percentage of bulk water in $\text{H}_2\text{O}/(\text{LiBr}+\text{IL})$ mixtures with ethylammonium nitrate, propylammonium nitrate, and ethylammonium chloride is higher than in $\text{H}_2\text{O}/\text{LiBr}$ at 20 °C, 40 °C, and 60 °C.

The percentage of bulk water in $\text{H}_2\text{O}/(\text{LiBr}+\text{IL})$ mixtures with 1-butyl-3-methylimidazolium bromide is higher than that of $\text{H}_2\text{O}/\text{LiBr}$ at 20 °C and 40 °C, and slightly lower at 60 °C.

Based on the requirements of the working fluid shown in Chapter I, the alkyl chain of [Bmim][Br] could negatively affect the transport properties of the working fluid due to its hydrophobicity and the larger size of ionic aggregates, which would be detrimental to the mass diffusion process.

The discussed results have guided the experimental development of the two following chapters, in which the thermophysical properties of $\text{H}_2\text{O}/(\text{LiBr}+\text{IL})$ mixtures are studied with more emphasis on the use of aprotic ionic liquids.

Chapter IV. Solid-liquid and vapour-liquid equilibria of H₂O/(LiBr+IL) mixtures

IV.1. Introduction

The work carried out to determine the solid-liquid and vapour-liquid equilibria of H₂O/(LiBr+IL) mixtures is discussed in this chapter.

Each phase of equilibria starts with an introduction regarding the conditions under which the experiments were carried out. Then, the experimental device and the experimental procedure are described. Subsequently, the phase equilibria of H₂O/LiBr are briefly discussed. Finally, the results are presented, discussed, and compared with those available in the literature.

IV.2. Solid-liquid equilibria

IV.2.1 Introduction

The temperature and composition ranges in which the solid-liquid equilibria (SLE) of H₂O/(LiBr+IL) mixtures were determined are shown in Table IV.1. These temperature and composition ranges are typical of absorption refrigeration and heat pump systems, in which the mass fraction of absorbent (w_{abs}) usually varies from 0.50 to 0.70, and the temperature of the mixture ranges from (30 to 100) °C.^[129–133]

Based on the results discussed in Chapter III, the SLE was determined at a mole fraction ratio between IL and LiBr (x_{IL}/x_{LiBr}) equal to 0.0205 for all the ionic liquids considered as additives of H₂O/LiBr. The solid-liquid equilibria was also determined at two other x_{IL}/x_{LiBr} ratios for the mixtures with aprotic ionic liquids ([Bmim][Br] and [Dmim][Cl]) to analyze the influence of the IL composition on the SLE.

Table IV.1. Summary of the conditions at which the SLE of H₂O/(LiBr+IL) mixtures was determined at atmospheric pressure. w_{abs} : mass fraction of absorbent; w_{IL}/w_{abs} : mass fraction ratio between IL and absorbent; x_{IL}/x_{LiBr} : mole fraction ratio between IL and LiBr.

Mixture	T (K)	w_{abs}	w_{IL}/w_{abs}	x_{IL}/x_{LiBr}
H ₂ O/(LiBr+[EA][NO ₃])	283 – 363	0.59 – 0.70	0.0252	0.0207
H ₂ O/(LiBr+[PA][NO ₃])	303 – 363	0.63 – 0.69	0.0281	0.0206
H ₂ O/(LiBr+ [EA][Cl])	283 – 363	0.59 – 0.70	0.0189	0.0205

Table IV.1. (continued)

$\text{H}_2\text{O}/(\text{LiBr}+[\text{Bmim}][\text{Br}])$	283 – 363	0.59 – 0.70	0.0297	0.0121
			0.0501	0.0209
			0.0706	0.0301
$\text{H}_2\text{O}/(\text{LiBr}+[\text{Dmim}][\text{Cl}])$	283 – 363	0.60 – 0.70	0.0304	0.0205
			0.0611	0.0426
			0.0698	0.0491

The experimental SLE of the mixtures with additive is compared with the SLE of $\text{H}_2\text{O}/\text{LiBr}$ to analyse the influence of each IL on the solid-liquid equilibria.

IV.2.2 Experimental device

The experimental device and its scheme are shown in Figure IV.1. The device consists of a glass cell, a Pt-100 temperature probe, a thermostatic bath, and a magnetic stirrer. The cell has three chambers: an inner chamber, where the phase equilibrium of the mixture to be studied is produced; an intermediate chamber, through which a thermostatic fluid circulates to control the equilibrium temperature; and an outer vacuum chamber, which contributes to thermal insulation and prevents condensation on the outer surface. The magnetic stirrer is introduced into the inner chamber to ensure homogeneous mixing of solute and solvent. The temperature of the mixture is determined with the temperature probe immersed at mid-height.

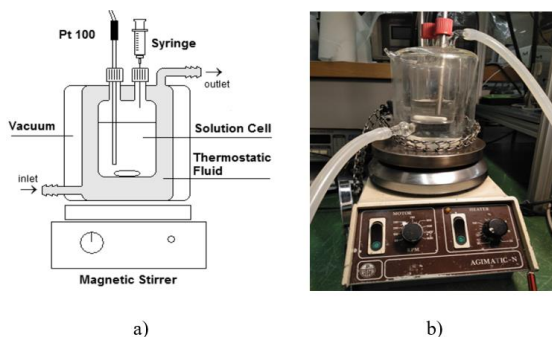


Figure IV.1. Experimental device used to determine the solid-liquid equilibria by means of the visual polythermal method. a) Scheme of the glass cell.^[22]
 b) Experimental setup.

IV.2.3 Experimental procedure

Sample preparation

Lithium bromide and solid-state ionic liquids at room temperature ([Bmim][Br], [Dmim][Cl], and [EA][Cl]) were dried in an oven at 373 K for 24 h before use. Ionic liquids in the liquid state at room temperature, namely [EA][NO₃] and [PA][NO₃], were subjected to vacuum with stirring and heating at 373 K for 24 h before use.

The H₂O/(LiBr+IL) mixtures were prepared by first adding the mass of lithium bromide, determined by means of a Mettler Toledo ME403 balance (resolution = 0.001 g). Then, the necessary amount of water was added to achieve a mass fraction of lithium bromide equal to 0.69 H₂O/LiBr mixture with a mass fraction of lithium bromide around 0.69. Subsequently, the stirrer was added, and the temperature of the thermostatic bath was set to 373 K until all crystals were dissolved. Finally, the required mass of ionic liquid was added to obtain the desired composition of the mixture.

Solid-liquid equilibria determination

To determine the temperature of the SLE at the measured composition, the first step is to precipitate the solid by setting the temperature of the thermostatic bath 5 K below the temperature at which precipitation is observed. The second step consists of increasing the temperature of the thermostatic bath by 0.5 K. The presence or absence of crystals is observed after waiting 15 min, during which the mixture is stirred to ensure thermal equilibrium and homogeneous composition. If crystals are still observed, then the temperature of the thermostatic bath is increased again by 0.5 K, and the process is repeated until no solid phase is observed.

The same procedure is then repeated with 0.1 K increments starting from the last temperature at which the solid phase was observed. The final phase change temperature is obtained as the average between the last temperature at which crystals were observed and the first temperature at which they were not observed.

Once the equilibrium temperature is determined, the mixture is diluted with a known mass of water to reach the next required composition. This process is repeated until the entire composition range is covered.

The inner chamber is washed with hot water, soap, and acetone after finishing the experiments. Then, the glass cell is placed in the oven for drying.

The combined uncertainty in temperature values is 0.06 K. The uncertainty in composition values is 0.001 in the mass fraction of absorbent.

IV.2.4 Reference mixture: H₂O/LiBr

The phase diagram of the H₂O/LiBr mixture at 1 bar is shown in Figure IV.2 with experimental solid-liquid equilibria data obtained from the literature.^[22,25,122,134] This figure represents temperature against lithium bromide mass fraction and illustrates the different phase boundaries of the mixture. For example: at a lithium bromide mass fraction of 0.45, the mixture is in liquid phase (dissolved LiBr) from 220 K onwards. At a LiBr mass fraction of 0.64, the mixture is in liquid phase at 314 K and above. Below each of these temperatures, H₂O/LiBr exists as a two-phase mixture of solid and liquid.

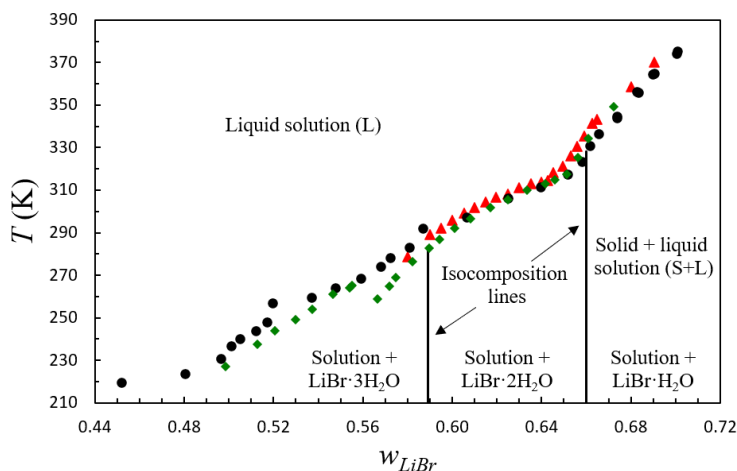


Figure IV.2. Solid-liquid equilibria of the H₂O/LiBr mixture at 1 bar. |: Pátek & Klomfar;^[134] ▲: Salavera *et al.*;^[22] ●: Boryta;^[122] ◆: Królikowska *et al.*^[25]

The SLE of this mixture can be formulated as follows:^[32]

Chapter IV

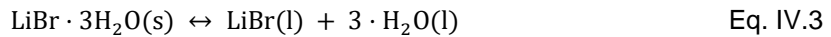
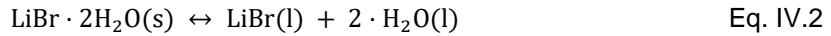
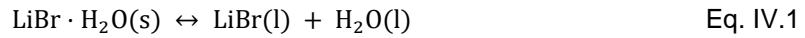


Table IV.2 shows the temperature and composition ranges in which each equilibrium takes place.^[134] These equilibria are represented as isocomposition lines in Figure IV.2, within the region with solid and liquid phases (S+L).

Table IV.2. Solid phase composition of H₂O/LiBr mixtures.^[134]

Solid phase composition	w_{LiBr}	T (K)
LiBr·3H ₂ O	0.482 – 0.589	223 – 277
LiBr·2H ₂ O	0.589 – 0.660	277 – 311
LiBr·H ₂ O	0.660 – 0.805	311 – 431

IV.2.5 Experimental results and discussion

Tables IV.3-IV.5 show the mass fraction of absorbent (LiBr+IL) at which the solid-liquid equilibria were determined along with the equilibrium temperature.

Table IV.3. Mass fraction of absorbent and temperature at the solid-liquid equilibria of H₂O/(LiBr+IL) mixtures using [EA][NO₃], [PA][NO₃] and [EA][Cl].

H ₂ O/(LiBr+[EA][NO ₃]) $w_{IL}/w_{abs} = 0.0252$				H ₂ O/(LiBr+[PA][NO ₃]) $w_{IL}/w_{abs} = 0.0281$				H ₂ O/(LiBr+[EA][Cl]) $w_{IL}/w_{abs} = 0.0189$			
w_{abs}	T (K)	w_{abs}	T (K)	w_{abs}	T (K)	w_{abs}	T (K)	w_{abs}	T (K)	w_{abs}	T (K)
0.696	362.6	0.647	310.0	0.693	359.5	0.663	319.3	0.695	366.3	0.649	312.0
0.692	358.7	0.641	308.0	0.689	355.0	0.661	314.8	0.692	362.9	0.643	310.2
0.689	354.6	0.636	305.7	0.686	351.1	0.658	313.5	0.688	358.9	0.638	308.1
0.685	350.4	0.631	303.4	0.682	346.4	0.654	312.5	0.685	354.8	0.631	304.9
0.681	345.4	0.626	300.8	0.679	341.8	0.650	311.3	0.681	350.4	0.624	301.7
0.677	340.3	0.622	298.2	0.675	337.2	0.646	309.6	0.677	345.8	0.618	298.4
0.673	335.0	0.617	295.5	0.673	333.3	0.642	308.0	0.674	341.0	0.613	295.1
0.670	330.6	0.614	293.4	0.669	328.5	0.638	306.3	0.670	336.3	0.607	291.5
0.667	325.9	0.610	290.9	0.666	323.9	0.633	304.3	0.666	331.0	0.603	288.8
0.664	321.2	0.606	288.5					0.663	325.6	0.599	285.8
0.661	316.3	0.603	285.8					0.659	320.2	0.595	282.9
0.658	314.1	0.599	282.6					0.656	314.6	0.592	279.9
0.656	313.2	0.595	279.3					0.652	313.4		
0.652	312.1										

Table IV.4. Mass fraction of absorbent and temperature at the solid-liquid equilibria of H₂O/(LiBr+[Bmim][Br]) mixtures at different IL/absorbent mass ratios.

H ₂ O/(LiBr+[Bmim][Br])											
$w_{IL}/w_{abs} = 0.0297$				$w_{IL}/w_{abs} = 0.0501$				$w_{IL}/w_{abs} = 0.0706$			
w_{abs}	T (K)	w_{abs}	T (K)	w_{abs}	T (K)	w_{abs}	T (K)	w_{abs}	T (K)	w_{abs}	T (K)
0.696	366.5	0.651	313.5	0.701	365.0	0.662	314.7	0.706	366.0	0.667	314.9
0.692	362.8	0.646	312.1	0.698	361.7	0.658	313.8	0.703	362.7	0.663	313.7
0.689	359.2	0.639	309.2	0.695	357.8	0.655	312.6	0.700	358.9	0.659	312.4
0.685	354.6	0.632	305.9	0.691	353.7	0.649	310.3	0.696	354.8	0.653	310.2
0.681	349.8	0.625	302.9	0.688	349.6	0.643	307.7	0.692	350.2	0.646	307.1
0.677	344.6	0.619	299.5	0.684	345.2	0.637	304.7	0.689	345.7	0.638	303.5
0.673	339.3	0.612	295.1	0.681	340.8	0.630	301.5	0.685	340.9	0.631	299.5
0.669	333.7	0.608	292.7	0.678	336.0	0.623	297.3	0.681	336.0	0.624	295.3
0.665	327.7	0.603	289.1	0.674	331.3	0.617	293.3	0.678	330.7	0.618	291.0
0.661	321.7	0.598	285.2	0.671	326.5	0.610	288.3	0.674	325.0	0.611	286.0
0.658	316.4	0.593	281.0	0.668	321.2	0.605	284.4	0.671	319.4	0.604	280.6
0.654	315.0			0.665	315.9	0.599	280.1	0.669	315.8	0.598	275.4

Table IV.5. Mass fraction of absorbent and temperature at the solid-liquid equilibria of H₂O/(LiBr+[Dmim][Cl]) mixtures at different IL/absorbent mass ratios.

H ₂ O/(LiBr+[Dmim][Cl])											
$w_{IL}/w_{abs} = 0.0304$				$w_{IL}/w_{abs} = 0.0611$				$w_{IL}/w_{abs} = 0.0698$			
w_{abs}	T (K)	w_{abs}	T (K)	w_{abs}	T (K)	w_{abs}	T (K)	w_{abs}	T (K)	w_{abs}	T (K)
0.697	366.6	0.652	312.5	0.694	350.3	0.635	299.7	0.705	361.4	0.663	310.2
0.693	362.6	0.648	311.3	0.680	332.7	0.627	295.4	0.702	357.5	0.660	309.3
0.690	358.6	0.644	309.9	0.672	322.3	0.620	290.9	0.698	353.0	0.654	307.1
0.686	353.8	0.639	307.7	0.665	311.8	0.614	286.9	0.693	348.3	0.647	304.5
0.682	348.9	0.631	304.4	0.659	309.9	0.607	281.5	0.689	343.2	0.641	301.5
0.678	344.5	0.624	300.9	0.652	307.3	0.599	275.3	0.685	337.6	0.635	298.4
0.674	339.2	0.617	296.8	0.643	303.6			0.681	332.0	0.628	294.9
0.670	333.7	0.610	292.1					0.678	328.5	0.622	291.2
0.666	328.5	0.603	287.2					0.675	324.3	0.616	287.3
0.662	322.7	0.598	283.3					0.672	319.5	0.611	283.2
0.659	317.0	0.593	279.5					0.669	314.5	0.607	279.7
0.655	313.6							0.666	311.2		

Chapter IV

The SLE of both H₂O/LiBr and H₂O/(LiBr+IL) mixtures was modelled with a quadratic equation correlating temperature with an absorbent mass fraction (Eq. IV.4).

$$T = p_1 \cdot w_{abs}^2 + p_2 \cdot w_{abs} + p_3 \quad \text{Eq. IV.4}$$

The fitting was carried out in two different regions taking into account the eutectic point, which is observable in all mixtures between 311 K and 315 K and involves a change in the number of water molecules precipitating together with lithium bromide in the solid phase (Table IV.2). The coefficients of Eq. IV.4 are given in Table IV.6. The root mean square error (Eq. IV.5) between the calculated temperature (T_{calc}) and the experimentally obtained temperature (T_{exp}) was minimized in the fit.

$$RMSE = \sqrt{\frac{1}{n} \cdot \sum_{i=1}^n (T_{calc} - T_{exp})^2} \quad \text{Eq. IV.5}$$

Table IV.6. Composition range, coefficients and *RMSE* of the SLE correlation for H₂O/(LiBr+IL) mixtures.

Mixture	w_{IL}/w_{LiBr}	w_{abs} range	p_1 (K)	p_2 (K)	p_3 (K)	<i>RMSE</i> (K)	w_{abs} range	p_1 (K)	p_2 (K)	p_3 (K)	<i>RMSE</i> (K)
H ₂ O/LiBr	-	0.580 – 0.643	-5818	7665	-2210	0.5456	0.643 – 0.690	-5094	7940	-2685	1.491
H ₂ O/(LiBr+[EA][NO ₃])	0.0252	0.595 – 0.658	-3910	5450	-1579	0.4183	0.658 – 0.696	-9198	13800	-4786	0.2438
H ₂ O/(LiBr+[PA][NO ₃])	0.0281	0.633 – 0.661	-2751	3933	-1083	0.1744	0.661 – 0.693	-8180	12450	-4338	0.5086
H ₂ O/(LiBr+[EA][Cl])	0.0189	0.592 – 0.656	-4134	5691	-1640	0.2309	0.656 – 0.695	-7833	11890	-4115	0.4236
	0.0297	0.593 – 0.658	-4073	5628	-1624	0.2945	0.658 – 0.696	-8565	12910	-4471	0.1677
H ₂ O/(LiBr+[Bmim][Br])	0.0501	0.599 – 0.665	-4115	5744	-1684	0.1948	0.665 – 0.701	-9259	13990	-4893	0.4399
	0.0706	0.598 – 0.668	-4274	5979	-1772	0.1465	0.668 – 0.706	-9931	14990	-5267	0.4629
	0.0304	0.593 – 0.655	-4484	6145	-1788	0.1406	0.655 – 0.697	-4184	6944	-2441	0.6262
H ₂ O/(LiBr+[Dmim][Cl])	0.0611	0.599 – 0.665	-4242	5914	-1745	0.1187	0.665 – 0.694	-5512	8813	-3111	0.3687
	0.0698	0.606 – 0.666	-4495	6246	-1855	0.2753	0.666 – 0.705	-6657	10420	-3677	0.4960

For a more comprehensive study, the SLE of $\text{H}_2\text{O}/(\text{LiBr}+\text{IL})$ mixtures have been analysed from three different and complementary points of view: at the same mass fraction of absorbent, at the same $\text{LiBr}/\text{H}_2\text{O}$ mole fraction ratio, and as a function of the chemical structure of the IL.

Solid-liquid equilibria analysis as a function of mass fraction of absorbent

This analysis, done as a function of the mass fraction of absorbent ($\text{LiBr}+\text{IL}$), is the one commonly found in the literature.^[22,135] When representing the absorbent composition as the sum of LiBr and IL , it should be noted that increasing the amount of the latter decreases the amount of the former, which has an immediate effect on the value of the absorbent mass fraction at which the phase change is observed.

Figure IV.3 shows the experimental SLE of $\text{H}_2\text{O}/(\text{LiBr}+\text{IL})$ mixtures along with the SLE of $\text{H}_2\text{O}/\text{LiBr}$ obtained by Salavera *et al.*,^[22] who used the same experimental device as in this work. As expected, a higher amount of absorbent can be dissolved in $\text{H}_2\text{O}/(\text{LiBr}+\text{IL})$ mixtures with respect to $\text{H}_2\text{O}/\text{LiBr}$ over the whole temperature range considered.

The influence of the composition of IL on the solubility can be analysed in $\text{H}_2\text{O}/(\text{LiBr}+[\text{Dmim}][\text{Cl}])$ and $\text{H}_2\text{O}/(\text{LiBr}+[\text{Bmim}][\text{Br}])$ mixtures. It is observed that the greater the amount of ionic liquid in the absorbent, the greater the amount of absorbent that can be dissolved in water at the same temperature. However, the solubility increase is not directly proportional to the IL composition, which suggests the existence of interactions between $\text{IL}-\text{H}_2\text{O}$ and $\text{IL}-\text{LiBr}$ that modify the solubility. This interpretation is in agreement with the findings discussed in Chapter III and with Królikowska *et al.*^[25] and Królikowska and Hofman^[32], who explained that the solubility increase in the presence of ILs as additives can be attributed to the interactions between lithium bromide and the ionic liquids.

Interpreting the SLE from the point of view of the absorbent composition is difficult because the observed greater solubility of $\text{H}_2\text{O}/(\text{LiBr}+\text{IL})$ mixtures is related to both the interactions between ions and molecules in the mixture and the replacement of part of the LiBr for IL . For this reason, in order to analyse the influence of the selected ionic liquids as additives on the solubility of lithium bromide in water, the mole ratio between lithium bromide and water is taken as a reference. From this point of view,

the analysis is independent of the nature of the IL in the absorbent and its composition. To the best of my knowledge, this is the first time that the SLE results have been analysed from this point of view.

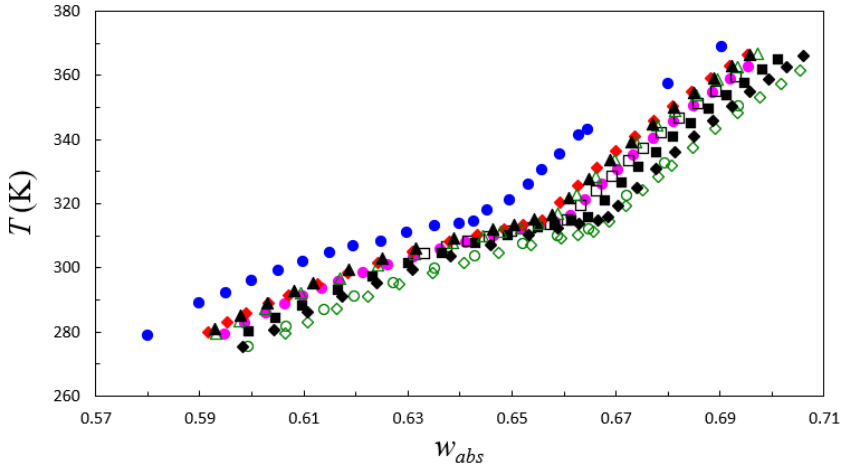


Figure IV.3. Solid-liquid equilibria of $\text{H}_2\text{O}/\text{LiBr}$ and $\text{H}_2\text{O}/(\text{LiBr}+\text{IL})$ mixtures. ●: $\text{H}_2\text{O}/\text{LiBr}$;^[22] ●: $\text{H}_2\text{O}/(\text{LiBr}+[\text{EA}][\text{NO}_3])$ with $w_{\text{IL}}/w_{\text{abs}} = 0.0501$; □: $\text{H}_2\text{O}/(\text{LiBr}+[\text{PA}][\text{NO}_3])$ with $w_{\text{IL}}/w_{\text{abs}} = 0.0501$; ◆: $\text{H}_2\text{O}/(\text{LiBr}+[\text{EA}][\text{Cl}])$ with $w_{\text{IL}}/w_{\text{abs}} = 0.0501$; ▲: $\text{H}_2\text{O}/(\text{LiBr}+[\text{Bmim}][\text{Br}])$ with $w_{\text{IL}}/w_{\text{abs}} = 0.0297$; ■: $\text{H}_2\text{O}/(\text{LiBr}+[\text{Bmim}][\text{Br}])$ with $w_{\text{IL}}/w_{\text{abs}} = 0.0501$; ◆: $\text{H}_2\text{O}/(\text{LiBr}+[\text{Bmim}][\text{Br}])$ with $w_{\text{IL}}/w_{\text{abs}} = 0.0706$; △: $\text{H}_2\text{O}/(\text{LiBr}+[\text{Dmim}][\text{Cl}])$ with $w_{\text{IL}}/w_{\text{abs}} = 0.0303$; ○: $\text{H}_2\text{O}/(\text{LiBr}+[\text{Dmim}][\text{Cl}])$ with $w_{\text{IL}}/w_{\text{abs}} = 0.0611$; ◇: $\text{H}_2\text{O}/(\text{LiBr}+[\text{Dmim}][\text{Cl}])$ with $w_{\text{IL}}/w_{\text{abs}} = 0.0698$.

Solid-liquid equilibria analysis as a function of $\text{LiBr}/\text{H}_2\text{O}$ mole ratio

Figure IV.4 shows the results for the mixtures with additive at $x_{\text{IL}}/x_{\text{LiBr}} \approx 0.0205$. It can be observed that all mixtures with additive have a higher $x_{\text{LiBr}}/x_{\text{H}_2\text{O}}$ ratio than $\text{H}_2\text{O}/\text{LiBr}$ over the entire temperature range.

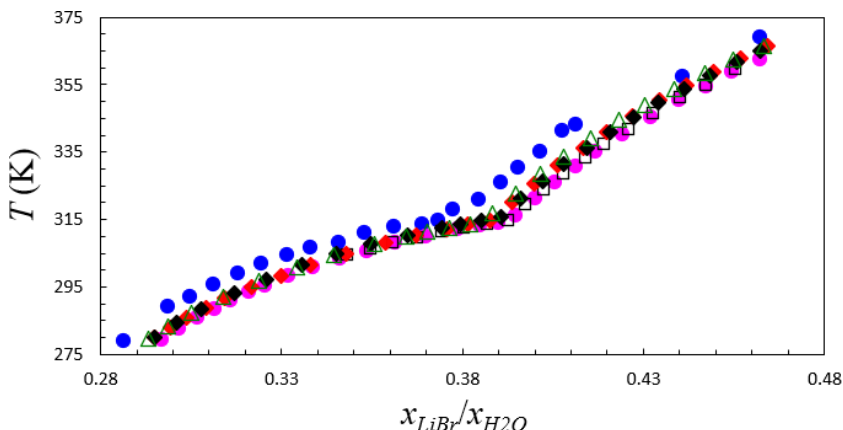


Figure IV.4. Solid-liquid equilibria of $\text{H}_2\text{O}/\text{LiBr}$ and $\text{H}_2\text{O}/(\text{LiBr}+\text{IL})$ mixtures at a similar $x_{\text{IL}}/x_{\text{LiBr}}$ ratio. ●: $\text{H}_2\text{O}/\text{LiBr}$;^[22] ●: $\text{H}_2\text{O}/(\text{LiBr}+[\text{EA}][\text{NO}_3])$ with $x_{\text{IL}}/x_{\text{LiBr}} = 0.0207$; □: $\text{H}_2\text{O}/(\text{LiBr}+[\text{PA}][\text{NO}_3])$ with $x_{\text{IL}}/x_{\text{LiBr}} = 0.0206$; ◆: $\text{H}_2\text{O}/(\text{LiBr}+[\text{EA}][\text{Cl}])$ with $x_{\text{IL}}/x_{\text{LiBr}} = 0.0205$; ◆: $\text{H}_2\text{O}/(\text{LiBr}+[\text{Bmim}][\text{Br}])$ with $x_{\text{IL}}/x_{\text{LiBr}} = 0.0209$; △: $\text{H}_2\text{O}/(\text{LiBr}+[\text{Dmim}][\text{Cl}])$ with $x_{\text{IL}}/x_{\text{LiBr}} = 0.0205$.

For instance: at 308 K, the $x_{\text{LiBr}}/x_{\text{H}_2\text{O}}$ ratio for the $\text{H}_2\text{O}/(\text{LiBr}+[\text{EA}][\text{NO}_3])$ mixture is 0.362, while for the $\text{H}_2\text{O}/\text{LiBr}$ mixture it is 0.346, i.e., more moles of LiBr can be dissolved per mole of water in the presence of IL. This comparison provides evidence that the solute-solute, solute-solvent, and solvent-solvent interactions in the mixtures with additive are different from those in the mixture without additive.

At $x_{\text{IL}}/x_{\text{LiBr}} \approx 0.0205$, even though there are not significant differences, the solubility of lithium bromide in water is slightly more increased with protic ILs ($[\text{EA}][\text{NO}_3]$, $[\text{PA}][\text{NO}_3]$, and $[\text{EA}][\text{Cl}]$) than with aprotic ILs ($[\text{Dmim}][\text{Cl}]$ and $[\text{Bmim}][\text{Br}]$). These results agree with those discussed in Section III.5.3 since the mixtures with protic ILs, which have a greater amount of bulk water, are more soluble than the mixtures with aprotic ILs which have a lower amount of bulk water.

The influence of the ionic liquid composition can be visualized in Figure IV.5, where the SLE of $\text{H}_2\text{O}/(\text{LiBr}+[\text{Bmim}][\text{Br}])$ and $\text{H}_2\text{O}/(\text{LiBr}+[\text{Dmim}][\text{Cl}])$ are plotted with different $x_{\text{IL}}/x_{\text{LiBr}}$. It is clearly observed that the solubility is not directly proportional to the amount of ionic liquid in the absorbent. On one hand, for the mixtures with $[\text{Bmim}][\text{Br}]$, it is observed that the maximum solubility increase of LiBr in H_2O happens

Chapter IV

at $x_{IL}/x_{LiBr} = 0.0209$, and that it slightly decreases at $x_{IL}/x_{LiBr} = 0.0301$. On the other hand, for the mixtures with [Dmim][Cl], there are not significant differences between the LiBr/H₂O ratio at $x_{IL}/x_{LiBr} = 0.0426$ and 0.0491 .

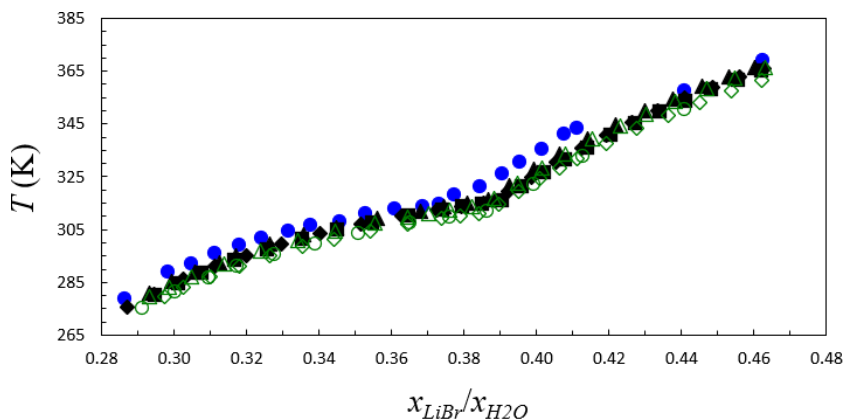


Figure IV.5. Solid-liquid equilibria of H₂O/LiBr and H₂O/(LiBr+IL) mixtures at different x_{IL}/x_{LiBr} ratios. ●: H₂O/LiBr;^[22] ▲: H₂O/(LiBr+[Bmim][Br]) with $x_{IL}/x_{LiBr} = 0.0121$; ■: H₂O/(LiBr+[Bmim][Br]) with $x_{IL}/x_{LiBr} = 0.0209$; ◆: H₂O/(LiBr+[Bmim][Br]) with $x_{IL}/x_{LiBr} = 0.0301$; △: H₂O/(LiBr+[Dmim][Cl]) with $x_{IL}/x_{LiBr} = 0.0205$; ○: H₂O/(LiBr+[Dmim][Cl]) with $x_{IL}/x_{LiBr} = 0.0426$; ◇: H₂O/(LiBr+[Dmim][Cl]) with $x_{IL}/x_{LiBr} = 0.0491$.

To facilitate the analysis, the x_{LiBr}/x_{H_2O} difference between the mixtures with and without additive is analysed in relative terms using Eq. IV.6.

$$\Delta x/x (\%) = 100 \cdot \frac{\left(\frac{x_{LiBr}}{x_{H_2O}}\right)_{H_2O/(LiBr+IL)} - \left(\frac{x_{LiBr}}{x_{H_2O}}\right)_{H_2O/LiBr}}{\left(\frac{x_{LiBr}}{x_{H_2O}}\right)_{H_2O/LiBr}} \quad \text{Eq. IV.6}$$

The results of this comparison are shown in Figure IV.6, where an increase in the solubility is observed in the presence of ionic liquids. The increase in solubility depends on temperature, which is not surprising considering that structural properties of ionic liquids and chemical species in the medium are temperature-dependent.^[136] The solubility change observed between 311 K and 315 K is consistent with the small

Chapter IV

transition temperature difference between lithium bromide dihydrate and monohydrate in the presence of ILs.^[25,32]

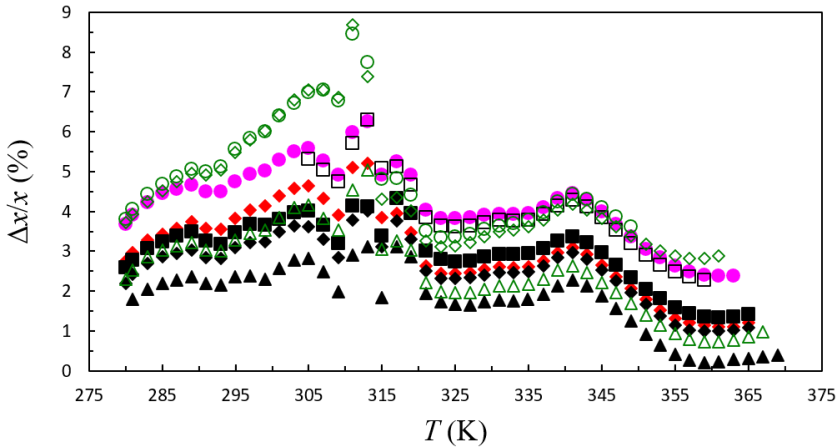


Figure IV.6. Relative LiBr/H₂O mole ratio difference between H₂O/(LiBr+IL) mixtures and H₂O/LiBr. ●: H₂O/(LiBr+[EA][NO₃]); □: H₂O/(LiBr+[PA][NO₃]); ◆: H₂O/(LiBr+[EA][Cl]); ▲: H₂O/(LiBr+[Bmim][Br]) with $w_{IL}/w_{abs} = 0.0297$; ■: H₂O/(LiBr+[Bmim][Br]) with $w_{IL}/w_{abs} = 0.0501$; ◆: H₂O/(LiBr+[Bmim][Br]) with $w_{IL}/w_{abs} = 0.0706$; △: H₂O/(LiBr+[Dmim][Cl]) with $w_{IL}/w_{abs} = 0.0304$; ○: H₂O/(LiBr+[Dmim][Cl]) with $w_{IL}/w_{abs} = 0.0611$; ◇: H₂O/(LiBr+[Dmim][Cl]) with $w_{IL}/w_{abs} = 0.0698$.

As a summary, Table IV.7 shows the average relative increase in the x_{LiBr}/x_{H_2O} ratio as a function of temperature and IL composition for each mixture.

Table IV.7. Summary of the average relative increase in x_{LiBr}/x_{H_2O} as a function of x_{IL}/x_{LiBr} and temperature. w_{IL}/w_{abs} : mass fraction ratio between ionic liquid and absorbent.

Mixture	w_{IL}/w_{abs}	x_{IL}/x_{LiBr}	$\Delta x/x$ (%)	
			(280 – 311) K	(311 – 365) K
H ₂ O/(LiBr+[EA][NO ₃])	0.0252	0.0207	4.8	3.9
H ₂ O/(LiBr+[PA][NO ₃])	0.0281	0.0206	4.6*	3.8*
H ₂ O/(LiBr+[EA][Cl])	0.0189	0.0205	3.9	2.5

*: Unavailable data in the whole temperature range considered.

Table IV.7 (continued)

H ₂ O/(LiBr+[Bmim][Br])	0.0297	0.0121	2.3	1.6
	0.0501	0.0209	3.5	2.7
	0.0706	0.0301	3.1	2.3
H ₂ O/(LiBr+[Dmim][Cl])	0.0304	0.0205	3.4	2.0
	0.0611	0.0426	5.7	4.3*
	0.0698	0.0491	5.7	3.8

*: Unavailable data in the whole temperature range considered.

Influence of the chemical structure of the ionic liquid on the solid-liquid equilibria

The results shown in the previous sections show that the changes in the solubility depend on the nature of the ionic liquid, its composition in the mixture, and the temperature.

It is striking to observe an increase in solubility in H₂O/(LiBr+IL) mixtures with [Bmim][Br], where the ionic liquid and lithium bromide have a common ion. This fact suggests that there is an interaction between the lithium cation and the cation of the ionic liquid that cancels the effect of the common ion. It is likely that this effect is occurring with the other ILs as well. Its significance can be visualized by performing a comparative analysis of the results shown in Figure IV.6 at $x_{IL}/x_{LiBr} \approx 0.0205$.

On one hand, the difference between the cations of [EA][NO₃] and [PA][NO₃] lies only in the size of the alkyl chain. Although the increase in the x_{LiBr}/x_{H_2O} ratio is slightly higher with [EA][NO₃] than with [PA][NO₃] (Table IV.7), the differences are not significant for the IL compositions used in this thesis. However, it is believed that the propyl group, which is larger than the ethyl group, is associated with a higher hydrophobicity that is not beneficial to dissolve more lithium bromide in water.^[25,32]

On the other hand, the difference between the cation of [EA][Cl] and [Dmim][Cl] lies simultaneously in the cation base – ammonium vs. imidazolium – and in the length of the alkyl chain. The experimental results evidence significant differences between these two additives in the solubility of LiBr in H₂O. Interpreting these differences is not simple because it requires information regarding interactions in the solution.

IV.2.6 Comparison of results with the literature

The number of studies where the SLE of H₂O/(LiBr+IL) mixtures has been experimentally determined is scarce, and the mass ratio between IL and absorbent varies from 0.1 to 0.3 in all of them, as was shown in Table I.3, which is considerably higher than the IL/absorbent mass ratios considered in this work (varying from 0.02 to 0.07).

The solubility comparison in these references was carried out as a function of the mass fraction of absorbent, either with mass fraction or mole fraction. However, as was discussed in the previous section, the most effective point of view for analysing the influence of ILs on the solubility of lithium bromide in water is based on the comparison of the mole fraction ratio between LiBr and H₂O.

For this purpose, the relative x_{LiBr}/x_{H_2O} differences between mixtures with and without additive (Eq. IV.6) have been quantified for the data available in the literature. The results are shown in Table IV.8.

Table IV.8. Summary of the average relative differences in x_{LiBr}/x_{H_2O} as a function of x_{IL}/x_{LiBr} and T for the SLE of H₂O/(LiBr+IL) found in the literature.^[25,32–34]

Mixture of H ₂ O/(LiBr+IL)	w_{IL}/w_{abs}	x_{IL}/x_{LiBr}	$\Delta x/x$ (%)	
			(280 – 311) K	(311 – 350) K
[Bmim][Br] ^[32,34]	0.108	0.048	3.8	7.6
	0.125	0.057	14.7*	12.4
	0.200	0.099	22.8*	25.9*
	0.201	0.100	6.8	8.0
	0.300	0.170	6.2	7.9
[C ₁ C ₂ MOR][Br] ^[32]	0.107	0.050	5.7	5.6
	0.207	0.108	9.7	10.2*
	0.297	0.175	14.5	15.2
[C ₁ C ₂ PIP][Br] ^[32]	0.100	0.047	3.7	3.4
	0.200	0.104	3.3	1.6*
	0.301	0.179	7.1	7.9*

*: Unavailable data in the whole temperature range considered.

Chapter IV

Table IV.8 (continued)

Mixture of H ₂ O/(LiBr+IL)	w_{IL}/w_{abs}	x_{IL}/x_{LiBr}	$\Delta x/x$ (%)	
			(280 – 311) K	(311 – 350) K
[C ₁ C ₄ MOR][Br] ^[32]	0.100	0.041	5.3	5.2
	0.202	0.092	6.9	10.8*
	0.307	0.162	10.9	12.7
[C ₁ C ₄ PIP][Br] ^[32]	0.102	0.042	4.3	4.5
	0.200	0.092	3.8	4.4*
	0.300	0.157	3.9	3.9
[C ₁ C ₄ PYR][Br] ^[32]	0.100	0.044	4.9	4.6
	0.200	0.098	6.2	7.3*
	0.301	0.168	3.5	5.0
[C ₁ C ₆ MOR][Br] ^[32]	0.100	0.036	4.7	4.6
	0.200	0.081	8.0	9.5
	0.301	0.141	7.8	9.4*
[C ₄ Py][Br] ^[32]	0.101	0.045	4.8	4.3
	0.201	0.101	4.1	5.7
	0.301	0.173	4.8	6.2*
[Emim][Cl] ^[33]	0.286	0.237	34.3	–
[IM _{1,2OH}][Br] ^[25]	0.300	0.180	12.9	15.4*
[MOR _{1,1(OOC)2}][Br] ^[25]	0.300	0.139	13.7	16.5*
[MOR _{1,1,2OH}][Br] ^[25]	0.301	0.165	16.4	20.5*
[MOR _{1,2(OOC)1}][Br] ^[25]	0.300	0.139	14.9	19.8
[N _{1,1,2OH,2OH}][Br] ^[25]	0.100	0.045	-8.3	-10.9
	0.200	0.101	13.5	14.9
	0.300	0.174	21.5	23.9
[N _{1,1,2OH,4}][Br] ^[25]	0.099	0.042	5.0	5.9
	0.200	0.096	6.8	8.2
	0.300	0.164	11.0	12.9

*: See note on previous page.

Chapter IV

Table IV.8 (continued)

Mixture of H ₂ O/(LiBr+IL)	w_{IL}/w_{abs}	x_{LiBr}/x_{LiBr}	$\Delta x/x$ (%)	
			(280 – 311) K	(280 – 311) K
[N _{2,2,2,1CN}][Br] ^[25]	0.100	0.044	-2.3	-2.0*
	0.200	0.098	-9.0	10.4
	0.300	0.169	-25.9	3.8*
[N _{2,2,2,2OH}][Br] ^[25]	0.100	0.043	6.2	7.5
	0.200	0.096	8.0	9.0
	0.300	0.165	12.1	14.5*
[N _{2,2,2,4}][Br] ^[32]	0.100	0.041	5.8	3.7
	0.200	0.091	3.5	4.7
	0.300	0.157	2.0	2.5
[Py ₂ OH][Br] ^[25]	0.300	0.182	12.2	14.2
[PYR _{1,2OH}][Br] ^[25]	0.301	0.178	14.2	18.5

*: Unavailable data in the whole temperature range considered.

Most of the ionic liquids listed in Table IV.8 increase the solubility of LiBr in H₂O, both when LiBr precipitates with two water molecules (275 K < T < 311 K) and with one water molecule (311 K < T < 431 K). The exceptions are the mixtures with [N_{1,1,1,2OH,2OH}][Br] at $x_{LiBr}/x_{LiBr} = 0.042$ and [N_{2,2,2,1CN}][Br] at $x_{LiBr}/x_{LiBr} = 0.044$ and temperatures ranging from (280 to 311) K.

In the data reported in the literature, the increase in solubility of lithium bromide in water is usually higher in the monohydrate region than in the dihydrate region, contrary to what was observed when analysing the experimental results of this PhD thesis. This may be because the composition of IL is considerably higher in the data published in the literature than in those shown in this work.

It can be observed in Table IV.8 that the influence of the IL composition in the absorbent also shows a limit in the solubility increase, which is consistent with the results discussed in this work.

Figure IV.7 shows the relative x_{LiBr}/x_{H_2O} difference between of different H₂O/(LiBr+[Bmim][Br]) mixtures with respect to H₂O/LiBr as a function of [Bmim][Br] composition and temperature. The increase in solubility of LiBr in H₂O is not

proportional to the composition of IL in the absorbent, as was discussed in previous sections. The x_{IL}/x_{LiBr} ratios, ordered from highest to lowest increase in solubility of LiBr in H₂O, are: 0.100 > 0.170 > 0.048 > 0.021 > 0.030 > 0.012. It is also noteworthy mentioning that the increase in the solubility of LiBr in the two mixtures with the highest [Bmim][Br] composition is greater than that produced by the rest of IL compositions.

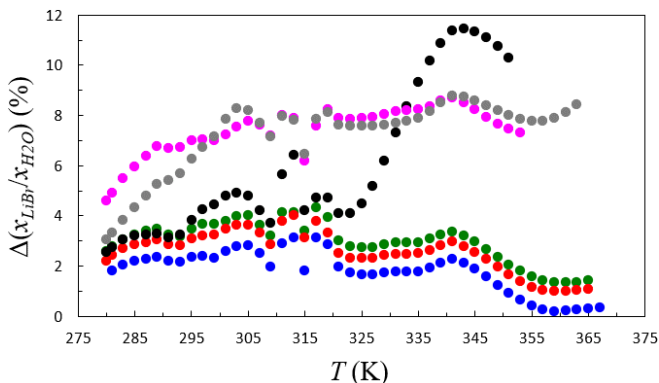


Figure IV.7. Influence of the amount of [Bmim][Br] on the solubility of LiBr in H₂O.

●: $x_{IL}/x_{LiBr} = 0.0121$, ●: $x_{IL}/x_{LiBr} = 0.0209$, ●: $x_{IL}/x_{LiBr} = 0.0301$;
 ●: $x_{IL}/x_{LiBr} = 0.048$, ●: $x_{IL}/x_{LiBr} = 0.100$, ●: $x_{IL}/x_{LiBr} = 0.170$.

IV.3. Vapour-liquid equilibria

IV.3.1 Introduction

Table IV.9 shows the composition and temperature ranges in which the vapour-liquid equilibria (VLE) of H₂O/(LiBr+IL) mixtures were determined. These conditions are typical of absorption refrigeration and heat pump systems. Based on the results obtained for solvation and solubility, the number of cases under study to determine the VLE was reduced, limiting it to the two aprotic ILs ([Bmim][Br] and [Dmim][Cl]), and the most promising protic ionic liquid ([EA][NO₃]).

Chapter IV

To evaluate the influence of the ionic liquid composition on the vapour pressure of H₂O/LiBr, this property was determined at two x_{IL}/x_{LiBr} ratios in H₂O/(LiBr+[Dmim][Cl]) mixtures.

Table IV.9. Summary of the conditions at which the vapor-liquid equilibria was determined for H₂O/(LiBr+IL) mixtures. x_{IL}/x_{LiBr} : mole fraction ratio between IL and LiBr; T : temperature; w_{abs} : mass fraction of absorbent; x_{abs} : mole fraction of absorbent.

Mixture	x_{IL}/x_{LiBr}	T (K)	w_{abs}	x_{abs}
H ₂ O/(LiBr+[EA][NO ₃])	0.0205	293 – 353	0.45 – 0.65	0.14 – 0.28
H ₂ O/(LiBr+[Bmim][Br])	0.0205	293 – 353	0.45 – 0.65	0.14 – 0.27
H ₂ O/(LiBr+[Dmim][Cl])	0.0204	293 – 353	0.45 – 0.65	0.17 – 0.28
	0.0427	293 – 393	0.44 – 0.62	0.14 – 0.25

IV.3.2 Experimental device

The device used to determine the vapour-liquid equilibrium is based on a static, isothermal, isochoric, synthetic method.^[137,138] It consists of an equilibrium cell (Figure IV.8) with an internal volume of approximately 10 mL made of stainless steel to withstand low and high pressures and temperatures, a magnetic stirrer, a Pt-100 temperature probe, a Druck pressure transducer (mod. UNIK5000) calibrated in the range from (0 to 1) bar and directly connected to the equilibrium cell, and a Julabo thermostatic bath (mod. SE) to keep the temperature constant.

The temperature probe was calibrated following the ITS-90 procedure.^[139] The pressure transducer was calibrated using the vapour pressure of pure water between 283.15 K and 353.15 K as the reference. The estimated uncertainties with a 95 % confidence level ($k = 2$) are $U(w_{abs}) = 0.001$, $U(T) = 0.05$ K, and $U(p) = 0.01$ kPa.

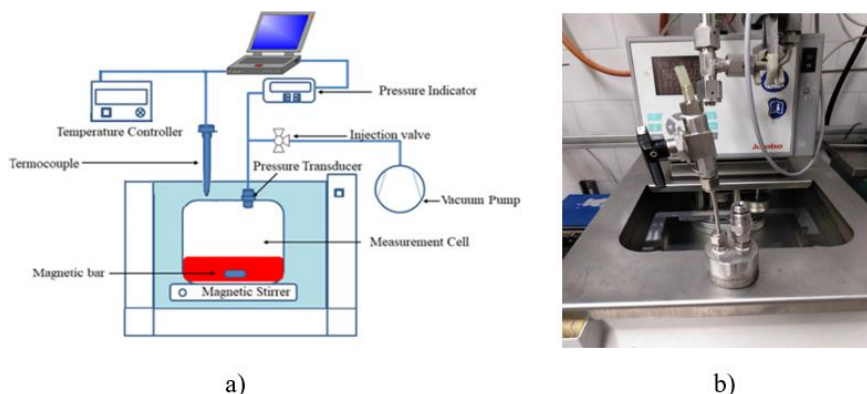


Figure IV.8. Experimental device used to determine the vapour-liquid equilibria by means of the static, isothermal, isochoric, synthetic, and variable pressure methods. a) Scheme of the system. b) Experimental setup.

IV.3.3 Experimental procedure

Sample preparation

The $\text{H}_2\text{O}/(\text{LiBr}+\text{IL})$ solutions are prepared outside the equilibrium cell. First, approximately 30 mL of the solution with the highest absorbent composition ($w_{abs} \approx 0.65$) are prepared by adding the estimated amount of lithium bromide. Then, the required amount of additive (IL) is used to reach the desired LiBr/IL ratio. Finally, the necessary amount of water is added. From this initial solution, successive solutions with lower absorbent composition are obtained by adding pure water.

The initial solution is stirred inside a closed vessel at 60 °C to achieve a homogeneous composition and avoid salt crystallisation. The rest of the solutions are stirred and heated at 40 °C for a minimum of 20 min before being introduced in the equilibrium cell.

Once the sample to be measured is ready, 5 mL of solution are introduced into the equilibrium cell using a syringe. The mass of the introduced sample is determined by weight difference with a Mettler Toledo ME403 analytical balance. Then, a magnetic stirrer is introduced, and the equilibrium cell is connected to the pressure transducer. The sample is finally degassed to remove the content of non-condensable gases,

especially air. The degassing process is carried out in three stages: 1) freezing, 2) vacuum, and 3) liquefaction.

Freezing of the solution is achieved by immersing the cell in liquid nitrogen for 15 min. Then, non-condensable gases are removed by applying vacuum for another 15 min while keeping the cell immersed in liquid nitrogen. Finally, the cell is immersed in a thermostatic bath at 50 °C for 20 min with constant stirring to liquefy the sample and evaporate any traces of air dissolved in the liquid phase. The degassing process is repeated three times to ensure that no air remains inside the cell.

Vapour-liquid equilibria determination

The VLE was determined between 20 °C and 120 °C each 10 °C, always starting at the highest temperature. To ensure thermodynamic equilibrium, the equilibrium cell was kept at constant temperature for 2 h. Pressure and temperature data were automatically recorded using an Agilent 34970A connected to a computer through a program created for these measurements with Keysight VEE software (version 9).

Regarding composition, it has been assumed that the composition of the liquid phase corresponds to the global composition, calculated from the masses added for each of the components of the mixture. This assumption is based on the fact that the estimated uncertainty of the composition is 0.001 in mass fraction of absorbent, while the variation in the composition over the temperature range considered has been estimated to be less than 0.0002 in mass fraction.

Once the experiments at each composition are finished, the equilibrium cell is removed from the experimental device and washed with hot water, soap, and acetone. Finally, it is placed in an oven at 80 °C for drying and subsequent use.

IV.3.4 Reference mixture: H₂O/LiBr

The pressure-temperature-composition diagram of the H₂O/LiBr mixture is plotted in Figure IV.9 with calculated values.^[123] The lines represent the equilibrium pressure as a function of temperature for different LiBr compositions and pure water. It is observed that the higher the temperature, the higher the equilibrium pressure, and the higher the mass fraction of lithium bromide, the lower the pressure. For example: the equilibrium pressure at $w_{LiBr} = 0.45$ and 293.15 K is 0.877 kPa. At that

Chapter IV

composition and temperature, if the pressure is higher than 0.877 kPa, the solution is a subcooled liquid, while if it is lower, the solution is a two-phase mixture of liquid and vapour. The crystallisation line, also included in Figure IV.9, represents SLE of the mixture and, therefore, indicates the operation limit for absorption refrigeration systems and heat pumps.

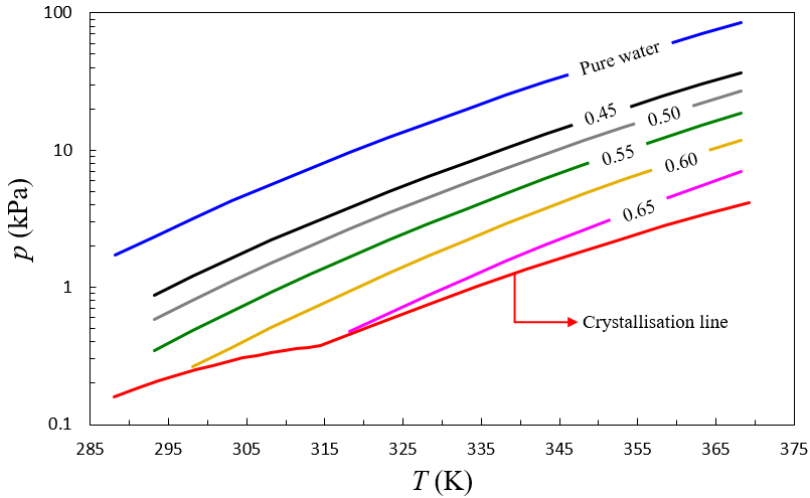


Figure IV.9. Pressure-temperature-composition phase diagram for the H₂O/LiBr mixture.^[123] —: Pure water;^[140] —: $w_{LiBr} = 0.45$; —: $w_{LiBr} = 0.50$; —: $w_{LiBr} = 0.55$; —: $w_{LiBr} = 0.60$; —: $w_{LiBr} = 0.65$; —: Crystallisation line.

In these solutions, lithium bromide is considered to be non-volatile,^[9] which means that the vapour-liquid equilibrium is established only with water (Eq. IV.7).



IV.3.5 Experimental results and discussion

Tables IV.10-IV.13 show the pressure values determined at the vapour-liquid equilibrium depending on the temperature and mass fraction of the absorbent.

Table IV.10. Vapour pressure of the H₂O/(LiBr+[EA][NO₃]) mixture with $x_{iL}/x_{LiBr} = 0.0205$.

w_{abs}	x_{abs}	p (kPa)						
		T (K)						
		293.15	303.15	313.15	323.15	333.15	343.15	353.15
0.449	0.144	0.99	1.86	3.20	5.55	9.13	14.41	22.31
0.555	0.205	0.43	0.84	1.44	2.46	4.14	6.71	10.27
0.648	0.275	-	-	0.59	1.08	1.70	2.66	4.38

Table IV.11. Vapour pressure of the H₂O/(LiBr+[Bmim][Br]) mixture with $x_{iL}/x_{LiBr} = 0.0205$.

w_{abs}	x_{abs}	p (kPa)						
		T (K)						
		293.15	303.15	313.15	323.15	333.15	343.15	353.15
0.450	0.141	1.01	1.86	3.23	5.40	8.77	13.90	21.32
0.500	0.168	0.77	1.39	2.37	3.93	6.36	10.08	15.57
0.550	0.197	0.43	0.84	1.49	2.53	4.17	6.72	10.51
0.599	0.231	0.27	0.50	0.89	1.50	2.52	4.11	6.49
0.650	0.272	-	-	0.56	0.91	1.48	2.37	3.77

Table IV.12. Vapour pressure of the H₂O/(LiBr+[Dmim][Cl]) mixture with $x_{iL}/x_{LiBr} = 0.0204$.

w_{abs}	x_{abs}	p (kPa)							
		T (K)							
		293.15	303.15	313.15	323.15	333.15	343.15	353.15	
0.450	0.144	1.12	1.96	3.32	5.48	8.83	13.91	21.43	
0.500	0.170	0.90	1.50	2.42	3.95	6.35	9.99	15.33	
0.550	0.201	0.55	0.94	1.56	2.56	4.12	6.56	10.20	
0.599	0.235	0.31	0.53	0.88	1.47	2.43	3.99	6.26	
0.650	0.276	-	-	0.55	0.89	1.46	2.37	3.74	

Table IV.13. Vapour pressure of the H₂O/(LiBr+[Dmim][Cl]) mixture with $x_{iL}/x_{LiBr} = 0.0427$.

w_{abs}	x_{abs}	p (kPa)								
		T (K)								
		293.15	303.15	313.15	323.15	333.15	343.15	353.15	373.15	393.15
0.443	0.139	0.90	1.66	2.86	4.87	8.01	12.53	19.40	42.22	85.69
0.474	0.155	0.69	1.26	2.37	4.11	6.81	10.60	16.01	34.02	69.51
0.519	0.180	0.52	0.99	1.68	2.95	4.85	8.01	12.22	25.65	51.95
0.576	0.216	0.29	0.57	1.00	1.60	2.73	4.29	6.61	15.81	32.58
0.622	0.251	-	-	0.53	0.96	1.50	2.40	3.98	9.30	20.83

Chapter IV

The VLE of $\text{H}_2\text{O}/(\text{LiBr}+\text{IL})$ mixtures has been modelled as a function of temperature and composition with two different correlations (Eqs. IV.8-IV.9), where p_0 and T_{ref} are 1 kPa and 273.15 K, respectively. The root mean square error (Eq. IV.10) between the calculated pressure (p_{calc}) and the experimentally obtained pressure (p_{exp}) was minimised in the fit.

The values of a_0 , b_0 , and c coefficients were obtained by modeling the vapour pressure values of pure water between 0.5 °C and 100 °C.^[140] Tables IV.14-IV.15 show the coefficients of Eqs. IV.8-IV.9 along with the *RMSE* of each fit.

$$\frac{p}{p_0} = \exp \left[\sum_{n=0}^2 \left(a_n \cdot w_{abs}^n + \frac{b_n \cdot w_{abs}^n}{\left(\frac{T}{T_{ref}}\right)} \right) + c \cdot \ln \left(\frac{T}{T_{ref}} \right) \right] \quad \text{Eq. IV.8}$$

$$\frac{p}{p_0} = \exp \left[\sum_{n=0}^2 \left(a_n \cdot x_{abs}^n + \frac{b_n \cdot x_{abs}^n}{\left(\frac{T}{T_{ref}}\right)} \right) + c \cdot \ln \left(\frac{T}{T_{ref}} \right) \right] \quad \text{Eq. IV.9}$$

$$RMSE = \sqrt{\frac{1}{n} \cdot \sum_{i=1}^n \left(\frac{p_{calc}}{p_0} - \frac{p_{exp}}{p_0} \right)^2} \quad \text{Eq. IV.10}$$

Table IV.14. Coefficients and *RMSE* of the VLE correlation for H₂O/(LiBr+IL) mixtures as a function of mass fraction of absorbent (w_{abs}).

Mixture	x_{iL}/x_{LiBr}	a_0	a_1	a_2	b_0	b_1	b_2	c	<i>RMSE</i>
H ₂ O/(LiBr+[EA][NO ₃])	0.0205	23.91	4.181	-10.25	-24.40	-1.625	0	-4.583	0.07644
H ₂ O/(LiBr+[Bmim][Br])	0.0205	23.91	0	-2.869	-24.40	3.710	-9.591	-4.583	0.1426
H ₂ O/(LiBr+[Dmim][Cl])	0.0204	23.91	-2.530	0	-24.40	7.211	-13.84	-4.583	0.1941
	0.0427	23.91	-1.297	0	-24.40	4.834	-12.98	-4.583	0.2968

Table IV.15. Coefficients and *RMSE* of the VLE correlation for H₂O/(LiBr+IL) mixtures as a function of mole fraction of absorbent (x_{abs}).

Mixture	x_{iL}/x_{LiBr}	a_0	a_1	a_2	b_0	b_1	b_2	c	<i>RMSE</i>
H ₂ O/(LiBr+[EA][NO ₃])	0.0205	23.91	0	-27.99	-24.40	-1.714	0	-4.583	0.1272
H ₂ O/(LiBr+[Bmim][Br])	0.0205	23.91	0	-31.30	-24.40	-1.780	0	-4.583	0.2021
H ₂ O/(LiBr+[Dmim][Cl])	0.0204	23.91	-8.624	1.794	-24.40	8.939	-40.21	-4.583	0.2701
	0.0427	23.91	0.8673	-29.78	-24.40	-4.125	0	-4.583	0.2299

Figures IV.10-IV.13 show the pressure-temperature-composition phase diagrams for the mixtures with additive. As expected, the vapour pressure increases with increasing temperature and decreases with increasing absorbent composition.

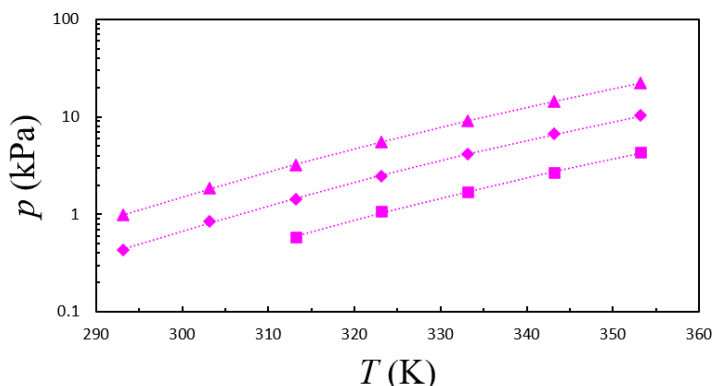


Figure IV.10. Pressure-temperature-composition phase diagram for the $\text{H}_2\text{O}/(\text{LiBr}+[\text{EA}][\text{NO}_3])$ mixture with $x_{\text{IL}}/x_{\text{LiBr}} = 0.0205$. \blacktriangle : $w_{\text{abs}} = 0.449$; \blacklozenge : $w_{\text{abs}} = 0.555$; \blacksquare : $w_{\text{abs}} = 0.648$. Dotted lines represent the calculated vapour pressure with the w_{abs} correlation.

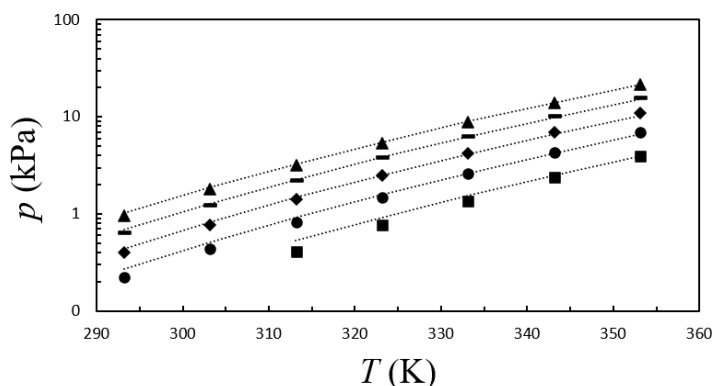


Figure IV.11. Pressure-temperature-composition phase diagram for the $\text{H}_2\text{O}/(\text{LiBr}+[\text{Bmim}][\text{Br}])$ mixture with $x_{\text{IL}}/x_{\text{LiBr}} = 0.0205$. \blacktriangle : $w_{\text{abs}} = 0.450$; $-$: $w_{\text{abs}} = 0.500$; \blacklozenge : $w_{\text{abs}} = 0.550$; \bullet : $w_{\text{abs}} = 0.599$; \blacksquare : $w_{\text{abs}} = 0.650$. Dotted lines represent the calculated vapour pressure with the w_{abs} correlation.

Chapter IV

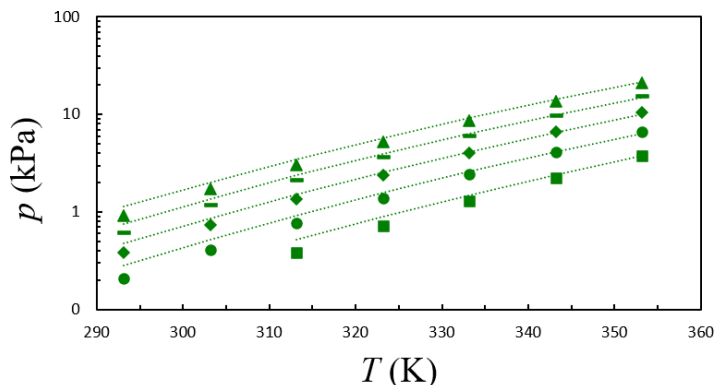


Figure IV.12. Pressure-temperature-composition phase diagram for the $\text{H}_2\text{O}/(\text{LiBr}+[\text{Dmim}][\text{Cl}])$ mixture with $x_{\text{IL}}/x_{\text{LiBr}} = 0.0204$. \blacktriangle : $w_{\text{abs}} = 0.450$; $-$: $w_{\text{abs}} = 0.500$; \blacklozenge : $w_{\text{abs}} = 0.550$; \bullet : $w_{\text{abs}} = 0.599$; \blacksquare : $w_{\text{abs}} = 0.650$. Dotted lines represent the calculated vapour pressure with the w_{abs} correlation.

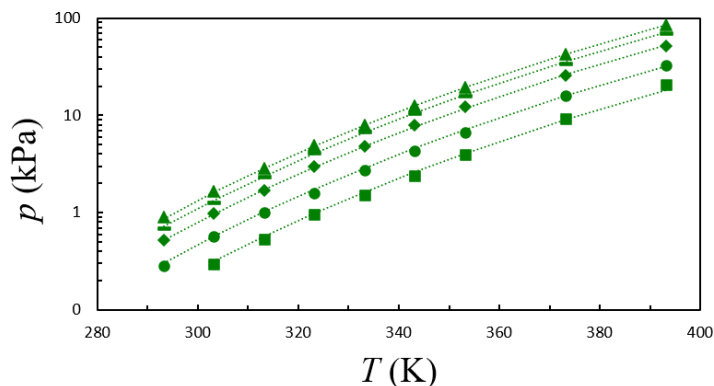


Figure IV.13. Pressure-temperature-composition phase diagram for the $\text{H}_2\text{O}/(\text{LiBr}+[\text{Dmim}][\text{Cl}])$ mixture with $x_{\text{IL}}/x_{\text{LiBr}} = 0.0427$. \blacktriangle : $w_{\text{abs}} = 0.443$; $-$: $w_{\text{abs}} = 0.474$; \blacklozenge : $w_{\text{abs}} = 0.519$; \bullet : $w_{\text{abs}} = 0.576$; \blacksquare : $w_{\text{abs}} = 0.622$. Dotted lines represent the calculated vapour pressure with the x_{abs} correlation.

Following the discussion conducted in Section IV.2.5, the vapour pressure of mixtures with additive is compared to that of $\text{H}_2\text{O}/\text{LiBr}$ as a function of the mole fraction ratio between LiBr and H_2O and temperature (Eq. IV.11). The results are plotted in Figures IV.14-IV.18.

Chapter IV

$$\Delta p/p (\%) = 100 \cdot \frac{p_{\text{H}_2\text{O}/(\text{LiBr}+\text{IL})} - p_{\text{H}_2\text{O}/\text{LiBr}}}{p_{\text{H}_2\text{O}/\text{LiBr}}} \quad \text{Eq. IV.11}$$

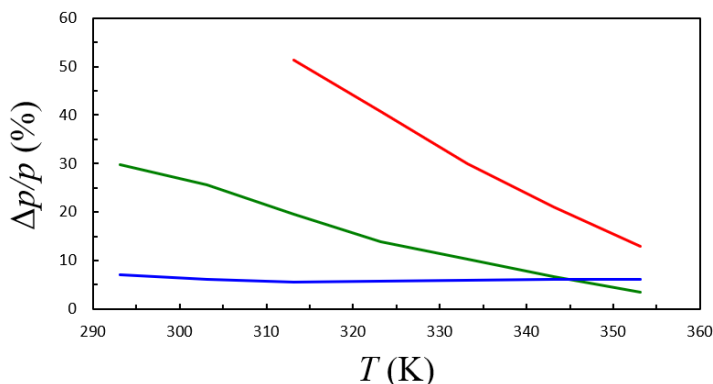


Figure IV.14. Relative vapour pressure difference between $\text{H}_2\text{O}/(\text{LiBr}+[\text{EA}][\text{NO}_3])$ and $\text{H}_2\text{O}/\text{LiBr}^{[123]}$ at $x_{\text{IL}}/x_{\text{LiBr}} = 0.0205$ against temperature. Blue line: $x_{\text{LiBr}}/x_{\text{H}_2\text{O}} = 0.170$; green line: $x_{\text{LiBr}}/x_{\text{H}_2\text{O}} = 0.270$; red line: $x_{\text{LiBr}}/x_{\text{H}_2\text{O}} = 0.370$.

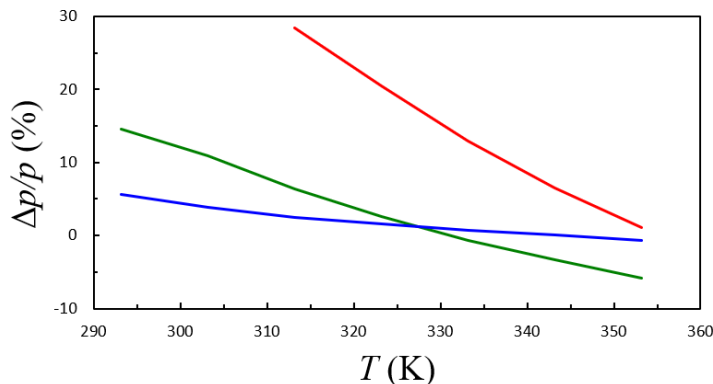


Figure IV.15. Relative vapour pressure difference between $\text{H}_2\text{O}/(\text{LiBr}+[\text{Bmim}][\text{Br}])$ and $\text{H}_2\text{O}/\text{LiBr}^{[123]}$ at $x_{\text{IL}}/x_{\text{LiBr}} = 0.0205$ against temperature. Blue line: $x_{\text{LiBr}}/x_{\text{H}_2\text{O}} = 0.165$; green line: $x_{\text{LiBr}}/x_{\text{H}_2\text{O}} = 0.265$; red line: $x_{\text{LiBr}}/x_{\text{H}_2\text{O}} = 0.365$.

Chapter IV

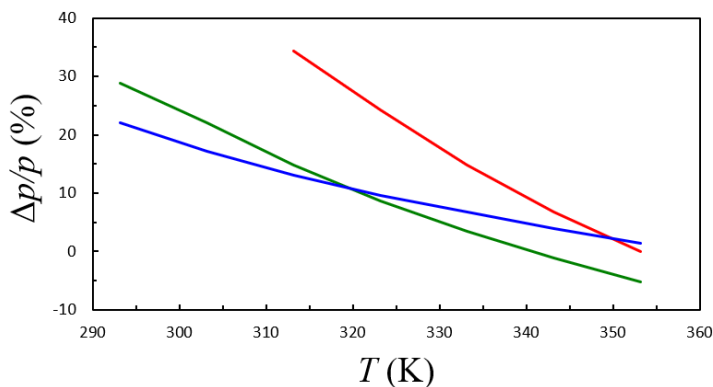


Figure IV.16. Relative vapour pressure difference between $\text{H}_2\text{O}/(\text{LiBr}+[\text{Dmim}][\text{Cl}])$ and $\text{H}_2\text{O}/\text{LiBr}^{[123]}$ at $x_{IL}/x_{\text{LiBr}} = 0.0204$ against temperature. Blue line: $x_{\text{LiBr}}/x_{\text{H}_2\text{O}} = 0.170$; green line: $x_{\text{LiBr}}/x_{\text{H}_2\text{O}} = 0.270$; red line: $x_{\text{LiBr}}/x_{\text{H}_2\text{O}} = 0.370$.

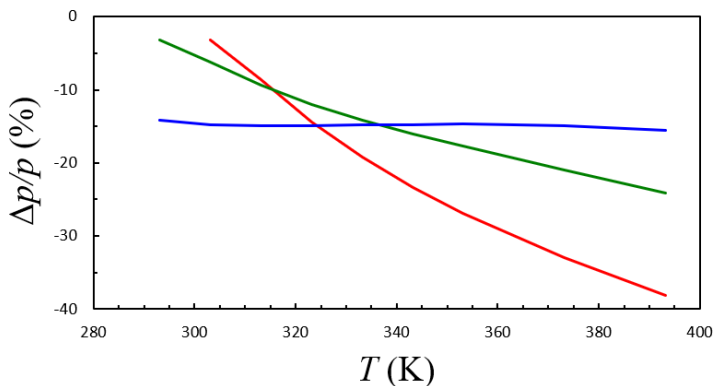


Figure IV.17. Relative vapour pressure difference between $\text{H}_2\text{O}/(\text{LiBr}+[\text{Dmim}][\text{Cl}])$ and $\text{H}_2\text{O}/\text{LiBr}^{[123]}$ at $x_{IL}/x_{\text{LiBr}} = 0.0427$ against temperature. Blue line: $x_{\text{LiBr}}/x_{\text{H}_2\text{O}} = 0.160$; green line: $x_{\text{LiBr}}/x_{\text{H}_2\text{O}} = 0.240$; red line: $x_{\text{LiBr}}/x_{\text{H}_2\text{O}} = 0.320$.

Chapter IV

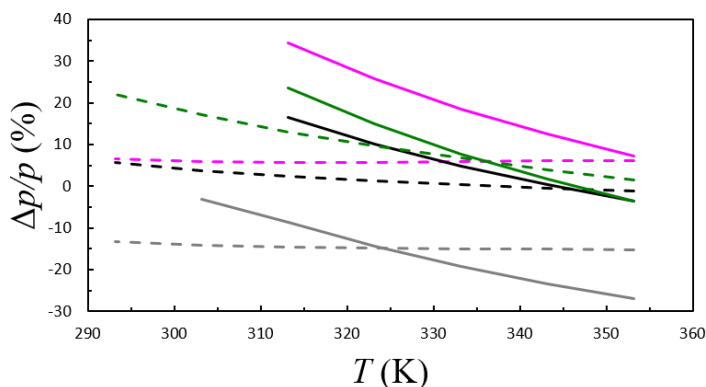


Figure IV.18. Summary of relative vapour pressure difference between $\text{H}_2\text{O}/(\text{LiBr}+\text{IL})$ mixtures and $\text{H}_2\text{O}/\text{LiBr}$ against temperature. Magenta data series: $\text{H}_2\text{O}/(\text{LiBr}+[\text{EA}][\text{NO}_3])$; black data series: $\text{H}_2\text{O}/(\text{LiBr}+[\text{Bmim}][\text{Br}])$; green data series: $\text{H}_2\text{O}/(\text{LiBr}+[\text{Dmim}][\text{Cl}])$ with $x_{\text{IL}}/x_{\text{LiBr}} = 0.0204$; grey data series: $\text{H}_2\text{O}/(\text{LiBr}+[\text{Dmim}][\text{Cl}])$ with $x_{\text{IL}}/x_{\text{LiBr}} = 0.0427$. Solid lines: $x_{\text{LiBr}}/x_{\text{H}_2\text{O}} = 0.32$; dashed lines: $x_{\text{LiBr}}/x_{\text{H}_2\text{O}} = 0.17$.

At $x_{\text{IL}}/x_{\text{LiBr}} \approx 0.0205$, the relative vapour pressure difference between the mixtures with and without additive tends to decrease with temperature and $x_{\text{LiBr}}/x_{\text{H}_2\text{O}}$, as can be seen individually in Figures IV.14-IV.16, and together in Figure IV.18

Remarkably, $\text{H}_2\text{O}/(\text{LiBr}+[\text{EA}][\text{NO}_3])$ is the only mixture with positive vapour pressure differences over the entire composition and temperature range. This result agrees with the higher amount of bulk water in $\text{H}_2\text{O}/(\text{LiBr}+\text{IL})$ mixtures with protic ionic liquids than with aprotic ionic liquids, discussed in Section III.5.3.

The relative pressure difference is significantly higher in mixtures with $[\text{Dmim}][\text{Cl}]$ than with $[\text{Bmim}][\text{Br}]$ at temperatures below 60°C . Based on the smaller radius of the chloride anion compared to that of the bromide anion,^[128] it can be assumed that Cl^- does not coordinate with as many water molecules as Br^- , causing an increase in the amount of water available to establish the vapour-liquid equilibrium (Eq. IV.7).

Figure IV.17 shows that the vapour pressure difference with $[\text{Dmim}][\text{Cl}]$ is negative in the composition and temperature range analysed at $x_{\text{IL}}/x_{\text{LiBr}} \approx 0.0427$. In this mixture, the pressure difference decreases significantly between 50°C and 120°C . This result suggests a limit to the cation-cation interactions between LiBr and

[Dmim][Cl]. The higher water absorption capacity of the H₂O/(LiBr+[Dmim][Cl]) mixture at $x_{IL}/x_{LiBr} = 0.0427$, compared to the other mixtures analysed at $x_{IL}/x_{LiBr} \approx 0.0205$, can be attributed to the water absorption capacity of the ionic liquids, as evidenced in Section III.3.

From these results, a first conclusion that can be drawn from the vapour pressure is that, at $x_{IL}/x_{LiBr} \approx 0.0205$, H₂O/(LiBr+IL) mixtures with [EA][NO₃], [Bmim][Br], and [Dmim][Cl] are good candidates as working fluids for absorption heat pumps, while the H₂O/(LiBr+[Dmim][Cl]) mixture with $x_{IL}/x_{LiBr} = 0.0427$ is a good candidate as a working pair for absorption refrigeration systems.

IV.3.6 Comparison of results with the literature

As discussed in Section I.3.3, there are only a few publications in which the vapour pressure of H₂O/(LiBr+IL) mixtures was experimentally determined. Table I.3 summarizes the x_{IL}/x_{LiBr} ratios along with temperature and absorbent composition range at which the vapour pressure was determined. In most of these works, the considered ILs are based on the imidazolium cation, and the IL/LiBr mole fraction ratio is significantly higher than those studied in this PhD thesis (maximum value of 0.0427).

The relative vapour pressure difference between mixtures with and without additive was calculated according to Eq. IV.11 with the data available in the literature. Table IV.16 shows the results depending on the ionic liquid and the x_{IL}/x_{LiBr} ratio.

Table IV.16. Average relative vapour pressure difference between H₂O/(LiBr+IL) mixtures and H₂O/LiBr.^[141] x_{abs} : mole fraction of absorbent.

Mixture of H ₂ O/(LiBr+IL)	x_{IL}/x_{LiBr}	$\Delta p/p$ (%)			
		$0 \leq x_{abs} < 0.15$		$0.15 \leq x_{abs} < 0.30$	
		T (K)			
		(295 – 350)	(350 – 440)	(295 – 350)	(350 – 440)
[EA][NO ₃]	0.0205 ^a	6.9	7.1	24.3	10.8
[Bmim][Br]	0.0205 ^a	2.2	-0.6	7.1	-4.2
[Dmim][Cl]	0.0204 ^a	9.2	2.6	17.2	-2.0
	0.0427 ^a	-14.3	-14.8	-14.4	-23.0

^a: this work.

Table IV.16 (continued)

Mixture of H ₂ O/(LiBr+IL)	x_{IL}/x_{LiBr}	$\Delta p/p$ (%)			
		$0 \leq x_{abs} < 0.15$		$0.15 \leq x_{abs} < 0.30$	
		T (K)			
		(295 – 350)	(350 – 440)	(295 – 350)	(350 – 440)
[Dmim][Cl]	0.218 ^[35]	-5.6	-6.4	-3.9	-10.5
[Dmim][BF ₄]	0.236 ^[35]	-1.5	-1.8	13.1	8.3
[Emim][Ac]	0.170 ^[36]	10.1	0.8	21.3	14.7
[Emim][Cl]	0.237 ^[33]	-	-	20.8	5.9
	0.296 ^[37]	-6.9	-8.5	-6.8	-9.3
[Emim][SO ₄]	0 – 1.68 ^[38]	-5.6	-	-	-
[Dmim][I]	0.194 ^[39]	-	-13.0	-	-9.3
[Emim][I]	0.091 ^[39]	-	-16.0	-	-6.2
[Dmim][DMP]	0.130 ^[41]	0.7	-16.3	327	249
[MOR _{1,3}][SO ₃]	0.167 ^[40]	-0.6	-0.1	17.0	17.5
[N _{1,1,2OH,2OH}][Br]	0.173 ^[40]	-4.6	-4.8	-4.4	-1.8
[N _{1,2OH,2OH,2OH}][Br]	0.167 ^[40]	-2.6	-2.9	-3.9	-4.2

^a: this work.

It is observed that the vapour pressure difference between H₂O/(LiBr+IL) and H₂O/LiBr mixtures generally shows negative increases with increasing temperature in the same composition range. It is also observed that the pressure differences tend to increase with absorbent composition.

From the point of view of absorption refrigeration and heat pump systems, the most relevant results in Table IV.16 are those within the interval $0.15 \leq x_{abs} < 0.30$. Compared to results obtained using data from the literature, the mixture of H₂O/(LiBr+[Dmim][Cl]) with $x_{IL}/x_{LiBr} = 0.0427$, proposed in this work, shows the most negative vapour pressure difference, even more than that of that same mixture with $x_{IL}/x_{LiBr} = 0.218$ ^[35]. This evidences that increasing ionic liquid composition in the absorbent does not necessarily decrease the vapour pressure of the mixture.

IV.4. Conclusions

The conclusions drawn in this chapter correspond to specific objectives 2, 3, and 5 (Section I.6).

The solubility of lithium bromide in water enhanced in the presence of the selected additives at all IL/LiBr considered ratios, effectively increasing the operation range of absorption refrigeration and heat pump systems.

The increase in solubility of lithium bromide is higher from (280 to 311) K than from (311 to 365) K, which shows that the properties of the mixture are strongly influenced by temperature.

At $x_{IL}/x_{LiBr} \approx 0.0205$, protic ILs increase the solubility of lithium bromide in water more than aprotic ILs as follows: $[EA][NO_3] \approx [PA][NO_3] > [EA][Cl] \approx [Bmim][Br] \approx [Dmim][Cl]$.

There is a limit to the increase in solubility of lithium bromide in water depending on the composition of the ionic liquid in the mixture.

At $x_{IL}/x_{LiBr} \approx 0.0205$, the vapour pressure of $H_2O/(LiBr+[EA][NO_3])$ is higher than that of $H_2O/LiBr$ over the entire composition and temperature range while the vapour pressure of mixtures with aprotic ILs ($[Bmim][Br]$ and $[Dmim][Cl]$) is lower than that of $H_2O/LiBr$ at certain compositions above 60 °C.

The vapour pressure of the $H_2O/(LiBr+[Dmim][Cl])$ mixture with $x_{IL}/x_{LiBr} = 0.0427$ is lower than that of $H_2O/LiBr$.

There is a limit to the vapour pressure reduction of the mixtures with additive as a function of the ionic liquid composition.

$H_2O/(LiBr+IL)$ mixtures with $x_{IL}/x_{LiBr} \approx 0.0205$, whose vapour pressure is generally higher than that of $H_2O/LiBr$, could be useful as working fluids in absorption heat pumps.

The $H_2O/(LiBr+[Dmim][Cl])$ mixture with $x_{IL}/x_{LiBr} = 0.0427$, whose vapour pressure is lower than that of $H_2O/LiBr$, may be of interest as a working pair in absorption refrigeration systems.

Chapter IV

The H₂O/(LiBr+[Dmim][Cl]) mixture with $x_{IL}/x_{LiBr} = 0.0427$ was selected to study its thermophysical properties based on the increased solubility and reduced vapour pressure with respect to H₂O/LiBr.

Chapter V. Thermophysical properties of liquid H₂O/(LiBr+IL) mixtures

V.1. Introduction

The thermophysical properties of the working fluids used in refrigeration and absorption heat pump systems are essential because they influence their performance.^[9] Hence, measuring those thermophysical properties relevant to the operation of the thermodynamic cycle is essential to determine the working fluid performance accurately. Analysing the thermophysical properties allows for the evaluation of the potential for improving the performance of H₂O/LiBr in the presence of ionic liquids as additives. It corroborates the decisions made based on previous hypotheses.

In this doctoral thesis, the thermophysical properties of some H₂O/(LiBr+IL) mixtures that have been experimentally determined are density, speed of sound, enthalpy of dilution, electrical conductivity, thermal conductivity, and dynamic viscosity. The role of these thermophysical properties of working fluids for absorption refrigeration and heat pumps was described in Sections I.3 and II.3. H₂O/(LiBr+IL) mixtures should have higher density, lower enthalpy of dilution, higher thermal conductivity, and lower dynamic viscosity than H₂O/LiBr to improve the performance of the working fluid.

Although the speed of sound and the electrical conductivity of the working fluid do not directly influence its performance in the considered application, they are valuable properties for analysing the influence of ILs on H₂O/LiBr from the point of view of thermophysical properties.

Subsequent sections are devoted to each thermophysical property, and all of them follow the same structure. The experimental devices are described in the first section. Secondly, the device and the experimental procedure used are described. Then, the reference values for H₂O/LiBr are briefly discussed. Finally, the experimental results are shown and discussed.

V.2. Density and speed of sound

V.2.1 Experimental device

Both the density (ρ) and the speed of sound (c) of the different mixtures were determined with an Anton-Paar DSA 5000 M. This densimeter is based on the vibrating tube method, which consists of a U-shaped tube whose natural frequency of vibration is inversely proportional to the density of the fluid.^[61] As for the speed of sound, the device is based on the time-of-flight method,^[62] where the time it takes for the wave to travel a known distance is measured.

Measurements were performed from (20 to 70) °C at atmospheric pressure. In the case of the H₂O/(LiBr+DmimCl) mixture with $x_{IL}/x_{LiBr} = 0.0423$, the density was also measured from 20 °C to 100 °C with an Anton-Paar DMA HPM at atmospheric pressure, to have values of this property at higher temperatures. The estimated uncertainties with a 95 % confidence level ($k = 2$) are $U(w_{abs}) = 0.001$, $U(T) = 0.01$ K, $U(\rho) = 0.1$ kg·m⁻³, and $U(c) = 0.5$ m·s⁻¹.

V.2.2 Experimental procedure

H₂O/(LiBr+IL) samples were prepared by weighing using a Mettler Toledo ME403 analytical balance. Starting from a mother solution with an absorbent (LiBr+IL) mass fraction of 0.58, the rest were prepared by dilution similarly to the vapour pressure measurement.

Once the solutions were prepared, they were injected into the densimeter (approximately 2 mL) and the measurement was performed automatically. Upon completion of the experiments for each sample, hot water and acetone were circulated through the equipment for cleaning and subsequent use.

Table V.1 shows the composition and conditions at which density and speed of sound were determined.

Chapter V

Table V.1. Summary of the conditions at which density and speed of sound were determined for H₂O/(LiBr+IL) mixtures. x_{IL}/x_{LiBr} : mole fraction ratio between IL and LiBr; w_{abs} : mass fraction of absorbent; x_{abs} : mole fraction of absorbent.

Mixture	x_{IL}/x_{LiBr}	T (K)	w_{abs}	x_{abs}
H ₂ O/(LiBr+[EA][NO ₃])	0.0205	293 – 343	0.05 – 0.58	0.01 – 0.22
H ₂ O/(LiBr+[PA][NO ₃])	0.0205	293 – 343	0.05 – 0.58	0.01 – 0.22
H ₂ O/(LiBr+[EA][Cl])	0.0205	293 – 343	0.05 – 0.58	0.01 – 0.22
H ₂ O/(LiBr+[Bmim][Br])	0.0208	293 – 343	0.03 – 0.58	0.01 – 0.22
H ₂ O/(LiBr+[Dmim][Cl])	0.0203	293 – 343	0.05 – 0.58	0.01 – 0.22
	0.0423*	293 – 373	0.42 – 0.57	0.13 – 0.21

*Only density is available for this mixture.

V.2.3 Reference mixture: H₂O/LiBr

The density of H₂O/LiBr was experimentally determined in the literature between -60 °C and 220 °C, and the mass fraction of LiBr ranged from 0.01 to 0.65.^[141]

Figure V.1 shows the density of three H₂O/LiBr solutions at different compositions between 0.2 and 0.6 in LiBr mass fraction, between 293.15 K and 373.15 K at 1 bar, calculated with a correlation available in the literature,^[123] together with the density of pure water.^[140] It is observed that density decreases with increasing temperature and increases with increasing lithium bromide composition.

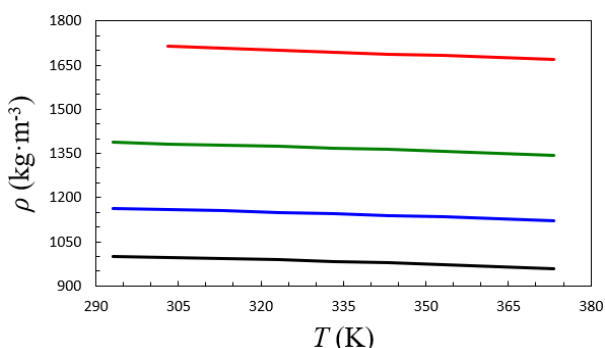


Figure V.1. Density of H₂O/LiBr solutions at 1 bar.^[123] Black series: pure water;^[140] blue series: $w_{LiBr} = 0.20$; green series: $w_{LiBr} = 0.40$; red series: $w_{LiBr} = 0.60$.

Chapter V

Only two works have been found in which the speed of sound of H₂O/LiBr was experimentally determined,^[75,142] whose values show significant discrepancies at similar compositions and temperatures. Given the differences between the experimental density values of H₂O/LiBr reported by Labra *et al.*^[142] and by other authors, both experimental^[75,143–145] and obtained by correlations,^[123,141] only the speed of sound values reported by Rohman *et al.*^[75] are considered for comparison.

Figure V.2 shows the speed of sound of H₂O/LiBr against temperature and composition. It is observed that the values of this property increase with increasing temperature and LiBr composition. However, the influence of temperature cannot be visualised at $w_{LiBr} = 0.55$, which could be attributed to the simultaneous influence of density and dynamic viscosity on this property.

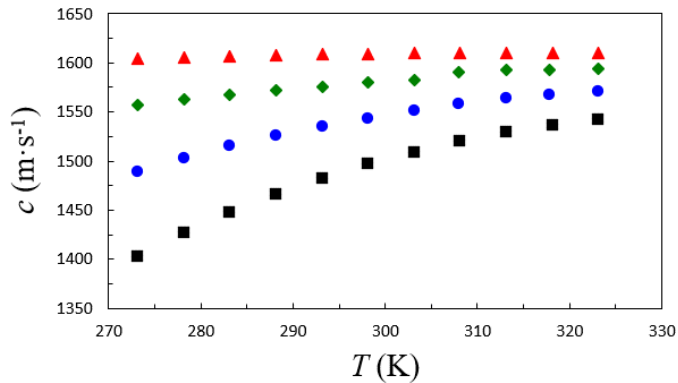


Figure V.2. Speed of sound of H₂O/LiBr solutions at 1 bar.^[75] ■: pure water;^[140] ●: $w_{LiBr} = 0.184$; ◆: $w_{LiBr} = 0.392$; ▲: $w_{LiBr} = 0.550$.

V.2.4 Experimental results and discussion

Tables V.2-V.7 show the experimental density and speed of sound of H₂O/(LiBr+IL) mixtures.

Table V.2. Density and speed of sound of the H₂O/(LiBr+[EA][NO₃]) mixture at $x_{iL}/x_{LiBr} = 0.0205$ and atmospheric pressure. w_{abs} : mass fraction of absorbent; x_{abs} : mole fraction of absorbent; T : temperature.

w_{abs}	x_{abs}	ρ (kg·m ⁻³)						c (m·s ⁻¹)					
		T (K)						T (K)					
		293.15	303.15	313.15	323.15	333.15	343.15	293.15	303.15	313.15	323.15	333.15	343.15
0.0500	0.0108	1035.6	1032.8	1029.1	1024.8	1019.8	1014.2	1494.4	1517.5	1535.2	1545.2	1548.5	1549.5
0.1504	0.0353	1117.5	1114.1	1110.2	1105.7	1100.7	1095.3	1525.2	1542.7	1552.7	1558.4	1559.4	1559.8
0.2499	0.0644	1209.2	1205.3	1201.0	1196.3	1191.2	1185.8	1551.7	1563.0	1568.0	1568.7	1569.4	1569.2
0.3504	0.1002	1314.6	1310.1	1305.4	1300.4	1295.2	1289.8	1574.2	1580.7	1581.8	1579.3	1576.3	1574.1
0.4540	0.1465	1441.1	1436.1	1430.8	1425.5	1420.0	1414.3	1591.7	1593.4	1590.4	1586.5	1582.7	1578.3
0.5502	0.2016	1586.7	1580.7	1574.8	1568.7	1562.7	1556.6	1612.7	1615.8	1604.1	1599.3	1593.5	1589.2
0.5801	0.2219	1642.9	1636.6	1630.2	1623.9	1617.6	1611.2	1626.9	1626.2	1616.4	1610.2	1602.5	1598.3

Table V.3. Density and speed of sound of the H₂O/(LiBr+[PA][NO₃]) mixture at $x_{Li}/x_{LiBr} = 0.0205$ and atmospheric pressure. w_{abs} : mass fraction of absorbent; x_{abs} : mole fraction of absorbent; T : temperature.

w_{abs}	x_{abs}	ρ (kg·m ⁻³)						c (m·s ⁻¹)					
		T (K)						T (K)					
		293.15	303.15	313.15	323.15	333.15	343.15	293.15	303.15	313.15	323.15	333.15	343.15
0.0502	0.0108	1038.4	1035.5	1031.9	1027.6	1022.7	1017.3	1497.2	-	1542.8	1549.6	1551.7	1551.8
0.1474	0.0343	1116.3	1112.9	1109.0	1104.5	1099.5	1094.1	1524.6	1543.3	1552.4	1556.6	1558.5	1558.6
0.2492	0.0639	1208.9	1205.0	1200.7	1196.0	1191.0	1185.6	1552.6	1564.3	1567.5	1567.8	1567.9	1566.4
0.3483	0.0991	1313.8	1309.3	1304.6	1299.6	1294.4	1288.9	1575.0	1581.2	1580.2	1577.1	1575.6	1572.9
0.4484	0.1433	1439.2	1434.1	1428.8	1423.4	1417.9	1412.2	1595.4	1594.3	1589.3	1584.7	1580.7	1577.1
0.5800	0.2213	1650.8	1644.4	1638.0	1631.6	1625.2	1618.7	1630.0	1627.0	1621.5	1617.1	1611.2	-

Table V.4. Density and speed of sound of the H₂O/(LiBr+[EA][Cl]) mixture at $x_{IL}/x_{LiBr} = 0.0205$ and atmospheric pressure. w_{abs} : mass fraction of absorbent; x_{abs} : mole fraction of absorbent; T : temperature.

w_{abs}	x_{abs}	ρ (kg·m ⁻³)						c (m·s ⁻¹)					
		T (K)						T (K)					
		293.15	303.15	313.15	323.15	333.15	343.15	293.15	303.15	313.15	323.15	333.15	343.15
0.0500	0.0108	1036.5	1033.7	1030.1	1025.8	1021.0	1015.5	1495.7	-	1552.5	1559.5	1554.5	1553.9
0.1499	0.0353	1118.1	1114.8	1110.8	1106.4	1101.4	1096.0	1525.3	1550.1	1560.9	1565.2	1564.3	1559.4
0.2496	0.0646	1211.3	1207.5	1203.2	1198.5	1193.5	1188.1	1554.3	1567.0	1572.8	1569.2	1570.9	1569.6
0.3506	0.1008	1318.8	1314.4	1309.8	1304.8	1299.7	1294.2	1573.5	1580.1	1583.9	1584.9	1577.8	1574.9
0.4502	0.1453	1444.4	1439.3	1434.1	1428.8	1423.3	1417.7	1591.2	1593.1	1593.0	1591.0	1587.1	1580.2
0.5509	0.2031	1598.4	1592.4	1586.4	1580.4	1574.4	1568.3	1619.7	1619.3	1614.4	1609.9	1598.9	1594.2
0.5803	0.2231	1653.3	1646.9	1640.5	1634.2	1627.9	1621.5	1627.8	1626.4	1622.6	1618.0	1608.0	1603.3

Table V.5. Density and speed of sound of the H₂O/(LiBr+[Bmim][Br]) mixture at $x_{Li}/x_{LiBr} = 0.0208$ and atmospheric pressure. w_{abs} : mass fraction of absorbent; x_{abs} : mole fraction of absorbent; T : temperature.

w_{abs}	x_{abs}	ρ (kg·m ⁻³)						c (m·s ⁻¹)					
		T (K)						T (K)					
		293.15	303.15	313.15	323.15	333.15	343.15	293.15	303.15	313.15	323.15	333.15	343.15
0.0296	0.0061	1022.2	1019.4	1015.8	1011.6	1006.7	1001.3	1486.7	1520.5	1538.6	1542.6	1547.1	1548.2
0.0920	0.0200	1063.1	1060.0	1056.3	1051.9	1047.0	1041.3	1502.6	1527.5	1541.5	1543.6	1547.8	1549.0
0.1524	0.0349	1109.5	1106.2	1102.3	1097.8	1092.9	1087.5	1519.9	1540.5	1552.3	1558.1	1555.6	1556.0
0.2083	0.0503	1155.7	1152.1	1148.0	1143.4	1138.4	1133.0	1535.7	1552.3	1561.3	1565.7	1566.0	1561.8
0.2739	0.0706	1213.6	1209.7	1205.4	1200.7	1195.6	1190.2	1552.0	1561.7	1567.2	1570.3	1570.1	1567.9
0.3361	0.0925	1274.9	1270.7	1266.2	1261.4	1256.2	1250.8	1566.7	1573.5	1574.4	1575.2	1573.0	1571.1
0.3963	0.1167	1340.7	1336.2	1331.4	1326.4	1321.1	1315.6	1578.5	1581.8	1580.2	1579.3	1576.4	1573.8
0.4586	0.1456	1414.6	1409.7	1404.6	1399.4	1394.0	1388.4	1588.5	1589.4	1585.2	1583.3	1579.4	1576.0
0.5204	0.1792	1494.8	1489.5	1484.1	1478.5	1472.9	1467.2	1597.8	1596.0	1589.7	1587.0	1583.6	1580.2
0.5773	0.2155	1586.0	1580.1	1574.2	1568.2	1562.2	1556.2	1614.1	1610.9	1602.3	1597.9	1593.1	1588.6

Table V.6. Density and speed of sound of the H₂O/(LiBr+[Dmim][Cl]) mixture at $x_{Li}/x_{LiBr} = 0.0203$ and atmospheric pressure. w_{abs} : mass fraction of absorbent; x_{abs} : mole fraction of absorbent; T : temperature.

w_{abs}	x_{abs}	ρ (kg·m ⁻³)						c (m·s ⁻¹)					
		T (K)						T (K)					
		293.15	303.15	313.15	323.15	333.15	343.15	293.15	303.15	313.15	323.15	333.15	343.15
0.0499	0.0107	1035.0	1032.2	1028.6	1024.3	1019.4	1014.0	1491.7	1512.9	1528.5	1536.8	1542.4	1544.8
0.0995	0.0222	1072.5	1069.4	1065.6	1061.2	1056.3	1050.6	1505.8	1524.8	1537.3	1543.8	-	-
0.1497	0.0349	1113.5	1110.2	1106.3	1101.8	1096.8	1091.3	1521.1	1535.5	1546.1	1553.2	-	-
0.1997	0.0487	1157.7	1154.1	1150.1	1145.5	1140.5	1135.1	1536.8	1549.8	1558.8	1562.4	1564.4	-
0.2505	0.0642	1205.7	1201.9	1197.6	1192.9	1187.9	1182.5	1549.9	1559.2	1565.4	1569.0	-	-
0.3005	0.0810	1256.5	1252.5	1248.0	1243.3	1238.2	1232.8	1566.7	1569.8	1574.2	1575.5	1573.9	-
0.3498	0.0995	1311.4	1307.1	1302.4	1297.5	1292.4	1287.0	1574.9	1580.3	1583.1	1581.9	1578.3	-
0.3997	0.1202	1370.6	1365.9	1361.1	1356.0	1350.7	1345.3	1580.5	1583.1	1582.0	1580.9	1579.7	1578.0
0.4515	0.1446	1435.7	1430.9	1425.9	1420.6	1415.2	1409.7	1590.3	1590.8	1588.3	1585.8	1583.3	-
0.4978	0.1691	1505.8	1500.5	1495.1	1489.5	1483.9	1478.2	1599.5	1598.5	1594.8	1590.1	1587.7	-
0.4978	0.2002	1589.6	1583.8	1578.0	1572.1	1566.1	1560.1	1615.2	1613.4	1607.5	1603.2	1599.5	1596.2
0.5494	0.2209	1649.4	1643.2	1636.9	1630.6	1624.3	1618.0	1636.0	1623.8	1620.5	1615.2	1609.6	1605.1

Table V.7. Density of the H₂O/(LiBr+[Dmim][Cl]) mixture at $x_{iL}/x_{LiBr} = 0.0423$ and atmospheric pressure. w_{abs} : mass fraction of absorbent; x_{abs} : mole fraction of absorbent; T : temperature.

w_{abs}	x_{abs}	ρ (kg·m ⁻³)								
		T (K)								
		293.15	303.15	313.15	323.15	333.15	343.15	353.15	363.15	373.15
0.4242	0.1302	1403.1	1399.6	1395.0	1389.4	1383.0	1375.5	1367.0	1357.5	1347.2
0.4710	0.1531	1474.8	1470.0	1464.5	1458.2	1451.1	1443.3	1434.7	1425.3	1415.2
0.5309	0.1869	1552.4	1548.3	1543.2	1537.0	1529.9	1521.7	1512.5	1502.3	1491.1
0.5675	0.2104	1626.7	1622.6	1617.5	1611.2	1603.8	1595.4	1585.9	1575.3	1563.7

Chapter V

The density values shown in Tables V.2-V.7 were fitted to Eqs. V.1-V.2 as a function of temperature (K) and absorbent composition. In these equations, T_c is the critical temperature of pure water (647.096 K).^[146] In the fit, the root mean square error (Eq. V.3) between the calculated density (ρ_{calc}) and the experimental value (ρ_{exp}) was minimized. The coefficients a_0 , b , c and d were obtained by modelling the density of pure water as a saturated liquid between 0.5 °C and 100 °C.^[140]

$$\rho = \sum_{n=0}^2 (a_n \cdot w_{abs}^n) + b \cdot \left(\frac{T}{T_c}\right)^{\frac{1}{3}} + c \cdot \left(\frac{T}{T_c}\right)^{\frac{2}{3}} + d \cdot \left(\frac{T}{T_c}\right)^{\frac{5}{3}} \quad \text{Eq. V.1}$$

$$\rho = \sum_{n=0}^2 (a_n \cdot x_{abs}^n) + b \cdot \left(\frac{T}{T_c}\right)^{\frac{1}{3}} + c \cdot \left(\frac{T}{T_c}\right)^{\frac{2}{3}} + d \cdot \left(\frac{T}{T_c}\right)^{\frac{5}{3}} \quad \text{Eq. V.2}$$

$$RMSE = \sqrt{\frac{1}{n} \cdot \sum_{i=1}^n (\rho_{calc} - \rho_{exp})^2} \quad \text{Eq. V.3}$$

Table V.8. Coefficients and *RMSE* of the density correlation for H₂O/(LiBr+IL) mixtures as a function of the mass fraction of absorbent.

Fluid	x_{IL}/x_{LiBr}	a_0 (kg·m ⁻³)	a_1 (kg·m ⁻³)	a_2 (kg·m ⁻³)	b (kg·m ⁻³)	c (kg·m ⁻³)	d (kg·m ⁻³)	<i>RMSE</i> (kg·m ⁻³)
H ₂ O/(LiBr+[EA][NO ₃])	0.0205	-6140	627.1	794.1	20990	-16170	2076	6.218
H ₂ O/(LiBr+[PA][NO ₃])	0.0205	-6140	623.6	828.6	20990	-16170	2076	6.908
H ₂ O/(LiBr+[EA][Cl])	0.0205	-6140	632.4	817.7	20990	-16170	2076	5.831
H ₂ O/(LiBr+[Bmim][Br])	0.0208	-6140	589.2	702.9	20990	-16170	2076	5.115
H ₂ O/(LiBr+[Dmim][Cl])	0.0203	-6140	599.7	849.8	20990	-16170	2076	6.297
	0.0423	-6140	519.2	992.1	20990	-16170	2076	8.901

Table V.9. Coefficients and *RMSE* of the density correlation for H₂O/(LiBr+IL) mixtures as a function of the mole fraction of absorbent.

Fluid	x_{IL}/x_{LiBr}	a_0 (kg·m ⁻³)	a_1 (kg·m ⁻³)	a_2 (kg·m ⁻³)	b (kg·m ⁻³)	c (kg·m ⁻³)	d (kg·m ⁻³)	<i>RMSE</i> (kg·m ⁻³)
H ₂ O/(LiBr+[EA][NO ₃])	0.0205	-6140	3353	-2218	20990	-16170	2076	3.770
H ₂ O/(LiBr+[PA][NO ₃])	0.0205	-6140	3381	-2114	20990	-16170	2076	3.756
H ₂ O/(LiBr+[EA][Cl])	0.0205	-6140	3385	-2193	20990	-16170	2076	3.325
H ₂ O/(LiBr+[Bmim][Br])	0.0208	-6140	3189	-2328	20990	-16170	2076	3.194
H ₂ O/(LiBr+[Dmim][Cl])	0.0203	-6140	3297	-1795	20990	-16170	2076	3.195
	0.0423	-6140	3301	-1790	20990	-16170	2076	8.649

Chapter V

The speed of sound of H₂O/(LiBr+IL) mixtures (Tables V.2-V.6) were fitted to a polynomial equation (Eq. V.4), where w_{abs} is the mass fraction of absorbent, T the temperature (K), and T_c the critical temperature of water (647.096 K).^[146] It was necessary to use a nine-parameter model due to the complex curvature of the data. The root mean square error (Eq. V.5) between the calculated (c_{calc}) and experimentally obtained (c_{exp}) speed of sound was minimised by the fit. The coefficients a_0 , b_0 , c_0 and d_0 were obtained for the speed of sound of pure water between 20 °C and 70 °C and 1 bar.^[140] The speed of sound of H₂O/LiBr reported by Rohman *et al.*^[75] was also modelled.

$$c = a_0 + \sum_{n=0}^2 (b_n \cdot w_{abs}^n) \cdot \left(\frac{T}{T_c}\right) + \sum_{n=0}^2 (c_n \cdot w_{abs}^n) \cdot \left(\frac{T}{T_c}\right)^2 + \sum_{n=0}^1 (d_n \cdot w_{abs}^n) \cdot \left(\frac{T}{T_c}\right)^3 \quad \text{Eq. V.4}$$

$$RMSE = \sqrt{\frac{1}{n} \cdot \sum_{i=1}^n (c_{calc} - c_{exp})^2} \quad \text{Eq. V.5}$$

Table V.10. Coefficients and $RMSE$ ($m \cdot s^{-1}$) of the speed of sound correlation for $H_2O/LiBr$ and $H_2O/(LiBr+IL)$ mixtures.

Fluid	x_{IL}/x_{LiBr}	a_0	b_0	b_1	b_2	c_0	c_1	c_2	d_0	d_1	$RMSE$
H_2O	-	-6125	$3.909 \cdot 10^4$	-	-	$-6.573 \cdot 10^4$	-	-	$3.644 \cdot 10^4$	-	0.040
$H_2O/LiBr$	-	-6125	$3.909 \cdot 10^4$	$2.287 \cdot 10^4$	-3480	$-6.573 \cdot 10^4$	$-8.505 \cdot 10^4$	6721	$3.644 \cdot 10^4$	$7.989 \cdot 10^4$	3.025
$H_2O/(LiBr+[EA][NO_3])$	0.0205	-6125	$3.909 \cdot 10^4$	$1.690 \cdot 10^4$	-2104	$-6.573 \cdot 10^4$	$-5.996 \cdot 10^4$	4281	$3.644 \cdot 10^4$	$5.311 \cdot 10^4$	3.386
$H_2O/(LiBr+[PA][NO_3])$	0.0205	-6125	$3.909 \cdot 10^4$	$1.760 \cdot 10^4$	-2778	$-6.573 \cdot 10^4$	$-6.209 \cdot 10^4$	5803	$3.644 \cdot 10^4$	$5.446 \cdot 10^4$	3.956
$H_2O/(LiBr+[EA][Cl])$	0.0205	-6125	$3.909 \cdot 10^4$	$1.428 \cdot 10^4$	-2491	$-6.573 \cdot 10^4$	$-4.886 \cdot 10^4$	5004	$3.644 \cdot 10^4$	$4.155 \cdot 10^4$	5.064
$H_2O/(LiBr+[Bmim][Br])$	0.0208	-6125	$3.909 \cdot 10^4$	$1.729 \cdot 10^4$	-2349	$-6.573 \cdot 10^4$	$-6.170 \cdot 10^4$	4672	$3.644 \cdot 10^4$	$5.499 \cdot 10^4$	3.323
$H_2O/(LiBr+[Dmim][Cl])$	0.0203	-6125	$3.909 \cdot 10^4$	$1.850 \cdot 10^4$	-2355	$-6.573 \cdot 10^4$	$-6.658 \cdot 10^4$	5002	$3.644 \cdot 10^4$	$5.974 \cdot 10^4$	4.872

Chapter V

To evaluate the influence of the ionic liquid on density, the relative density difference was calculated between the mixtures with and without additive as a function of the x_{LiBr}/x_{H_2O} ratio and temperature (Eqs. IV.6-IV.7). The density of H₂O/LiBr was estimated using a correlation.^[123]

$$\Delta\rho/\rho (\%) = 100 \cdot \frac{\rho_{H_2O/(LiBr+IL)} - \rho_{H_2O/LiBr}}{\rho_{H_2O/LiBr}} \quad \text{Eq. V.6}$$

Table V.11 and Figure V.3 show the average values of the relative density difference. Since the density of the solutions decreases the lower the solute composition, the results suggest that the higher percentage of bulk water in the mixtures with additive is related to a lower density. However, at $x_{IL}/x_{LiBr} \approx 0.0205$, the order of additives from largest to smallest relative density difference is: [PA][NO₃] \approx [EA][Cl] > [Dmim][Cl] \approx [EA][NO₃] > [Bmim][Br]. This order, which does not match that of the amount of bulk water discussed in Chapter III ([EA][Cl] > [EA][NO₃] \approx [PA][NO₃] \approx [Dmim][Cl] > [Bmim][Br]), evidences that these results cannot be interpreted solely based on bulk water due to the complexity of the interactions.

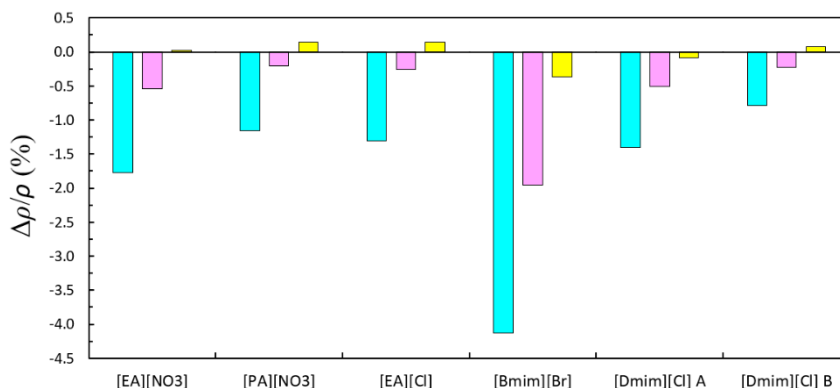


Figure V.3. Summary of density differences between H₂O/(LiBr+IL) mixtures and H₂O/LiBr over the entire temperature and composition range. Cyan: most negative difference; pink: average difference; yellow: most positive difference. Mixtures with additive have an approximate x_{IL}/x_{LiBr} ratio of 0.0205, except for [Dmim][Cl] B, in which case it is 0.0423.

From the point of view of the selected application, a lower density implies a lower mass flow rate for the same volume flow rate. This means that increasing the volume

Chapter V

flow rate through the solution pump would be required to exchange the same amount of heat.

A better interpretation of the influence of the additive on the molecular structure of H₂O/LiBr can be made in terms of the apparent molar volume and isentropic compressibility, which can be calculated from the density and speed of sound. The results of this analysis are discussed in Chapter VI.

Table V.11. Average relative density difference between H₂O/(LiBr+IL) and H₂O/LiBr mixtures from (293.15 to 343.15) K as as function of x_{LiBr}/x_{H_2O} .

x_{LiBr}/x_{H_2O}	$\Delta\rho/\rho$ (%)					
	[EA][NO ₃]	[PA][NO ₃]	[EA][Cl]	[Bmim][Br]	[Dmim][Cl]	
	$x_{IL}/x_{LiBr} = 0.0205$	$x_{IL}/x_{LiBr} = 0.0205$	$x_{IL}/x_{LiBr} = 0.0205$	$x_{IL}/x_{LiBr} = 0.0208$	$x_{IL}/x_{LiBr} = 0.0203$	$x_{IL}/x_{LiBr} = 0.0423$
0.025	-0.01	0.06	0.07	-0.40	-0.11	0.05 ^a
0.050	-0.03	0.11	0.11	-0.75	-0.18	0.11 ^a
0.10	-0.21	0.06	0.04	-1.47	-0.33	0.12 ^a
0.15	-0.54	-0.14	-0.20	-2.25	-0.56	-0.01
0.20	-0.98	-0.46	-0.57	-3.03	-0.80	-0.21
0.25	-1.45	-0.83	-0.98	-3.83	-1.09	-0.46

^a: extrapolated.

V.3. Enthalpy of dilution

V.3.1 Experimental device

The experimental device used to determine the enthalpy of dilution of $\text{H}_2\text{O}/(\text{LiBr}+\text{IL})$ mixtures (Figure V.4) using a calorimetric method has been widely used in previous works.^[147–150] The main part of this system is a Setaram C80 differential calorimeter with an adapted flow-mixing cell.^[147,148] The calorimeter is housed inside the calorimeter block, whose temperature is controlled by a Setaram G11 electronic controller.

The signal produced by heat absorption or rejection when mixed streams are detected inside the flow mixing cell by thermopiles. In addition to the calorimeter, the system contains two Teledyne ISCO Model 260D syringe pumps, two internal heat exchangers (in the calorimeter block) and two external heat exchangers to achieve thermal equilibrium between the fluids and the calorimeter, and a Circle Seal pressure regulator to regulate the pressure at which the experiments are conducted. The fluids flow from the pumps to the calorimeter and from the calorimeter to the collection vessel (pressure buffers) through stainless steel tubes with outer and inner diameters of 1.6 mm and 1 mm, respectively.

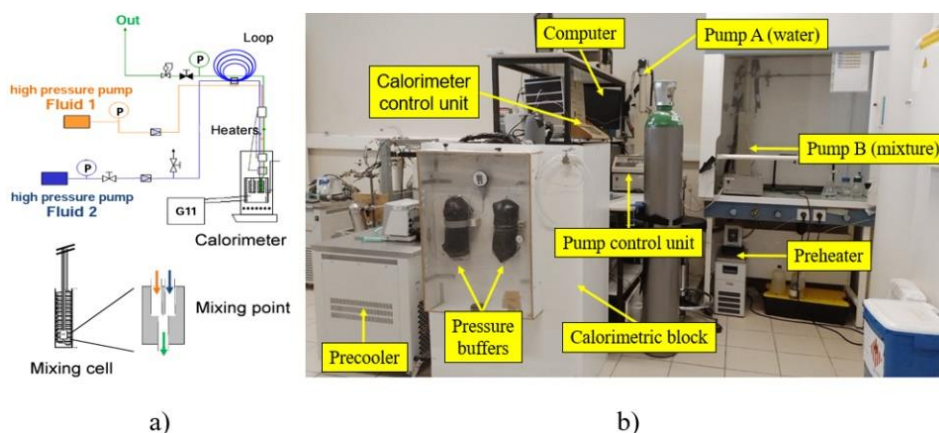


Figure V.4. Experimental device used to determine the enthalpy of dilution. a) Scheme of the system.^[149] b) Experimental setup.

Based on previously reported work,^[147,148] the uncertainty of the mole flow rate is less than 1.5 %, the uncertainty of the signal difference ranges from 1 % to 3 %, and the uncertainty of the calibration constant is less than 5 %.

V.3.2 Experimental procedure

About 200 mL of each mixture, with and without additive, were prepared with a mass fraction of absorbent equal to 0.58 by weighing using an Ohaus Adventurer ARC120 balance (resolution = 0.01 g). For the additive mixtures, the ionic liquid mass was weighed using an Ohaus Explorer Semi-Micro EX225D/AD balance (resolution = 0.00001 g). Each mixture was then loaded into one of the syringe pumps, while the other was filled with pure water.

The experiments were carried out at pressures between 2.4 bar and 3.4 bar. The baseline of the signal collected by the thermopiles must be determined for each measurement. For this purpose, a volumetric flow rate of $0.06 \text{ cm}^3 \cdot \text{min}^{-1}$ of pure water was circulated for at least 1.5 h until the signal stabilised.

The different compositions of the resulting solution were achieved by varying the volumetric flow rates of each stream. The thermopiles detected a stable signal between (30 and 60) min after setting a new pair of volumetric flow rates.

After the experiments were finished, the pump where the mixture had previously been stored was rinsed with 260 cm^3 of pure water. This water was then removed from the pump and refilled with pure water, which was circulated through the tubing, the calorimeter, and the flow mixing cell. Finally, the resulting solution was removed from the system.

The enthalpy of dilution of $\text{H}_2\text{O}/\text{LiBr}$, calculated from Eq. II.19 with literature data,^[151] was used to determine the calibration constant of the calorimeter at $25 \text{ }^\circ\text{C}$ using Eq. II.18 (Section II.3.4).

Table V.12 shows the mixtures and composition and pressure ranges at which the enthalpy of dilution was determined at $25 \text{ }^\circ\text{C}$.

Chapter V

Table V.12. Summary of the conditions at which the enthalpy of dilution was determined at 298.15 K. x_{IL}/x_{LiBr} : mole fraction ratio between IL and LiBr; w_{abs} : mass fraction of absorbent; x_{abs} : mole fraction of absorbent.

Mixture	x_{IL}/x_{LiBr}	w_{abs}	x_{abs}
H ₂ O/LiBr	-	0.46 – 0.54	0.17 – 0.20
H ₂ O/(LiBr+[EA][NO ₃])	0.0205	0.46 – 0.55	0.15 – 0.20
H ₂ O/(LiBr+[PA][NO ₃])	0.0205	0.44 – 0.55	0.14 – 0.20
H ₂ O/(LiBr+[EA][Cl])	0.0206	0.46 – 0.55	0.15 – 0.20
H ₂ O/(LiBr+[Dmim][Cl])	0.0207	0.43 – 0.55	0.14 – 0.20

V.3.3 Reference mixture: H₂O/LiBr

Smith-Magowan and Goldberg^[152] created an extensive reference collection of experimental data on constant pressure heat capacity, enthalpy of dissolution and enthalpy of dilution of aqueous electrolyte mixtures. The enthalpy of dilution of H₂O/LiBr at 25 °C was determined by Fortier *et al.*^[153] and Vaslow^[154] in very dilute initial solutions ($w_{LiBr} < 0.15$). The enthalpy of dilution can be calculated at 25 °C from measurements by Lange and Schwartz^[155] at LiBr mass fractions between 0 and 0.61, and from calculations by Parker's data^[151] at LiBr mass fractions between 0 and 0.60, obtained using the chord-area method.^[156]

Figure V.5 shows the enthalpy of dilution of H₂O/LiBr at 25 °C starting from an initial solution with a LiBr mole fraction of 0.23. It is observed that the more the initial sample is diluted, the lower the enthalpy of dilution. Negative values are indicative of an exothermic process when diluting the initial mixture. At LiBr mass fractions higher than 0.50 ($x_{LiBr} > 0.172$), typical of the operating conditions in the selected application, the enthalpy of dilution follows a linear trend with the lithium bromide mole fraction (area shown in Figure V.5).

Chapter V

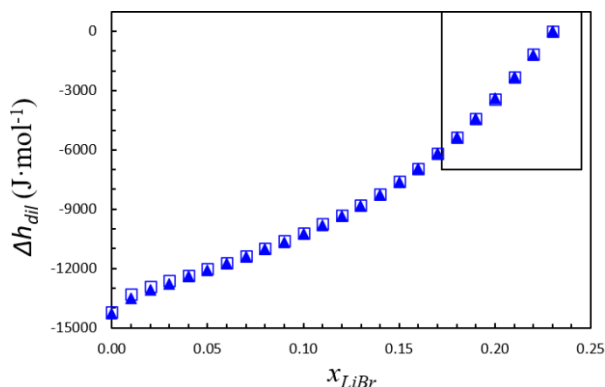


Figure V.5. Calculated enthalpy of dilution of H₂O/LiBr solutions at 298.15 K starting from an initial solution with mole fraction of lithium bromide equal to 0.23. ▲: Lange and Schwartz's data^[155] with Parker's correction^[151]; □: Parker^[151]. The area inside the small rectangle indicates the typical composition range of LiBr in absorption refrigeration and heat pump systems.

V.3.4 Experimental results and discussion

Figure V.6 shows the experimental results of enthalpy of dilution of the mixtures with and without additive. As expected, it increases linearly and negatively in the mixtures with additive. The negative values are characteristic of an exothermic process, representing that the processes of solute-solute and solvent-solvent bond breaking, which are endothermic, are energetically lower than the process of solute-solvent bond formation, which is exothermic.^[157,158]

It is observed that the enthalpy of dilution of H₂O/(LiBr+IL) mixtures with [EA][NO₃], [PA][NO₃], and [Dmim][Cl] is slightly lower than that of H₂O/LiBr, while that of the mixture with [EA][Cl] is slightly higher than that of H₂O/LiBr. Explaining this finding is complex since it must be considered that ionic liquids are also diluted in these mixtures, but their enthalpies of dilution are not known. One possible explanation is that the absorbent (LiBr+IL) does not interact as much with water when the added ionic liquid is [EA][Cl], as discussed in Section III.5, so that not as much heat is released as with the other ionic liquids. In H₂O/(LiBr+IL) mixtures with [EA][NO₃] and [Dmim][Cl], whose ILs share cation and anion with [EA][Cl], respectively, the enthalpy of dilution is slightly lower than in H₂O/LiBr.

The influence of the alkyl chain on the enthalpy of dilution of H₂O/(LiBr+IL) mixtures can be observed by comparing the values of mixtures with [EA][NO₃] and [PA][NO₃]. In the analysed composition range, the enthalpy of dilution is slightly lower in the mixture with [EA][NO₃] than in the mixture with [PA][NO₃], which is indicative of a higher hydrophobicity of the absorbent in the mixtures with propylammonium nitrate at the same absorbent mole fraction.

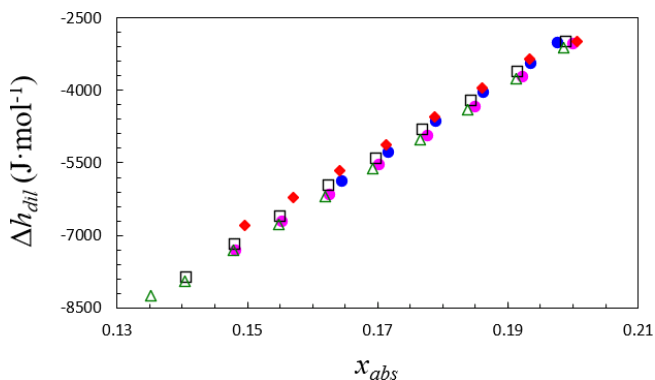


Figure V.6. Experimental enthalpy of dilution of H₂O/LiBr and H₂O/(LiBr+IL) mixtures at 298.15 K. ●: H₂O/LiBr from $x_{abs} = 0.228$; ●: H₂O/(LiBr+[EA][NO₃]) from $x_{abs} = 0.233$; □: H₂O/(LiBr+[PA][NO₃]) from $x_{abs} = 0.232$; ◆: H₂O/(LiBr+[EA][Cl]) from $x_{abs} = 0.232$; △: H₂O/(LiBr+[Dmim][Cl]) from $x_{abs} = 0.232$.

The results of mixtures with and without additives were compared by analysing the relative differences in the enthalpy of dilution at the same mole fraction ratio between lithium bromide and water at 25 °C (Eq. V.7).

$$\Delta(\Delta h_{dil})/\Delta h_{dil} (\%) = 100 \cdot \frac{\Delta h_{dil_{H_2O/(LiBr+IL)}} - \Delta h_{dil_{H_2O/LiBr}}}{\Delta h_{dil_{H_2O/LiBr}}} \quad \text{Eq. V.7}$$

The negative values observed for all the mixtures (Figure V.7) indicate that the heat released in the dilution process is lower in the presence of the ionic liquid. This result shows that the interactions between solute (LiBr+IL) and solvent (H₂O) in the presence of the ionic liquid are not as favoured as in its absence. A more detailed explanation of these results requires knowing the interactions of the ions in these mixtures, which could be studied by Molecular Dynamics simulations.^[109,125,159]

Chapter V

Comparatively, the enthalpy of dilution of the mixtures with protic ionic liquids ([EA][NO₃], [PA][NO₃], and [EA][Cl]) is lower than that of the mixture with [Dmim][Cl], suggesting that the degree of hydration of LiBr is lower in mixtures with protic ILs, as already discussed in Chapter III.

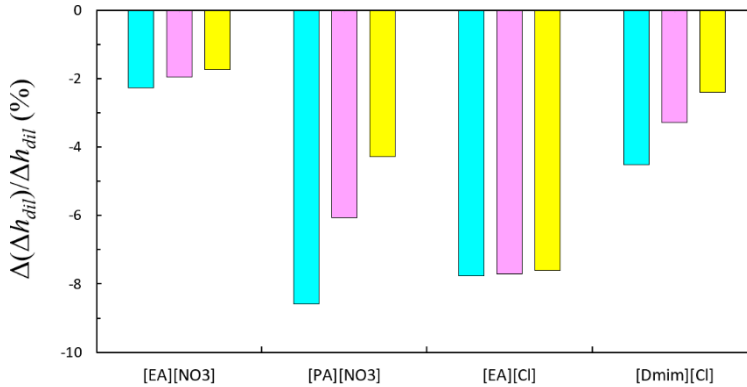


Figure V.7. Summary of enthalpy of dilution relative difference between H₂O/(LiBr+IL) and H₂O/LiBr mixtures at 298.15 K and $x_{IL}/x_{LiBr} \approx 0.0205$. Cyan: most negative difference; pink: average difference; yellow: most positive difference.

The general order of the relative enthalpy of dilution difference is: [EA][Cl] < [PA][NO₃] < [Dmim][Cl] \approx [EA][NO₃]. From the point of view of absorption refrigeration and heat pump systems, it is desirable to have a working pair with low enthalpy of dilution since the size of the generator and absorber could be reduced. In this sense, ionic liquids based on the ammonium cation would be better than those based on the imidazolium cation.

V.4. Electrical conductivity

V.4.1 Experimental device

The electrical conductivity was determined at atmospheric pressure with a Crison model 5298 platinum electrode connected to a Crison Conductimeter BASIC 30. Based on the electrode contact method, this equipment measures the electrical

conductivity at room temperature. Then, the device compensates for the value obtained to obtain the electrical conductivity at 20 °C and 25 °C.

The estimated uncertainties with a confidence level of 95 % ($k = 2$) are $U(w_{abs}) = 0.001$, $U(T) = 0.5$ K, and $U(\sigma) = 5$ %.

V.4.2 Experimental procedure

The analysed H₂O/(LiBr+IL) solutions (Table V.13) were prepared by weighing using a Mettler Toledo analytical balance model ME403. The successive solutions were prepared from a stock solution with an absorbent mass fraction of 0.60 by adding pure water. About 10 mL of each sample was used for each measurement.

The platinum cell with the electrodes was immersed in the solution until the sensor reading reached stability. The experiment was repeated several times at each composition to calculate an average value. At the end of the measurement, the device was cleaned with hot water and acetone.

Table V.13. Summary of the conditions at which the electrical conductivity was determined for H₂O/(LiBr+IL) mixtures. x_{IL}/x_{LiBr} : mole fraction ratio between IL and LiBr; T : temperature; w_{abs} : mass fraction of absorbent; x_{abs} : mole fraction of absorbent.

Mixture	x_{IL}/x_{LiBr}	w_{abs} range	T (K)
H ₂ O/(LiBr+[EA][NO ₃])	0.0204	0.10 – 0.60	293, 298
H ₂ O/(LiBr+[EA][Cl])	0.0209	0.05 – 0.60	293, 298
H ₂ O/(LiBr+[Dmim][Cl])	0.0203	0.05 – 0.60	293, 298
	0.0421	0.10 – 0.60	293, 298

V.4.3 Reference mixture: H₂O/LiBr

Table V.14 summarises the literature data regarding the electrical conductivity of the H₂O/LiBr mixture and the temperature and composition ranges, represented in Figure V.8.

Table V.14. Summary of available electrical conductivity values of H₂O/LiBr in the literature.

Reference	w_{abs}	T (K)
Labra <i>et al.</i> ^[142]	0.45 – 0.65	308 – 353
Molena ^t ^[160]	0.01 – 0.54	298
Baron and Scherba ^[161]	0.05 – 0.50	213 – 363
Fried and Segal ^[162]	0.41 – 0.64	288 – 353
Wu <i>et al.</i> ^[163]	0 – 0.44	293

It is observed that the electrical conductivity increases with temperature, as already demonstrated by Arrhenius,^[164] and that it reaches a maximum at a given composition. Wu *et al.*^[163] explained that this behaviour is governed by the phenomena of solvation and ion pairing and that the observed change in trend can be attributed to the predominance of ion pairing over ion solvation.

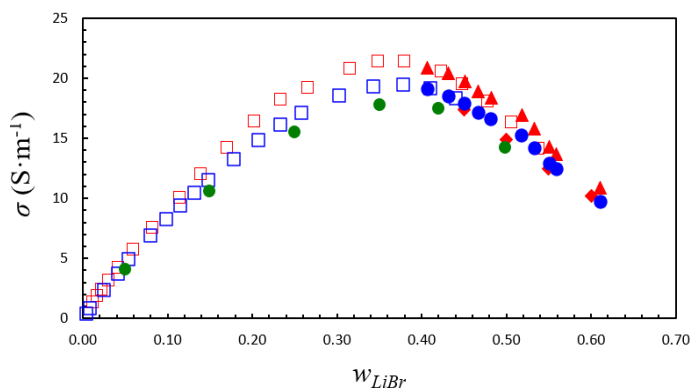


Figure V.8. Literature data of electrical conductivity of H₂O/LiBr against mass fraction of lithium bromide. Green series: 288.15 K; blue series: 293.15 K; red series: 298.15 K. ●: Baron and Scherba^[161]; □: Wu *et al.*^[163] ●: Fried and Segal^[162] □: Molena^t^[160] ▲: Fried and Segal^[162] ◆: Labra *et al.*^[142].

V.4.4 Experimental results and discussion

Tables V.15-V.18 show the experimental electrical conductivity of H₂O/(LiBr+IL) mixtures. These values are plotted in Figures V.9-V.10 along with those of H₂O/LiBr as a function of mass fraction of absorbent at 20 °C and 25 °C.

Chapter V

The behaviour of the mixtures with additives is similar to that of H₂O/LiBr. In general, there are no differences between the behaviour of the mixtures with ILs based on the ammonium cation and the mixture with IL based on the imidazolium cation. On average, the electrical conductivity of the mixtures in the presence of ILs decreases compared to that of H₂O/LiBr. Wu *et al.*^[163] attributed this fact to ion pairing and ion mobility. In this sense, the cation-cation interactions between ILs and LiBr would impair the mobility of the ions, resulting in lower electrical conductivity values.

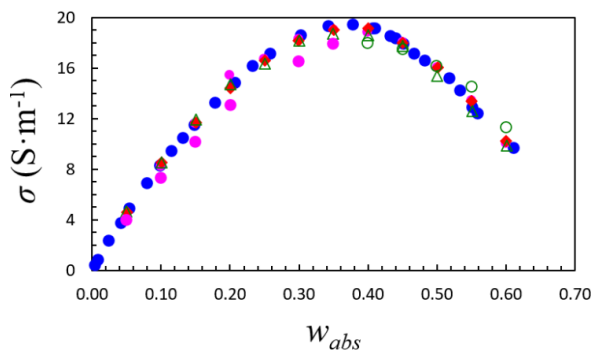


Figure V.9. Electrical conductivity of H₂O/(LiBr+IL) solutions at 293.15 K against mass fraction of absorbent. ●: H₂O/LiBr;^[162,163] ●: H₂O/(LiBr+[EA][NO₃]); ◆: H₂O/(LiBr+[EA][Cl]); △: H₂O/(LiBr+[Dmim][Cl]) with $x_{IL}/x_{LiBr} = 0.0203$; ○: H₂O/(LiBr+[Dmim][Cl]) with $x_{IL}/x_{LiBr} = 0.0421$.

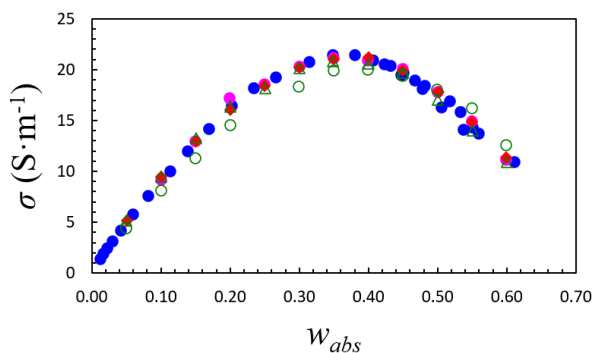


Figure V.10. Electrical conductivity of H₂O/(LiBr+IL) solutions at 298.15 K against mass fraction of absorbent. ●: H₂O/LiBr;^[160,162] ●: H₂O/(LiBr+[EA][NO₃]); ◆: H₂O/(LiBr+[EA][Cl]); △: H₂O/(LiBr+[Dmim][Cl]) with $x_{IL}/x_{LiBr} = 0.0203$; ○: H₂O/(LiBr+[Dmim][Cl]) with $x_{IL}/x_{LiBr} = 0.0421$.

Table V.15. Electrical conductivity of H₂O/(LiBr+[EA][NO₃]) solutions with $x_{IL}/x_{LiBr} = 0.0204$. w_{abs} : mass fraction of absorbent; x_{abs} : mole fraction of absorbent.

w_{abs}	x_{abs}	σ (S·m ⁻¹)	
		293.15 K	298.15 K
0.100	0.022	8.25	9.17
0.150	0.035	11.65	12.95
0.200	0.049	15.46	17.18
0.250	0.064	16.72	18.58
0.300	0.081	18.29	20.33
0.350	0.100	19.02	21.14
0.399	0.121	18.81	20.90
0.450	0.144	18.06	20.08
0.500	0.171	16.06	17.84
0.550	0.201	13.46	14.95
0.600	0.236	10.05	11.17

Table V.16. Electrical conductivity of H₂O/(LiBr+[EA][Cl]) solutions with $x_{IL}/x_{LiBr} = 0.0209$. w_{abs} : mass fraction of absorbent; x_{abs} : mole fraction of absorbent.

w_{abs}	x_{abs}	σ (S·m ⁻¹)	
		293.15 K	298.15 K
0.050	0.011	4.62	5.14
0.100	0.023	8.54	9.49
0.151	0.036	11.70	12.96
0.200	0.049	14.41	16.03
0.250	0.065	16.61	18.43
0.300	0.082	18.19	20.21
0.350	0.101	18.98	21.09
0.400	0.122	19.11	21.23
0.450	0.145	17.95	19.94
0.501	0.173	16.01	17.81
0.550	0.202	13.36	14.85
0.600	0.237	10.24	11.40

Table V.17. Electrical conductivity of H₂O/(LiBr+[Dmim][Cl]) solutions with $x_{iL}/x_{LiBr} = 0.0203$. w_{abs} : mass fraction of absorbent; x_{abs} : mole fraction of absorbent.

w_{abs}	x_{abs}	σ (S·m ⁻¹)	
		293.15 K	298.15 K
0.050	0.011	4.67	5.19
0.100	0.022	8.56	9.51
0.150	0.035	11.92	13.24
0.200	0.049	14.72	16.36
0.250	0.064	16.36	18.18
0.300	0.081	18.14	20.16
0.349	0.099	18.73	20.79
0.400	0.120	18.56	20.63
0.450	0.144	17.71	19.67
0.500	0.171	15.35	17.07
0.551	0.201	12.61	14.02
0.601	0.236	9.85	10.94

Table V.18. Electrical conductivity of H₂O/(LiBr+[Dmim][Cl]) solutions with $x_{iL}/x_{LiBr} = 0.0421$. w_{abs} : mass fraction of absorbent; x_{abs} : mole fraction of absorbent.

w_{abs}	x_{abs}	σ (S·m ⁻¹)	
		293.15 K	298.15 K
0.050	0.011	3.99	4.43
0.100	0.022	7.30	8.11
0.150	0.035	10.19	11.28
0.200	0.048	13.06	14.52
0.300	0.080	16.50	18.33
0.349	0.098	17.93	19.92
0.399	0.119	17.98	19.99
0.450	0.142	17.47	19.42
0.499	0.168	16.16	18.03
0.550	0.199	14.55	16.19
0.600	0.233	11.34	12.58

Chapter V

The electrical conductivity values of H₂O/LiBr and H₂O/(LiBr+IL) mixtures were correlated at 20 °C and 25 °C according to the transformed Casteel-Amis equation^[165,166] (Eq. V.8), where σ , b , x , and y are the electrical conductivity, molality, and two fitting coefficients, respectively. σ_p and b_p correspond to the maximum electrical conductivity and the molality at which it occurs.

Experimental data from Molenat,^[160] Fried and Segal,^[162] and Wu *et al.*^[163] were used to model the electrical conductivity of H₂O/LiBr. The root mean square error (Eq. V.9) between the calculated and experimentally obtained electrical conductivity was minimised in the fit.

$$\frac{\sigma}{\sigma_p} = \left(\frac{b}{b_p}\right)^x \cdot \exp \left[-y \cdot b_p^2 \cdot \left(\frac{b}{b_p} - 1\right)^2 - x \cdot \left(\frac{b}{b_p} - 1\right) \right] \quad \text{Eq. V.8}$$

$$RMSE = \sqrt{\frac{1}{n} \cdot \sum_{i=1}^n \left(\frac{\sigma_{calc}}{\sigma_p} - \frac{\sigma_{exp}}{\sigma_p} \right)^2} \quad \text{Eq. V.9}$$

Table V.19 shows the values of x and y coefficients together with the *RMSE* obtained for each fitting.

Table V.19. Coefficients and *RMSE* of the electrical conductivity correlation for H₂O/LiBr and H₂O/(LiBr+IL) mixtures. x_{IL}/x_{LiBr} : mole fraction ratio between IL and LiBr.

Mixture	x_{IL}/x_{LiBr}	<i>x</i>	<i>y</i>	<i>RMSE</i>	<i>x</i>	<i>y</i>	<i>RMSE</i>
		293.15 K			298.15 K		
H ₂ O/LiBr	-	0.8673	$2.656 \cdot 10^{-3}$	0.0119	0.8434	$3.460 \cdot 10^{-3}$	0.0236
H ₂ O/(LiBr+[EA][NO ₃])	0.0204	1.117	$-2.135 \cdot 10^{-3}$	0.0242	1.117	$-2.131 \cdot 10^{-3}$	0.0242
H ₂ O/(LiBr+[EA][Cl])	0.0209	0.6735	$3.838 \cdot 10^{-3}$	0.0325	0.6752	$3.810 \cdot 10^{-3}$	0.0322
H ₂ O/(LiBr+[Dmim][Cl])	0.0203	1.055	$-1.504 \cdot 10^{-3}$	0.0193	1.053	$-1.507 \cdot 10^{-3}$	0.0193
	0.0421	0.9173	$4.995 \cdot 10^{-3}$	0.0106	0.9195	$4.953 \cdot 10^{-3}$	0.0106

V.5. Thermal conductivity

V.5.1 Experimental device

Thermal conductivity was determined at atmospheric pressure with a Decagon KD2 Pro connected to a Thermal Analyzer based on the transient hot wire method.

The estimated uncertainties with a 95 % confidence level ($k = 2$) are $U(w_{abs}) = 0.001$, $U(T) = 0.5$ °C, and $U(\lambda) = 5$ %.

V.5.2 Experimental procedure

The analysed $\text{H}_2\text{O}/(\text{LiBr}+[\text{Dmim}][\text{Cl}])$ samples were prepared separately by weighing using a Mettler Toledo ME403 analytical balance. Approximately 15 mL of solution were prepared for each composition.

The sample is placed in a special glass beaker immersed in a water bath; the temperature is kept constant using a Julabo thermostatic bath (mod. ME). The measuring probe is inserted vertically. Once thermal equilibrium is reached, the measurement is repeated up to 6 times at 15 min intervals to ensure thermal equilibrium.

The thermal conductivity of $\text{H}_2\text{O}/(\text{LiBr}+[\text{Dmim}][\text{Cl}])$ mixture at $x_{\text{IL}}/x_{\text{LiBr}} = 0.0449$ was determined from (20 to 34) °C at absorbent mass fractions between 0.401 and 0.536.

V.5.3 Reference mixture: $\text{H}_2\text{O}/\text{LiBr}$

The thermal conductivity of aqueous lithium bromide has been experimentally determined in the literature.^[167–169] Figure V.11 shows the thermal conductivity of $\text{H}_2\text{O}/\text{LiBr}$ as a function of temperature at different LiBr compositions, calculated using a literature correlation.^[123] It is observed that the thermal conductivity increases with temperature and decreases with lithium bromide composition.

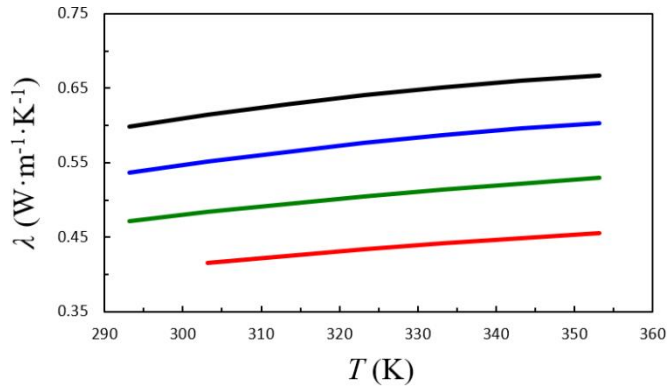


Figure V.11. Thermal conductivity of H₂O/LiBr as a function of mass fraction of lithium bromide and temperature.^[123] Black line: pure water ($w_{LiBr} = 0$);^[140] blue line: $w_{LiBr} = 0.20$; green line: $w_{LiBr} = 0.40$; red line: $w_{LiBr} = 0.60$.

V.5.4 Experimental results and discussion

Table V.20 and Figure V.12 show the experimental values of thermal conductivity of H₂O/(LiBr+[Dmim][Cl]) at $x_{IL}/x_{LiBr} = 0.0449$. As expected, based on the behaviour of H₂O/LiBr, the thermal conductivity of this mixture increases with temperature and decreases with solute composition. The decrease in thermal conductivity with solute composition can be attributed to a lower vibration of the molecular bonds of pure water^[109] due to an increase in solute-solvent and solute-solute interactions.

Table V.20. Thermal conductivity of H₂O/(LiBr+[Dmim][Cl]) with $x_{IL}/x_{LiBr} = 0.0449$. w_{abs} : mass fraction of absorbent. x_{abs} : mole fraction of absorbent.

w_{abs}	x_{abs}	T (K)	λ (W·m ⁻¹ ·K ⁻¹)
0.401	0.119	293.2	0.448
		297.9	0.458
		302.6	0.462
		307.3	0.469
0.445	0.140	293.3	0.430
		297.9	0.438
		302.8	0.441
		307.4	0.446

Chapter V

Table V.20 (continued)

w_{abs}	x_{abs}	T (K)	λ ($\text{W}\cdot\text{m}^{-1}\cdot\text{K}^{-1}$)
0.501	0.169	293.2	0.420
		298.0	0.428
		302.8	0.431
		307.3	0.433
0.536	0.190	293.3	0.405
		298.0	0.412
		302.8	0.415
		307.5	0.419

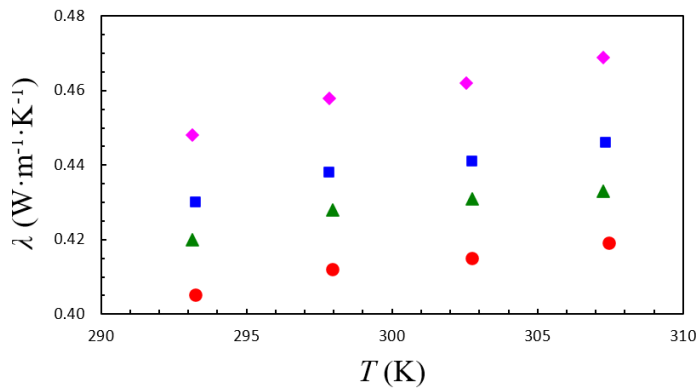


Figure V.12. Thermal conductivity of $\text{H}_2\text{O}/(\text{LiBr}+[\text{Dmim}][\text{Cl}])$ with $x_{IL}/x_{LiBr} = 0.0449$. \blacklozenge : $w_{abs} = 0.401$; \blacksquare : $w_{abs} = 0.455$; \blacktriangle : $w_{abs} = 0.501$; \bullet : $w_{abs} = 0.536$.

The thermal conductivity of $\text{H}_2\text{O}/(\text{LiBr}+[\text{Dmim}][\text{Cl}])$ has been modelled with a polynomial equation (Eq. V.10), where T is the temperature (K), w_{abs} is the mass fraction of absorbent, and a , b , and c are the fit coefficients. The root mean square error between the calculated and the experimental thermal conductivity was minimised in the fit (Eq. V.11).

Chapter V

$$\lambda = a + b \cdot w_{abs} \cdot T + c \cdot w_{abs} \cdot T^2 \quad \text{Eq. V.10}$$

$$RMSE = \sqrt{\frac{1}{n} \cdot \sum_{i=1}^n (\lambda_{calc} - \lambda_{exp})^2} \quad \text{Eq. V.11}$$

Table V.21 shows the values of the correlation coefficients and *RMSE*.

Table V.21. Coefficients and *RMSE* of the correlation for the thermal conductivity of H₂O/(LiBr+[Dmim][Cl]) with $x_{IL}/x_{LiBr} = 0.0449$.

<i>a</i> (W·m ⁻¹ ·K ⁻¹)	<i>b</i> (W·m ⁻¹ ·K ⁻²)	<i>c</i> (W·m ⁻¹ ·K ⁻³)	<i>RMSE</i> (W·m ⁻¹ ·K ⁻¹)
0.5869	-0.00438	1.1·10 ⁻⁵	0.003969

The thermal conductivity of the mixture with additive has been compared with that of the mixture without additive according to Eq. V.12 as a function of the x_{LiBr}/x_{H_2O} ratio and temperature.

$$\Delta\lambda/\lambda (\%) = 100 \cdot \frac{\lambda_{H_2O/(LiBr+IL)} - \lambda_{H_2O/LiBr}}{\lambda_{H_2O/LiBr}} \quad \text{Eq. V.12}$$

Figure V.13 shows that the relative difference in thermal conductivity is always negative in the analysed composition and temperature range. Interpreting the change in trend at different x_{LiBr}/x_{H_2O} ratios would require knowledge of the influence of temperature on both the molecular structures of the ionic liquid and those of water. Again, helpful information for this analysis could be obtained from computational studies based on Molecular Dynamics simulations.

The lower thermal conductivity of this H₂O/(LiBr+[Dmim][Cl]) mixture compared to H₂O/LiBr contrasts with the higher amount of bulk water in the mixtures with additive, discussed in Chapter III. This fact evidences the relevance of solute-solute interactions in the values of this property in these mixtures.

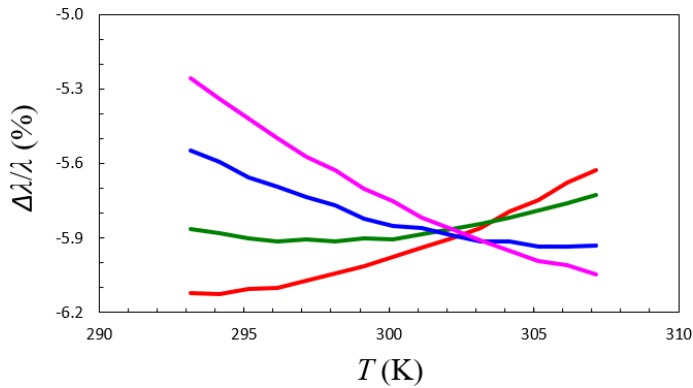


Figure V.13. Relative thermal conductivity difference between $\text{H}_2\text{O}/(\text{LiBr}+[\text{Dmim}][\text{Cl}])$ with $x_{\text{IL}}/x_{\text{LiBr}} = 0.0449$ and $\text{H}_2\text{O}/\text{LiBr}$. Pink series: $x_{\text{LiBr}}/x_{\text{H}_2\text{O}} = 0.130$; blue series: $x_{\text{LiBr}}/x_{\text{H}_2\text{O}} = 0.156$; green series: $x_{\text{LiBr}}/x_{\text{H}_2\text{O}} = 0.195$; red series: $x_{\text{LiBr}}/x_{\text{H}_2\text{O}} = 0.224$.

From the point of view of the application, a lower thermal conductivity will result in a higher difficulty in transferring heat. Hence, the area of the heat exchangers should increase in the presence of this IL, impairing the performance of the working fluid.

V.6. Dynamic viscosity

V.6.1 Experimental device

Dynamic viscosity was determined at atmospheric pressure using the Cambridge Viscosity ViscoPro 2000 viscometer, based on the movement of a piston through the solution.

The estimated uncertainties with a 95 % confidence level ($k = 2$) are $U(w_{abs}) = 0.001$, $U(T) = 0.05$ °C, and $U(\eta) = 0.05$ mPa·s.

V.6.2 Experimental procedure

$\text{H}_2\text{O}/(\text{LiBr}+\text{IL})$ samples were prepared separately by weighing using a Mettler Toledo analytical balance model ME403. About 25 mL of sample were prepared for each composition.

Upon completion of the experiments, the viscometer was cleaned by rinsing it with hot water and acetone and applying vacuum.

The dynamic viscosity of the $\text{H}_2\text{O}/(\text{LiBr}+[\text{Dmim}][\text{Cl}])$ mixture at $x_{\text{IL}}/x_{\text{LiBr}} = 0.0423$ was determined from (20 to 100) °C and absorbent mass fraction ranging from 0.401 to 0.536.

V.6.3 Reference mixture: $\text{H}_2\text{O}/\text{LiBr}$

In a recent work, Fleßner and Ziegler^[170] developed an empirical correlation to estimate the dynamic viscosity of $\text{H}_2\text{O}/\text{LiBr}$ using experimental data reported in the literature (Figure V.14). It is observed that the values decrease with temperature and increase the higher the LiBr composition in the solution. On the one hand, the increase in flow resistance with absorbent composition can be attributed to interactions in the solution, which are significantly influenced by the breakdown of the molecular structure of water and ion pairing.^[171,172] On the other hand, the decrease in dynamic viscosity with temperature can be attributed to the higher kinetic energy of the molecules, which decreases the attractive forces between the molecules, reducing their resistance to flow.

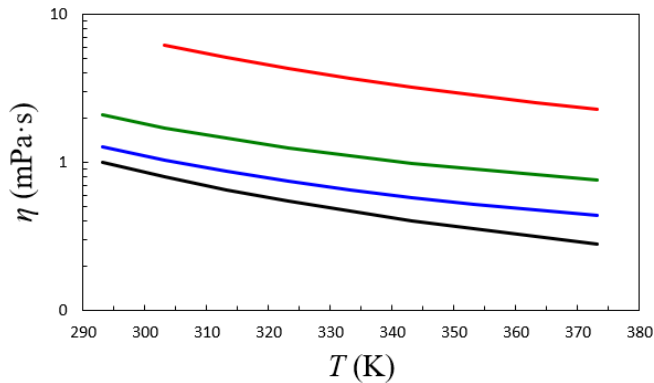


Figure V.14. Estimated dynamic viscosity of $\text{H}_2\text{O}/\text{LiBr}$ against temperature and mass fraction of lithium bromide using Fleßner and Ziegler's correlation.^[170] Black line: pure water ($w_{\text{LiBr}} = 0$);^[140] blue line: $w_{\text{LiBr}} = 0.20$; green line: $w_{\text{LiBr}} = 0.40$; red line: $w_{\text{LiBr}} = 0.60$.

V.6.4 Experimental results and discussion

Table V.22 and Figure V.15 show the experimental values of dynamic viscosity of the $\text{H}_2\text{O}/(\text{LiBr}+[\text{Dmim}][\text{Cl}])$ mixture with $x_{\text{IL}}/x_{\text{LiBr}} = 0.0423$. As for $\text{H}_2\text{O}/\text{LiBr}$, the viscosity of this mixture increases with absorbent composition and decreases with temperature.

Table V.22. Dynamic viscosity of H₂O/(LiBr+[Dmim][Cl]) with $x_{IL}/x_{LiBr} = 0.0423$. w_{abs} : mass fraction of absorbent; x_{abs} : mole fraction of absorbent.

w_{abs}	x_{abs}	η (mPa·s)								
		T (K)								
		293.15	303.15	313.15	323.15	333.15	343.15	353.15	363.15	373.15
0.424	0.130	2.53	2.02	1.65	1.37	1.17	1.01	0.88	0.78	0.70
0.531	0.187	3.81	3.05	2.51	2.12	1.83	1.61	1.44	1.30	1.20
0.568	0.210	7.52	5.54	4.23	3.33	2.71	2.33	1.91	1.65	1.45

Chapter V

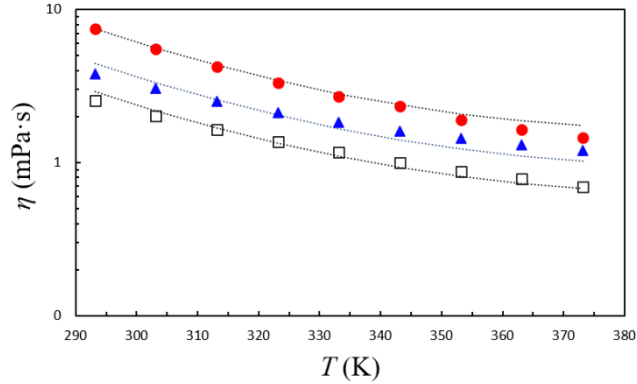


Figure V.15. Dynamic viscosity of the $\text{H}_2\text{O}/(\text{LiBr}+[\text{Dmim}][\text{Cl}])$ mixture with $x_{\text{IL}}/x_{\text{LiBr}} = 0.0423$ against temperature and mass fraction of absorbent. \square : $w_{\text{abs}} = 0.424$; \blacklozenge : $w_{\text{abs}} = 0.531$; \blacktriangle : $w_{\text{abs}} = 0.568$. Dotted lines represent the calculated dynamic viscosity with the proposed correlation.

The experimental viscosity values were modeled with an exponential equation (Eq. V.13), where $\eta_0 = 1$ mPa·s, T is the temperature (K), w_{abs} the mass fraction of absorbent, a , b_1 , b_2 , c_1 , and c_2 the fitting coefficients. The root mean square error between the calculated and experimentally obtained thermal conductivity was minimized in the fit (Eq. V.14).

$$\frac{\eta}{\eta_0} = \exp \left[a + \sum_{n=1}^2 (b_n \cdot w_{\text{abs}}^n + c_n \cdot T^n) \right] \quad \text{Eq. V.13}$$

$$RMSE = \sqrt{\frac{1}{n} \cdot \sum_{i=1}^n \left(\frac{\eta_{\text{calc}}}{\eta_0} - \frac{\eta_{\text{exp}}}{\eta_0} \right)^2} \quad \text{Eq. V.14}$$

Table V.23 shows the values of the correlation coefficients and $RMSE$.

Table V.23. Coefficients and $RMSE$ of the correlation for the dynamic viscosity of $\text{H}_2\text{O}/(\text{LiBr}+[\text{Dmim}][\text{Cl}])$ with $x_{\text{IL}}/x_{\text{LiBr}} = 0.0423$.

a	b_1	b_2	c_1	c_2	$RMSE$
37.65	-63.95	71.07	-0.1211	$1.543 \cdot 10^{-4}$	0.2158

The comparison between the values of the mixtures with and without additive was carried out by calculating the relative difference in dynamic viscosity as a function of the $x_{\text{LiBr}}/x_{\text{H}_2\text{O}}$ ratio and temperature (Eq. V.15).

$$\Delta\eta/\eta (\%) = 100 \cdot \frac{\eta_{\text{H}_2\text{O}/(\text{LiBr}+\text{IL})} - \eta_{\text{H}_2\text{O}/\text{LiBr}}}{\eta_{\text{H}_2\text{O}/\text{LiBr}}} \quad \text{Eq. V.15}$$

The relative difference in dynamic viscosity at absorbent mass fractions lower than 0.531 is generally negative, indicating that the mixture with additive is less viscous than $\text{H}_2\text{O}/\text{LiBr}$. However, between 20 °C and 50 °C and $x_{\text{LiBr}}/x_{\text{H}_2\text{O}} > 0.20$ ($w_{\text{abs}} > 0.50$), which are typical absorber working conditions in the considered application, this effect is reversed, with an average value of the relative dynamic viscosity difference of 11.7 %. This behaviour is similar to that already seen when analysing the thermal conductivity and cannot be explained solely in terms of the higher percentage of bulk water in the presence of ionic liquid. In this case, in addition to solute-solute, solute-solvent, and solvent-solvent interactions, it is also necessary to consider that the viscosity of ionic liquids is higher than that of water.^[173]

The presence of the ionic liquid impairs the performance of the working fluid since the higher resistance to flow is associated with higher power consumption in the solution pump.

V.7. Summary of the influence of ILs on the thermophysical properties of $\text{H}_2\text{O}/\text{LiBr}$

Figure V.16 shows the average relative difference of the analysed thermophysical properties between the mixtures with and without additive, discussed in the previous sections, as a function of the ionic liquid and its composition.

Regarding thermodynamic properties, $\text{H}_2\text{O}/(\text{LiBr}+\text{IL})$ mixtures have, in general, lower density, speed of sound, and enthalpy of dilution than $\text{H}_2\text{O}/\text{LiBr}$. These values can be directly related to the higher amount of bulk water in the mixtures with additive. Lower density in the presence of the ionic liquid can be expected to impair the performance of the working fluid, while lower enthalpy of dilution has the opposite effect. Even though the speed of sound does not influence the operation of absorption

Chapter V

refrigeration and heat pump systems, it will be used to comparatively analyse solute-solvent interactions in Chapter VI.

With respect to transport properties, the $\text{H}_2\text{O}/(\text{LiBr}+\text{IL})$ mixtures have, in general, lower values of electrical conductivity, thermal conductivity, and dynamic viscosity than $\text{H}_2\text{O}/\text{LiBr}$. The changes in these properties in the presence of additive cannot be directly related to the higher amount of bulk water in the mixtures with additive. Compared to $\text{H}_2\text{O}/\text{LiBr}$, the lower thermal conductivity and higher dynamic viscosity of $\text{H}_2\text{O}/(\text{LiBr}+[\text{Dmim}][\text{Cl}])$ at typical working conditions for the selected application impairs the performance of the working fluid.

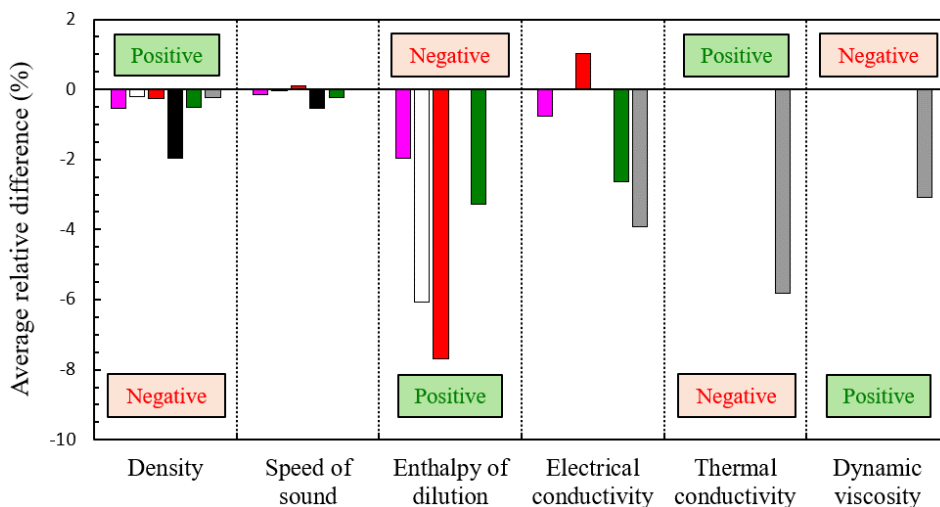


Figure V.16. Summary of average relative difference of the experimentally determined thermophysical properties of $\text{H}_2\text{O}/(\text{LiBr}+\text{IL})$ mixtures with respect to $\text{H}_2\text{O}/\text{LiBr}$. Magenta: $[\text{EA}][\text{NO}_3]$; white: $[\text{PA}][\text{NO}_3]$; red: $[\text{EA}][\text{Cl}]$; black: $[\text{Bmim}][\text{Br}]$; green and grey: $[\text{Dmim}][\text{Cl}]$. All bars show results at $x_{\text{IL}}/x_{\text{LiBr}} \approx 0.0205$, except for grey bar ($[\text{Dmim}][\text{Cl}]$), at $x_{\text{IL}}/x_{\text{LiBr}} \approx 0.0435$. Positive and negative labels indicate whether the influence of the ionic liquid on each property is beneficial or not in the application.

V.8. Conclusions

The conclusions drawn in this chapter correspond to specific objectives 4 and 5 (Section I.6).

The average relative difference in properties between $\text{H}_2\text{O}/(\text{LiBr}+\text{IL})$ and $\text{H}_2\text{O}/\text{LiBr}$ was analysed, and its effect on the application was discussed.

According to the discussed results, the use of the ionic liquids considered enhances the enthalpy of dilution of the working fluid but impairs other relevant properties that directly influence its performance: lower density, thermal conductivity, and higher dynamic viscosity.

The influence of ionic liquids on the analysed thermodynamic properties (density, speed of sound, and enthalpy of dilution) of $\text{H}_2\text{O}/(\text{LiBr}+\text{IL})$ mixtures can be related to their higher percentage of bulk water.

The influence of the ionic liquid on the analysed transport properties (electrical conductivity, thermal conductivity, and dynamic viscosity) of the $\text{H}_2\text{O}/(\text{LiBr}+\text{IL})$ mixture cannot be directly related to their higher amount of bulk water.

The analysis of thermophysical properties and the results obtained from NIR+MCR-ALS provide useful complementary information for interpreting the influence of ionic liquids on the thermophysical properties of $\text{H}_2\text{O}/\text{LiBr}$.

Chapter VI. Analysis of the influence of ionic liquid on the solute-solvent interaction in H₂O/(LiBr+IL) mixtures using derived volumetric properties

VI.1. Introduction

Derived volumetric properties of electrolyte solutions allow the analysis of solute-solvent, solute-solute, and solvent-solvent interactions from a thermodynamic point of view.^[70]

In the context of the application considered in this doctoral thesis, the interest lies in using these properties to analyse the influence of the ionic liquid on the interaction between solute (LiBr+IL) and solvent (H₂O). To achieve this, estimating the properties at infinite dilution conditions is necessary, where solute-solute interactions can be assumed to be negligible.^[43,71]

The properties considered for the analysis are the apparent molar volume at infinite dilution, the isentropic compressibility, and the limiting apparent molar isentropic compressibility.

To discuss the results, a comparative analysis of the derived volumetric properties has been carried out, assuming that the solute consists of both lithium bromide and ionic liquid (LiBr+IL).

As described in Section II.4, obtaining properties at infinite dilution requires knowledge of the apparent molar properties, which have been calculated using the experimental density and speed of sound data reported in Section V.2 (Tables V.2-V.6). Table VI.1 summarises the temperature and composition range in which the derived volumetric properties were analysed.

Table VI.1. Summary of conditions at which the analysis was carried out for each mixture. x_{IL}/x_{LiBr} : mole fraction ratio between IL and LiBr; T : temperature; b : molality; x_{LiBr}/x_{H_2O} : mole fraction ratio between LiBr and H₂O.

Mixture	x_{IL}/x_{LiBr}	T (K)	b (mol·kg ⁻¹)	x_{LiBr}/x_{H_2O}
H ₂ O/LiBr	-	293 – 343	0.6 – 15	0.01 – 0.28
H ₂ O/(LiBr+[EA][NO ₃])	0.0205	293 – 343	0.6 – 16	0.01 – 0.28
H ₂ O/(LiBr+[PA][NO ₃])	0.0205	293 – 343	0.6 – 16	0.01 – 0.28
H ₂ O/(LiBr+[EA][Cl])	0.0205	293 – 343	0.6 – 16	0.01 – 0.28
H ₂ O/(LiBr+[Bmim][Br])	0.0208	293 – 343	0.3 – 15	0.01 – 0.27
H ₂ O/(LiBr+[Dmim][Cl])	0.0203	293 – 343	0.6 – 16	0.01 – 0.28

The application of the successive equations has required estimation of both the molar mass of the solute in solution and the coefficients V_{φ}^0 , S_V , and B_V of the Redlich-Rosenfeld-Meyer equation (Eq. II.32, Section II.4.1).

The molar mass of the solute (LiBr+IL) was calculated as the weighted sum of the molar masses as a function of the mole fractions of these compounds (Eq. VI.1).

$$M_{solute} = \frac{x_{LiBr} \cdot M_{LiBr} + x_{IL} \cdot M_{IL}}{x_{LiBr} + x_{IL}} \quad \text{Eq. VI.1}$$

The apparent molar volume (V_{φ}) in H₂O/LiBr solutions was calculated from density values estimated using literature data.^[123] The apparent molar volume at infinite dilution (V_{φ}^0) of these solutions was obtained from (20 to 40) °C using data from Bagheri *et al.*^[43] and from (50 to 70) °C using data from Millero.^[70] S_V and B_V parameters in H₂O/LiBr solutions were calculated from the values reported by Bagheri *et al.*^[43]

Comparative analysis of the results for the different solutes was also conducted using Hepler's constant,^[73] isentropic compressibility (κ_S), and limiting apparent molar isentropic compressibility (κ_{φ}^0), defined in Section II.4.

The isentropic compressibility of H₂O/LiBr solutions was estimated based on density data referenced in the literature^[123] and the speed of sound fit shown in Section V.2 with data from Rohman *et al.*^[75]

VI.2. Apparent molar volume at infinite dilution

The apparent molar volume is a property defined to isolate the contribution of the solute to the non-ideality of the mixture. Its value depends on the interactions relative to the solute, i.e. solute-solute and solute-solvent interactions.

Table VI.2 shows the results of the apparent molar volume of lithium bromide in H₂O/LiBr solutions. It is observed that the values increase with the solute composition and with temperature from 20 °C to 50 °C, then decrease from 50 °C to 70 °C. On the one hand, the increase in the apparent molar volume with solute composition may indicate the formation of more significant ion pairs as the amount of solvent decreases. On the other hand, the increase in V_{φ} with temperature up to 50 °C is not surprising, considering that the increase in kinetic energy of the molecules facilitates

Chapter VI

their mobility and causes more significant expansion. The decrease at higher temperatures suggests structural changes in the solvent,^[174,175] the solute, and/or specific interactions between molecules in solution.

Table VI.2. Apparent molar volume of H₂O/LiBr solutions. *b*: molality; $x_{\text{LiBr}}/x_{\text{H}_2\text{O}}$: mole fraction ratio between LiBr and H₂O; *T*: temperature.

<i>b</i> (mol·kg ⁻¹)	$x_{\text{LiBr}}/x_{\text{H}_2\text{O}}$	$10^6 \cdot V_\phi$ (m ³ ·mol ⁻¹)						$U(V_\phi)$ (m ³ ·mol ⁻¹)
		<i>T</i> (K)						
		293.15	303.15	313.15	323.15	333.15	343.15	
0.594	0.011	24.2	25.2	25.7	25.8	25.8	25.6	8.6
1.79	0.036	25.5	25.8	25.9	25.8	25.7	25.5	2.9
3.30	0.067	25.8	26.0	26.0	26.0	25.8	25.7	1.6
6.05	0.109	26.0	26.1	26.2	26.1	26.0	25.9	0.90
9.21	0.168	26.1	26.2	26.3	26.3	26.2	26.2	0.60
15.5	0.247	26.1	26.3	26.4	26.5	26.5	26.5	0.37

The apparent molar volume of the LiBr+IL solutes analysed in H₂O/(LiBr+IL) solutions is shown in Tables VI.3-VI.7. As an example, Figure VI.1 shows the values obtained for solutions with protic ([EA][NO₃]) and aprotic ([Dmim][Cl]) ionic liquids. In both cases, the behaviour with temperature and composition follows the trend already discussed for H₂O/LiBr solutions. Comparatively, the apparent molar volume in mixtures with additive is more significant than in H₂O/LiBr in the considered temperature and composition range.

Chapter VI

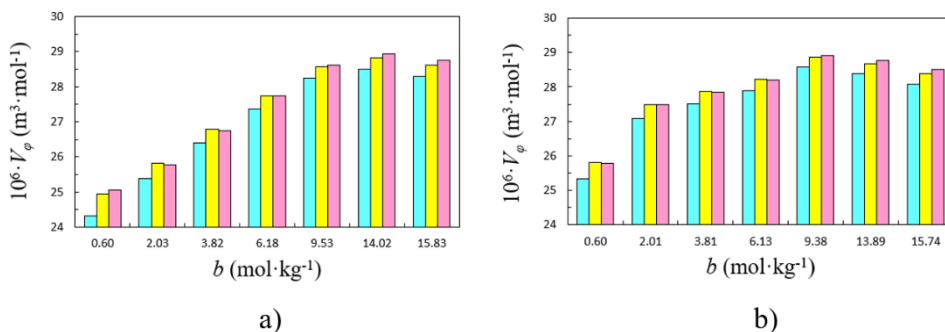


Figure VI.1. Apparent molar volume of (LiBr+IL) in H₂O/(LiBr+IL) mixtures as a function of molality and temperature. a) LiBr+[EA][NO₃]; b) LiBr+[Dmim][Cl]. Cyan: 293.15 K; yellow: 313.15 K; pink: 333.15 K.

Table VI.3. Apparent molar volume of H₂O/(LiBr+[EA][NO₃]) solutions with $x_{iL}/x_{LiBr} = 0.0205$. b : molality; x_{LiBr}/x_{H_2O} : mole fraction ratio between LiBr and H₂O; T : temperature.

b (mol·kg ⁻¹)	x_{LiBr}/x_{H_2O}	$10^6 \cdot V_\phi$ (m ³ ·mol ⁻¹)					
		T (K)					
		293.15	303.15	313.15	323.15	333.15	343.15
0.603	0.011	24.3	24.6	24.9	25.0	25.1	25.2
2.03	0.036	25.4	25.7	25.8	25.9	25.8	25.6
3.82	0.067	26.4	26.7	26.8	26.8	26.8	26.6
6.18	0.109	27.4	27.6	27.7	27.8	27.7	27.6
9.53	0.168	28.2	28.4	28.6	28.6	28.6	28.6
14.0	0.247	28.5	28.7	28.8	28.9	28.9	28.9
15.8	0.279	28.3	28.5	28.6	28.7	28.8	28.8
$10^6 \cdot U(V_\phi) = 1.3 \text{ m}^3 \cdot \text{mol}^{-1}$							

Chapter VI

Table VI.4. Apparent molar volume of $\text{H}_2\text{O}/(\text{LiBr}+[\text{PA}][\text{NO}_3])$ solutions with $x_{\text{IL}}/x_{\text{LiBr}} = 0.0205$. b : molality; $x_{\text{LiBr}}/x_{\text{H}_2\text{O}}$: mole fraction ratio between LiBr and H_2O ; T : temperature.

b (mol·kg ⁻¹)	$x_{\text{LiBr}}/x_{\text{H}_2\text{O}}$	$10^6 \cdot V_\phi$ (m ³ ·mol ⁻¹)					
		T (K)					
		293.15	303.15	313.15	323.15	333.15	343.15
0.60	0.011	20.1	20.5	20.6	20.6	20.5	20.2
1.97	0.035	24.7	25.1	25.2	25.2	25.1	24.9
3.79	0.067	26.4	26.6	26.7	26.8	26.7	26.5
6.10	0.108	27.2	27.5	27.6	27.6	27.6	27.5
9.29	0.164	27.8	28.0	28.1	28.2	28.2	28.1
15.8	0.278	27.9	28.1	28.3	28.4	28.4	28.4
$10^6 \cdot U(V_\phi) = 1.3 \text{ m}^3 \cdot \text{mol}^{-1}$.							

Table VI.5. Apparent molar volume of $\text{H}_2\text{O}/(\text{LiBr}+[\text{EA}][\text{Cl}])$ solutions with $x_{\text{IL}}/x_{\text{LiBr}} = 0.0205$. b : molality; $x_{\text{LiBr}}/x_{\text{H}_2\text{O}}$: mole fraction ratio between LiBr and H_2O ; T : temperature.

b (mol·kg ⁻¹)	$x_{\text{LiBr}}/x_{\text{H}_2\text{O}}$	$10^6 \cdot V_\phi$ (m ³ ·mol ⁻¹)					
		T (K)					
		293.15	303.15	313.15	323.15	333.15	343.15
0.607	0.011	22.8	23.0	23.2	23.2	23.0	22.8
2.03	0.036	24.8	25.0	25.2	25.2	25.1	24.9
3.84	0.068	25.7	25.9	26.0	26.0	25.9	25.8
6.22	0.110	26.6	26.9	27.0	27.0	26.9	26.8
9.44	0.167	27.3	27.5	27.6	27.6	27.6	27.6
14.1	0.250	27.7	27.9	28.0	28.1	28.1	28.1
15.9	0.281	27.6	27.8	27.9	28.0	28.0	28.0
$10^6 \cdot U(V_\phi) = 1.3 \text{ m}^3 \cdot \text{mol}^{-1}$.							

Chapter VI

Table VI.6. Apparent molar volume of $\text{H}_2\text{O}/(\text{LiBr}+[\text{Bmim}][\text{Br}])$ solutions with $x_{\text{IL}}/x_{\text{LiBr}} = 0.0208$. b : molality; $x_{\text{LiBr}}/x_{\text{H}_2\text{O}}$: mole fraction ratio between LiBr and H_2O ; T : temperature.

b (mol·kg ⁻¹)	$x_{\text{LiBr}}/x_{\text{H}_2\text{O}}$	$10^6 \cdot V_\phi$ (m ³ ·mol ⁻¹)					
		T (K)					
		293.15	303.15	313.15	323.15	333.15	343.15
0.341	0.006	18.7	19.2	19.5	19.4	19.3	18.9
1.13	0.020	30.2	30.6	30.8	30.8	30.8	30.9
2.01	0.035	30.7	31.0	31.1	31.2	31.1	30.9
2.94	0.052	31.0	31.3	31.5	31.5	31.5	31.4
4.21	0.074	31.6	31.8	32.0	32.0	32.0	31.9
5.66	0.100	31.8	32.0	32.2	32.2	32.2	32.1
7.33	0.129	31.9	32.1	32.2	32.3	32.3	32.2
9.46	0.167	32.1	32.3	32.5	32.5	32.6	32.5
12.1	0.214	32.4	32.6	32.8	32.9	32.9	32.9
15.3	0.269	32.1	32.3	32.5	32.5	32.6	32.6
$10^6 \cdot U(V_\phi) = 2.5 \text{ m}^3 \cdot \text{mol}^{-1}$							

Table VI.7. Apparent molar volume of $\text{H}_2\text{O}/(\text{LiBr}+[\text{Dmim}][\text{Cl}])$ solutions with $x_{\text{IL}}/x_{\text{LiBr}} = 0.0203$. b : molality; $x_{\text{LiBr}}/x_{\text{H}_2\text{O}}$: mole fraction ratio between LiBr and H_2O ; T : temperature.

b (mol·kg ⁻¹)	$x_{\text{LiBr}}/x_{\text{H}_2\text{O}}$	$10^6 \cdot V_\phi$ (m ³ ·mol ⁻¹)					
		T (K)					
		293.15	303.15	313.15	323.15	333.15	343.15
0.599	0.011	25.3	25.6	25.8	25.9	25.8	25.5
1.26	0.022	26.7	27.1	27.3	27.3	27.2	27.2
2.01	0.035	27.1	27.4	27.5	27.5	27.5	27.4
2.84	0.050	27.3	27.5	27.6	27.7	27.6	27.5
3.81	0.067	27.5	27.8	27.9	27.9	27.8	27.7
4.90	0.086	27.8	28.0	28.1	28.1	28.1	28.0
6.13	0.108	27.9	28.1	28.2	28.3	28.2	28.1
$10^6 \cdot U(V_\phi) = 1.3 \text{ m}^3 \cdot \text{mol}^{-1}$							

Chapter VI

Table VI.7 (continued)

b (mol·kg ⁻¹)	$x_{\text{LiBr}}/x_{\text{H}_2\text{O}}$	$10^6 \cdot V_\varphi$ (m ³ ·mol ⁻¹)					
		T (K)					
		293.15	303.15	313.15	323.15	333.15	343.15
7.59	0.134	28.2	28.4	28.5	28.5	28.5	28.4
9.38	0.166	28.6	28.8	28.9	28.9	28.9	28.9
11.3	0.199	28.4	28.6	28.7	28.8	28.8	28.7
13.9	0.245	28.4	28.6	28.7	28.8	28.8	28.8
15.7	0.278	28.1	28.3	28.4	28.5	28.5	28.5
$10^6 \cdot U(V_\varphi) = 1.3 \text{ m}^3 \cdot \text{mol}^{-1}$							

To simplify the comparative analysis of the influence of the IL on the apparent volume of the solute, its values in H₂O/LiBr and H₂O/(LiBr+IL) solutions are calculated at infinite dilution. The values obtained are shown in Tables VI.8-VI.9, together with the empirical parameters S_V and B_V of the Redlich-Rosenfeld-Meyer equation.

Table VI.8. Redlich-Rosenfeld-Meyer fitting of the apparent molar volume of H₂O/LiBr solutions.^[43,70] V_φ^0 : apparent molar volume at infinite dilution; S_V and B_V : empirical parameters.

Solute	Parameter	T (K)					
		293.15	303.15	313.15	323.15	333.15	343.15
LiBr	$10^6 \cdot V_\varphi^0$ (m ³ ·mol ⁻¹)	23.39	23.84	24.27	24.25	23.96	23.58
	$10^6 \cdot S_V$ (m ³ ·kg ^{1/2} ·mol ^{-3/2})	4.65	4.38	4.11	3.84	3.57	3.31
	$10^6 \cdot B_V$ (m ³ ·kg·mol ⁻²)	-1.09	-0.44	0.09	0.50	0.79	0.97
$10^6 \cdot U(V_\varphi^0) = 0.080 \text{ (m}^3 \cdot \text{mol}^{-1})^{[43]}$							

Table VI.9. Redlich-Rosenfeld-Meyer fitting of the apparent molar volume of H₂O/(LiBr+IL) solutions. V_{ϕ}^0 : apparent molar volume at infinite dilution; S_V and B_V : empirical parameters.

Solution	Parameter	T (K)					
		293.15	303.15	313.15	323.15	333.15	343.15
H ₂ O/(LiBr+[EA][NO ₃])	$10^6 \cdot V_{\phi}^0$ (m ³ ·mol ⁻¹)	22.1	22.4	22.9	22.9	23.1	23.4
	$10^6 \cdot S_V$ (m ³ ·kg ^{1/2} ·mol ^{-3/2})	3.0	2.9	2.6	2.6	2.4	2.1
	$10^6 \cdot B_V$ (m ³ ·kg·mol ⁻²)	-0.34	-0.33	-0.29	-0.28	-0.23	-0.16
H ₂ O/(LiBr+[PA][NO ₃])	$10^6 \cdot V_{\phi}^0$ (m ³ ·mol ⁻¹)	14.9	15.5	15.6	15.6	15.5	15.0
	$10^6 \cdot S_V$ (m ³ ·kg ^{1/2} ·mol ^{-3/2})	8.2	8.0	8.0	8.0	8.0	8.2
	$10^6 \cdot B_V$ (m ³ ·kg·mol ⁻²)	-1.27	-1.23	-1.23	-1.23	-1.22	-1.24
H ₂ O/(LiBr+[EA][Cl])	$10^6 \cdot V_{\phi}^0$ (m ³ ·mol ⁻¹)	20.1	20.4	20.6	20.7	20.3	20.2
	$10^6 \cdot S_V$ (m ³ ·kg ^{1/2} ·mol ^{-3/2})	3.9	3.8	3.8	3.7	3.9	3.8
	$10^6 \cdot B_V$ (m ³ ·kg·mol ⁻²)	-0.50	-0.49	-0.48	-0.47	-0.49	-0.47
H ₂ O/(LiBr+[Bmim][Br])	$10^6 \cdot V_{\phi}^0$ (m ³ ·mol ⁻¹)	26.4	26.8	27.2	27.5	27.1	27.3
	$10^6 \cdot S_V$ (m ³ ·kg ^{1/2} ·mol ^{-3/2})	3.7	3.6	3.4	3.2	3.4	3.2
	$10^6 \cdot B_V$ (m ³ ·kg·mol ⁻²)	-0.57	-0.56	-0.52	-0.49	-0.52	-0.46
H ₂ O/(LiBr+[Dmim][Cl])	$10^6 \cdot V_{\phi}^0$ (m ³ ·mol ⁻¹)	24.5	25.7	25.5	25.7	25.5	25.7
	$10^6 \cdot S_V$ (m ³ ·kg ^{1/2} ·mol ^{-3/2})	2.1	1.4	1.7	1.6	1.6	1.4
	$10^6 \cdot B_V$ (m ³ ·kg·mol ⁻²)	-0.29	-0.17	-0.23	-0.22	-0.21	-0.17
$10^6 \cdot U(V_{\phi}^0) = 2.1$ m ³ ·mol ⁻¹ ; $10^6 \cdot U(S_V) = 2.0$ m ³ ·kg ^{1/2} ·mol ^{-3/2} ; $10^6 \cdot U(B_V) = 0.42$ m ³ ·kg·mol ⁻²							

To facilitate the analysis, the values of V_{φ}^0 in $\text{H}_2\text{O}/\text{LiBr}$ and $\text{H}_2\text{O}/(\text{LiBr}+\text{IL})$ solutions are plotted together in Figure VI.2. It is observed that the apparent molar volume at infinite dilution is positive for all solutes analysed, and that its value increases with temperature. The sequence of the values at any temperature obeys the following decreasing order: $\text{H}_2\text{O}/(\text{LiBr}+[\text{Bmim}][\text{Br}]) > \text{H}_2\text{O}/(\text{LiBr}+[\text{Dmim}][\text{Cl}]) > \text{H}_2\text{O}/\text{LiBr} > \text{H}_2\text{O}/(\text{LiBr}+[\text{EA}][\text{NO}_3]) > \text{H}_2\text{O}/(\text{LiBr}+[\text{EA}][\text{Cl}]) > \text{H}_2\text{O}/(\text{LiBr}+[\text{PA}][\text{NO}_3])$.

The higher values of V_{φ}^0 in the solutions with ionic liquids based on the imidazolium cation agree with lower solute-solvent interactions and higher amount of bulk water, as discussed in Chapter III. In addition, the size of the $[\text{Bmim}]^+$ and $[\text{Dmim}]^+$ cations could contribute to an increase in the value of V_{φ}^0 due to the cation volume itself and the change in the solvent volume around the solute.^[72] However, the values of apparent molar volume at infinite dilution in $\text{H}_2\text{O}/(\text{LiBr}+\text{IL})$ mixtures with protic ionic liquids are lower than those obtained for $\text{H}_2\text{O}/\text{LiBr}$ mixtures, even though a higher amount of bulk water was also observed in those solutions. This fact could be related to a higher contribution of the change in the volume of the solution due to solute-solvent interactions,^[72] as well as to the formation of complex structures through hydrogen bonding by ionic liquids based on the ammonium cation.^[108,176,177]

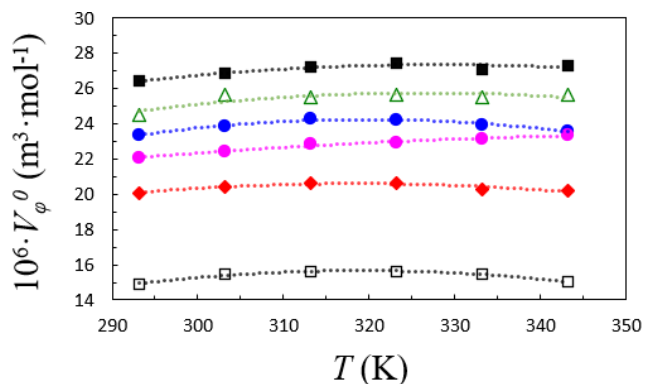


Figure VI.2. Apparent molar volume at infinite dilution of LiBr and $\text{LiBr}+\text{IL}$ in aqueous solutions at $x_{\text{IL}}/x_{\text{LiBr}} \approx 0.0205$. ●: $\text{H}_2\text{O}/\text{LiBr}$;^[43,70] ●: $\text{H}_2\text{O}/(\text{LiBr}+[\text{EA}][\text{NO}_3])$; □: $\text{H}_2\text{O}/(\text{LiBr}+[\text{PA}][\text{NO}_3])$; ◆: $\text{H}_2\text{O}/(\text{LiBr}+[\text{EA}][\text{Cl}])$; ■: $\text{H}_2\text{O}/(\text{LiBr}+[\text{Bmim}][\text{Br}])$; △: $\text{H}_2\text{O}/(\text{LiBr}+[\text{Dmim}][\text{Cl}])$. Dotted lines represent the fitting shown in Eq. VI.2.

Chapter VI

In the literature,^[44,71,178] the apparent molar volume at infinite dilution is correlated with temperature using a polynomial equation (Eq. VI.2), where A , B , and C are empirical coefficients. The results of this quadratic fit are shown in Table VI.10 and plotted in Figure VI.2.

$$V_{\phi}^0 = A + B \cdot T + C \cdot T^2 \quad \text{Eq. VI.2}$$

Table VI.10. A , B and C coefficients of the apparent molar volume at infinite dilution of $\text{H}_2\text{O}/\text{LiBr}$ and $\text{H}_2\text{O}/(\text{LiBr}+\text{IL})$ solutions from (293.15 to 343.15) K.

Solution	$10^5 \cdot A$ ($\text{m}^3 \cdot \text{mol}^{-1}$)	$10^7 \cdot B$ ($\text{m}^3 \cdot \text{mol}^{-1} \cdot \text{K}^{-1}$)	$10^{10} \cdot C$ ($\text{m}^3 \cdot \text{mol}^{-1} \cdot \text{K}^{-2}$)
$\text{H}_2\text{O}/\text{LiBr}$	-10.4	8.02	-12.6
$\text{H}_2\text{O}/(\text{LiBr}+[\text{EA}][\text{NO}_3])$	-0.66	1.61	-2.1
$\text{H}_2\text{O}/(\text{LiBr}+[\text{PA}][\text{NO}_3])$	-9.86	7.17	-11.3
$\text{H}_2\text{O}/(\text{LiBr}+[\text{EA}][\text{Cl}])$	-5.92	5.01	-7.9
$\text{H}_2\text{O}/(\text{LiBr}+[\text{Bmim}][\text{Br}])$	-5.38	4.94	-7.5
$\text{H}_2\text{O}/(\text{LiBr}+[\text{Dmim}][\text{Cl}])$	-6.98	5.84	-8.9

Since Hepler's constant^[73] is commonly used to interpret solute-solvent interactions,^[42,43] its value has been calculated for all mixtures (Eq. VI.3).

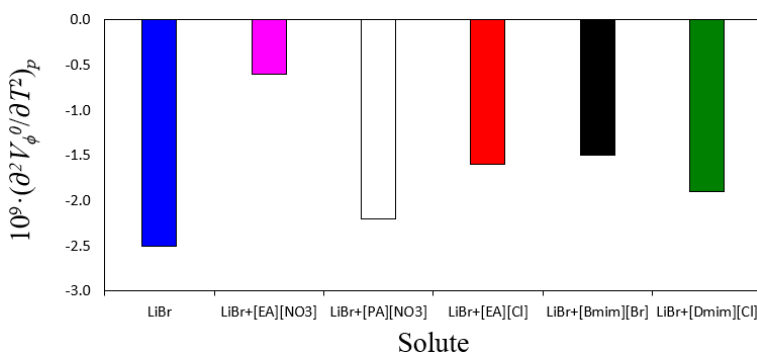
$$\left(\frac{\partial^2 V_{\phi}^0}{\partial T^2} \right)_p = 2 \cdot C \quad \text{Eq. VI.3}$$

The results are shown in Table VI.11 and Figure VI.3. As expected, Hepler's constant is negative in all cases, which evidences that all these solutes break the molecular structure of water. However, the values obtained are lower in the presence of the ionic liquid, indicating that the solute ($\text{LiBr}+\text{IL}$) tends to break the water structure less than lithium bromide at $x_{\text{IL}}/x_{\text{LiBr}} \approx 0.0205$, which could justify the higher percentage of bulk water observed in the solutions with ionic liquid.

Chapter VI

Table VI.11. Hepler's constant for H₂O/LiBr and H₂O/(LiBr) solutions with $x_{Li}/x_{LiBr} \approx 0.0205$ from (293.15 to 343.15) K

Solution	$10^9 \cdot \left(\frac{\partial^2 V_\phi^0}{\partial T^2} \right)_p$ (m ³ ·mol ⁻¹ ·K ⁻²)
H ₂ O/LiBr	-2.5
H ₂ O/(LiBr+[EA][NO ₃])	-0.4
H ₂ O/(LiBr+[PA][NO ₃])	-2.3
H ₂ O/(LiBr+[EA][Cl])	-1.6
H ₂ O/(LiBr+[Bmim][Br])	-1.5
H ₂ O/(LiBr+[Dmim][Cl])	-1.8

Figure VI.3. Hepler's constant solutes in H₂O/LiBr and H₂O/(LiBr+IL) solutions in water from (293.15 to 343.15) K. Blue: LiBr; magenta: LiBr+[EA][NO₃]; white: LiBr+[PA][NO₃]; red: LiBr+[EA][Cl]; black: LiBr+[Bmim][Br]; green: LiBr+[Dmim][Cl].

VI.3. Isentropic compressibility

The isentropic compressibility of electrolyte solutions indicates the change in volume of the solution with pressure, and its value depends on both density and speed of sound. Therefore, this property is expected to be influenced by the factors discussed in the previous section: solute-solute, solute-solvent, and solvent-solvent interactions. Low isentropic compressibility values can generally be anticipated when the net balance of interactions is high.

Chapter VI

Tables VI.12-VI.17 show the κ_S values for all the considered mixtures. An analysis of these results reveals that, regardless of temperature, the values decrease as solute composition increases.

Table VI.12. Isentropic compressibility of H₂O/LiBr solutions. *b*: molality; x_{LiBr}/x_{H_2O} : mole fraction ratio between LiBr and H₂O; *T*: temperature.

<i>b</i> (mol·kg ⁻¹)	x_{LiBr}/x_{H_2O}	$10^{10} \cdot \kappa_S$ (Pa ⁻¹)			
		<i>T</i> (K)			
		293.15	303.15	313.15	323.15
0.594	0.011	4.308	4.189	4.112	4.068
1.79	0.036	3.908	3.829	3.780	3.752
3.30	0.067	3.534	3.485	3.457	3.442
6.05	0.109	3.069	3.051	3.041	3.035
9.21	0.168	2.725	2.722	2.722	2.718
15.5	0.247	2.319	2.329	2.334	2.329
$10^{10} \cdot U(\kappa_S) = 0.048 \text{ Pa}^{-1}$					

Table VI.13. Isentropic compressibility of H₂O/(LiBr+[EA][NO₃]) solutions with $x_{IL}/x_{LiBr} = 0.0205$. *b*: molality; x_{LiBr}/x_{H_2O} : mole fraction ratio between LiBr and H₂O; *T*: temperature.

<i>b</i> (mol·kg ⁻¹)	x_{LiBr}/x_{H_2O}	$10^{10} \cdot \kappa_S$ (Pa ⁻¹)					
		<i>T</i> (K)					
		293.15	303.15	313.15	323.15	333.15	343.15
0.603	0.011	4.324	4.205	4.123	4.087	4.089	4.107
2.03	0.036	3.847	3.772	3.736	3.724	3.736	3.753
3.82	0.067	3.435	3.396	3.387	3.397	3.408	3.425
6.18	0.109	3.070	3.055	3.062	3.083	3.107	3.129
9.53	0.168	2.739	2.743	2.763	2.787	2.811	2.838
14.0	0.247	2.423	2.423	2.468	2.492	2.520	2.544
15.8	0.279	2.300	2.311	2.348	2.375	2.407	2.430
$10^{10} \cdot U(\kappa_S) = 0.003 \text{ Pa}^{-1}$							

Chapter VI

Table VI.14. Isentropic compressibility of $\text{H}_2\text{O}/(\text{LiBr}+[\text{PA}][\text{NO}_3])$ solutions with $x_{\text{IL}}/x_{\text{LiBr}} = 0.0205$. b : molality; $x_{\text{LiBr}}/x_{\text{H}_2\text{O}}$: mole fraction ratio between LiBr and H_2O ; T : temperature.

b (mol·kg ⁻¹)	$x_{\text{LiBr}}/x_{\text{H}_2\text{O}}$	$10^{10} \cdot \kappa_S$ (Pa ⁻¹)					
		T (K)					
		293.15	303.15	313.15	323.15	333.15	343.15
0.60	0.011	4.296	-	4.071	4.053	4.061	4.082
1.97	0.035	3.854	3.773	3.742	3.737	3.745	3.763
3.79	0.067	3.432	3.391	3.390	3.402	3.416	3.438
6.10	0.108	3.068	3.055	3.070	3.094	3.112	3.136
9.29	0.164	2.730	2.743	2.771	2.798	2.823	2.847
15.8	0.278	2.280	2.297	2.322	2.344	2.370	-
$10^{10} \cdot U(\kappa_S) = 0.003 \text{ Pa}^{-1}$							

Table VI.15. Isentropic compressibility of $\text{H}_2\text{O}/(\text{LiBr}+[\text{EA}][\text{Cl}])$ solutions with $x_{\text{IL}}/x_{\text{LiBr}} = 0.0205$. b : molality; $x_{\text{LiBr}}/x_{\text{H}_2\text{O}}$: mole fraction ratio between LiBr and H_2O ; T : temperature.

b (mol·kg ⁻¹)	$x_{\text{LiBr}}/x_{\text{H}_2\text{O}}$	$10^{10} \cdot \kappa_S$ (Pa ⁻¹)					
		T (K)					
		293.15	303.15	313.15	323.15	333.15	343.15
0.607	0.011	4.313	-	4.028	4.008	4.053	4.078
2.03	0.036	3.844	3.733	3.695	3.689	3.710	3.752
3.84	0.068	3.417	3.373	3.360	3.388	3.395	3.416
6.22	0.110	3.063	3.047	3.043	3.051	3.091	3.115
9.44	0.167	2.734	2.738	2.748	2.765	2.789	2.825
14.1	0.250	2.385	2.395	2.419	2.441	2.485	2.509
15.9	0.281	2.283	2.296	2.315	2.337	2.376	2.399
$10^{10} \cdot U(\kappa_S) = 0.003 \text{ Pa}^{-1}$							

Chapter VI

Table VI.16. Isentropic compressibility of $\text{H}_2\text{O}/(\text{LiBr}+[\text{Bmim}][\text{Br}])$ solutions with $x_{\text{IL}}/x_{\text{LiBr}} = 0.0208$. b : molality; $x_{\text{LiBr}}/x_{\text{H}_2\text{O}}$: mole fraction ratio between LiBr and H_2O ; T : temperature.

b (mol·kg ⁻¹)	$x_{\text{LiBr}}/x_{\text{H}_2\text{O}}$	$10^{10} \cdot \kappa_S$ (Pa ⁻¹)					
		T (K)					
		293.15	303.15	313.15	323.15	333.15	343.15
0.341	0.006	4.426	4.243	4.159	4.154	4.150	4.167
1.13	0.020	4.166	4.043	3.984	3.990	3.987	4.002
2.01	0.035	3.902	3.809	3.765	3.752	3.781	3.798
2.94	0.052	3.669	3.602	3.573	3.568	3.582	3.618
4.21	0.074	3.421	3.389	3.378	3.378	3.393	3.418
5.66	0.100	3.196	3.179	3.186	3.195	3.217	3.239
7.33	0.129	2.993	2.991	3.008	3.023	3.046	3.069
9.46	0.167	2.802	2.808	2.833	2.851	2.876	2.900
12.1	0.214	2.620	2.636	2.666	2.685	2.707	2.730
15.3	0.269	2.420	2.439	2.474	2.497	2.522	2.546
$10^{10} \cdot U(\kappa_S) = 0.003 \text{ Pa}^{-1}$							

Table VI.17. Isentropic compressibility of $\text{H}_2\text{O}/(\text{LiBr}+[\text{Dmim}][\text{Cl}])$ solutions with $x_{\text{IL}}/x_{\text{LiBr}} = 0.0203$. b : molality; $x_{\text{LiBr}}/x_{\text{H}_2\text{O}}$: mole fraction ratio between LiBr and H_2O ; T : temperature.

b (mol·kg ⁻¹)	$x_{\text{LiBr}}/x_{\text{H}_2\text{O}}$	$10^{10} \cdot \kappa_S$ (Pa ⁻¹)					
		T (K)					
		293.15	303.15	313.15	323.15	333.15	343.15
0.599	0.011	4.342	4.233	4.161	4.134	4.123	4.133
1.26	0.022	4.112	4.022	3.971	3.954	-	-
2.01	0.035	3.881	3.820	3.781	3.762	-	-
2.84	0.050	3.657	3.607	3.578	3.576	3.583	-
3.81	0.067	3.453	3.422	3.408	3.405	-	-
4.90	0.086	3.242	3.240	3.233	3.240	3.260	-
6.13	0.108	3.074	3.063	3.064	3.080	3.106	-
7.59	0.134	2.921	2.921	2.936	2.951	2.967	2.985
$10^{10} \cdot U(\kappa_S) = 0.003 \text{ Pa}^{-1}$							

Table VI.17 (continued)

b (mol·kg ⁻¹)	x_{LiBr}/x_{H_2O}	$10^{10} \cdot \kappa_S$ (Pa ⁻¹)					
		T (K)					
		293.15	303.15	313.15	323.15	333.15	343.15
9.38	0.166	2.754	2.762	2.780	2.799	2.819	-
11.3	0.199	2.596	2.608	2.630	2.655	2.673	-
13.9	0.245	2.411	2.426	2.452	2.475	2.496	2.516
15.7	0.278	2.265	2.308	2.326	2.351	2.376	2.399

$10^{10} \cdot U(\kappa_S) = 0.003 \text{ Pa}^{-1}$

All mixtures have a composition in which the isentropic compressibility does not vary significantly with temperature (Table VI.18). Rohman *et al.*^[75,179] observed this phenomenon, referred to as the convergence point, in H₂O/LiBr solutions and was attributed to the beginning of the predominance of ion pairing over ion hydration. Their analysis^[75] evidence that in H₂O/LiBr, the convergence point is reached at a significantly higher molality of 10.8 mol·kg⁻¹ than in the case of H₂O/(LiBr+IL) mixtures, where the molality ranges from (3.79 to 4.90) mol·kg⁻¹.

Although it is not possible to analyse the influence of the ionic liquids on isentropic compressibility, as its values strongly depend on the composition, it is observed that the predominance of ion pairing over ion hydration begins at a significantly lower solute composition in the presence of ionic liquids. This finding suggests the existence of stronger solute-solute interactions in these solutions and could be related to weaker solute-solvent interactions, which would justify the higher amount of bulk water in H₂O/(LiBr+IL) solutions, discussed in Chapter III.

Table VI.18. Convergence points of isentropic compressibility of H₂O/LiBr and H₂O/(LiBr+IL) solutions at $x_{IL}/x_{LiBr} \approx 0.0205$. b : molality; x_{LiBr}/x_{H_2O} : mole fraction ratio between LiBr and H₂O.

Solution	$10^{10} \cdot \kappa_S$ (Pa ⁻¹)	b (mol·kg ⁻¹)	x_{LiBr}/x_{H_2O}
H ₂ O/LiBr ^[75]	2.61	10.8	0.195
H ₂ O/(LiBr+[EA][NO ₃])	3.41	3.82	0.067
H ₂ O/(LiBr+[PA][NO ₃])	3.41	3.79	0.067
H ₂ O/(LiBr+[EA][Cl])	3.39	3.84	0.068

Chapter VI

Table VI.18 (continued)

Solution	$10^{10} \cdot \kappa_S$ (Pa ⁻¹)	b (mol·kg ⁻¹)	x_{LiBr}/x_{H_2O}
H ₂ O/(LiBr+[Bmim][Br])	3.40	4.21	0.074
H ₂ O/(LiBr+[Dmim][Cl])	3.24	4.90	0.086

Similar to what was discussed in the previous section, the analysis of the influence of the ionic liquid on the isentropic compressibility of H₂O/(LiBr+IL) mixtures with respect to H₂O/LiBr is simplified by considering infinite dilution conditions as the reference point. As introduced in Section II.4, estimating this property requires the calculation of the molar apparent isentropic compressibility. Tables VI.19-VI.24 show the results obtained for the different solutions. The values are negative over the whole composition and temperature range and increase with solute composition.

Table VI.19. Apparent molar isentropic compressibility of H₂O/LiBr solutions. b : molality; x_{LiBr}/x_{H_2O} : mole fraction ratio between LiBr and H₂O; T : temperature.

b (mol·kg ⁻¹)	x_{LiBr}/x_{H_2O}	$10^{15} \cdot \kappa_\varphi$ (m ³ ·mol ⁻¹ ·Pa ⁻¹)				$10^{15} \cdot U(\kappa_\varphi)$ (m ³ ·mol ⁻¹)
		T (K)				
		293.15	303.15	313.15	323.15	
0.594	0.011	-32.0	-26.7	-23.3	-21.1	13
1.79	0.036	-26.5	-22.8	-20.2	-18.7	6.2
3.30	0.067	-22.0	-19.1	-17.1	-16.0	4.3
6.05	0.109	-16.7	-14.6	-13.2	-12.5	3.0
9.21	0.168	-12.8	-11.3	-10.2	-9.72	2.0
15.5	0.247	-8.4	-7.4	-6.7	-6.4	1.6

Chapter VI

Table VI.20. Apparent molar isentropic compressibility of $\text{H}_2\text{O}/(\text{LiBr}+[\text{EA}][\text{NO}_3])$ solutions with $x_{\text{IL}}/x_{\text{LiBr}} = 0.0205$. b : molality; $x_{\text{LiBr}}/x_{\text{H}_2\text{O}}$: mole fraction ratio between LiBr and H_2O ; T : temperature.

b (mol·kg ⁻¹)	$x_{\text{LiBr}}/x_{\text{H}_2\text{O}}$	$10^{15} \cdot \kappa_\varphi$ (m ³ ·mol ⁻¹ ·Pa ⁻¹)					
		T (K)					
		293.15	303.15	313.15	323.15	333.15	343.15
0.603	0.011	-28.5	-23.8	-21.2	-17.7	-13.1	-10.7
2.03	0.036	-25.4	-21.9	-18.9	-16.8	-15.0	-14.5
3.82	0.067	-20.4	-17.6	-15.3	-13.6	-12.7	-12.5
6.18	0.109	-15.7	-13.6	-11.9	-10.6	-9.8	-9.6
9.53	0.168	-11.4	-9.8	-8.5	-7.6	-7.1	-6.8
14.0	0.247	-8.4	-7.3	-6.1	-5.5	-5.1	-5.0
15.8	0.279	-7.8	-6.7	-5.8	-5.2	-4.8	-4.7
$10^{15} \cdot U(\kappa_\varphi) = 1.1 \text{ m}^3 \cdot \text{mol}^{-1} \cdot \text{Pa}^{-1}$							

Table VI.21. Apparent molar isentropic compressibility of $\text{H}_2\text{O}/\text{LiBr}+[\text{PA}][\text{NO}_3])$ solutions with $x_{\text{IL}}/x_{\text{LiBr}} = 0.0205$. b : molality; $x_{\text{LiBr}}/x_{\text{H}_2\text{O}}$: mole fraction ratio between LiBr and H_2O ; T : temperature.

b (mol·kg ⁻¹)	$x_{\text{LiBr}}/x_{\text{H}_2\text{O}}$	$10^{15} \cdot \kappa_\varphi$ (m ³ ·mol ⁻¹ ·Pa ⁻¹)					
		T (K)					
		293.15	303.15	313.15	323.15	333.15	343.15
0.60	0.011	-35.1	-	-31.7	-25.3	-19.9	-17.0
1.97	0.035	-26.2	-23.0	-19.7	-17.1	-15.5	-14.9
3.79	0.067	-20.8	-18.0	-15.4	-13.6	-12.7	-12.3
6.10	0.108	-16.1	-13.9	-12.0	-10.7	-10.0	-9.7
9.29	0.164	-12.2	-10.4	-8.9	-8.0	-7.4	-7.2
15.8	0.278	-8.1	-7.0	-6.2	-5.6	-5.2	-
$10^{15} \cdot U(\kappa_\varphi) = 1.1 \text{ m}^3 \cdot \text{mol}^{-1} \cdot \text{Pa}^{-1}$							

Chapter VI

Table VI.22. Apparent molar isentropic compressibility of $\text{H}_2\text{O}/(\text{LiBr}+[\text{EA}][\text{Cl}])$ solutions with $x_{\text{IL}}/x_{\text{LiBr}} = 0.0205$. b : molality; $x_{\text{LiBr}}/x_{\text{H}_2\text{O}}$: mole fraction ratio between LiBr and H_2O ; T : temperature.

b (mol·kg ⁻¹)	$x_{\text{LiBr}}/x_{\text{H}_2\text{O}}$	$10^{15} \cdot \kappa_\phi$ (m ³ ·mol ⁻¹ ·Pa ⁻¹)					
		T (K)					
		293.15	303.15	313.15	323.15	333.15	343.15
0.607	0.011	-30.8	-	-37.8	-31.5	-20.0	-16.4
2.03	0.036	-25.7	-24.1	-21.3	-18.8	-16.6	-14.8
3.84	0.068	-21.1	-18.4	-16.3	-14.0	-13.3	-12.9
6.22	0.110	-15.9	-13.8	-12.3	-11.3	-10.3	-10.0
9.44	0.167	-11.9	-10.3	-9.1	-8.3	-7.8	-7.4
14.1	0.250	-8.8	-7.6	-6.7	-6.1	-5.6	-5.4
15.9	0.281	-8.0	-7.0	-6.2	-5.6	-5.2	-5.0
$10^{15} \cdot U(\kappa_\phi) = 1.1 \text{ m}^3 \cdot \text{mol}^{-1} \cdot \text{Pa}^{-1}$							

Table VI.23. Apparent molar isentropic compressibility of $\text{H}_2\text{O}/(\text{LiBr}+[\text{Bmim}][\text{Br}])$ solutions with $x_{\text{IL}}/x_{\text{LiBr}} = 0.0208$. b : molality; $x_{\text{LiBr}}/x_{\text{H}_2\text{O}}$: mole fraction ratio between LiBr and H_2O ; T : temperature.

b (mol·kg ⁻¹)	$x_{\text{LiBr}}/x_{\text{H}_2\text{O}}$	$10^{15} \cdot \kappa_\phi$ (m ³ ·mol ⁻¹ ·Pa ⁻¹)					
		T (K)					
		293.15	303.15	313.15	323.15	333.15	343.15
0.341	0.006	-30.8	-41.0	-37.1	-21.4	-15.2	-11.4
1.13	0.020	-22.2	-20.1	-16.9	-11.3	-9.4	-8.3
2.01	0.035	-20.8	-18.2	-15.7	-13.6	-10.9	-10.3
2.94	0.052	-19.0	-16.3	-14.1	-12.4	-11.1	-10.0
4.21	0.074	-16.3	-13.5	-11.5	-10.2	-9.3	-8.8
5.66	0.100	-14.0	-11.7	-9.8	-8.7	-7.8	-7.5
7.33	0.129	-11.8	-9.8	-8.2	-7.2	-6.6	-6.3
9.46	0.167	-9.6	-7.9	-6.5	-5.7	-5.2	-5.0
12.1	0.214	-7.5	-6.1	-4.9	-4.3	-3.9	-3.7
15.3	0.269	-6.3	-5.1	-4.1	-3.5	-3.2	-3.0
$10^{15} \cdot U(\kappa_\phi) = 2.4 \text{ m}^3 \cdot \text{mol}^{-1} \cdot \text{Pa}^{-1}$							

Chapter VI

Table VI.24. Apparent molar isentropic compressibility of $\text{H}_2\text{O}/(\text{LiBr}+[\text{Dmim}][\text{Cl}])$ solutions with $x_{\text{IL}}/x_{\text{LiBr}} = 0.0203$. b : molality; $x_{\text{LiBr}}/x_{\text{H}_2\text{O}}$: mole fraction ratio between LiBr and H_2O ; T : temperature.

b (mol·kg ⁻¹)	$x_{\text{LiBr}}/x_{\text{H}_2\text{O}}$	$10^{15} \cdot \kappa_\varphi$ (m ³ ·mol ⁻¹ ·Pa ⁻¹)					
		T (K)					
		293.15	303.15	313.15	323.15	333.15	343.15
0.599	0.011	-25.3	-18.9	-14.6	-9.5	-7.2	-6.3
1.26	0.022	-24.6	-20.0	-16.4	-13.3	-	-
2.01	0.035	-23.3	-19.1	-16.2	-14.4	-	-
2.84	0.050	-21.8	-18.4	-16.1	-14.2	-13.2	-
3.81	0.067	-19.6	-16.6	-14.4	-13.0	-	-
4.90	0.086	-17.9	-14.9	-13.1	-11.8	-11.0	-
6.13	0.108	-15.7	-13.4	-11.9	-10.7	-9.8	-
7.59	0.134	-13.4	-11.4	-9.9	-9.0	-8.5	-8.3
9.38	0.166	-11.4	-9.7	-8.4	-7.6	-7.1	-
11.3	0.199	-10.0	-8.6	-7.5	-6.7	-6.3	-
13.9	0.245	-8.6	-7.4	-6.5	-5.8	-5.5	-5.4
15.7	0.278	-8.2	-6.9	-6.1	-5.5	-5.2	-5.1
$10^{15} \cdot U(\kappa_\varphi) = 1.1 \text{ m}^3 \cdot \text{mol}^{-1} \cdot \text{Pa}^{-1}$							

The dependence of κ_φ on molality is fitted to an equation of the Redlich-Rosenfeld-Meyer type (Eq. II.36, Section II.4), which allows estimating the value of this property at infinite dilution. The results of κ_φ^0 y S_κ empirical parameters obtained in the fit are shown in Table VI.25. It should be noted that the estimated values of the limiting apparent molar isentropic compressibility of $\text{H}_2\text{O}/\text{LiBr}$ agree with those reported by Bagheri *et al.*^[43]

Table VI.25. Fitting of the apparent molar isentropic compressibility of H₂O/(LiBr+IL) solutions. κ_{ϕ}^0 : limiting apparent molar isentropic compressibility; S_{κ} : empirical parameter.

Solution	Parameter	T (K)					
		293.15	303.15	313.15	323.15	333.15	343.15
H ₂ O/LiBr	$10^{15} \cdot \kappa_{\phi}^0$ (m ³ ·mol ⁻¹ ·Pa ⁻¹)	-36.5	-30.8	-27.8	-24.7	-	-
	$10^{15} \cdot S_{\kappa}$ (m ³ ·kg ^{1/2} ·mol ^{-3/2} ·Pa ⁻¹)	7.52	6.23	5.78	4.79	-	-
H ₂ O/(LiBr+[EA][NO ₃])	$10^{15} \cdot \kappa_{\phi}^0$ (m ³ ·mol ⁻¹ ·Pa ⁻¹)	-33.9	-28.7	-25.3	-21.7	-20.5	-20.0
	$10^{15} \cdot S_{\kappa}$ (m ³ ·kg ^{1/2} ·mol ^{-3/2} ·Pa ⁻¹)	6.86	5.75	5.13	4.31	4.12	4.10
H ₂ O/(LiBr+[PA][NO ₃])	$10^{15} \cdot \kappa_{\phi}^0$ (m ³ ·mol ⁻¹ ·Pa ⁻¹)	-38.7	-30.4	-28.9	-24.9	-22.4	-20.7
	$10^{15} \cdot S_{\kappa}$ (m ³ ·kg ^{1/2} ·mol ^{-3/2} ·Pa ⁻¹)	8.34	6.21	6.56	5.55	4.90	4.40
H ₂ O/(LiBr+[EA][Cl])	$10^{15} \cdot \kappa_{\phi}^0$ (m ³ ·mol ⁻¹ ·Pa ⁻¹)	-35.6	-31.6	-30.2	-24.3	-23.0	-19.7
	$10^{15} \cdot S_{\kappa}$ (m ³ ·kg ^{1/2} ·mol ^{-3/2} ·Pa ⁻¹)	7.25	6.48	6.25	4.90	4.70	3.79
H ₂ O/(LiBr+[Bmim][Br])	$10^{15} \cdot \kappa_{\phi}^0$ (m ³ ·mol ⁻¹ ·Pa ⁻¹)	-30.4	-26.9	-23.5	-20.3	-16.4	-13.8
	$10^{15} \cdot S_{\kappa}$ (m ³ ·kg ^{1/2} ·mol ^{-3/2} ·Pa ⁻¹)	6.75	6.15	5.52	4.74	3.60	2.74
H ₂ O/(LiBr+[Dmim][Cl])	$10^{15} \cdot \kappa_{\phi}^0$ (m ³ ·mol ⁻¹ ·Pa ⁻¹)	-31.1	-26.1	-22.1	-19.4	-18.9	-
	$10^{15} \cdot S_{\kappa}$ (m ³ ·kg ^{1/2} ·mol ^{-3/2} ·Pa ⁻¹)	6.08	5.09	4.21	3.64	3.64	-
$10^{15} \cdot U(\kappa_{\phi}^0) = 1.7 \text{ m}^3 \cdot \text{mol}^{-1} \cdot \text{Pa}^{-1}$; $10^{15} \cdot U(S_{\kappa}) = 0.64 \text{ m}^3 \cdot \text{kg}^{1/2} \cdot \text{mol}^{-3/2} \cdot \text{Pa}^{-1}$							

Chapter VI

To comparatively analyse the results, Figure VI.4 shows the values obtained for the limiting apparent molar isentropic compressibility of all the solutions considered. These values are always negative due to the strong interaction between solute and solvent.^[76] Regardless of temperature, the values of κ_{ϕ}^0 in H₂O/(LiBr+IL) mixtures with ionic liquids based on imidazolium cations ([Bmim]⁺ and [Dmim]⁺) are less negative than those of H₂O/LiBr, suggesting that the compressibility is higher in the presence of these ionic liquids. This agrees with the higher percentage of bulk water in those mixtures, discussed in Chapter III.

On the contrary, κ_{ϕ}^0 values H₂O/(LiBr+IL) mixtures based on the [EA]⁺ and [PA]⁺ cations are more negative than those found for the mixture without additive, suggesting that their compressibility is lower than that of the lithium bromide solutions. Again, since the amount of bulk water in these mixtures is also higher than that of H₂O/LiBr, the behaviour of this property can be attributed to the stiffness of the structures originated in the presence of these ILs by caging of the Li⁺ ions in solution.^[108,176,177] This information could be useful for interpreting the transport properties in H₂O/(LiBr+IL) mixtures.

κ_{ϕ}^0 values in the different solutions vary slightly with temperature. At 20 °C, the decreasing order is as follows: H₂O/(LiBr+[Bmim][Br]) \approx H₂O/(LiBr+[Dmim][Cl]) > H₂O/(LiBr+[EA][NO₃]) > H₂O/(LiBr+[EA][Cl]) \approx H₂O/LiBr > H₂O/(LiBr+[PA][NO₃]).

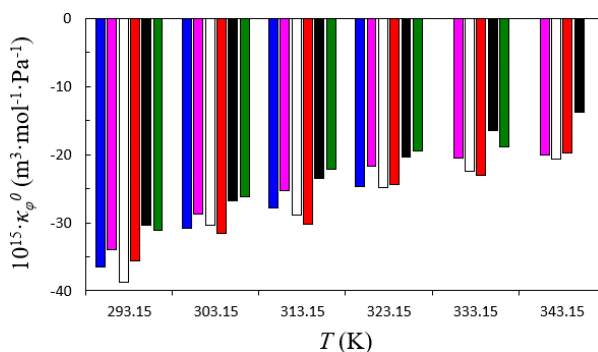


Figure VI.4. Limiting apparent molar isentropic compressibility of LiBr and LiBr+IL in aqueous solutions at $x_{IL}/x_{LiBr} \approx 0.0205$. Blue: H₂O/LiBr; magenta: H₂O/(LiBr+[EA][NO₃]); white: H₂O/(LiBr+[PA][NO₃]); red: H₂O/(LiBr+[EA][Cl]); black: H₂O/(LiBr+[Bmim][Br]); green: H₂O/(LiBr+[Dmim][Cl]).

VI.4. Conclusions

The conclusions drawn in this chapter correspond to the specific objective 6 (Section I.6).

The analysis of derived volumetric properties (in this work, apparent molar volume at infinite dilution, isentropic compressibility, and limiting apparent molar isentropic compressibility) is a valuable tool for analysing the influence of ionic liquids on solute-solvent interactions in $\text{H}_2\text{O}/(\text{LiBr}+\text{IL})$ solutions.

Both the apparent molar volume at infinite dilution and the limiting apparent molar compressibility generally decrease in the following order: $\text{H}_2\text{O}/(\text{LiBr}+[\text{Bmim}][\text{Br}]) > \text{H}_2\text{O}/(\text{LiBr}+[\text{Dmim}][\text{Cl}]) > \text{H}_2\text{O}/\text{LiBr} > \text{H}_2\text{O}/(\text{LiBr}+[\text{EA}][\text{NO}_3]) > \text{H}_2\text{O}/(\text{LiBr}+[\text{EA}][\text{Cl}]) > \text{H}_2\text{O}/(\text{LiBr}+[\text{PA}][\text{NO}_3])$. The higher values observed in mixtures with aprotic ionic liquids compared to the mixture without additive are consistent with their higher amount of bulk water. However, in $\text{H}_2\text{O}/(\text{LiBr}+\text{IL})$ solutions with protic ionic liquids, forming complex structures by hydrogen bonding would justify the lower values obtained in these properties.

Hepler's constant values are lower for $\text{H}_2\text{O}/(\text{LiBr}+\text{IL})$ mixtures than for $\text{H}_2\text{O}/\text{LiBr}$, which evidences lower solute-solvent interactions in the presence of ionic liquids. Based on the isentropic compressibility analysis, it is interpreted that ion pairing begins predominating over ion hydration at significantly lower solute composition in solutions with additive, which is related to greater solute-solute interactions and, therefore, higher amount of bulk water in these solutions.

The discussion in this chapter evidences that the NIR+MCR-ALS approach and the derived volumetric properties are complementary approaches to analyse the influence of ionic liquids on solute-solvent interactions.

Chapter VII. Conclusions and future work

VII.1. Conclusions

This doctoral thesis aims to establish an analysis strategy to estimate the influence of ionic liquids as additives on the thermophysical properties of the H₂O/LiBr working pair, which could facilitate the selection of an optimal additive. The strategy has been based on the solvation analysis through near-infrared spectroscopy coupled with the multivariate curve resolution method based on alternating least squares to estimate quantitatively the amount of bulk water and solvated water in the solutions. The conclusions derived from these results have been contrasted with the results found from the experimental determination of solid-liquid and vapour-liquid equilibria and some thermophysical properties: density, speed of sound, enthalpy of dilution, electrical conductivity, thermal conductivity, and dynamic viscosity. Finally, some derived volumetric properties have been calculated to compare solute-solvent and solute-solute interactions between solutions with and without additive. The ionic liquids used as additives of H₂O/LiBr are ethylammonium nitrate ([EA][NO₃]), propylammonium nitrate ([PA][NO₃]), ethylammonium chloride ([EA][Cl]), 1-butyl-3-methylimidazolium bromide ([Bmim][Br]), and 1,3-dimethylimidazolium chloride ([Dmim][Cl]).

The main findings of this thesis lead to the following conclusions:

- 1) In aqueous LiBr solutions, as a consequence of the solvation process of Li⁺ and Br⁻ ions, there is a certain amount of water that preserves the characteristic molecular structure of pure water (bulk water) and an amount of water bound to the ionic forms (hydrated ions and/or ionic pairs) of LiBr (water in the solvate).
- 2) The solvation process causes changes in the effective solute and solvent compositions, varying the mole fractions of water and lithium bromide calculated from the anhydrous number of moles in the solutions.
- 3) In the H₂O/LiBr mixture, in which the coordination numbers of Li⁺ and Br⁻ ions are known, the vapour pressure of the solutions at 20 °C was estimated using Raoult's law from the water mole fraction calculated using the amounts of bulk water and water in the solvate, estimated by NIR+MCR-ALS. The values

Chapter VII

obtained agree with those referenced in the literature. Therefore, it is assumed that this comparison validates the goodness of the bulk water results estimated by NIR+MCR-ALS to discuss solute-solvent interactions in the different solutions considered in this thesis.

- 4) In $\text{H}_2\text{O}/(\text{LiBr}+[\text{Dmim}][\text{Cl}])$ solutions, it was evidenced that, when working at high ionic liquid composition, the amount of bulk water would compromise the water absorption capacity in the application of interest. Therefore, it is concluded that the maximum mole ratio considered between 1,3-dimethylimidazolium chloride and LiBr should be less than 0.0942.
- 5) There are no significant differences in the percentage of bulk water in $\text{H}_2\text{O}/(\text{LiBr}+[\text{Dmim}][\text{Cl}])$ mixtures at ionic liquid/lithium bromide mole ratios of 0.0202, 0.0418 and 0.0648. For this reason, the mole fraction ratio of 0.0205 was considered for successive analyses of solvation in $\text{H}_2\text{O}/(\text{LiBr}+\text{IL})$ mixtures with $[\text{EA}][\text{NO}_3]$, $[\text{PA}][\text{NO}_3]$, $[\text{EA}][\text{Cl}]$, and $[\text{Bmim}][\text{Br}]$.
- 6) Generally, the amount of bulk water in all $\text{H}_2\text{O}/(\text{LiBr}+\text{IL})$ solutions is higher than that of $\text{H}_2\text{O}/\text{LiBr}$ at the same solute composition, regardless of the ionic liquid considered. Since the amount of bulk water is small in $\text{H}_2\text{O}/\text{IL}$ solutions, the higher amount of bulk water in the presence of ionic liquids suggests that they compete with water for the Li^+ and Br^- ions in the solution.
- 7) The percentage of bulk water in $\text{H}_2\text{O}/\text{LiBr}$ and $\text{H}_2\text{O}/(\text{LiBr}+\text{IL})$ solutions does not vary significantly between 20 °C and 60°C, decreasing according to the following general order: $\text{H}_2\text{O}/(\text{LiBr}+[\text{EA}][\text{Cl}]) > \text{H}_2\text{O}/(\text{LiBr}+[\text{EA}][\text{NO}_3]) \approx \text{H}_2\text{O}/(\text{LiBr}+[\text{PA}][\text{NO}_3]) \approx \text{H}_2\text{O}/(\text{LiBr}+[\text{Dmim}][\text{Cl}]) > \text{H}_2\text{O}/(\text{LiBr}+[\text{Bmim}][\text{Br}])$.
- 8) The solubility of lithium bromide in water is improved in the presence of the ionic liquids considered. At a mole fraction ratio between ionic liquid and lithium bromide of approximately 0.0205, the solubility increases 4.4 % from (10 to 40) °C for the mixtures with protic ionic liquids, and 4.6 % for the mixtures with aprotic ionic liquids. In the temperature range from 40 °C to 90 °C, the

Chapter VII

solubility increase in mixtures with [EA][NO₃], [PA][NO₃], and [EA][Cl] is 3.4 %, and 3.5 % in mixtures with [Bmim][Br] and [Dmim][Cl]. This finding has been attributed to the competitive reaction between the ionic liquid and water for Li⁺ and Br⁻ ions, which results in more bulk water in the presence of these additives.

- 9) The higher amount of bulk water in H₂O/(LiBr+IL) mixtures compared to H₂O/LiBr does not always correspond to higher vapour pressure in mixtures with additive. At an approximate IL to LiBr mole fraction ratio of 0.0205 and temperatures from (20 to 50) °C, the vapour pressure of mixtures with [EA][NO₃], [Bmim][Br], and [Dmim][Cl] is always higher than that of H₂O/LiBr, with relative differences ranging from 2.4 % to 49.6 %. However, when the temperature increases, the mixtures with [Bmim][Br] and [Dmim][Cl] show lower vapour pressure than the mixture without additive. At a mole ratio between ionic liquid and lithium bromide equal to 0.0427, the vapour pressure of H₂O/(LiBr+[Dmim][Cl]) is between 6.4 % and 39.2 % lower than that of H₂O/LiBr over the entire composition and temperature ranges. Explaining these results requires knowledge of the solvation structures in the solution.
- 10) The presence of ionic liquids causes the working fluid to be less dense than H₂O/LiBr, which acts to the detriment of the application under consideration, since a higher volume flow rate will have to be pumped to achieve the same mass flow rate. At $x_{IL}/x_{LiBr} \approx 0.0205$, the decreasing order of density of H₂O/(LiBr+IL) mixtures as a function of the ionic liquid is: [PA][NO₃] \approx [EA][Cl] > [Dmim][Cl] \approx [EA][NO₃] > [Bmim][Br].
- 11) The presence of ionic liquids causes lower enthalpy of dilution in the working fluid, improving its performance in the considered application, since the size of the absorber and generator could be reduced. The enthalpy of dilution of H₂O/(LiBr+IL) mixtures at $x_{IL}/x_{LiBr} \approx 0.0205$ decreases as follows: H₂O/(LiBr+[EA][Cl]) < H₂O/(LiBr+[PA][NO₃]) < H₂O/(LiBr+[Dmim][Cl]) \approx H₂O/(LiBr+[EA][NO₃]).

Chapter VII

- 12) The electrical conductivity does not vary significantly in the presence of the ionic liquids in the composition range analysed at 20 °C and 25 °C.
- 13) The thermal conductivity of $\text{H}_2\text{O}/(\text{LiBr}+[\text{Dmim}][\text{Cl}])$ at $x_{\text{IL}}/x_{\text{LiBr}} \approx 0.0449$ is 5.9 % lower than that of $\text{H}_2\text{O}/\text{LiBr}$ between 20 °C and 35 °C, which indicates greater difficulty in heat transfer in the presence of ionic liquid. Therefore, if a mixture with an additive is used in the application, the area of the heat exchangers through which the working fluid circulates would need to be increased to reject and/or absorb a certain amount of heat.
- 14) The dynamic viscosity of the $\text{H}_2\text{O}/(\text{LiBr}+[\text{Dmim}][\text{Cl}])$ mixture at absorbent mass fraction ranging from 0.424 to 0.568, and between 20 °C and 100 °C, is, on average, 3.1 % lower than that of $\text{H}_2\text{O}/\text{LiBr}$. However, at typical composition conditions of the application (temperature above 50 °C and mass fraction of absorbent above 0.50), the viscosity is 11.7 % higher than that of the mixture without additive, which is associated with a greater electricity consumption required in the pump to circulate the fluid.
- 15) Generally, there is a direct relationship between the increase of bulk water in the presence of ionic liquids and thermodynamic properties (density, speed of sound, and enthalpy of dilution). Nevertheless, it is not possible to directly relate the higher amount of bulk water in $\text{H}_2\text{O}/(\text{LiBr}+\text{IL})$ mixtures to the transport properties (electrical conductivity, thermal conductivity, and dynamic viscosity).
- 16) The apparent molar volume of the solute (LiBr or $\text{LiBr}+\text{IL}$) in $\text{H}_2\text{O}/\text{LiBr}$ and $\text{H}_2\text{O}/(\text{LiBr}+\text{IL})$ solutions at infinite dilution decreases according to the following order: $\text{H}_2\text{O}/(\text{LiBr}+[\text{Bmim}][\text{Br}]) > \text{H}_2\text{O}/(\text{LiBr}+[\text{Dmim}][\text{Cl}]) > \text{H}_2\text{O}/\text{LiBr} > \text{H}_2\text{O}/(\text{LiBr}+[\text{EA}][\text{NO}_3]) > \text{H}_2\text{O}/(\text{LiBr}+[\text{EA}][\text{Cl}]) > \text{H}_2\text{O}/(\text{LiBr}+[\text{PA}][\text{NO}_3])$. At 20 °C, the limiting apparent molar isentropic compressibility in $\text{H}_2\text{O}/(\text{LiBr}+\text{IL})$ solutions decreases as follows: $\text{H}_2\text{O}/(\text{LiBr}+[\text{Bmim}][\text{Br}]) \approx \text{H}_2\text{O}/(\text{LiBr}+[\text{Dmim}][\text{Cl}]) > \text{H}_2\text{O}/(\text{LiBr}+[\text{EA}][\text{NO}_3]) > \text{H}_2\text{O}/(\text{LiBr}+[\text{EA}][\text{Cl}]) \approx \text{H}_2\text{O}/\text{LiBr} > \text{H}_2\text{O}/(\text{LiBr}+[\text{PA}][\text{NO}_3])$. The results for mixtures with ionic liquids based on the imidazolium cation are directly related to the more significant bulk water percentage in the presence of

ionic liquids. The results obtained for mixtures with ionic liquids based on the ammonium cation are justified as a consequence of ion caging caused by the formation of complex structures by hydrogen bonding.

VII.2. Future work

Future work regarding the analysis of the influence of ionic liquids as additives in working fluids for refrigeration and absorption heat pump systems, which will be focused on overcoming the limitations mentioned and evidenced in this doctoral thesis, is summarised in the following points:

- 1) A thorough knowledge of the changes in the molecular structures of ions in the presence of ionic liquids is necessary. It would be helpful to predict the amount of water bound to the different ionic species in mixtures with additive to estimate, based on Raoult's law, the vapour pressure of the solution considering the amount of bulk water. This information could be obtained from computational calculations based on Molecular Dynamics simulations.
- 2) More experimental data regarding solubility, vapour pressure, and viscosity of mixtures with protic ionic liquids are needed to confirm the conclusions drawn in this work. The experimental part of those properties determined at reduced composition and/or temperature ranges should be extended.
- 3) To analyze the influence of ionic liquids on the performance of the working fluid in the considered application, new thermophysical properties, such as heat capacity at constant pressure, surface tension, and mass diffusion coefficient, would be of interest.
- 4) To complement the information extracted from the analysis of derived volumetric properties, it would be interesting to analyse solute-solute, solute-solvent, and solvent-solvent interactions in $\text{H}_2\text{O}/(\text{LiBr}+\text{IL})$ mixtures using the Jones-Dole viscosity equation coefficients. This requires experimental data on the dynamic viscosity of these mixtures over a wide composition range.

References

1. Ahmad, T., & Zhang, D. (2020). A critical review of comparative global historical energy consumption and future demand: The story told so far. *Energy Reports*, 6, 1973–1991. <https://doi.org/10.1016/j.egy.2020.07.020>
2. Yolcan, O. O. (2023). World energy outlook and state of renewable energy: 10-Year evaluation. *Innovation and Green Development*, 2(4). <https://doi.org/10.1016/j.igd.2023.100070>
3. International Energy Agency, I. (2023). *World Energy Outlook 2023*. <https://iea.blob.core.windows.net/assets/86ede39e-4436-42d7-ba2a-edf61467e070/WorldEnergyOutlook2023.pdf>
4. Zhao, X., Yin, Y., He, Z., & Deng, Z. (2023). State-of-the-art, challenges and new perspectives of thermal comfort demand law for on-demand intelligent control of heating, ventilation, and air conditioning systems. *Energy and Buildings*, 295. <https://doi.org/10.1016/j.enbuild.2023.113325>
5. McLinden, M. O., & Huber, M. L. (2020). (R)Evolution of Refrigerants. *Journal of Chemical and Engineering Data*, 65(9), 4176–4193. <https://doi.org/10.1021/acs.jced.0c00338>
6. Nikbakhti, R., Wang, X., Hussein, A. K., & Iranmanesh, A. (2020). Absorption cooling systems – Review of various techniques for energy performance enhancement. *Alexandria Engineering Journal*, 59(2), 707–738. <https://doi.org/10.1016/j.aej.2020.01.036>
7. Srikhirin, P., Aphornratana, S., & Chungpaibulpatana, S. (2001). A review of absorption refrigeration technologies. *Renewable and Sustainable Energy Reviews*, 5(4), 343–372. [https://doi.org/10.1016/S1364-0321\(01\)00003-X](https://doi.org/10.1016/S1364-0321(01)00003-X)
8. Wang, X., & Chua, H. T. (2009). Absorption cooling: A review of lithium bromide-water chiller technologies. *Recent Patents on Mechanical Engineering*, 2(3), 193–213. <https://doi.org/10.2174/1874477x10902030193>
9. Herold, K. E., Radermacher, R., & Klein, S. A. (2016). *Absorption Chillers and Heat Pumps* (Second Edition). CRC Press. <https://doi.org/doi.org/10.1201/b19625>

References

10. Salavera Muñoz, D. (2005). *Propiedades termofísicas de nuevos fluidos de trabajo (H₂O+LiBr+LiNO₃+LiCl+LiI, NH₃+H₂O+NaOH y NH₃+H₂O+KOH) para sistemas de refrigeración por absorción*. Universitat Rovira i Virgili.
11. Ji, L., Shukla, S. K., Zuo, Z., Lu, X., Ji, X., & Wang, C. (2023). An overview of the progress of new working pairs in absorption heat pumps. *Energy Reports*, 9, 703–729. <https://doi.org/10.1016/j.egy.2022.11.143>
12. Khamooshi, M., Parham, K., & Atikol, U. (2013). Overview of ionic liquids used as working fluids in absorption cycles. *Advances in Mechanical Engineering*, 5, 620592. <https://doi.org/10.1155/2013/620592>
13. Sun, J., Fu, L., & Zhang, S. (2012). A review of working fluids of absorption cycles. *Renewable and Sustainable Energy Reviews*, 16(4), 1899–1906. <https://doi.org/10.1016/j.rser.2012.01.011>
14. Królikowska, M., Skonieczny, M., & Padaszyński, K. (2023). Physicochemical and thermodynamic investigation of ethanolic solution of phosphonium-based Ionic Liquids—Measurements, correlations, and application to absorption cycles. *Journal of Chemical and Engineering Data*, 68(12), 3377–3397. <https://doi.org/10.1021/acs.jced.3c00537>
15. Hallett, J. P., & Welton, T. (2011). Room-temperature ionic liquids: Solvents for synthesis and catalysis. 2. *Chemical Reviews*, 111(5), 3508–3576. <https://doi.org/10.1021/cr1003248>
16. Zhang, S., Sun, N., He, X., Lu, X., & Zhang, X. (2006). Physical properties of ionic liquids: Database and evaluation. *Journal of Physical and Chemical Reference Data*, 35(4), 1475–1517. <https://doi.org/10.1063/1.2204959>
17. Królikowska, M., & Nędzi, F. (2021). Experimental data on the physicochemical and thermodynamic properties of the aqueous lithium bromide modified by the addition of lithium salt. *Journal of Chemical Thermodynamics*, 161. <https://doi.org/10.1016/j.jct.2021.106514>
18. Iyoki, S., Yamanaka, R., & Uemura, T. (1993). Physical and thermal properties of the water-lithium bromide-lithium nitrate system. *International Journal of Refrigeration*, 16(3), 191–200. [https://doi.org/10.1016/0140-7007\(93\)90048-D](https://doi.org/10.1016/0140-7007(93)90048-D)

References

19. Iyoki, S., & Uemura, T. (1989). Physical and thermal properties of the water-lithium bromide zinc chloride-calcium bromide system. *International Journal of Refrigeration*, 12(5), 272–277. [https://doi.org/10.1016/0140-7007\(89\)90093-5](https://doi.org/10.1016/0140-7007(89)90093-5)
20. Iyoki, S., & Uemura, T. (1990). Physical and thermal properties of the water-lithium bromide-zinc bromide-lithium chloride system. *ASHRAE TRANSACTIONS*, 96(2), 323–328.
21. Inada, T., Tomita, H., Takemura, F., Tsubouchi, O., & Hihara, E. (2019). Crystallization temperature, vapor pressure, density and viscosity of lithium bromide + lithium iodide + ethylene glycol + water system for absorption refrigerators for automotive use. *International Journal of Refrigeration*, 100, 274–283. <https://doi.org/10.1016/j.ijrefrig.2019.02.016>
22. Salavera, D., Esteve, X., Patil, K. R., Mainar, A. M., & Coronas, A. (2004). Solubility, heat capacity, and density of lithium bromide + lithium iodide + lithium nitrate + lithium chloride aqueous solutions at several compositions and temperatures. *Journal of Chemical and Engineering Data*, 49(3), 613–619. <https://doi.org/10.1021/je034202x>
23. Donate, M., Rodriguez, L., Lucas, A. De, & Rodríguez, J. F. (2006). Thermodynamic evaluation of new absorbent mixtures of lithium bromide and organic salts for absorption refrigeration machines. *International Journal of Refrigeration*, 29(1), 30–35. <https://doi.org/10.1016/j.ijrefrig.2005.05.005>
24. Królikowska, M., & Zawadzki, M. (2018). The experimental study on influence of zwitterionic compounds on solubility of lithium bromide in water. *Fluid Phase Equilibria*, 475, 18–24. <https://doi.org/10.1016/j.fluid.2018.07.021>
25. Królikowska, M., Zawadzki, M., & Skonieczny, M. (2018). The influence of bromide-based ionic liquids on solubility of {LiBr (1) + water (2)} system. Experimental (solid + liquid) phase equilibrium data. Part 2. *Journal of Molecular Liquids*, 265, 316–326. <https://doi.org/10.1016/j.molliq.2018.06.006>
26. Kim, J.-S., Park, Y., & Lee, H. (1996). Solubilities and vapor pressures of the water + lithium bromide + ethanolamine system. *Journal of Chemical Engineering Data*, 41(2), 279–281. <https://doi.org/https://doi.org/10.1021/je950249+>

References

27. Chi, C. W., Robert, A. M., & Rush, W. F. (1971). Secondary alcohol additives for lithium bromide-water absorption refrigeration system (Patent 3609087). In *21) Appl. No (3609087)*. <https://patents.google.com/patent/US3609087A>
28. Park, Y., Kim, J. S., & Lee, H. (1997). Thermodynamic properties of the lithium bromide + diethanolamine + water system. *ASHRAE TRANSACTIONS*, *103*(Part 2), 175–181.
29. Kim, J. S., & Lee, H. (2001). Solubilities, vapor pressures, densities, and viscosities of the LiBr + Lil + HO(CH₂)₃OH + H₂O system. *Journal of Chemical and Engineering Data*, *46*(1), 79–83. <https://doi.org/10.1021/je000154u>
30. Park, Y., Kim, J.-S., Lee, H., & Yu, S. II. (1997). Density, vapor pressure, solubility, and viscosity for water + lithium bromide + lithium bitrate + 1,3-propanediol. *Journal of Chemical Engineering Data*, *42*(1), 145–148. <https://doi.org/10.1021/je960233z>
31. Park, Y., Kim, J.-S., & Lee, H. (1997). Physical properties of the lithium bromide + 1,3-propanediol + water system. *Int J. Refrig*, *20*(5), 319–325. [https://doi.org/10.1016/S0140-7007\(97\)00021-2](https://doi.org/10.1016/S0140-7007(97)00021-2)
32. Królikowska, M., & Hofman, T. (2019). The influence of bromide-based ionic liquids on solubility of {LiBr (1) + water (2)} system. Experimental (solid + liquid) phase equilibrium data. Part 1. *Journal of Molecular Liquids*, *273*, 606–614. <https://doi.org/10.1016/j.molliq.2018.09.104>
33. Yang, D., Zhu, Y., Liu, S., Lv, H., & Luo, C. (2019). Thermodynamic properties of a ternary AHP working pair: lithium bromide + 1-ethyl-3-methylimidazolium chloride + H₂O. *Journal of Chemical and Engineering Data*, *64*(2), 574–583. <https://doi.org/10.1021/acs.jced.8b00771>
34. Kim, KS., Demberehnyamba, D., Shin, BK., Yeon, SH., Choi, S., Cha, JH., Lee, H., Lee, CS., & Shim, JJ. (2006). Surface tension and viscosity of 1-butyl-3-methylimidazolium iodide and 1-butyl-3-methylimidazolium tetrafluoroborate, and solubility of lithium bromide+1-butyl-3-methylimidazolium bromide in water. *Korean Journal of Chemical Engineering*, *23*(1), 113–116. <https://doi.org/https://doi.org/10.1007/BF02705701>
35. Jing, L., Danxing, Z., Lihua, F., Xianghong, W., & Li, D. (2011). Vapor pressure measurement of the ternary systems H₂O + LiBr + [Dmim]Cl, H₂O + LiBr +

References

- [Dmim]BF₄, H₂O + LiCl + [Dmim]Cl, and H₂O + LiCl + [Dmim]BF₄. *Journal of Chemical and Engineering Data*, 56(1), 97–101. <https://doi.org/10.1021/je1009202>
36. Zhang, X., Gao, N., Wu, Y., & Chen, G. (2018). Vapor pressure measurement for the ternary system of sater, lithium bromide, and 1-ethyl-3-methylimidazolium acetate. *Journal of Chemical and Engineering Data*, 63(3), 781–786. <https://doi.org/10.1021/acs.jced.7b00951>
37. Xuan, Y., Ding, X., Gao, N., Ding, Y., Meng, X., & Chen, G. (2019). Vapor pressure measurement of ternary systems LiCl + [Emim]Cl + H₂O, LiBr + [Emim]Cl + H₂O, and LiCl + [Emim]Br + H₂O. *Journal of Chemical and Engineering Data*, 64(6), 2406–2413. <https://doi.org/10.1021/acs.jced.8b01217>
38. Rafiee, H. R., & Frouzesh, F. (2016). Vapor-liquid equilibria and volumetric properties for new working fluid ([C₆H₁₁N₂][HSO₄] + LiBr + H₂O) and corresponding binary systems at different temperatures and ambient pressure. *Fluid Phase Equilibria*, 429, 137–148. <https://doi.org/10.1016/j.fluid.2016.08.036>
39. Xuan, Y., Fang, K., Duan, B., Gao, N., & Chen, G. (2020). Vapor pressure measurement of ternary systems LiBr + [Emim]I + H₂O and LiBr + [Dmim]I + H₂O. *Journal of Chemical and Engineering Data*, 65(2), 487–494. <https://doi.org/10.1021/acs.jced.9b00614>
40. Królikowska, M., Skonieczny, M., Padaszyński, K., & Zawadzki, M. (2021). Vapor pressure and physicochemical properties of {LiBr + IL-based additive + Water} mixtures: experimental data and COSMO-RS predictions. *Journal of Solution Chemistry*. <https://doi.org/10.1007/s10953-021-01071-w>
41. Dong, L., Nie, N., & Zheng, D. (2012). Vapor-liquid equilibrium measurements for the H₂O+LiBr+[DMIM]DMP and H₂O+LiCl+[DMIM]DMP ternary systems. *Journal of Beijing University of Chemical Technology*, 39(3), 7–11. <http://www.journal.buct.edu.cn>
42. Shekaari, H., Taghi Zafarani-Moattar, M., & Golmohammadi, B. (2020). Thermodynamic and transport properties of ionic liquids, 1-alkyl-3-methylimidazolium thiocyanate in the aqueous lithium halides solutions. *Journal of Chemical Thermodynamics*, 141. <https://doi.org/10.1016/j.jct.2019.105953>

References

43. Bagheri, M., Shekaari, H., Ghaffari, F., & Mousavi, F. (2024). Solute- solvent interactions between ethanolamine-based protic ionic liquids and lithium bromide in aqueous media using volumetric, acoustic and transport properties. *Journal of Molecular Liquids*, 397. <https://doi.org/10.1016/j.molliq.2024.124125>
44. Rafiee, H. R., & Frouzesh, F. (2015). Study of apparent molar volumes for ionic liquid, 1-ethyl-3-methyl imidazolium chloride in aqueous lithium nitrate, lithium bromide, and lithium chloride solutions at temperatures (298.15 to 318.15) K. *Journal of Chemical and Engineering Data*, 60(10), 2958–2965. <https://doi.org/10.1021/acs.jced.5b00329>
45. Lawton, W. H., & Sylvestre, E. A. (1971). Self modeling curve resolution. *Technometrics*, 13(3), 617–633. <https://doi.org/10.1080/00401706.1971.10488823>
46. Vandeginste, B., Essers, R., Bosman, T., Reijnen, J., & Kateman, G. (1985). Three-component curve resolution in liquid chromatography with multiwavelength diode array detection. *Analytical Chemistry*, 57(6), 971–985. <https://doi.org/10.1021/ac00283a005>
47. Borgen, O. S., & Kowalski, B. R. (1985). An extension of the multivariate component-resolution method to three components. *Analytica Chimica Acta*, 174, 1–26. [https://doi.org/10.1016/S0003-2670\(00\)84361-5](https://doi.org/10.1016/S0003-2670(00)84361-5)
48. Tauler, R., Kowalski, B., & Fleming, S. (1993). Multivariate curve resolution applied to spectral data from multiple runs of an industrial process. *Anal. Chem*, 65(15), 2040–2047. <https://doi.org/https://doi.org/10.1021/ac00063a019>
49. Malinowski, E. R. (1999). Abstract factor analysis of data with multiple sources of error and a modified Faber–Kowalski f-test. *Journal of Chemometrics*, 13, 69–81. [https://doi.org/10.1002/\(SICI\)1099-128X\(199903/04\)13:2%3C69::AID-CEM526%3E3.0.CO;2-W](https://doi.org/10.1002/(SICI)1099-128X(199903/04)13:2%3C69::AID-CEM526%3E3.0.CO;2-W)
50. Massart, D. L., Vandeginste, B. G. M., Deming, S. N., Michotte, Y., & Kaufman, L. (1988). Chemometrics: a textbook. Part B. In *Chemometrics: a textbook. Part B* (Issue 4). Elsevier.
51. Massart, D. L., Vandeginste, B. G. M., Buydens, L. M. C., De Jong, S., Lewi, P. J., & Smeyers-Verbeke, J. (1997). Handbook of Chemometrics and Qualimetrics:

References

Part A. In *Journal of Chemical Information and Computer Sciences* (Vols. 20, Part A, Issue 6). Elsevier.

52. Elyashberg, M. E., Serov, V. V, Martirosyan, E. R., Zlatina, L. A., Karasev, Y. Z., Koldashov, V. N., & Yampolskiy, Y. Y. (1991). An expert system for molecular structure elucidation based on spectral data. *Journal of Molecular Structure (Theochem)*, *230*, 191–203. [https://doi.org/https://doi.org/10.1016/0166-1280\(91\)85178-A](https://doi.org/https://doi.org/10.1016/0166-1280(91)85178-A)

53. Maeder, M., & Zuberbuehler, A. D. (1986). The resolution of overlapping chromatographic peaks by evolving factor analysis. *Analytica Chimica Acta*, *181*, 287–291. [https://doi.org/https://doi.org/10.1016/S0003-2670\(00\)85248-4](https://doi.org/https://doi.org/10.1016/S0003-2670(00)85248-4)

54. Tauler, R., Izquierdo-Ridorsa, A., & Casassas, E. (1993). Simultaneous analysis of several spectroscopic titrations with self-modelling curve resolution. *Chemometrics and Intelligent Laboratory Systems*, *18*, 293–300. [https://doi.org/https://doi.org/10.1016/0169-7439\(93\)85006-3](https://doi.org/https://doi.org/10.1016/0169-7439(93)85006-3)

55. Tauler, R., Casassas, E., & Izquierdo-Ridorsa, A. (1991). Self-modelling curve resolution in studies of spectrometric titrations of multi-equilibria systems by factor analysis. *Analytica Chimica Acta*, *248*(2), 447–458. [https://doi.org/https://doi.org/10.1016/S0003-2670\(00\)84662-0](https://doi.org/https://doi.org/10.1016/S0003-2670(00)84662-0)

56. Bro, R., & De Jong, S. (1997). A fast non-negativity-constrained least squares algorithm. *Journal of Chemometrics*, *11*(5), 393–401. [https://doi.org/10.1002/\(SICI\)1099-128X\(199709/10\)11:5%3C393::AID-CEM483%3E3.0.CO;2-L](https://doi.org/10.1002/(SICI)1099-128X(199709/10)11:5%3C393::AID-CEM483%3E3.0.CO;2-L)

57. Gargallo, R., Tauler, R., Cuesta-Sánchez, F., & Massart, D. L. (1996). Validation of alternating least-squares multivariate curve resolution for chromatographic resolution and quantitation. *TrAC Trends in Analytical Chemistry*, *15*(7), 279–286. [https://doi.org/https://doi.org/10.1016/0165-9936\(96\)00048-9](https://doi.org/https://doi.org/10.1016/0165-9936(96)00048-9)

58. de Juan, A., Vander Heyden, Y., Tauler, R., & Massart, D. L. (1997). Assessment of new constraints applied to the alternating least squares method. *Analytica Chimica Acta*, *346*(3), 307–318. [https://doi.org/10.1016/S0003-2670\(97\)90069-6](https://doi.org/10.1016/S0003-2670(97)90069-6)

59. solubility. (2014). In *The IUPAC Compendium of Chemical Terminology*. International Union of Pure and Applied Chemistry (IUPAC). <https://doi.org/10.1351/goldbook.S05740>

References

60. Pérez Velilla, E. (2007). *Equilibrio de fases y solubilidades en fluidos supercríticos*. Universidad Complutense de Madrid.
61. Spieweck, F., & Bettin, H. (1992). Review: solid and liquid density determination. *Technisches Messen*, 59(8), 237–244. <https://doi.org/10.1524/teme.1992.59.6.237>
62. Goodwin, A. R. H., & Trusler, J. P. M. (2003). 6 - Speed of sound. In *Experimental Thermodynamics* (Vol. 6, pp. 237–323). Elsevier Inc. [https://doi.org/10.1016/S1874-5644\(03\)80009-7](https://doi.org/10.1016/S1874-5644(03)80009-7)
63. Ott, J. B., & Boerio-Goates, J. (2000). Chapter 7 - The thermodynamic properties of solutions. In *Chemical Thermodynamics: Principles and Applications* (pp. 325–382). Elsevier. <https://doi.org/10.1016/B978-012530990-5/50008-0>
64. John O'M. Bockris, & Amulya K. N. Reddy. (1998). *Volume 1: Modern Electrochemistry* (Second Edition). Springer. <https://doi.org/10.1007/b114546>
65. Yizhak Marcus. (2015). *Ions in solution and their solvation*. John Wiley & Sons, Inc. <https://doi.org/10.1002/9781118892336>
66. Hahn, D. W., & Özisik, M. N. (2012). *Heat Conduction* (Third Edition). John Wiley & Sons, Inc. <https://doi.org/10.1002/9781118411285>
67. Dabir S. Viswanath, Tushar K. Ghosh, Dasika H. L. Prasad, Nidamarty V. K. Dutt, & Kalipatnapu Y. Rani. (2007). Chapter 1. Introduction. In *Viscosity of Liquids. Theory, Estimation, Experiment, and Data* (pp. 1–8). Springer. <https://doi.org/10.1007/978-1-4020-5482-2>
68. Ira N. Levine. (2009). *Physical Chemistry* (Sixth Edition). McGraw-Hill.
69. Redlich, O., & Meyer, D. M. (1964). The molal volumes of electrolytes. *Chemical Reviews*, 64(3), 221–227. <https://doi.org/10.1021/cr60229a001>
70. Millero, F. J. (1971). Molal volumes of electrolytes. *Chemical Reviews*, 71(2), 147–176. <https://doi.org/10.1021/cr60270a001>
71. Królikowska, M., Zawadzki, M., & Kuna, T. (2019). Physicochemical and thermodynamic properties of the {1-alkyl-1-methylpiperidinium bromide [C₁C_n=2,4PIP][Br], or 1-butylpyridinium bromide, [C₄Py][Br], or tri(ethyl)butylammonium bromide [N_{2,2,2,4}][Br] + water} binary systems. *Thermochimica Acta*, 671, 220–231. <https://doi.org/10.1016/j.tca.2018.11.018>

References

72. Marcinkowski, Ł., Olszewska, T., Kloskowski, A., & Warmińska, D. (2014). Apparent molar volumes and expansivities of ionic liquids based on N-Alkyl-N-methylmorpholinium cations in acetonitrile. *Journal of Chemical and Engineering Data*, 59(3), 718–725. <https://doi.org/10.1021/je400790d>
73. Hepler, L. G. (1969). Thermal expansion and structure in water and aqueous solutions. *Canadian Journal of Chemistry*, 47, 4613–4617. <https://doi.org/10.1139/v69-762>
74. Apelblat, A. (2007). Thermodynamic properties of aqueous electrolyte solutions. Compressibility studies in 0.1, 0.5 and 1.0 mol·kg⁻¹ lithium chloride solutions at temperatures from 278.15 to 323.15 K. *Journal of Solution Chemistry*, 36(11–12), 1437–1456. <https://doi.org/10.1007/s10953-007-9195-5>
75. Rohman, N., N. Dass, N., & Mahiuddin, S. (2002). Isentropic compressibility, effective pressure, classical sound absorption and shear relaxation time of aqueous lithium bromide, sodium bromide and potassium bromide solutions. *Journal of Molecular Liquids*, 100(3), 265–290. [https://doi.org/10.1016/S0167-7322\(02\)00047-8](https://doi.org/10.1016/S0167-7322(02)00047-8)
76. Bahadur, I., & Deenadayalu, N. (2013). Apparent molar volume and apparent molar isentropic compressibility for the binary systems {methyltrioctylammoniumbis(trifluoromethylsulfonyl) imide + ethyl acetate or ethanol} at different temperatures under atmospheric pressure. *Thermochimica Acta*, 566, 77–83. <https://doi.org/10.1016/j.tca.2013.05.015>
77. Ohtaki, H., & Radnai, T. (1993). Structure and dynamics of hydrated ions. *Chemical Reviews*, 93(3), 1157–1204. <https://doi.org/10.1021/cr00019a014>
78. Marcus, Y., & Hefter, G. (2006). Ion pairing. *Chemical Reviews*, 106(11), 4585–4621. <https://doi.org/10.1021/cr040087x>
79. Frank, H. S. (1941). Local dielectric constant and solute activity. A hydration-association model for strong electrolytes. *Journal of the American Chemical Society*, 63(7), 1789–1799. <https://doi.org/10.1021/ja01852a003>
80. Stokes, R. H., & Robinson, R. A. (1973). Solvation equilibria in very concentrated electrolyte solutions. *Journal of Solution Chemistry*, 2(2–3), 173–191. <https://doi.org/10.1007/BF00651972>

References

81. Cheng-long Lin, Hsieng-cheng Tseng, & Llang-sun Lee. (1998). A three-characteristic-parameter correlation model for strong electrolyte solutions. *Fluid Phase Equilibria*, 152(2), 169–185. [https://doi.org/10.1016/S0378-3812\(98\)00393-8](https://doi.org/10.1016/S0378-3812(98)00393-8)
82. Rabie, H. R., Wilczek-Vera, G., & Vera, J. H. (1999). Activities of individual ions from infinite dilution to saturated solutions. *Journal of Solution Chemistry*, 28(7), 885–913. <https://doi.org/10.1023/a:1021736315580>
83. Pazuki, G. R., & Rohani, A. A. (2006). A new model for the activity coefficients of individual ions in aqueous electrolyte solutions. *Fluid Phase Equilibria*, 242(1), 65–71. <https://doi.org/10.1016/j.fluid.2006.01.004>
84. Temoltzi-Avila, J., Iglesias-Silva, G. A., Ramos-Estrada, M., & Hall, K. R. (2019). An extended solvation theory for electrolyte osmotic and activity coefficients. I. Application at 298.15 K. *Fluid Phase Equilibria*, 499. <https://doi.org/10.1016/j.fluid.2019.112243>
85. Heyrovská, R. (1997). Degrees of dissociation and hydration numbers of alkali halides in aqueous solutions at 25 °C (some up to saturation). *Croatica Chemica Acta*, 1, 39–54. <https://hrcak.srce.hr/135604>
86. Heyrovská, R. (2011). Partial dissociation and hydration quantitatively explain the properties of aqueous electrolyte solutions and hence empirical activity concepts are unnecessary. *Nature Precedings*. <https://doi.org/10.1038/npre.2011.6416.1>
87. Karelin, A. I., & Tarasenko, V. A. (2019). Hydration numbers of perchloric acid: Estimation method based on the Raoult law. *Chemical Physics*, 523, 211–221. <https://doi.org/10.1016/j.chemphys.2019.04.004>
88. Zavitsas, A. A. (2020). Ideal thermodynamic behaviors of aqueous electrolyte solutions at very high concentrations. *Chemical Physics Letters*, 759. <https://doi.org/10.1016/j.cplett.2020.137941>
89. Zavitsas, A. A. (2022). Properties of aqueous solutions. A treatise against osmotic and activity coefficients. *Journal of Molecular Liquids*, 348. <https://doi.org/10.1016/j.molliq.2021.118410>
90. Reynolds, J. G., Graham, T. R., & Pearce, C. I. (2022). Extending Zavitsas' hydration model to the thermodynamics of solute mixtures in water. *Journal of Molecular Liquids*, 347. <https://doi.org/10.1016/j.molliq.2021.118309>

References

91. Wilson, A. D., & Stetson, C. (2021). Modeling solution vapor equilibria with solvation and solute assembly. *Journal of Molecular Liquids*, 336. <https://doi.org/10.1016/j.molliq.2021.116272>
92. Chialvo, A. A., & Simonson, J. M. (2006). Ion association in aqueous LiCl solutions at high concentration: Predicted results via molecular simulation. *Journal of Chemical Physics*, 124(15). <https://doi.org/10.1063/1.2186641>
93. Vlcek, L., & Chialvo, A. A. (2016). Single-ion hydration thermodynamics from clusters to bulk solutions: Recent insights from molecular modeling. *Fluid Phase Equilibria*, 407, 58–75. <https://doi.org/10.1016/j.fluid.2015.05.048>
94. Gujt, J., Bešter-Rogač, M., & Hribar-Lee, B. (2014). An investigation of ion-pairing of alkali metal halides in aqueous solutions using the electrical conductivity and the Monte Carlo computer simulation methods. *Journal of Molecular Liquids*, 190, 34–41. <https://doi.org/10.1016/j.molliq.2013.09.025>
95. Wilson, A. D., Lee, H., & Stetson, C. (2021). Mass action model of solution activity via speciation by solvation and ion pairing equilibria. *Communications Chemistry*, 4(1). <https://doi.org/10.1038/s42004-021-00599-8>
96. Wishaw, B. F., & Stokes, R. H. (1954). The diffusion coefficients and conductances of some concentrated electrolyte solutions at 25 °. *Journal of the American Chemical Society*, 76(8), 2065–2071. <https://doi.org/10.1021/ja01637a011>
97. Das, D. (2008). Ion association and solvation behavior of some lithium salts in tetrahydrofuran. A conductivity and raman spectroscopic study. *Journal of Solution Chemistry*, 37(7), 947–955. <https://doi.org/10.1007/s10953-008-9288-9>
98. Neilson, G. W., & Enderby, J. E. (1979). Neutron and X-ray diffraction studies of concentrated aqueous electrolyte solutions. *Annual Reports on the Progress of Chemistry - Section C*, 76, 185–220. <https://doi.org/10.1039/PC9797600185>
99. Dougan, L., Bates, S. P., Hargreaves, R., Fox, J. P., Crain, J., Finney, J. L., Réat, V., & Soper, A. K. (2004). Methanol-water solutions: A bi-percolating liquid mixture. *Journal of Chemical Physics*, 121(13), 6456–6462. <https://doi.org/10.1063/1.1789951>
100. Pereiro, A. B., Araújo, J. M. M., Oliveira, F. S., Esperança, J. M. S. S., Canongia Lopes, J. N., Marrucho, I. M., & Rebelo, L. P. N. (2012). Solubility of inorganic salts

References

- in pure ionic liquids. *Journal of Chemical Thermodynamics*, *55*, 29–36.
<https://doi.org/10.1016/j.jct.2012.06.007>
101. Fennell, C. J., Bizjak, A., Vlachy, V., & Dill, K. A. (2009). Ion pairing in molecular simulations of aqueous alkali halide solutions. *Journal of Physical Chemistry B*, *113*(19), 6782–6791. <https://doi.org/10.1021/jp809782z>
102. Prasetyo, N., Canaval, L. R., Wijaya, K., & Armunanto, R. (2015). Lithium(I) in liquid ammonia: A quantum mechanical charge field (QMCF) molecular dynamics simulation study. *Chemical Physics Letters*, *619*, 158–162.
<https://doi.org/10.1016/j.cplett.2014.11.066>
103. Workman, Jerry., & Weyer, Lois. (2008). *Practical guide to interpretive near-infrared spectroscopy*. CRC Press.
104. Mazivila, S. J., & Santos, J. L. M. (2022). A review on multivariate curve resolution applied to spectroscopic and chromatographic data acquired during the real-time monitoring of evolving multi-component processes: From process analytical chemistry (PAC) to process analytical technology (PAT). *TrAC - Trends in Analytical Chemistry*, *157*. <https://doi.org/10.1016/j.trac.2022.116698>
105. Garrido, M., Rius, F. X., & Larrechi, M. S. (2008). Multivariate curve resolution-alternating least squares (MCR-ALS) applied to spectroscopic data from monitoring chemical reactions processes. *Analytical and Bioanalytical Chemistry*, *390*(8), 2059–2066. <https://doi.org/10.1007/s00216-008-1955-6>
106. Barba, M. I., Larrechi, M. S., & Coronas, A. (2016). Quantitative analysis of the hydration of lithium salts in water using multivariate curve resolution of near-infrared spectra. *Analytica Chimica Acta*, *919*, 20–27.
<https://doi.org/10.1016/j.aca.2016.03.022>
107. Barba, M. I., Larrechi, M. S., & Coronas, A. (2019). Quantitative analysis of free water in ionic liquid-water mixtures. *Talanta*, *199*, 407–414.
<https://doi.org/10.1016/j.talanta.2019.02.087>
108. Rodríguez-Barrios, M. S., Rodríguez-Forteza, A., Varela, L. M., Salavera, D., Larrechi, M. S., & Coronas, A. (2021). Structural and quantitative analysis of water association in ethylammonium nitrate mixtures using soft modeling resolution of NIR

References

- spectra and molecular dynamics simulations. *Journal of Molecular Liquids*, *327*, 114789. <https://doi.org/10.1016/j.molliq.2020.114789>
109. Latorre-Arca, D., Soledad Larrechi, M., Salavera, D., Coronas, A., Rodríguez-Forteza, A., Rivera-Pousa, A., Méndez-Morales, T., & Varela, L. M. (2022). Quantitative and structural analysis of water association in water-lithium bromide-1,3-dimethylimidazolium chloride mixtures. *Journal of Molecular Liquids*, *368*(B), 120828. <https://doi.org/10.1016/j.molliq.2022.120828>
110. Jaumot, J., de Juan, A., & Tauler, R. (2015). MCR-ALS GUI 2.0: New features and applications. *Chemometrics and Intelligent Laboratory Systems*, *140*, 1–12. <https://doi.org/10.1016/j.chemolab.2014.10.003>
111. Rudolph, W., Brooker, M. H., & Pye, C. C. (1995). Hydration of lithium ion in aqueous solution. *J. Phys. Chem*, *99*(11), 3793–3797. <https://doi.org/10.1021/j100011a055>
112. Savoj, R., Agnew, H., Zhou, R., & Paesani, F. (2024). Molecular Insights into the Influence of Ions on the Water Structure. I. Alkali Metal Ions in Solution. *The Journal of Physical Chemistry B*, *128*(7), 1953–1962. <https://doi.org/10.1021/acs.jpcc.3c08150>
113. Stokes, R. H., & Robinson, R. A. (1948). Ionic hydration and activity in electrolyte solutions. *Journal of the American Chemical Society*, *70*(5), 1870–1878. <https://doi.org/10.1021/ja01185a065>
114. Fennell, C. J., Bizjak, A., Vlachy, V., & Dill, K. A. (2009). Ion pairing in molecular simulations of aqueous alkali halide solutions. *Journal of Physical Chemistry B*, *113*(19), 6782–6791. <https://doi.org/10.1021/jp809782z>
115. Chen, A. A., & Pappu, R. V. (2007). Quantitative characterization of ion pairing and cluster formation in strong 1:1 electrolytes. *Journal of Physical Chemistry B*, *111*(23), 6469–6478. <https://doi.org/10.1021/jp0708547>
116. Izvekov, S., & Philpott, M. R. (2000). Ab initio molecular dynamics simulation of LiBr association in water. *Journal of Chemical Physics*, *113*(23), 10676–10684. <https://doi.org/10.1063/1.1311965>
117. Lee, S. H., & Rasaiah, J. C. (1996). Molecular Dynamics simulation of ion mobility. 2. Alkali metal and halide ions using the SPC/E model for water at 25 °C.

References

-
- Journal of Physical Chemistry*, 100(4), 1420–1425.
<https://doi.org/https://doi.org/10.1021/jp953050c>
118. Rasaiah, J. C., & Lynden-Bell, R. M. (2001). Computer simulation studies of the structure and dynamics of ions and non-polar solutes in water. *Philosophical Transactions of the Royal Society A: Mathematical, Physical and Engineering Sciences*, 359(1785), 1545–1574. <https://doi.org/10.1098/rsta.2001.0865>
119. Daub, C. D., Hänninen, V., & Halonen, L. (2019). Ab initio Molecular Dynamics simulations of the influence of lithium bromide on the structure of the aqueous solution-air interface. *Journal of Physical Chemistry B*, 123(3), 729–737. <https://doi.org/10.1021/acs.jpcc.8b10552>
120. Marcus, Y. (2009). Effect of ions on the structure of water: Structure making and breaking. *Chemical Reviews*, 109(3), 1346–1370. <https://doi.org/10.1021/cr8003828>
121. Reiser, S., Horsch, M., & Hasse, H. (2014). Temperature dependence of the density of aqueous alkali halide salt solutions by experiment and molecular simulation. *Journal of Chemical and Engineering Data*, 59(11), 3434–3448. <https://doi.org/10.1021/je500420g>
122. Boryta, D. A. (1961). Solubility of lithium bromide in water between -50° and +100° C. (45 to 70% lithium bromide). *Journal of Chemical and Engineering Data*, 15(1), 142–144. <https://doi.org/https://doi.org/10.1021/je60044a030>
123. SSC. (1998). *Transport property data for aqueous lithium bromide*. Unpublished.
124. Kacenauskaite, L., Van Wyck, S. J., Moncada Cohen, M., & Fayer, M. D. (2023). Water-in-Salt: Fast Dynamics, Structure, Thermodynamics, and Bulk Properties. *The Journal of Physical Chemistry B*, 128(1), 291–302. <https://doi.org/10.1021/acs.jpcc.3c07711>
125. Méndez-Morales, T., Carrete, J., Cabeza, Ó., Russina, O., Triolo, A., Gallego, L. J., & Varela, L. M. (2014). Solvation of lithium salts in protic ionic liquids: A molecular dynamics study. *Journal of Physical Chemistry B*, 118(3), 761–770. <https://doi.org/10.1021/jp410090f>
126. Cammarata, L., Kazarian, S. G., Salter, P. A., & Welton, T. (2001). Molecular states of water in room temperature ionic liquids. *Physical Chemistry Chemical Physics*, 3(23), 5192–5200. <https://doi.org/10.1039/b106900d>
-

References

127. Köddermann, T., Wertz, C., Heintz, A., & Ludwig, R. (2006). The association of water in ionic liquids: A reliable measure of polarity. *Angewandte Chemie - International Edition*, 45(22), 3697–3702. <https://doi.org/10.1002/anie.200504471>
128. Haynes, W. M., Lide, D. R., & Bruno, T. J. (2017). *CRC Handbook of Chemistry and Physics* (97th Edition). CRC Press.
129. Killion, J. D., & Garimella, S. (2003). A review of experimental investigations of absorption of water vapor in liquid films falling over horizontal tubes. *HVAC and R Research*, 9(2), 111–136. <https://doi.org/10.1080/10789669.2003.10391060>
130. Yoon, J. I., Phan, T. T., Moon, C. G., Lee, H. S., & Jeong, S. K. (2008). Heat and mass transfer characteristics of a horizontal tube falling film absorber with small diameter tubes. *Heat and Mass Transfer/Waerme- Und Stoffuebertragung*, 44(4), 437–444. <https://doi.org/10.1007/s00231-007-0261-8>
131. Eisa, M. A. R., Devotta, S., & Holland, F. A. (1986). Thermodynamic design data for absorption heat pump systems operating on water-lithium bromide: Part III— Simultaneous cooling and heating. *Applied Energy*, 25(2), 83–96. [https://doi.org/10.1016/0306-2619\(86\)90068-1](https://doi.org/10.1016/0306-2619(86)90068-1)
132. Eisa, M. A. R., Devotta, S., & Holland, F. A. (1986). Thermodynamic design data for absorption heat pump systems operating on water-lithium bromide: Part I— Cooling. *Applied Energy*, 24(4), 287–301. [https://doi.org/10.1016/0306-2619\(86\)90007-3](https://doi.org/10.1016/0306-2619(86)90007-3)
133. Eisa, M. A. R., Rashed, I. G. A., Devotta, S., & Holland, F. A. (1986). Thermodynamic design data for absorption heat pump systems operating on water-lithium bromide: Part II: Heating. *Applied Energy*, 25(1), 71–82. [https://doi.org/10.1016/0306-2619\(86\)90062-0](https://doi.org/10.1016/0306-2619(86)90062-0)
134. Pátek, J., & Klomfar, J. (2006). Solid-liquid phase equilibrium in the systems of LiBr-H₂O and LiCl-H₂O. *Fluid Phase Equilibria*, 250(1–2), 138–149. <https://doi.org/10.1016/j.fluid.2006.09.005>
135. Koo, K.-K., Lee, H.-R., Jeong, S., Oh, Y.-S., Park, D.-R., & Back, Y.-S. (1999). Solubilities, vapor pressures, and heat capacities of the water + lithium bromide + lithium nitrate + lithium iodide + lithium chloride system. *International Journal of*

References

- Thermophysics*, 20(2), 589–600.
<https://doi.org/https://doi.org/10.1023/A:1022661222237>
136. D'Agostino, C., Mantle, M. D., Mullan, C. L., Hardacre, C., & Gladden, L. F. (2018). Diffusion, ion pairing and aggregation in 1-ethyl-3-methylimidazolium-based ionic liquids studied by ¹H and ¹⁹F PFG NMR: effect of temperature, anion and glucose dissolution. *ChemPhysChem*, 19(9), 1081–1088.
<https://doi.org/10.1002/cphc.201701354>
137. Cera-Manjarres, A., Salavera, D., & Coronas, A. (2018). Vapour pressure measurements of ammonia/ionic liquids mixtures as suitable alternative working fluids for absorption refrigeration technology. *Fluid Phase Equilibria*, 476(B), 48–60.
<https://doi.org/10.1016/j.fluid.2018.01.006>
138. Chaudhari, S. K., Salavera, D., & Coronas, A. (2011). Densities, viscosities, heat capacities, and vapor-liquid equilibria of ammonia + sodium thiocyanate solutions at several temperatures. *Journal of Chemical and Engineering Data*, 56(6), 2861–2869.
<https://doi.org/10.1021/je200038n>
139. H. Preston-Thomas. (1990). The international temperature scale of 1990 (ITS-90). *Metrologia*, 27(2), 3–10. <https://doi.org/10.1088/0026-1394/27/1/002>
140. Lemmon, E. W., Bell, I. H., Huber, M. L., & McLinden, M. O. (n.d.). *Thermophysical properties of fluid systems*. NIST Chemistry WebBook; National Institute of Standards and Technology. <https://doi.org/10.18434/T4D303>
141. Yuan, Z., & Herold, K. E. (2005). Thermodynamic properties of aqueous lithium bromide using a multiproperty free energy correlation. *HVAC&R Research*, 11(3), 377–393. <https://doi.org/10.1080/10789669.2005.10391144>
142. Labra, L., Juárez-Romero, D., Siqueiros, J., Coronas, A., & Salavera, D. (2017). Measurement of properties of a lithium bromide aqueous solution for the determination of the concentration for a prototype absorption machine. *Applied Thermal Engineering*, 114, 1186–1192.
<https://doi.org/10.1016/j.applthermaleng.2016.10.162>
143. Stankus, S. V., Khairulin, R. A., Gruzdev, V. A., & Verba, O. I. (2007). The density of aqueous solutions of lithium bromide at high temperatures and concentrations. *High Temperature*, 45(3), 429–431. <https://doi.org/10.1134/S0018151X07030212>

References

144. Kiepe, J., De Araújo Rodrigues, A. K., Horstmann, S., & Gmehling, J. (2003). Experimental determination and correlation of liquid density data of electrolyte mixtures containing water or methanol. *Industrial and Engineering Chemistry Research*, 42(9), 2022–2029. <https://doi.org/10.1021/ie020936b>
145. Khairulin, R. A., Gruzdev, V. A., Stankus, S. V, & Verba, O. I. (2006). Experimental study of the density of aqueous solutions of lithium bromide at temperature of up to 250 °C in the range of mass concentrations from 30 to 65 %. *Thermophysics and Aeromechanics*, 13(4), 575–583. <https://doi.org/10.1134/S0869864306040111>
146. Wagner, W., & Pruß, A. (2002). The IAPWS formulation 1995 for the thermodynamic properties of ordinary water substance for general and scientific use. *Journal of Physical and Chemical Reference Data*, 31(2), 387–535. <https://doi.org/10.1063/1.1461829>
147. Koschel, D., Coxam, J. Y., Rodier, L., & Majer, V. (2006). Enthalpy and solubility data of CO₂ in water and NaCl(aq) at conditions of interest for geological sequestration. *Fluid Phase Equilibria*, 247(1–2), 107–120. <https://doi.org/10.1016/j.fluid.2006.06.006>
148. Arcis, H., Ballerat-Busserolles, K., Rodier, L., & Coxam, J. Y. (2011). Enthalpy of solution of carbon dioxide in aqueous solutions of monoethanolamine at temperatures of 322.5 K and 372.9 K and pressures up to 5 MPa. *Journal of Chemical and Engineering Data*, 56(8), 3351–3362. <https://doi.org/10.1021/je2002946>
149. Simond, M. R., Ballerat-Busserolles, K., Coulier, Y., & Coxam, J.-Y. (2013). Flow calorimetry: a technique for characterisation of liquid-liquid and liquid-gas systems. *Proceedings of the XXXIX Jeep – 39th Edition of the Joint European Days on Equilibrium Between Phases 2013*, 3, 67–70. <https://doi.org/10.1051/mateconf/20130301024>
150. Hajlaoui, A., Salat, L., Rodier, L., Andanson, J.-M., Coulier, Y., & Thermody, Y. C. (2023). Thermodynamic study of working fluid pairs for an absorption refrigeration process. *Proceedings of the 26th IIR International Congress of Refrigeration*, 567–578. <https://hal.science/hal-04224702>

References

151. Parker, V. B. (1965). *Thermal properties of aqueous uni-univalent electrolytes*.
<https://doi.org/10.6028/NBS.NSRDS.2>
152. Smith-Magowan, D., & Goldberg, R. N. (1979). *A bibliography of sources of experimental data leading to thermal properties of binary aqueous electrolyte solutions*. <https://doi.org/10.6028/NBS.SP.537>
153. Fortier, J.-L., Leduc, P.-A., & Desnoyers ' ', J. E. (1974). Thermodynamic properties of alkali halides. II. Enthalpies of dilution and heat capacities in water at 25 °C. *Journal of Solution Chemistry*, 3(4), 323–349.
<https://doi.org/10.1007/BF00648229>
154. Vaslow, F. (1971). Salt-induced critical-type transitions in aqueous solution. Heats of dilution of the lithium and sodium halides. *The Journal of Physical Chemistry*, 75(21), 3317–3321. <https://doi.org/10.1021/j100690a020>
155. Lange, E., & Schwartz, E. (1928). Lösungs-und Verdünnungswärmen von Salzen von der äussersten Verdünnung bis zur Sättigung. IV. Lithinbromid. *Zeitschrift Für Physikalische Chemie*, 133, 129–150. <https://doi.org/10.1515/zpch-1928-13311>
156. Young, T. F., & Vogel, O. G. (1932). The relative heat contents of the constituents of aqueous sodium chloride solutions. *Journal of the American Chemical Society*, 54(8), 3030–3040. <https://doi.org/10.1021/ja01347a002>
157. Stolov, M. A., Zaitseva, K. V., Varfolomeev, M. A., & Acree, W. E. (2017). Enthalpies of solution and enthalpies of solvation of organic solutes in ethylene glycol at 298.15 K: Prediction and analysis of intermolecular interaction contributions. *Thermochimica Acta*, 648, 91–99. <https://doi.org/10.1016/j.tca.2016.12.015>
158. Varfolomeev, M. A., Khachatrian, A. A., Akhmadeev, B. S., & Solomonov, B. N. (2016). Thermodynamics of hydrogen bonding and van der Waals interactions of organic solutes in solutions of imidazolium based ionic liquids: “Structure-property” relationships. *Thermochimica Acta*, 633, 12–23.
<https://doi.org/10.1016/j.tca.2016.03.036>
159. Russina, O., Caminiti, R., Méndez-Morales, T., Carrete, J., Cabeza, O., Gallego, L. J., Varela, L. M., & Triolo, A. (2015). How does lithium nitrate dissolve in a protic

References

- ionic liquid? *Journal of Molecular Liquids*, 205, 16–21.
<https://doi.org/10.1016/j.molliq.2014.08.007>
160. Molenat, J. (1969). Étude systématique de la conductivité à 25 °C dans les solutions concentrées des halogénures alcalins. *Journal de Chimie Physique*, 66, 825–833. <https://doi.org/10.1051/jcp/1969660825>
161. Baron, N. M., & Scherba, M. U. (1971). Electrical conductivity of aqueous solutions of LiCl, LiBr and LiI at low and medium temperatures. *Zhurnal Prikladnoi Khimii*, 44, 2118–2120.
162. Fried, I., & Segal, M. (1983). Electrical conductivity of concentrated lithium bromide aqueous solutions. *Journal of Chemical & Engineering Data*, 28(1), 127–130. <https://doi.org/10.1021/je00031a033>
163. Wu, X., Gong, Y., Xu, S., Yan, Z., Zhang, X., & Yang, S. (2019). Electrical conductivity of lithium chloride, lithium bromide, and lithium iodide electrolytes in methanol, water, and their binary mixtures. *Journal of Chemical and Engineering Data*, 64(10), 4319–4329. <https://doi.org/10.1021/acs.jced.9b00405>
164. Arrhenius, S. (1889). Über die Dissociationswärme und den Einfluss der Temperatur auf den Dissociationsgrad der Elektrolyte. *Zeitschrift Für Physikalische Chemie*, 4, 96–116. <https://doi.org/10.1515/zpch-1889-0408>
165. Casteel Edward S Amis, J. F. (1972). Specific conductance of concentrated solutions of magnesium salts in water-ethanol system. *Journal of Chemical & Engineering Data*, 17(1), 55–59. <https://doi.org/10.1021/je60052a029>
166. Ding, M. S. (2004). Casteel-Amis equation: Its extension from univariate to multivariate and its use as a two-parameter function. *Journal of Chemical & Engineering Data*, 49(5), 1469–1474. <https://doi.org/10.1021/je049839a>
167. Alloush, A., Gosney, W. B., & Wakeham, W. A. (1982). A transient hot-wire instrument for thermal conductivity measurements in electrically conducting liquids at elevated temperatures. *International Journal of Thermophysics*, 3(3), 225–235. <https://doi.org/10.1007/BF00503318>
168. Abdulagatov, I. M., & Magomedov, U. B. (1997). Measurements of thermal conductivity of aqueous LiCl and LiBr solutions from 293 to 473 K at pressures up to

References

- 100 MPa. *Berichte Der Bunsengesellschaft Für Physikalische Chemie*, 101(4), 708–711. <https://doi.org/10.1002/bbpc.19971010411>
169. Kawamata, K., Nagasaka, Y., & Nagashima, A. (1988). Measurements of the thermal conductivity of aqueous LiBr solutions at pressures up to 40 MPa. *International Journal of Thermophysics*, 9(3), 317–329. <https://doi.org/10.1007/BF00513074>
170. Fleßner, C., & Ziegler, F. (2023). Viscosity correlation for aqueous lithium bromide solution. *International Journal of Thermophysics*, 44(2). <https://doi.org/10.1007/s10765-022-03122-w>
171. Reynolds, J. G., Mauss, B. M., & Daniel, R. C. (2019). The importance of ion interactions on electrolyte solution viscosities determined by comparing concentrated sodium carbonate and nitrate solutions. *Journal of Molecular Liquids*, 288. <https://doi.org/10.1016/j.molliq.2019.111022>
172. Peng, H., & Nguyen, A. V. (2018). A link between viscosity and cation-anion contact pairs: Adventure on the concept of structure-making/breaking for concentrated salt solutions. *Journal of Molecular Liquids*, 263, 109–117. <https://doi.org/10.1016/j.molliq.2018.04.145>
173. Plechkova, N. V., & Seddon, K. R. (2008). Applications of ionic liquids in the chemical industry. *Chemical Society Reviews*, 37(1), 123–150. <https://doi.org/10.1039/b006677j>
174. Stillinger, F. H., & Rahman, A. (1972). Molecular dynamics study of temperature effects on water structure and kinetics. *The Journal of Chemical Physics*, 57(3), 1281–1292. <https://doi.org/10.1063/1.1678388>
175. Nilsson, A., & Pettersson, L. G. M. (2011). Perspective on the structure of liquid water. *Chemical Physics*, 389(1–3), 1–34. <https://doi.org/10.1016/j.chemphys.2011.07.021>
176. Segade, L., Cabanas, M., Domínguez-Pérez, M., Rilo, E., García-Garabal, S., Turmine, M., Varela, L. M., Gómez-González, V., Docampo-Alvarez, B., & Cabeza, O. (2016). Surface and bulk characterisation of mixtures containing alkylammonium nitrates and water or ethanol: Experimental and simulated properties at 298.15 K.

References

-
- Journal of Molecular Liquids*, 222, 663–670.
<https://doi.org/10.1016/j.molliq.2016.07.107>
177. Docampo-Álvarez, B., Gómez-González, V., Méndez-Morales, T., Carrete, J., Rodríguez, J. R., Cabeza, Ó., Gallego, L. J., & Varela, L. M. (2014). Mixtures of protic ionic liquids and molecular cosolvents: A molecular dynamics simulation. *Journal of Chemical Physics*, 140(21). <https://doi.org/10.1063/1.4879660>
178. Zafarani-Moattar, M. T., & Shekaari, H. (2005). Apparent molar volume and isentropic compressibility of ionic liquid 1-butyl-3-methylimidazolium bromide in water, methanol, and ethanol at T = (298.15 to 318.15) K. *Journal of Chemical Thermodynamics*, 37(10), 1029–1035. <https://doi.org/10.1016/j.jct.2005.01.009>
179. Rohman, N., Mahiuddin, S., Dass, N. N., & Yoo, K.-P. (2002). Isentropic compressibility of aqueous and methanolic electrolytic solution. *Korean Journal of Chemical Engineering*, 19(4), 679–684. <https://doi.org/10.1007/BF02699317>

UNIVERSITAT ROVIRA I VIRGILI
QUANTITATIVE ANALYSIS OF BULK WATER IN WATER/LITHIUM BROMIDE MIXTURES WITH IONIC LIQUIDS
AS A WORKING FLUID IN ABSORPTION HEAT PUMPS AND INFLUENCE ON THE THERMOPHYSICAL PROPERTIES
David Latorre Arca

UNIVERSITAT ROVIRA I VIRGILI
QUANTITATIVE ANALYSIS OF BULK WATER IN WATER/LITHIUM BROMIDE MIXTURES WITH IONIC LIQUIDS
AS A WORKING FLUID IN ABSORPTION HEAT PUMPS AND INFLUENCE ON THE THERMOPHYSICAL PROPERTIES
David Latorre Arca

UNIVERSITAT ROVIRA I VIRGILI
QUANTITATIVE ANALYSIS OF BULK WATER IN WATER/LITHIUM BROMIDE MIXTURES WITH IONIC LIQUIDS
AS A WORKING FLUID IN ABSORPTION HEAT PUMPS AND INFLUENCE ON THE THERMOPHYSICAL PROPERTIES
David Latorre Arca

UNIVERSITAT ROVIRA I VIRGILI
QUANTITATIVE ANALYSIS OF BULK WATER IN WATER/LITHIUM BROMIDE MIXTURES WITH IONIC LIQUIDS
AS A WORKING FLUID IN ABSORPTION HEAT PUMPS AND INFLUENCE ON THE THERMOPHYSICAL PROPERTIES
David Latorre Arca

UNIVERSITAT ROVIRA I VIRGILI
QUANTITATIVE ANALYSIS OF BULK WATER IN WATER/LITHIUM BROMIDE MIXTURES WITH IONIC LIQUIDS
AS A WORKING FLUID IN ABSORPTION HEAT PUMPS AND INFLUENCE ON THE THERMOPHYSICAL PROPERTIES
David Latorre Arca



UNIVERSITAT
ROVIRA i VIRGILI